THE ORIGIN OF THE GEOLOGICAL STRUCTURES, DIAPIRS, GRABENS, AND BARITE VEINS IN THE FLINDERS RANGES, SOUTH AUSTRALIA

by

Premalal J. Mendis

A thesis submitted in fulfilment of the requirements for the degree of

Doctor of Philosophy in Geology

Department of Geology and Geophysics
University of Adelaide, South Australia
November 2002

ABSTRACT

The Adelaide Fold Belt in South Australia consists of a sequence of sedimentary rocks from Neoproterozoic to Cambrian in age, deposited on a granitic basement and deformed by two shortening deformations during the 500-480 Ma Delamerian Orogeny. Significant features of the Fold Belt, especially in the central Flinders Ranges, are a large number of barite vein deposits and mud breccia deposits known as diapirs.

During the D_1 deformation, a series of F_1 gentle folds were formed with NNW orientation. Fractures and faults trending NNE and ENE were also formed across F_1 anticlines, initiating boundary faults for grabens on both limbs of the anticlines. Sequences on limbs of anticlines, but dominantly those on eastern limbs, and within boundary faults of grabens, were thrust over décollement faults, forming a series of imbricate type fault-propagation folds, verging WSW, and grabens across the axial traces of anticlines. Décollement faults that formed over the basement continued as listric thrust faults through the sedimentary sequence, up to Cambrian aged sediments. Breccia was produced during gouging along these thrust surfaces, and included basement rocks and Neoproterozoic sedimentary rocks. The breccias were subsequently deposited along the décollement faults, in the cores of anticlines, adjacent to apices of grabens and extruded into adjacent hosts.

Structures produced by the D_2 deformation include major F_2 gentle, fault-propagation folds oriented ENE, and superimposed onto F_1 folds to form dome and basin egg-carton-like structure, thus remobilising breccia, dominantly into domes. The D_2 deformation also caused a series of dextral kinks along F_1 axial traces, including the Nackara Arc.

Barite veins were mainly formed in three sets of essentially unconnected and near-vertical tensional fractures, following the antitaxial mechanism, during NE-SW major compression of the D_1 deformation. The dominant set was oriented NE-SW, while two subordinate en échelon sets were formed with NNE and ENE orientations in conjugate shear zones. The veins were then subjected to displacement and rotation during progressive deformation, especially within the grabens, thus producing a complex vein array as shown by the Oraparinna deposits in Bunkers Graben of the central Flinders Ranges.

The most favourable host stratigraphic unit for barite veins in the Adelaide Fold Belt is the Brachina Formation, accounting for approximately 60 % of barite production+reserves. Siltstone, alone or in association with other lithologies, mainly shale, is the most important

lithology, hosting approximately 70 % of barite production+reserves. Siltstone is the dominant lithology in the Brachina Formation. K-feldspars in the Brachina Formation contain up to 1.2 wt% Ba and are the most likely source of Ba^{2+} ions which migrated into vein-depositional sites during deformation.

Barite veins of the Adelaide Fold Belt are characterized by a simple mineralogy, consisting of barite with minor, but variable, amounts of carbonates and quartz, and only trace amounts of sulphide minerals. $^{87}Sr/^{86}Sr$ ratios of the veins range from 0.710695 to 0.733382 and $\delta^{34}S$ values of barite range from 16.8 to 31.0 ‰. The combined isotope data suggest both Sr^{2+} and SO_4^{2-} ions were derived mainly from host formations and connate waters of marine origin, but in some cases Cambrian seawater and/or diapirs may have been additional sources of these components. Fluid inclusion data indicate the veins formed from fluids with temperature of less than 150°C.

Dilational fractures that host the barite veins formed abundantly near both the décollement and listric thrust fault surfaces along which most of the diapirs were produced. However, the supply of ingredients to the veins was limited to those veins within about 100 m from diapirs, as seen at the Oraparinna Diapir in the central Flinders Ranges.

STATEMENT OF ORIGINALITY

This work contains no material which has been accepted for the award of any other degree or diploma in any university or other tertiary institution and, to the best of my knowledge and belief, contains no material previously published or written by another person, except where due reference has been made in the text.

I give consent to this copy of my thesis, when deposited in the University Library, being available for loan and photocopying.

Premalal J. Mendis

(Email: lalmendis@yahoo.com.au)

ACKNOWLEDGMENTS

I would like to thank Drs Ross Both and Pat James of the Department of Geology and Geophysics of the University of Adelaide, for their guidance and helpful discussions throughout the research. Sincere thanks to the late Dr Robin Oliver, whose long contact with Sri Lanka was instrumental in my arrival at the University of Adelaide.

The work was supported by a scholarship from the Australian International Development Assistance Bureau and a Post-graduate Scholarship in Structural Geology from the University of Adelaide. It was further supported by research grants to Ross Both from the ARC and an analytical fund from Commercial Minerals Ltd, administered through Lew Barnes.

Sincere thanks to W.C. McCallum, Greg Jenkins and J. Townsend of PIRSA, Lew Barnes of Commercial Minerals Ltd and Alan Pring of South Australian Museum for assistance.

The fieldwork phase was made enjoyable because of great kindness and help from Bernnie Wright, Marree Wright, Peter Wright and Dick from the Oraparinna Barite Mine. Thank you all.

The author thanks many people who helped in the Department of Geology and Geophysics for assistance, guidance and company. Even though it is a long list of names, a few names need to be mentioned. Discussions and assistance of Graziella Caprarelli, J. Mawby, Mrs. Ding, John Foden, Colin Windsor, John Stanly, Rick Barrett, Wayne Mussared and Sherry Proferes, and association with Ali, Basim and Paul Polito were gratefully appreciated.

During the time of thesis writing, helpful discussions, encouragement and assistance from Parakrama Ediriweera, Palitha Welgama, Somasiri Agalawatta, Gamini Withanachchi, Dana Hapugoda and Jaliya and Lucki Kumaratilake were greatly appreciated to keep the work on track. Positive and parallel thinking about the geological structure of the Flinders Ranges from Bob Dalgarno and John Parker was a great relief and decreased the fear of forwarding a new theory for the Ranges. I am particularly grateful to B.G. Forbes and Brenda Bradley for proof reading and encouragement.

Great appreciations for late parents Nimala and Vini, sisters Shantha, Chandrika, Pathmarani and brother Sisira who wished and encouraged my education right through the lifetime.

Finally, those who shared the rock-hard time during studies: wife Padma, son Rangana and daughter Victoria are greatly appreciated for testing their patience. Special thanks to Rangana for using his skills for type setting the thesis.

For their encouragement, patience, assistance and endurance; this thesis is offered to:

Deceased mother and father, Nimala and Vini Mendis

Padma

Rangana

Victoria

Shantha, Percy

Chandrika, Jayantha

Pathmarani, Nelson

Sisira, Kumari

and

Teachers, relatives and friends.

TABLE OF CONTENTS

LIST OF FIGURES

* ^ Symbol denotes cartoon figures constructed from photographs of serial sections.

LIST OF TABLES

LIST OF APPENDICES

PUBLICATIONS

Mendis, P.J. (Lal); James, P.R. & Both, R.A. 2002. Geological structure of the Flinders ranges, South Australia. *In: Geoscience 2002: Expanding Horizons. Abstracts of the 16th Australian Geological Convention* (edited by Preiss, V.P.) **No. 67**, Adelaide Convention Centre, Adelaide, SA, Australia, p183.

Mendis, P.J. (Lal); Both, R.A. & James, P.R. 2002. Structural and geochemical control of barite veins in the Flinders ranges, South Australia. *In: Geoscience 2002: Expanding Horizons. Abstracts of the 16th Australian Geological Convention* (edited by Preiss, V.P.) **No. 67**, Adelaide Convention Centre, Adelaide, SA, Australia, p337.

Mendis, P.J. (Lal); James, P.R. & Both, R.A. 2002. Origin of diapirs in the Adelaide Fold Belt: Synsedimentary or syntectonic? *In: Geoscience 2002: Expanding Horizons. Abstracts of the 16th Australian Geological Convention* (edited by Preiss, V.P.) **No. 67**, Adelaide Convention Centre, Adelaide, SA, Australia, p384.

GLOSSARY

Diapir A vertical columnar plug of less dense rock or magma that is forced through a more dense rock. The process, called diapirism, may be caused by buoyancy (less dense material rising through denser rocks), tectonic forces, or a combination of the two. For example, the deformation of a succession of sedimentary strata containing highly incompetent material such as rock salt often results in the upward intrusion of the salt through the overlying layers. Diapirism forms both igneous and non-igneous intrusions (e.g. salt plugs) and is accompanied by doming and piercement of the overlying strata (Lapidus, 1987).

PIRSA Primary Industries and Resources, South Australia includes the former Department of Mines and Energy South Australia (MESA) and the Geological Survey of South Australia.

Lode Used in reference to barite deposits of the Adelaide Fold Belt is equivalent to "vein".

Chapter 1

THE PROJECT

1.1 Introduction

The Adelaide Fold Belt in South Australia is composed of Neoproterozoic and Cambrian deformed sedimentary rocks of the Adelaide Geosyncline (Sprigg, 1952), bordering the older, relatively undeformed Gawler Craton (Preiss, 1987; Von der Borch, 1980; Sandiford *et al.*, 1998). The Fold Belt is subdivided into four main structural subdomains: the northern, central and southern Flinders Ranges, and the southern Adelaide Fold Belt (Fig. 1.1).

The central Flinders Ranges are situated about 500 km north of the State capital of Adelaide. Both the central and northern Flinders Ranges are located bordering the cratonic block of the Gawler Craton (to the west) and the Curnamona Craton (to the east). The Flinders Ranges consist of broad, open dome (e.g. Blinman Dome) and basin (e.g. Wilpena Pound) structures (Dalgarno and Johnson, 1966; Fig. 1.2). Dips on the limbs of these structures are gentle to moderate, and only locally steep. Cleavage is generally not developed.

The Flinders Ranges have been well studied for sedimentary aspects and breccia deposits, described as diapirs, by many authors (Mawson, 1942; Sprigg, 1952; Parkin *et al.*, 1953; Webb, 1960, 1961; Coats, 1964a; Mincham, 1964; Dalgarno and Johnson, 1964, 1965, 1968; Barnes, 1972; Mount, 1975; White, 1983; Preiss, 1985, 1987; Clarke, 1986; Lemon, 1988; Dyson, 1992, 1996, 2002a,b; Reilly *et al.*, 2002). The origin of the diapirs has been the subject of much debate, with both syntectonic (Mount, 1975; White, 1983) and synsedimentary (Lemon, 1988; Dyson, 1992, 1996, 1999) proponents. The geological structure of the northern Flinders Ranges, the southern Flinders Ranges including the Nackara Arc, and the southern Fold Belt has been studied in detail. It has been suggested the Nackara Arc resulted from a NW tapering orogenic wedge during the Delamerian deformation where the sediment thickness increased to the SE, by northwestward tectonic transportation (Marshak and Flottmann, 1996; Paul *et al.*, 1999). However, the central Flinders Ranges has received little attention for its structural geology, possibly due to the low intensity of deformation within the sequences (Preiss, 1999; see attached maps in the back pocket, Map 1 of Reid and Preiss, 1999, and Map 2 of Callen and Reid, 1994).

The Adelaide Fold Belt is a barite rich province. Both diapirs and barite deposits are relatively abundant in the Flinders Ranges but sparse elsewhere in the Fold Belt (Fig. 1.3; Mount, 1975).

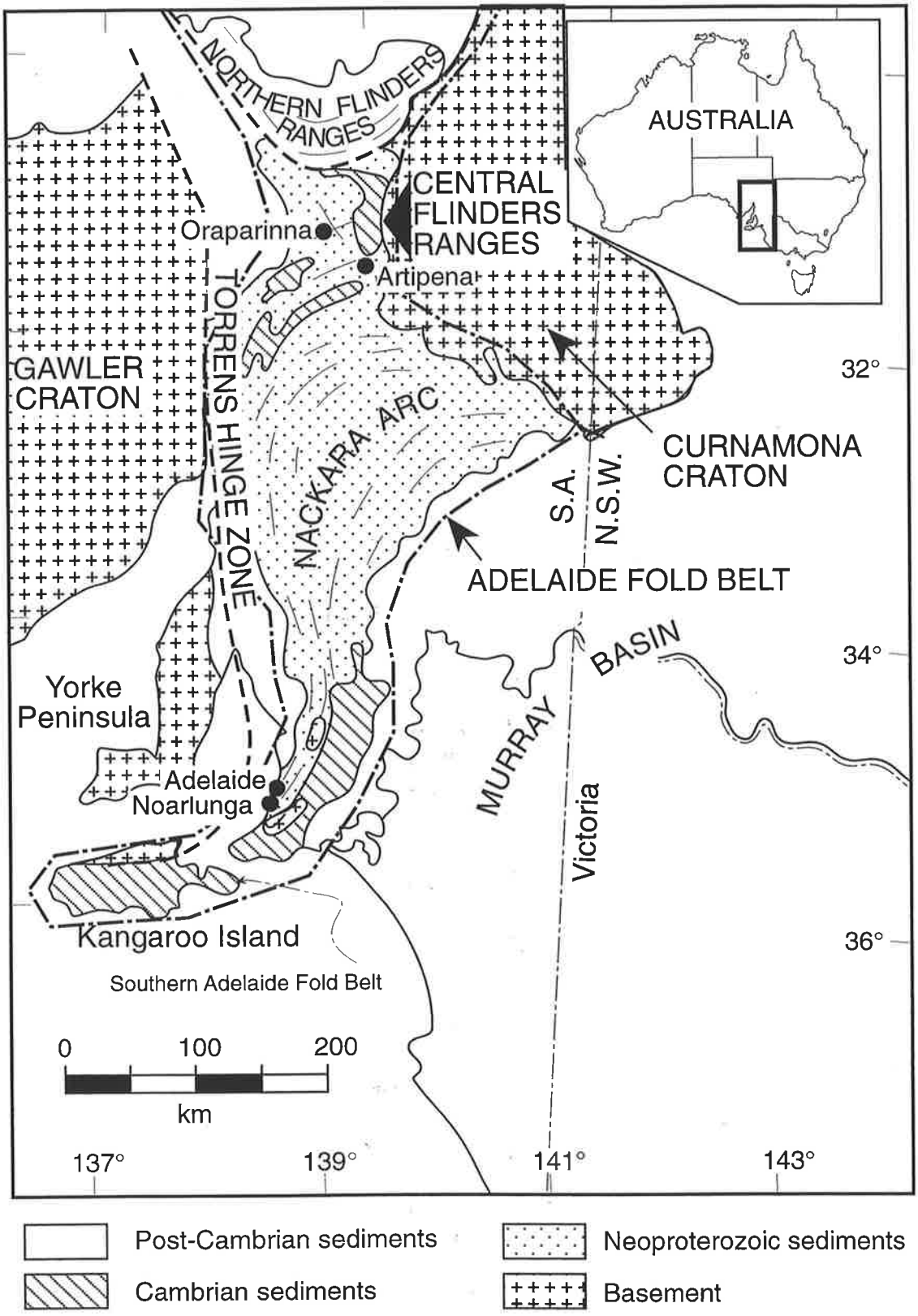

Fig. 1.1: Regional map of the Adelaide Fold Belt (after T.Flöttmann).

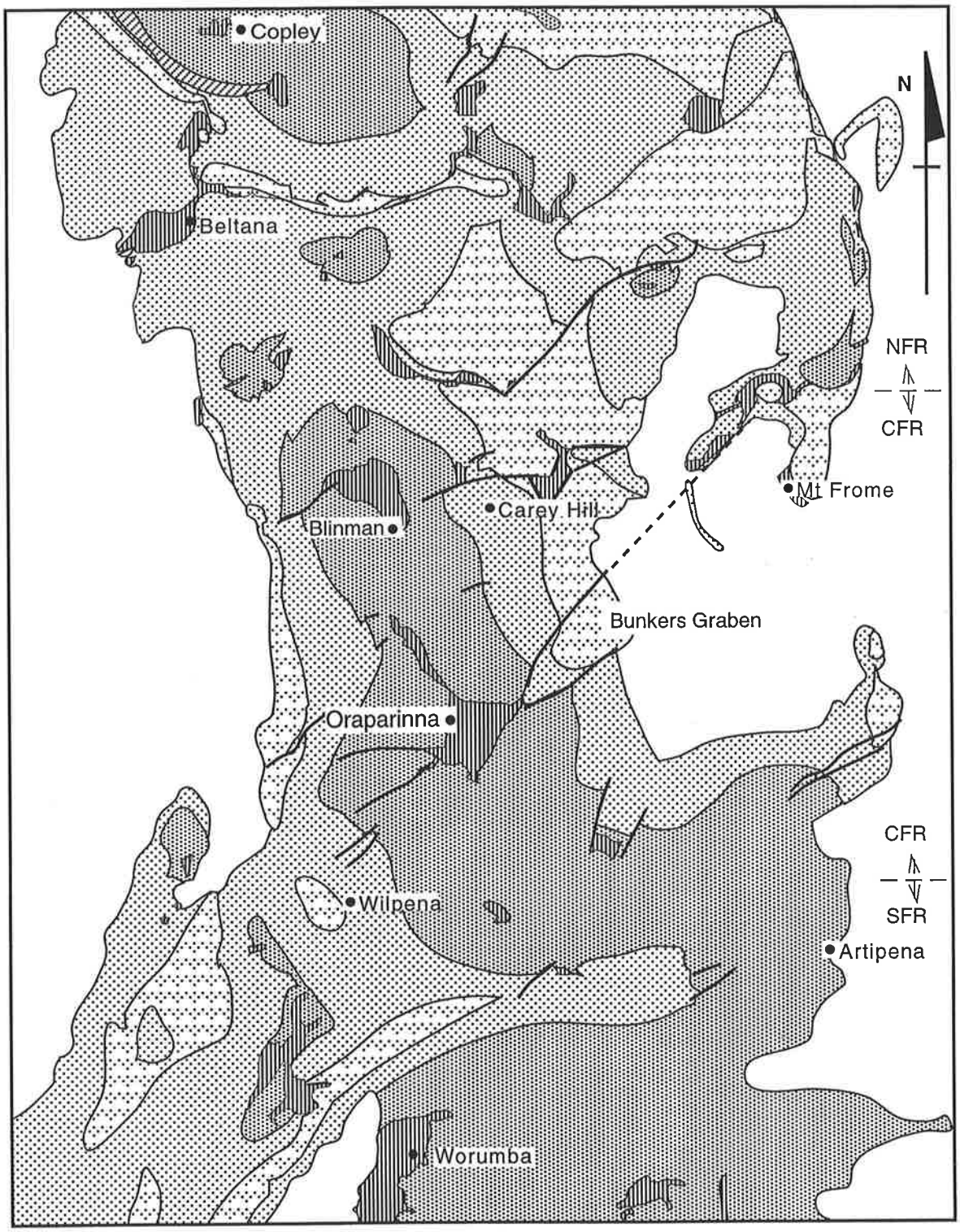

Fig. 1.2: General stratigraphy of the central Flinders Ranges (CFR) and adjacent northern Flinders Ranges (NFR) and southern Flinders Ranges (SFR). Localities of vein barite deposits at Artipena, Carey Hill and Mt Frome are also shown.

GEOLOGY FROM PARACHILNA 1:250000 SHEET.

QUAT. — Superficial deposits.

PALAEOZOIC, Cambrian — UNDIFFERENTIATED: Wilkawillina Lst. Parara Lst. Bunkers sst., Oraparinna Shale, Billy Creek Formation.

PROTEROZOIC, Adelaide System:

- RAWNSLEY QUARTZITE: White quartzite and red feldspathic sandstone.
- WONOKA FORMATION: Calcareous shale and flaggy limestone.
- BUNYEROO FORMATION: Purple and green dolomitic shale.
- A.B.C. RANGE QUARTZITE.
- Pw — BRACHINA FORMATION: Greenish grey siltstone with lenticular sandstone interbeds.
- NUCCALEENA FORMATION: Brown weathering purple dolomite.
- ELATINA FORMATION: Pink sandstone and feldspathic greywacke.
- TREZONA FORMATION: Grey shale with interbeds of purple limestone.

PROTEROZOIC, Adelaide System:

- ENORAMA SHALE: Purple weathering green shale.
- ETINA FORMATION: Sandy-limestone and grey shale.
- WOCKERAWIRRA DOLOMITE.
- Pu — TAPLEY HILL FORMATION: Blue grey laminated siltstone.
- Mount Caernarvon Greywacke Member.
- WILYERPA FORMATION: Arkosic quartzite and siltstone. Includes Holowilena Ironstone

Dolomite, dolomitic siltstone and breccias.

Fault.

TURLEY LODE — Barite Deposit.

SCALE 1:250 000

km. 5 0 5 10 km.

Fig. 1.3

	DEPARTMENT OF MINES AND ENERGY SOUTH AUSTRALIA	SCALE 1:250000
COMPILED: L. Barnes.	BARITE DEPOSITS — ORAPARINNA DIAPIR	DATE 29-5-78
DRN: G.J.T. CKD:	LOCATION & REGIONAL GEOLOGY	PLAN NUMBER S13421

526

Barite deposits predominantly occur closer to diapirs, thus barite was suggested to be genetically related to diapirs (McCallum, 1982, 1988, 1990). The deposits mainly occur as veins at several stratigraphic levels in the Neoproterozoic to Early Cambrian sedimentary host rocks. These veins vary from micro scale to 350 m or more in length and 1-3 m in width, with some portions as wide as 5 m. Compared to most barite veins elsewhere in the world, these deposits are unusual, containing only very small amounts of sulphide minerals plus minor carbonate and quartz in most of the deposits.

A total of 669,980 tonnes of barite worth $A15,428,500, was produced from the first recorded mining in 1910 up to 1998, from various deposits of the Adelaide Fold Belt (Pers. comm. J. Townsend of PIRSA). The most important known deposits are those at Oraparinna within the Bunkers Graben, currently mined by UNIMIN Australia Ltd (Fig. 1.3). The Oraparinna Mine has accounted for more than 50% of South Australia's barite production, including nearly 90% of the industrial grade barite and for many years was the largest supplier of industrial grade barite in Australia (McCallum, 1998, 1990). The major uses of barite are in mixing with circulating drilling mud to strengthen weak walls against collapsing, especially in oil wells, in the manufacture of lithopone (a white pigment used in paper manufacture), as a flux in glass manufacture, and also as a filler and extender in rubber, paint, paper, textiles, linoleum and other industrial products (McCallum, 1982).

1.2 Previous Investigations

It has been speculated that the central Flinders Ranges suffered two phases of deformation during the Delamerian Orogeny in the Cambro-Ordovician period, forming ENE and NNW trending folds that interfered to form domes and basins (Haslett, 1976; Li and Powell, 1993). Much controversy surrounds the origin of these domes and basins as was noted by Preiss (1999), "It is still uncertain whether the domes and basins formed during a single deformation or are the product of interference of two separate fold phases, since there is little tectonic foliation and no unequivocal evidence of overprinting relationships". According to Haslett (1976), the cross-fold features or interference structures localised diapirs but Lemon (1988) suggested the diapirs occur irrespective of the geological structure and thus were not controlled by the Delamerian structure.

The characters of the diapirs have been intensively recorded, in particular by Mount (1975) who favoured a syntectonic origin. To the contrary, Lemon (1988) and Dyson (1996, 1999, 2002a,b)

suggested a synsedimentary origin, which has been widely accepted by the geological community in South Australia.

Lemon (1988) modelled diapirs in the laboratory using a sandbox model, an expansion of the works of Currie (1956). The box was constructed with glass on one side and no lid. A stiff rubber membrane was laid over the bottom of the box and was pulled up slowly by a thread attached to the centre of the membrane, while evenly distributing coloured sand into the box, simulating sedimentation (Fig. 1.4). He interpreted the shapes produced by the rising membrane as three stages of diapir development, namely the Pillow, Diapir and Post-diapir Stage, comparing them with the natural salt domes of Iran (Fig. 1.5; Seni and Jackson, 1983a,b). Lemon used tension applied through the thread to create these models, mainly to show the shapes of diapirs including formation of peripheral sinks, and thickening and thinning of sequences around diapirs. The synsedimentary theory for the origin of diapirs is in agreement with many previous authors (Webb, 1960, 1961; Coats, 1973) and it was suggested that breccia was mobilised until late Delamerian phases of deformation (Preiss, 1985; Lemon, 1988).

The diapirs dominantly contain breccia clasts recognised as originating from granitic basement and lower Adelaidean sequences such as the Callanna Beds and the Burra Group (Mount, 1975; Preiss, 1987; Lemon, 1988). Therefore, it was widely believed that the Ba-rich brines, which originated from the basement were transported through the diapirs and subsequently through fractures, to meet with sea or connate water flowing downwards, eventually to form barite deposits (Robertson, 1981; McCallum, 1982, 1988, 1990; Cawley, 1983).

Cawley (1983) reported that feldspar in siltstones of the Brachina Formation near the Oraparinna deposits was enriched in barium (up to 0.6 wt %), and that adjacent to the veins the feldspar had been altered to sericite, thus releasing barium. Therefore, Cawley suggested there was additional input of Ba from the hosts. The sulphur was suggested to have been derived from Proterozoic seawater, possibly via connate water or dissolution of evaporites, (Robertson, 1981; Cawley, 1983).

There is a clear spatial relationship between diapirs and certain barite deposits, but not all the deposits of the Fold Belt occur adjacent to diapirs, e.g. the Noarlunga deposits of the southern Adelaide Fold Belt are not associated with any known diapirs. The spatial relationship with diapirs may be due to fluids taking advantage of fractures around the periphery of diapirs, and there may not necessarily be a genetic relationship in terms of fluid evolution or source of components. Therefore, even though the studies of Robertson (1981) and Cawley (1983) were essentially preliminary, the results did cast doubts on the widely held belief (e.g. McCallum, 1988, 1990) that

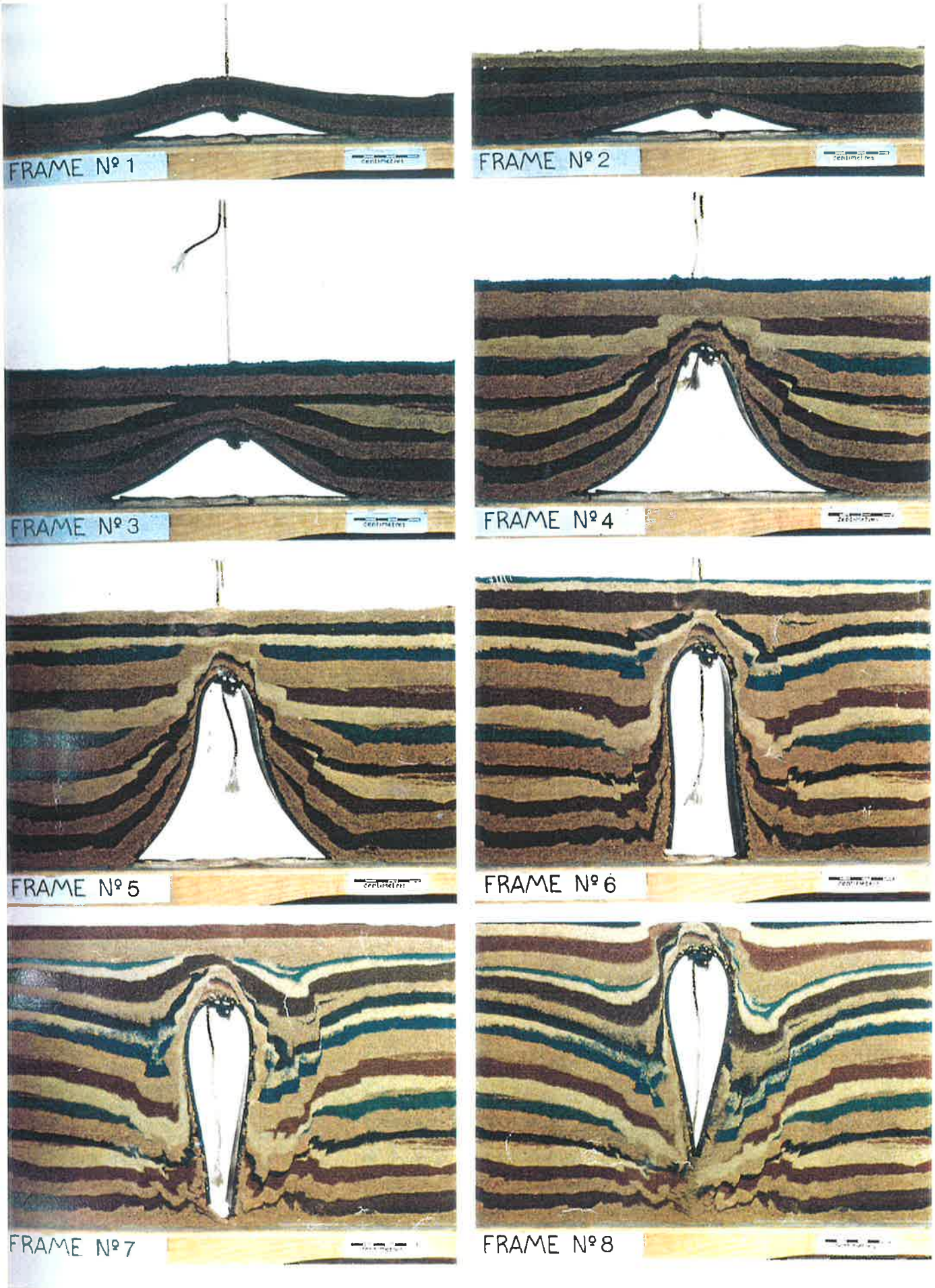

Fig. 1.4: Modelling of a synsedimentary diapir by a laboratory sandbox (after Lemon, 1988); by using tension on a thread attached to a stiff rubber membrane. Coloured sand layers denote sedimentation. Note: 'Inward dipping' peripheral sinks have developed from Frame Nos 6 to 8 during rise, due to collapse of flanks resulting from noncontinuous supply of breccia. These shapes are yet to be demonstrated in the Adelaide Fold Belt.

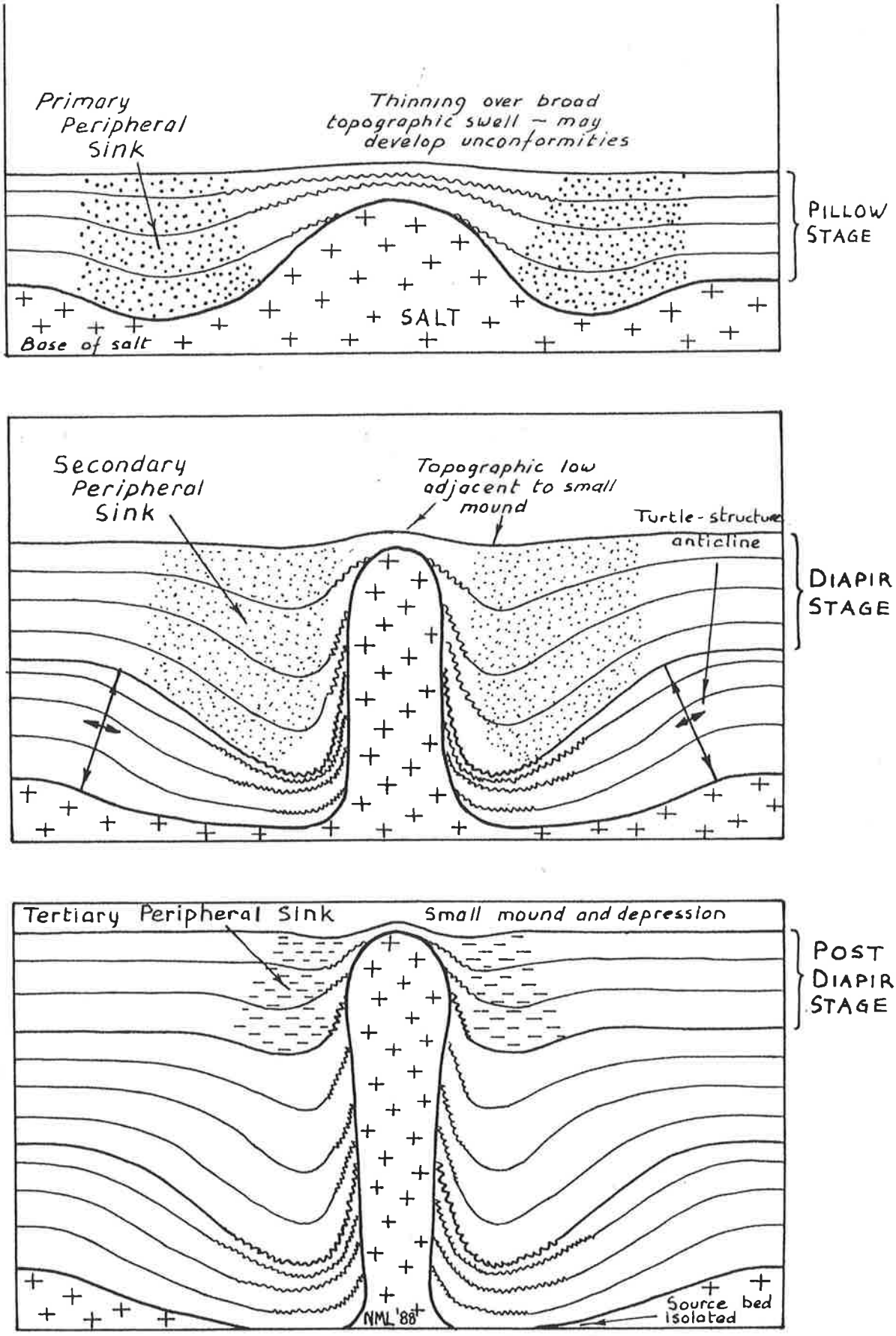

Fig. 1.5: Three stages of salt movement (after Lemon, 1988). Note: Development of 'inward dipping' primary, secondary, and tertiary peripheral sinks, based on the sandbox experiments (Fig. 1.4).

the barite veins have a direct genetic relationship with diapirs in the Adelaide Fold Belt. Resolution of this question is fundamental to exploration concepts for further high-grade deposits. Timing of vein formation has also not been previously studied; whether the veins were formed throughout multiple events during the depositional time of the sedimentary rocks, or through a simple event in the Early Cambrian. Therefore, for this thesis project, the structural geology and geochemistry of barite veins and the host rocks have been studied, together with an investigation of the relationship of veins with diapirs, and minor and major geological structures of the central Flinders Ranges with the aim of resolving these questions.

1.3 Aims and scope of investigation

An understanding of the geological structure of the Flinders Ranges is important to gain an insight into the genesis, structural and geochemical control, and timing of barite vein formation and deformation. The previously proposed supply of Ba rich brines generated from the basement and distributed through diapirs into the sediments is initially dependent upon the origin and timing of diapirs, thought to have syntectonic (Mount, 1975; Haslett, 1976; White, 1983) or synsedimentary (Webb, 1960, 1961; Coats, 1973; Lemon. 1988; Dyson, 1992, 1996, 2002a,b) origins. Even though some authors preferred a structural control of diapirs (Mount, 1975; Haslett, 1976), Lemon (1988) counter-argued that diapirs are synsedimentary structures not controlled by the structure. Therefore, the structure of the central Flinders Ranges, including the problem of origin of diapirs, was studied in an attempt to explain the deformational history of the Ranges. The study includes major and minor structures and their relationship to diapirs, grabens, and barite veins. The main fieldwork phase consisted of mapping and data collection of the geological structures associated with the Oraparinna barite deposits and elsewhere in the central Flinders Ranges.

Initially, it was considered necessary to make a preliminary examination of many barite occurrences in the Adelaide Fold Belt in order to select a smaller number of representative deposits for detailed geological study. The Oraparinna Barite Mine and other barite vein deposits around the Oraparinna Diapir, viz. the Dunbar (also known as Linke's), Hall, Bowering and Turley Lodes were chosen for study (Fig. 1.3). Other deposits such as McRae (Fig. 1.3) and Artipena (42 km SE of the Oraparinna Diapir) and Noarlunga (Fig. 1.1) were selected to include a range of geological environments and stratigraphic levels. Results were compared with the previous work of Robertson (1981) and Cawley (1983).

Techniques used in the study were:

(a) Review of the general geological structure of the central Flinders Ranges, using available maps and data. A variety of geological structures was mapped across the Ranges in order to produce a balanced cross section across the major Enorama Diapir.

(b) Mapping to determine the relationship between veins and associated minor structures of the host rocks, and the relationship of these to the major structures.

(c) Vein orientation and morphology was studied at a variety of scales in order to understand the mechanism of vein formation.

(d) Whole rock analyses were made of host rocks adjacent to barite veins.

(e) Electron microprobe analyses were performed of mineral phases in the veins and wall-rock alteration zones, i.e. barite, feldspar and sheet silicates.

(f) Strontium isotope analyses of barite veins were undertaken to provide information on the source of the hydrothermal fluids.

(g) Sulphur isotope analyses of barite were undertaken to investigate the sulphur source.

(h) Fluid inclusions in barite and associated quartz were investigated, to provide data on composition and temperature of the fluids.

Chapter 2

GEOLOGICAL AND STRUCTURAL SETTING

2.1 The Adelaide Fold Belt

Many previous workers have studied the structural evolution of the southern Adelaide Fold Belt and the Nackara Arc in detail (Fig 1.1; Jenkins, 1990; Mancktelow, 1990; Flottmann *et al.*, 1994; Marshak and Flottmann, 1996; Flottmann and James, 1997; Yassaghi, 1998; Yassaghi *et al.*, 2000). Deformation of the Fold Belt has involved the basement, which is now exposed as a series of inliers in the north (the Mount Painter and Mount Babbage Inliers), in the east (the Willyama Inliers), and in the south (the Houghton and Myponga Inliers). Elsewhere the deformation has detached the cover sequences from the underlying basement (e.g. the Nackara Arc in the southern Flinders Ranges; Sandiford *et al.*, 1998).

In map view, the Fold Belt between Kangaroo Island in the south and the MacDonald Fault Zone in the NE resembles an upright letter 'S' shape (Coney *et al.*, 1990; Fig. 1.1), the origin of which has been argued as resulting from lateral variations in basin geometry (Daily *et al.*, 1973), a NW-trending strike-slip sinistral shear couple (Coward, 1976), or shearing between two EW trending dextral strike-slip faults (Crawford and Campbel, 1973; Clarke and Powell, 1989). The Fleurieu Arc was suggested to be due to decompression against a curved cratonic margin (Mancktelow, 1981, 1990). After detailed structural analysis including fold and fault geometry, fabric orientation and style and kinematic indicators of sections across the Fold Belt, Marshak and Flottmann (1996) suggested that in the Nackara Arc, the fold belt consists of open detachment folds that probably formed above an evaporite-hosted décollement, whereas in the Fleurieu Arc the belt consists of an imbricate fan (Boyer and Elliot, 1982) of basement-involved thrusts. These authors further suggested the curvature of the Fleurieu Arc reflects oroclinal rotation of the early formed thrust sheets of the fold-thrust belt when it impinged on the southeastern corner of the Gawler Craton, while the curvature of the Nackara Arc reflects the control of basin stratigraphy on the width of a fold-thrust belt.

In the southern Adelaide Fold-Thrust Belt, basement-involved and detached deformation was observed within an imbricate zone with overall shortening in the order of 50%, and with the majority of strain localised at the base of the sedimentary package (Flottmann *et al.*, 1994; Yassaghi, 1998). In contrast, the northern Flinders Ranges show shortening of only about 10 - 20%, and are strongly influenced by thick skinned, basement-involved deformation which is largely coupled with

the overlying Neoproterozoic and Cambrian cover (Paul *et al.,* 1999). The main structural characteristics here are open, mainly south-verging folds resulting from southward tectonic transportation, involved with intracratonic basin inversion associated with pop-up geometries formed between steeply dipping reverse faults (Paul *et al.,* 1999). In contrast, the central and southern Flinders Ranges have shortened by <5% and between 10 – 20%, respectively (Marshak and Flottmann, 1996; Paul *et al.,* 1999). Thin-skinned tectonics for the southern Adelaide Fold Belt and Nackara Arc, and thick-skin tectonics for the Flinders Ranges were suggested by Flottmann and James (1997).

Dalgarno and Johnson (1966) mapped broad, open, dome and basin-shaped folds without regional cleavage on the Parachilna Sheet (Map 1). No refolded folds or overprinted tectonic foliation were observed, thus they were uncertain whether the domes and basins were formed in a single folding event or were due to two interfering phases. In a detailed study of the eastern part of the northern Flinders Ranges, Richert (1976) reported two phases of folding. The first phase constitutes isolated folds with steep fold axes, varying in plunge from NE to SE. Richert (1976) used the observations of two phases of folding to reinterpret the tectonic sketches given in the Parachilna Sheet mapped by Dalgarno and Johnson (1966) and the Copley Sheet by Coats (1973), and speculated that the two sets of folds shown on these maps produced typical interference patterns. Two phases of deformation of the central Flinders Ranges were further supported by Li and Powell (1993), based on palaeomagnetic data from mid-Cambrian rocks. These authors suggested that, after bedding rotation during formation of the regional NNW- trending folds in the central Flinders Ranges, there was a younger phase of NNW-SSE directed tectonic shortening during the Delamerian Orogeny. Preiss (1987) suggested these two trends of folds in the central Flinders Ranges are approximately perpendicular to each other and produced the domes and basins. In the northern Flinders Ranges, these folds have been deformed and rotated producing interference patterns by a second phase of folding, plunging shallowly to the east, during the southward tectonic transportation of Paul *et al.,* (1999).

Preiss (1995) tabulated informal nomenclatures used by many previous workers for the deformation phases (D_1, D_2) of the Delamerian (***D***) Orogeny, which affected the whole Adelaide Fold Belt. The ***D***D_1 (? late Cambrian) first phase of deformation formed recumbent folds and décollements in the Callanna Group developed from bedding parallel detachment in the central Flinders Ranges. The ***D***D_{2a} (? earliest Ordovician) followed next forming upright, open, concentric folds with NNW - SSE trending axes. The ***D***D_{2b} (early Ordovician) followed, forming upright, open, concentric cross-folds with ENE - WSW trending axes and similarly oriented cross-faults. No folding phases were observed in ***D***D_3 (? Ordovician), but possible ENE – WSW trending

wrench faults linking diapirs were postulated. Preiss (1995) summarised that the D_{2a} folds interfered with D_{2b} folds to produce the dome and basin style folds of the central Flinders Ranges. The deformation phases D_{2a} and D_{2b}, are discussed in detail in this thesis, but for easy identification, these phases are here denoted as D_1 and D_2, respectively. Following Richart (1976); Li and Powell (1993) and Preiss (1995), it is considered the D_1 phase of deformation that formed NNW-SSE trending folds in the central Flinders Ranges, predated the D_2 phase of deformation that formed ENE-WSW trending folds. This interpretation is further discussed in this thesis.

2.2 The central Flinders Ranges

The central Flinders Ranges contain a continuous sequence of Neoproterozoic Adelaidean sediments, unconformably overlain by Cambrian and finally by Cainozoic sediments. The regional geology of the Adelaidean, including the central Flinders Ranges, is well documented in Bulletins 53 and 54 of the South Australian Department of Mines and Energy (Preiss, 1987, 1995), and is summarised in the 1:250,000 Parachilna Sheet geological map by Dalgarno and Johnson (1966), revised by Reid and Preiss (1999).

The continuous stratigraphic sequence of the central Flinders Ranges is exposed from the lowest beds of the Pualco Tillite, on the eastern margin of a N-S trending fault at the southern end of the Oraparinna Diapir (Map 2, Fig. 2.1). The Tillite is a blue-grey gritty siltstone, exposed for about 1 km in length along the fault, and is less than 50 m in width. The Tillite is thrust up over the younger Holowilena Ironstone on the western margin of the fault. The fault dies out towards the south, exposing the Holowilena Ironstone on both sides of the fault. The Ironstone is a dark, thinly laminated, iron-rich siltstone and is further exposed on the eastern flanks between the Enorama and Oraparinna Diapirs, where it dips 75° towards the NE (Fig. 2.1).

The next overlying unit is the green siltstone of the Wilyerpa Formation, which occupies both the western and eastern flanks of the Oraparinna Diapir, and also lies on the eastern flank between the two diapirs. On the western flank, the Wilyerpa Formation dips moderately, 50° - 55° SW, but on the eastern flank it dips steeply to moderately (80° – 60°), and is overturned adjacent to the southeastern flank of the Oraparinna Diapir. Within 600 m from the margins of the diapir, the overturning gradually changes from 80° NW to 80° SE, towards the upper boundary of the formation.

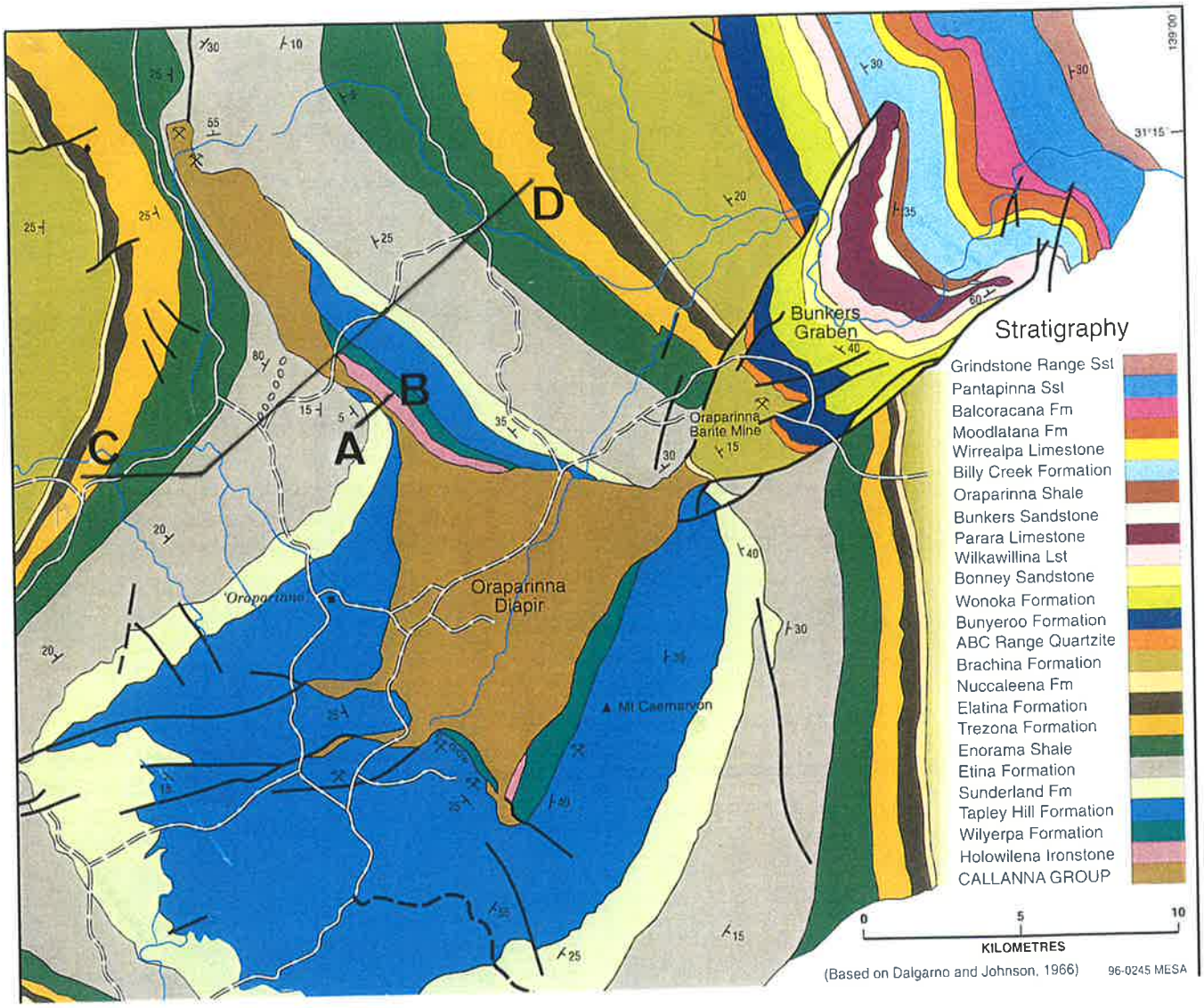

Fig. 2.1: Geology around the Oraparinna and Enorama Diapirs (after Dyson, 1996). The narrow NW-trending diapir to the NW of the Oraparinna diapir is the Enorama Diapir. Geological sections, AB (Fig. 3.1) and CD (Fig. 3.8a).

Next in the sequence is the Tapley Hill Formation, a finely laminated grey-green siltstone. It occurs all around the Oraparinna Diapir and between the two diapirs as well. The Formation dips 10° - 40° W on the western flank of the diapir, 25° - 60° SE on the southeastern flank, and 45° NE between the two diapirs. Overlying this is the Sunderland Formation, a calcareous siltstone that dips 15° - 30° westerly on the western flank and 35° - 45° easterly on the eastern flanks of the Oraparinna and Enorama Diapirs. Oolitic and stromatolitic limestone of the Etina Formation follows next and dips 17° - 20° and 17° - 30° in westerly and easterly directions, respectively on the western and eastern flanks.

The grey-green, laminated Enorama Shale, greenish grey shale of the Trezona Formation and red brown arkosic sandstone of the Elatina Formation are next in sequence. The dips on the eastern flanks of the diapirs are steep or overturned adjacent to the margins and decrease to gentle, away from the diapir, but dips on the western flank change from moderate to gentle. The Neoproterozoic sediments from the Pualco Tillite to the Elatina Formation are from Sturtian to Marinoan age and belong to the Umberatana Group (Map 1). Overlying these is a sequence from the Nuccaleena Formation up to the Rawnsley Quartzite of the Wilpena Group.

The sediments from the Neoproterozoic to Cambrian continue around the Enorama – Oraparinna Diapirs, but none of the Umberatana Group sediments occur in the Bunkers Graben on the eastern flank of the Oraparinna Diapir (Map 2). The lowest stratigrapic unit in the graben is the Nuccaleena Formation that is exposed on the apex, on the northeastern edge of the Oraparinna Diapir (Fig. 2.1). The Nuccaleena Formation is a fine-grained, competent, laminated dolomicrite, with thickness varying from 2 to 5 m and is used as a marker bed in the Adelaide Fold Belt, due to its wide geographic spread. The Nuccaleena Formation dips 10° - 25° outwards around the Enorama and Oraparinna Diapirs, but is nearly vertical within the Bunkers Graben, adjacent to the apex.

The Brachina Formation of grey-green siltstones, which hosts the Oraparinna barite deposits, lies next in the sequence, and dips at between 15° to 45° around the diapirs, but the dip gradually decreases from 80° to 40° from the lower boundary to the upper boundary, within the graben (Map 1). The cross-bedded ABC Range Quartzite is the next unit and is followed by the brick-red shale of the Bunyeroo Formation, the carbonate siliciclastic sequence of the Wonoka Formation, the red silty Bonney Sandstone and the white cross-bedded Rawnsley Quartzite, which continue both within and outside of the graben.

The Adelaidean in the central Flinders Ranges consists of the Neoproterozoic Paulco Tillite to the Rawnsley Quartzite. The sediments from the Nuccaleena Formation to the Rawnsley Quartzite are of Marinoan age, and belong to the Wilpena Group. The Cambrian sequence of silty, sandy and calcareous lithologies overlies the Neoproterozoic sequence and occurs in both the Bunkers Graben and elsewhere in the Flinders Ranges.

2.3 Diapirs

Large bodies of carbonate-cemented breccia are common in the Flinders Ranges and rare in the southern Adelaide Fold Belt. They were originally regarded as "complex crush zones" (Parkin *et al.*, 1953) or "plug upthrusts" (Sprigg, 1952) and were first interpreted as diapirs by Webb (1960, 1961). The breccias include massive to flow banded, pink to buff, carbonate-cemented, angular to rounded clasts, with a wide range of sizes from sand to boulder. Xenoclasts up to 3 km long, most of which are grey micaceous siltstone and fine-grained sandstone with interbeds of heavy-mineral cross-bedded sandstone and micaceous shale, have been reported from the Blinman Diapir (Coats, 1964a). The diapiric clasts generally consist of dolomite, siltstone, micaceous sandstone as well as dolerite and basalt. Breccia in the diapirs is known to have been derived largely from the evaporitic clastic and carbonate sediments of the Callanna Group (Coats, 1964a; Mount, 1975; Preiss, 1985; Lemon, 1988). However, in the Beltana Diapir (Leeson, 1970), xenoclasts of crystalline basement rocks (granite, amphibolite), Neoproterozoic sediments from the Callanna and Burra Groups, as well as fossiliferous Cambrian limestone, are also present (Preiss, 1987). Despite the known difficulties of identifying source rocks of diapiric breccia, Mount (1975) and Preiss (1985) at the Arkaba and Worumba Anticlines, respectively, noted that in addition to the deep-seated Adelaidean and the intrusive volcanic fragments, the diapirs carry breccia largely derived from the Callanna Beds and stratigraphically up to and including the Cambrian formations. The diapir-rocks are always structurally, metamorphically, and stratigraphically incompatible with adjacent host-rocks (Mount, 1975).

Mount (1975) suggested the diapirs or breccia plugs were essentially mud flows emplaced, at least in part, syn-tectonically related to thrusting during a late, tensional phase of the Delamerian Orogeny. This view was supported by White (1983), who suggested the diapirs intruded under very high pressure, due to the appearance of clastic breccia pipes containing a jumble of xenoliths from all levels of crust through which they have passed. White (1983) noted that breccia indiscriminately intruded, brecciated and stoped all formations in the Adelaidean sequence up to the middle

Cambrian, with emplacement into structurally controlled zones and was syntectonic with the Delamerian Orogeny. Therefore, both Mount (1975) and White (1983) proposed a tectonic origin for diapirs as later piercement of breccia into the Adelaidean.

In contrast, Lemon (1988) modelled the Flinders Ranges diapirs in the laboratory and interpreted a synsedimentary origin (Chapter 1).

2.3.1 The Enorama and Oraparinna Diapirs

The Enorama Diapir and the Oraparinna Diapir trend between NW and NNW, and are connected by a narrow strip of breccia (Maps, 1,2; Fig. 2.1). Both the northern end of the Enorama Diapir and the southern end of the Oraparinna Diapir are overlain by NW-NNW trending and gently folded Neoproterozoic sequences (Dalgarno and Johnson, 1966).

Unconformable breccia flows including boulder beds have been reported from more than eight locations along the western flank of the Enorama Diapir (Dalgarno and Johnson, 1968). The authors observed that individual units grade from cross-bedded, sandy, oolitic limestone to pebbly sandstone and finally to boulder conglomerate where they are in contact with the diapir. Most of such occurrences emanating from the Enorama Diapir commonly occur for about 200 m but no more than 500 m. Further, Lemon (1988) reported occurrences of breccia between the boundaries of the Umberatana and Wilpena Groups, more than 5 km east of the Enorama Diapir as well. Lemon (1988) assumed that all these breccia on the flanks of diapirs occurred as erosional features formed during non-depositional times. According to Lemon, here was also cannibalisation of diapiric debris from the top of the diapir-structures onto the surrounding sediments, during pulses of differential loading (Figs. 2.2, 2.3). Lemon suggested the discharged diapiric debris was then carried away along the seabed by the action of waves, forming tongues of sediments grading from coarse to fine away from the diapir and further causing temporal changes in composition of surrounding sediments. However, these suggestions were not confirmed by studies on breccia movement directions. According to Lemon, mud breccia movement was aided by limited salt occurrences, similar to salt tectonics, as the governing force for the formation of these breccia plugs (Fig. 1.5).

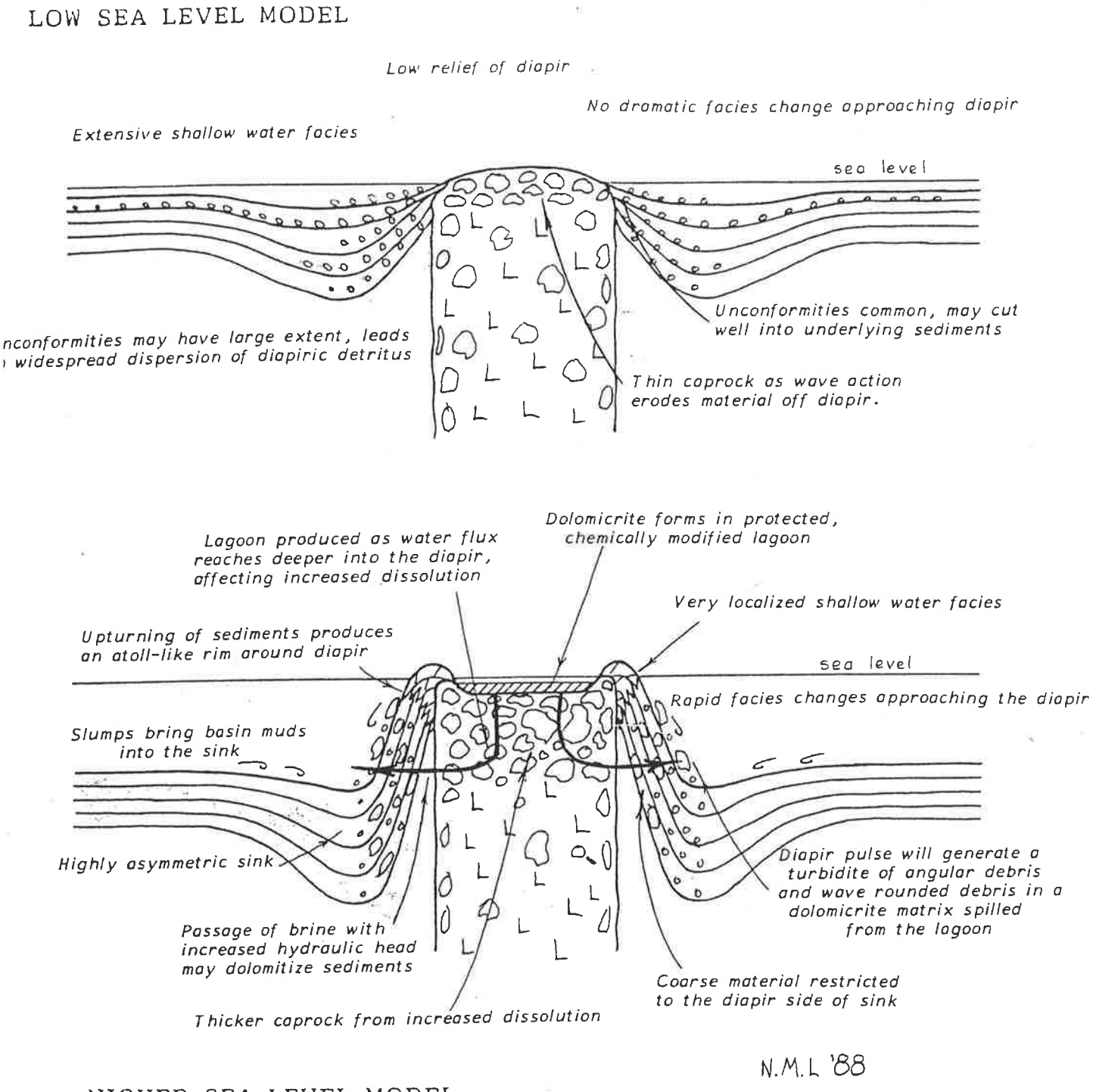

Fig. 2.2: Models for exposed diapirs (after Lemon, 1988). Note: Troughs of peripheral sinks are likely to have collected largest debris like boulders that spilled from the rising diapir.

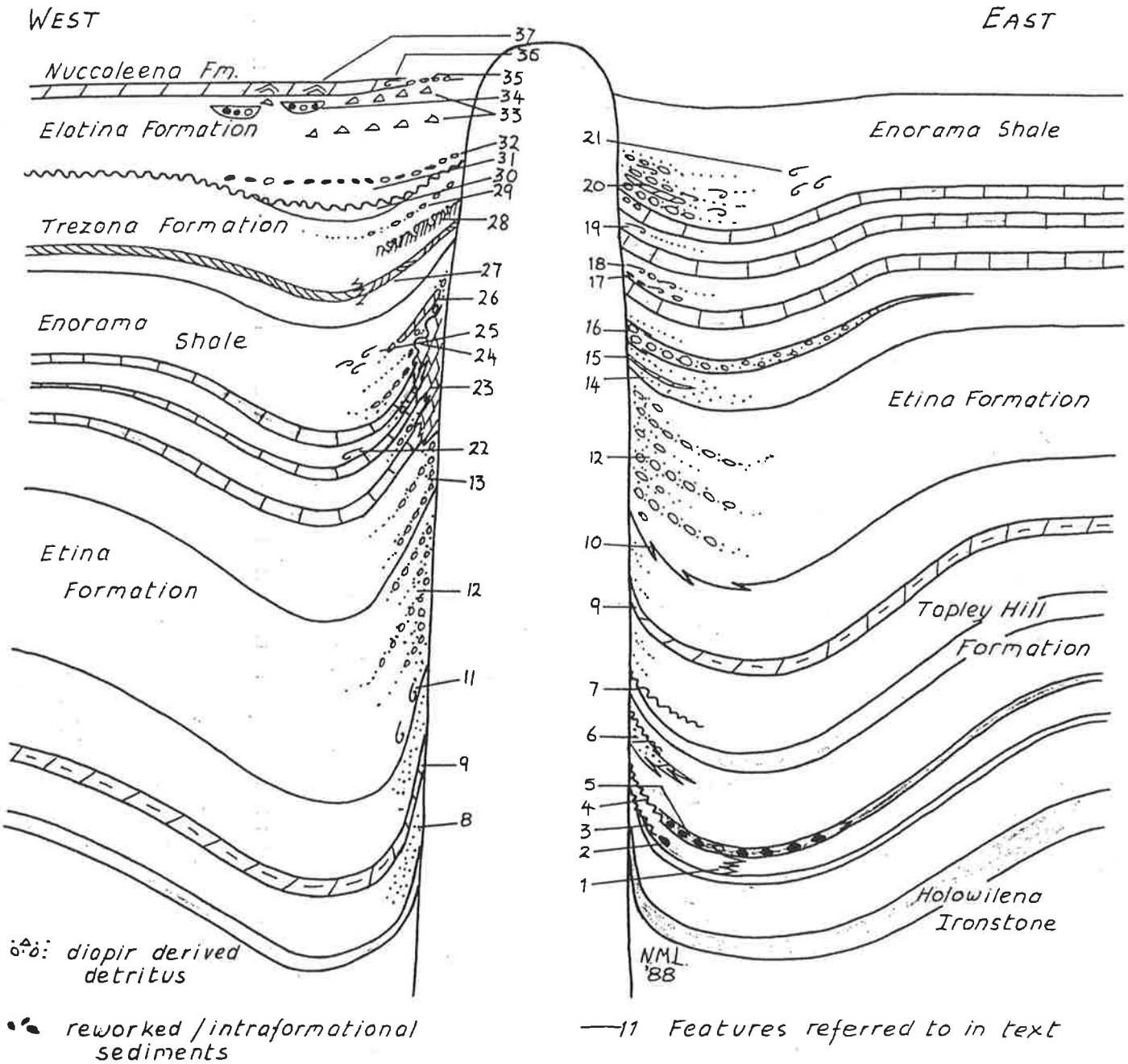

Fig, 2.3: Enorama Diapir; a summary of the influence on surrounding sediments (after Lemon, 1988). Note the occurrence of 'inward dipping' peripheral sinks on both sides of the diapir.

2.3.2 The Moralana Diapir

The Moralana Diapir in the west of the central Flinders Ranges is hosted by a continuous series of sequences from Warcowie Dolomite to Brachina Formation (Fig. 2.4). Dyson (1992, 1996) interpreted olistostromes and large-scale submarine channels and also breccia occurrences between boundaries of host sequences in the Umberatana and overlying Wilpena Groups around the Moralana Diapir, which were interpreted as having been derived from the diapir during erosion (cf. Lemon, 1988). Dyson (1992, 1996, 1997, 1998, 1999, 2002a,b) suggested the diapir formation was based on salt tectonics initiated by regional extensional events during passive margin developments of the Adelaide Geosyncline, following break-up of the Neoproterozoic super-continent. He agreed with the proposal of Lemon (1988) and many previous authors for a syndepostional origin for the diapirs.

2.3.3 The Bunkers Graben

The Bunkers Graben is the only significant graben in the Flinders Ranges (Maps 1 & 2; Figs. 1.2, 2.1). The graben is bounded by two major boundary faults, trending in a northeastly direction. The southwestern ends of the faults converge towards an apex in the Oraparinna Diapir and, according to Dalgarno and Johnson (1968), the northeastern ends extend to about 50 km along nearly parallel faults. The sequences inside the graben continue in the same order as outside, but are variably offset along the boundary faults and many other faults parallel to them within the graben. Along the northeastern boundary fault, the sequences offset both northeasterly and southwesterly, respectively adjacent to the open end and apex. This has been considered unexplainable by a single event (Lemon, 1988). The formations within the graben are highly faulted, and show uneven and irregular thicknesses, compared to those outside. The Wonoka Formation and some of the Cambrian formations (viz. the shaley limestone of the Mernmerna Formation or the Parara Limestone, the Bunkers Sandstone, the Oraparinna Shale, and the thin limestone banded siltstone and shale of the Balcoracana Formation) show increased thicknesses within the graben, compared to those outside (Map 2; Fig. 2.1). In contrast to this, some of the competent formations such as the ABC Range Quartzite, Bunyeroo Formation, Bonny Sandstone and Rawnsley Quartzite show no change of thicknesses either within or outside the graben. The lower boundary of the Brachina Formation dips 80° NE near its base but this gradually decreases to 45° NE over approximate 3 km of lateral thickness towards its upper boundary. Therefore, it is difficult to estimate the true thickness of the Brachina Formations without detailed geological mapping.

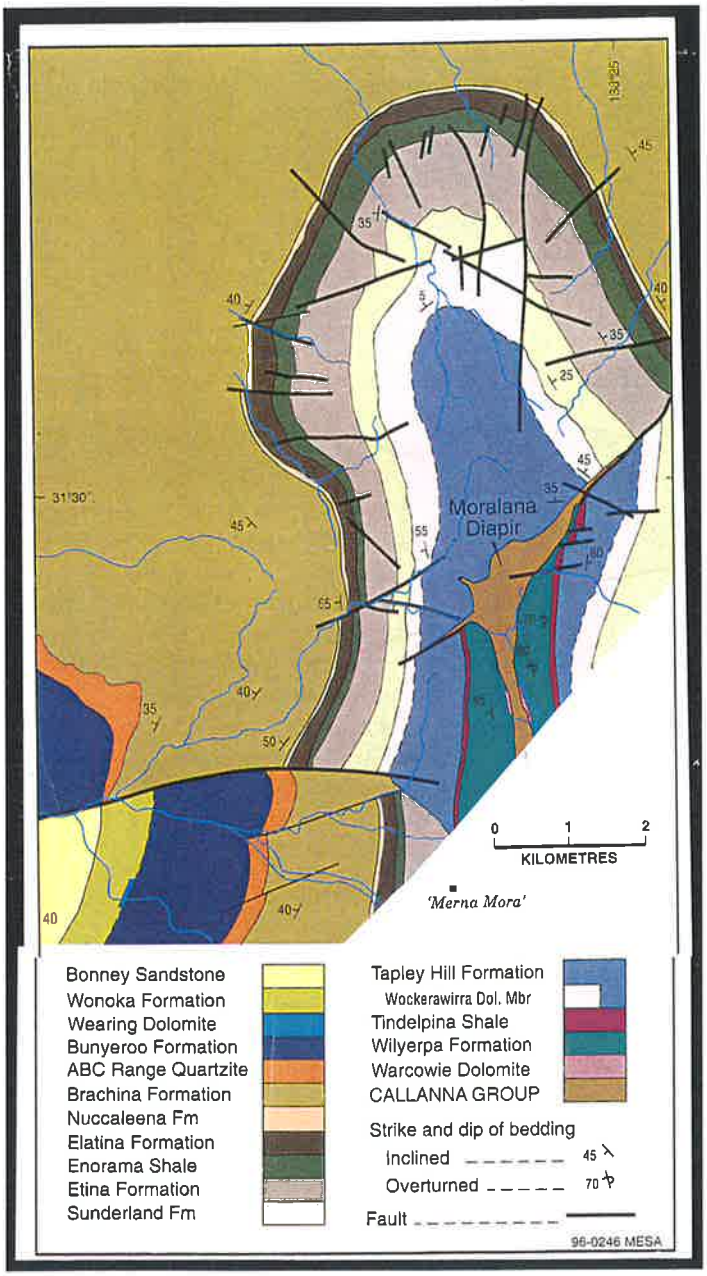

Fig. 2.4: Geology of the Moralana Anticline (after Dyson, 1996). Note the occurrence of the Moralana Diapir along the hinge zone of the southern part of the anticline that has been uplifted against its northern part, along a NE trending fault.

2.4 The Oraparinna Barite Mine and adjacent barite lodes

The Oraparinna Mine is hosted by the Brachina Formation, which generally strikes EW and dips gently to moderately to the north, in the mine. The mine is currently working and has been deepened to the 9th level underground. Several other worked out lodes occur in the vicinity of the Oraparinna Mine, namely the Belsen Lode, Western Lodes, Bainbridge Lodes and Roberts Lode (Fig. 2.5). Except from the Belsen Lode, which is hosted by the Bunyeroo Formation, the Brachina Formation hosts all the other lodes. The host rocks are complexly folded, faulted and sheared (McCallum, 1982). A major fault zone tens of kilometres long and about 50 m thick lies to the south of these lodes. The fault zone strikes between NE and ENE, and dips moderately to steeply to the NW and has displaced the sequences for more than 1.6 km of surface offset (McCallum, 1982).

The barite lodes in these vein complexes generally strike between NW and east and dips vary from gentle to steep, where most of the veins shear off along keels parallel to bedding as well as on numerous faults (Broadhurst, 1946, 1968; Gibson, 1957; Hiern and Olliver, 1973; Forsyth, 1978; McCallum, 1982).

2.5 Artipena Lodes

Geological sequences from the Wilyerpa Formation to the Brachina Formation continue in the Artipena area and are partly covered by the Quaternary alluvium (Fig. 2.6; Robertson, 1981; Barnes and Robertson, 1983, 1985). The Neoproterozoic is folded into a major syncline, formed during the latter part of the Delamerian deformation in the Cambro – Ordovician, approximately between 480 – 500 Ma ago. The syncline is tens of kilometres in wavelength, gently plunging towards ENE and is offset by major faults trending between north and NNE. Some of these faults extend for more than 10 km and act as host for most of the major barite veins (Lode nos. 1, 2, 4 and 5). The other major lode, no.3 Lode, trends ENE.

The Artipena Lodes are hosted by rocks from the lowermost Etina Formation (approx. 650 Ma) to the uppermost Brachina Formation (600 Ma). The no.2 Lode is hosted by the Etina Formation, both the nos. 3 and 4 Lodes are hosted by the Enorama Shale (approx. 640 Ma). The no.1 Lode is located along a fault between the Elatina Formation (approx. 620 Ma) and the Trezona Formation (approx. 630 Ma); and no.5 Lode is located along a fault between the uppermost Brachina

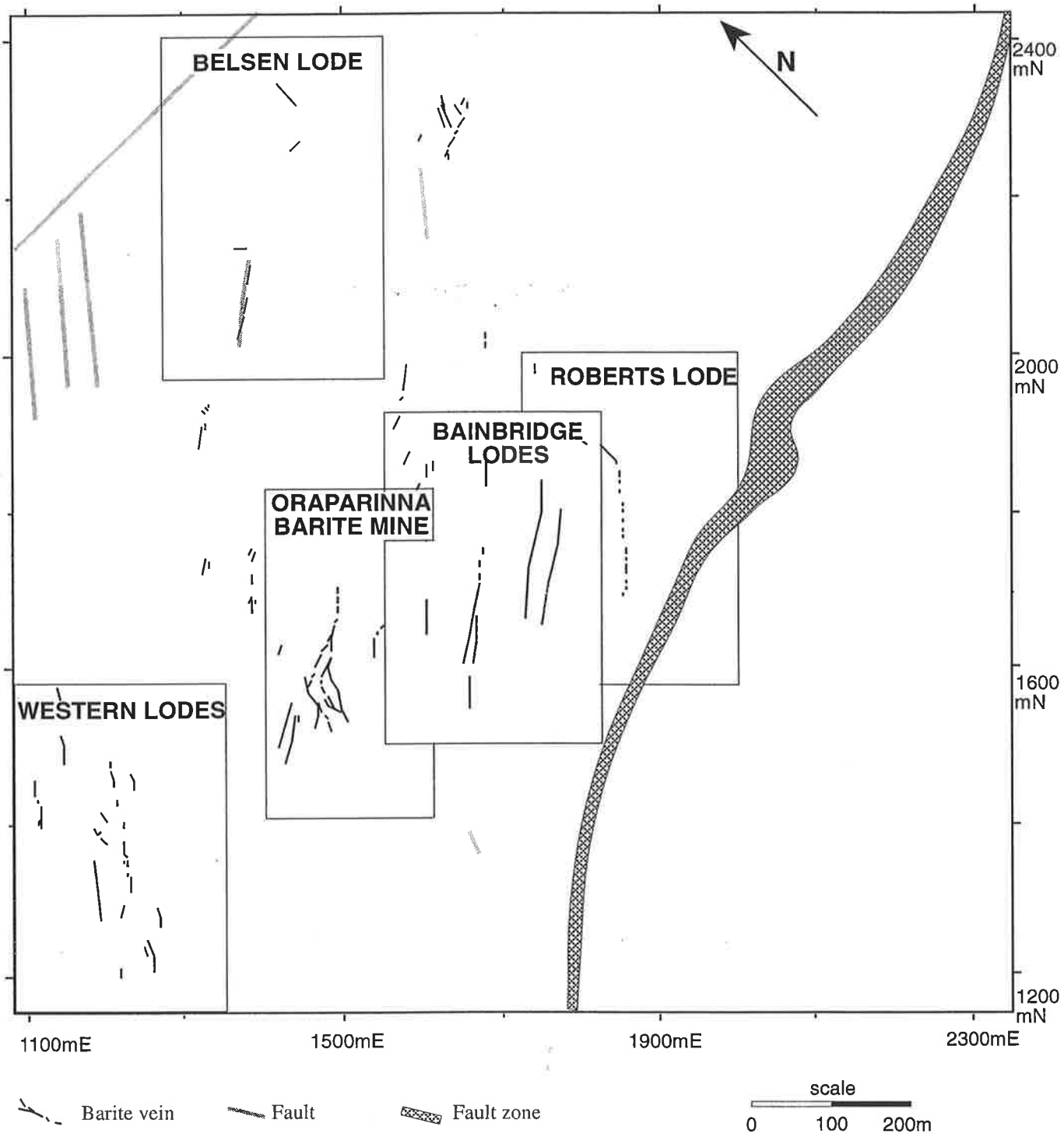

Fig. 2.5: The Oraparinna Barite Mine and adjacent barite lode systems.

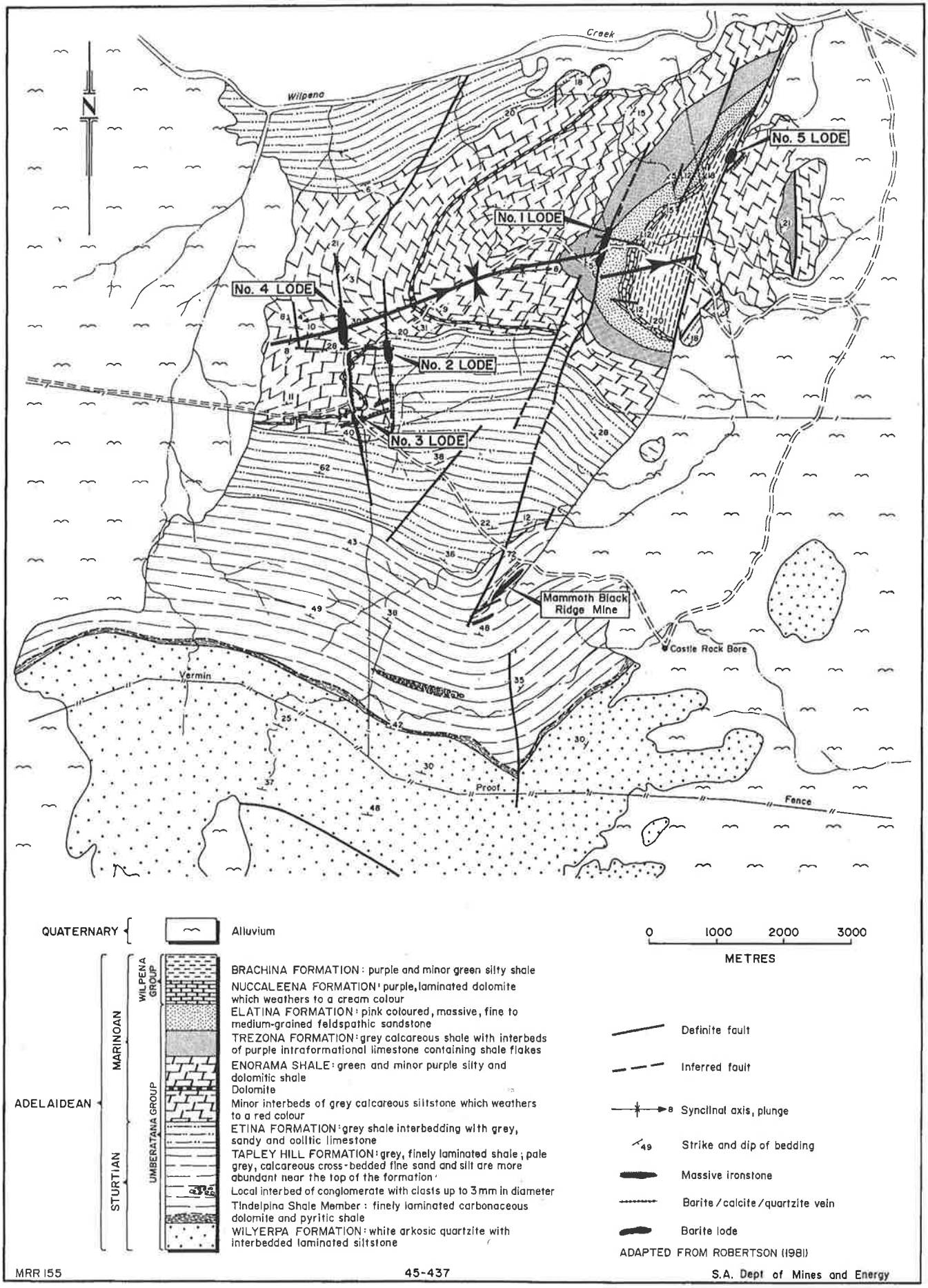

Fig. 2.6: Geological plan of the Artipena barite deposits, modified after Barnes and Robertson (1985), showing fault-controlled vein barite occurrences crosscutting Delamerian folds.

Formation and the Enorama Shale. All the lodes show some close proximity to the axial trace of the major syncline.

2.6 Noarlunga Lodes

The Noarlunga Lodes are hosted by a short continuous Neoproterozoic sequence from the Elatina Formation (approx. 620 Ma) to the Brachina Formation (approx. 600 Ma) in the southern Adelaide Fold Belt (Forbes, 1983; Fig. 2.7). The Seacliff Sandstone (approx. age 610 Ma) between these two formations is calcareous and fine-grained, and occupies the same stratigraphic position as the calcareous Nuccaleena Formation in the north (Preiss, 1987). The formations are folded into a major Delamerian syncline, oriented between NNE and NE, and gently plunging SW, in the trough of which lies the Brachina Formation. The lodes strike NE – SW and are associated with the syncline, similar to the Artipena Lodes. The Neoproterozoic is overlain by Cainozoic sediments.

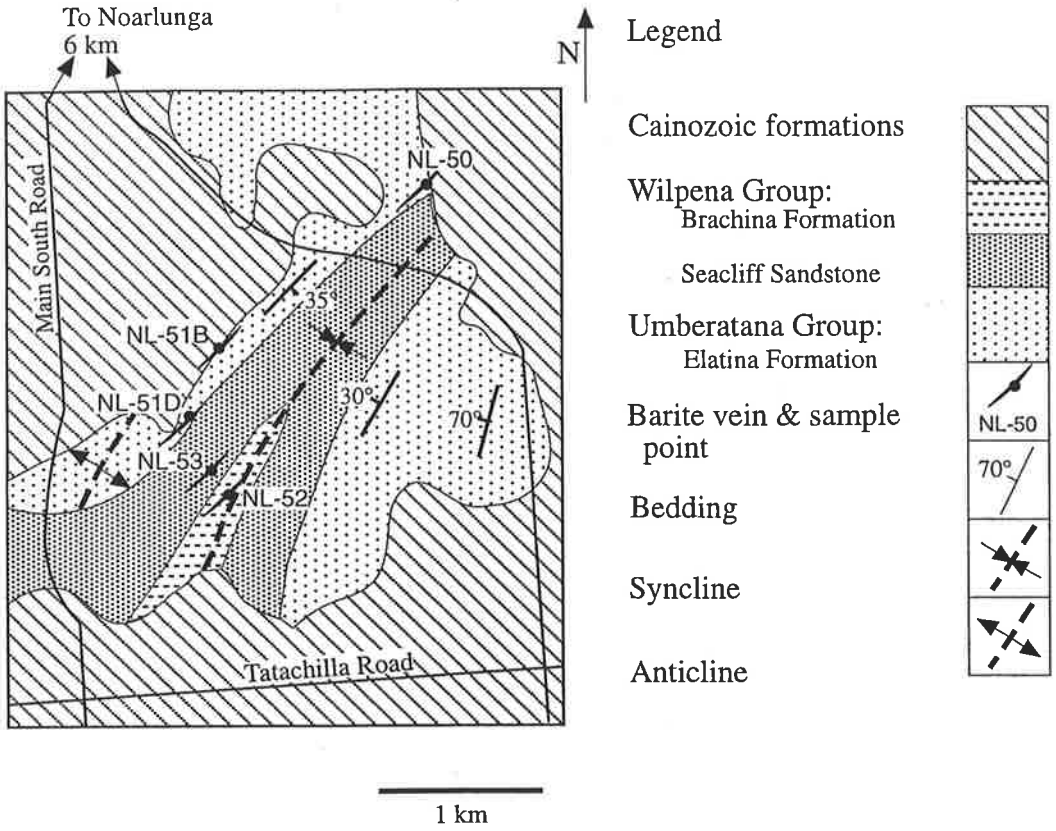

Fig. 2.7: Sample location map and general geology of the sample area at Noarlunga. Modified from the preliminary geological map, Noarlunga 1:50,000; 6627-iv & PT 6527-1, MESA (1983).

Chapter 3

MAJOR STRUCTURE OF THE CENTRAL FLINDERS RANGES

3.1 Introduction

Major geological structures in the central Flinders Ranges are the Blinman and Oraparinna Domes and the Enorama Anticline, which all include diapirs, and the Bunkers Graben (Map 1). The diapirs vary in surface extension and shape, as shown by the Blinman Diapir (12x7 km), Enorama Diapir (12x2 km), and Oraparinna Diapir (13x12 km; see attached maps in the back pocket, Map 1 of Reid and Preiss, 1999, and Map 2 of Callen and Reid, 1994).

The central Flinders Ranges have been considered to lack a fold-thrust belt structural assemblage and are treated as a completely separate structural entity from the neighbouring, northern and southern Flinders Ranges (Coward, 1976; Rutland *et al.*, 1981; Preiss, 1985, 1987; Clarke and Powell, 1989; and Marshak and Flottmann, 1996). The Nackara Arc that is bordering the central Flinders Ranges in the south was considered to have a foreland edge around the arc to coinciding with a 'blind ramp' whose strike parallels fold axes of the arc (Marshak and Flottmann, 1996). Previous authors pointed out the lack of continuation of the fold trends from the central Flinders Ranges, to both the adjoining northern Flinders Ranges and the southern Flinders Ranges that continues its fold trends to the southern Adelaide Fold Belt.

Controversy surrounds the origin of diapirs, because of the prominent occurrence of these deposits in cores of domes and their preferred manifestation along a basement fault system (Dalgarno and Johnson, 1968). Correspondingly, Richert (1976) reinterpreted the Parachilna (Dalgarno and Johnson 1966) and Copley (Coats 1973); 1:250,000 geological maps in the central Flinders Ranges and noted that it is in the cross-fold feature that the diapirs are mainly localised, suggesting the main control for the position of diapirs, or piercing structures, is a structural phenomenon. Brecciation has taken place in fault zones and fold hinges as well, and along stratiform, possibly originally evaporite bearing layers (Preiss, 1985). Lemon (1988) reassessed the occurrence of diapirs: (a) in the hinge zones of anticlines (Dalgarno and Johnson, 1966; Haslett, 1976); (b) on the limbs of anticlines (encountered during drilling of the Blinman-2 drill hole on the eastern limb of the Blinman Anticline by the Frontier Exploration, see Preiss, 1999); and (c) in the synclines (Wirrealpa Diapir). Therefore, Lemon argued that diapirs associated with anticlines, synclines and limbs of Delamerian folds predated the Cambro-Ordovician Delamerian Deformation. Lemon

interpreted the diapirs were synsedimentary structures which rose as a result of their buoyancy, similar to salt diapirs (Figs. 1.4, 1.5; Seni and Jackson, 1983a&b; Jackson *et al.*, 1990).

Even though Lemon's model has been widely accepted, a profile of a diapir in the Adelaide Fold Belt has not been documented or observed; therefore, the compatibility of Lemon's experimental shapes with diapirs in the Fold Belt remains unchallenged. Along the eastern border of the Enorama – Oraparinna Diapirs, Lemon observed a ten kilometre long thrust surface that repeated the Holowilena Ironstone including a slice of a breccia layer (Fig. 3.1). The author suggested the thrust surface was accompanied by a late phase of Delamerian Deformation, but on the contrary, thought it was not related to a thrust origin of the diapirs. These previous works suggesting syntectonic and synsedimentary origins for diapirs lead naturally into a fuller investigation of the origin of diapirs.

The Bunkers Graben was presumed to have sunk along normal faults into the northeastern crestal sequences of the Oraparinna Diapir, simultaneously with rise of the diapir (Lemon, 1988). The author further suggested that at least part of the movement occurred in the Middle Cambrian because of folding of the Cambrian sequences across the northern fault margin of the Bunkers Graben. He assumed that one simple graben-forming model could not explain why the beds from the Nuccaleena Formation to the Etina Formation within the graben are upturned along the northern margin (Maps 1, 2).

Thickening of some of the sequences within the graben as well as on the flanks of the Enorama Diapir was interpreted as deposition during rise of the diapir, which was credited to a synsedimentary process (Fig. 1.4; Lemon, 1988). Some of the rocks from the Tapley Hill Formation on the western border of the Oraparinna Diapir, to the Nuccaleena Formation on the eastern border between the Bunkers Graben, apparently have been brecciated and added into the diapir, and this remains unexplained.

The purpose of this chapter is to study the major structure of the Flinders Ranges and its likely impact on diapirs and graben formation.

3.2 Method

All the available geological and structural maps of the Flinders Ranges were reinterpreted to produce a new series of 1:625,000 scale structural maps, which have been compiled to form Figure

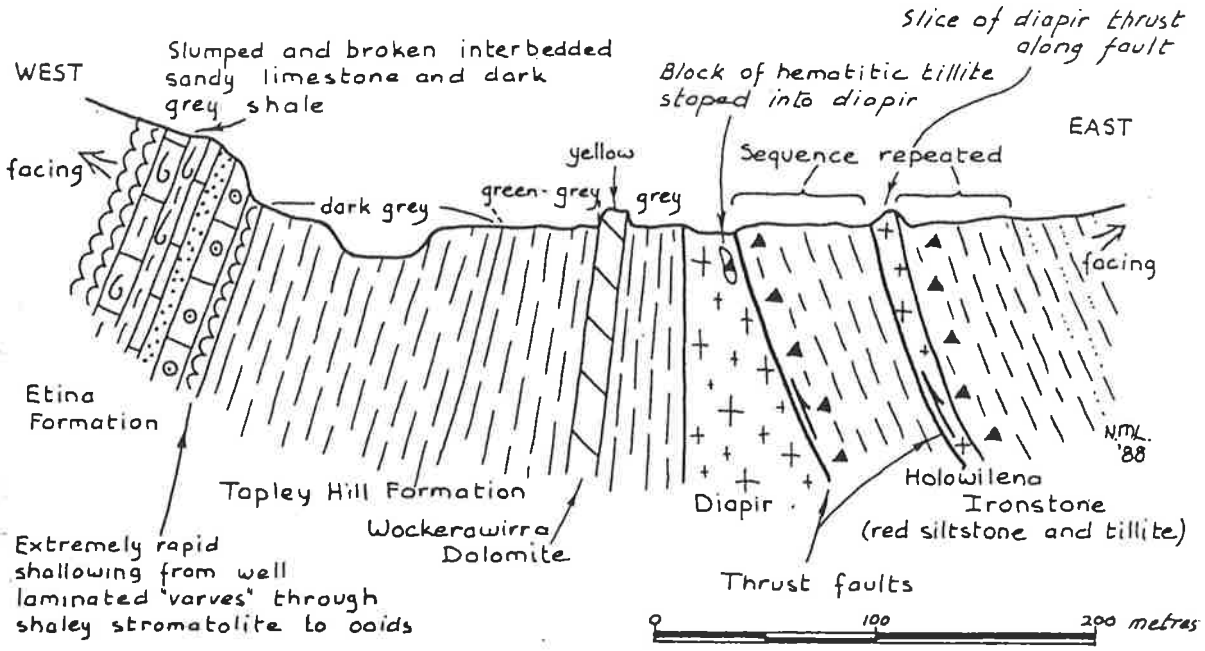

Fig. 3.1: Sketch section across Enorama – Oraparinna Diapirs (after Lemon, 1988); along AB in Figure 2.1. Note occurrence of west verging thrusts along listric thrust faults on the east of the diapir, resulting in the repetition of the Holowilena Ironstone, including a slice of diapiric breccia.

1.2. These maps include the 1:000,000 Adelaide Geosyncline (Preiss, 1983); 1:250,000 Parachilna (Dalgarno and Johnson, 1966; Reid and Preiss, 1999 i.e. Map 1) and 1:250,000 Copley (Coats, 1973) geological series; 1:75,000 Flinders Ranges National Park (Callen and Reid, 1994 i.e. Map 2), the Flinders Ranges (Hobbs *et al.,* 1976) and unpublished maps and diagrams by Mount (1975) and Lemon (1988). The maps produced were used to establish the initial relationships between folds, diapirs, faults and grabens in the Ranges. A detailed geometric profile across the major Enorama Anticline that includes the Enorama Diapir was constructed to explore the relationship between the diapir and the anticline.

3.3 Folds

Two types of major folds were identified during the study and were denoted as F_1 and F_2, and related to D_1 and D_2 deformations, respectively (Chapter 2).

3.3.1 F_1 folds

The Flinders Ranges maps reveal a series of major F_1 fold axial traces trending between NNW and NW (Fig. 3.2). A continuous anticlinal axial trace occurs through the Greenwell, Warraweena North and Beltana Anticlines in the northern Flinders Ranges and continues through the Blinman, Enorama and Oraparinna Anticlines in the central Flinders Ranges; Upalinna and Worumba Anticlines in the southern Flinders Ranges; and further into the southern Adelaide Fold Belt. Other F_1 axial traces in the southern Flinders Ranges pass through the Moralana Anticline, Mernmerna Syncline, Arkaba Anticline and Wilpena Syncline, and then disappear under the Cainozoic cover in the north. Both axial traces of the Puttapa - Angepena Hill syncline and Copley anticline of the northern Flinders Ranges are displaced along a northeasterly trending fault to the NE of Blinman and thereafter continue towards the SE and disappear under the Cainozoic cover to the NE of Wirrealpa. An additional pair of parasitic anticline and syncline axial traces is exposed at Wirrealpa, between the southeastern continuation of the Angepena Hill Syncline and the Blinman - Enorama anticlines. The F_1 axial traces in the Flinders Ranges are doubly plunging, and show near parallelism between alternating series of anticlines and synclines, similar to the pattern of corrugated cardboard. The F_1 folds suggest a dominant ENE – WSW compression, even though this varied at times.

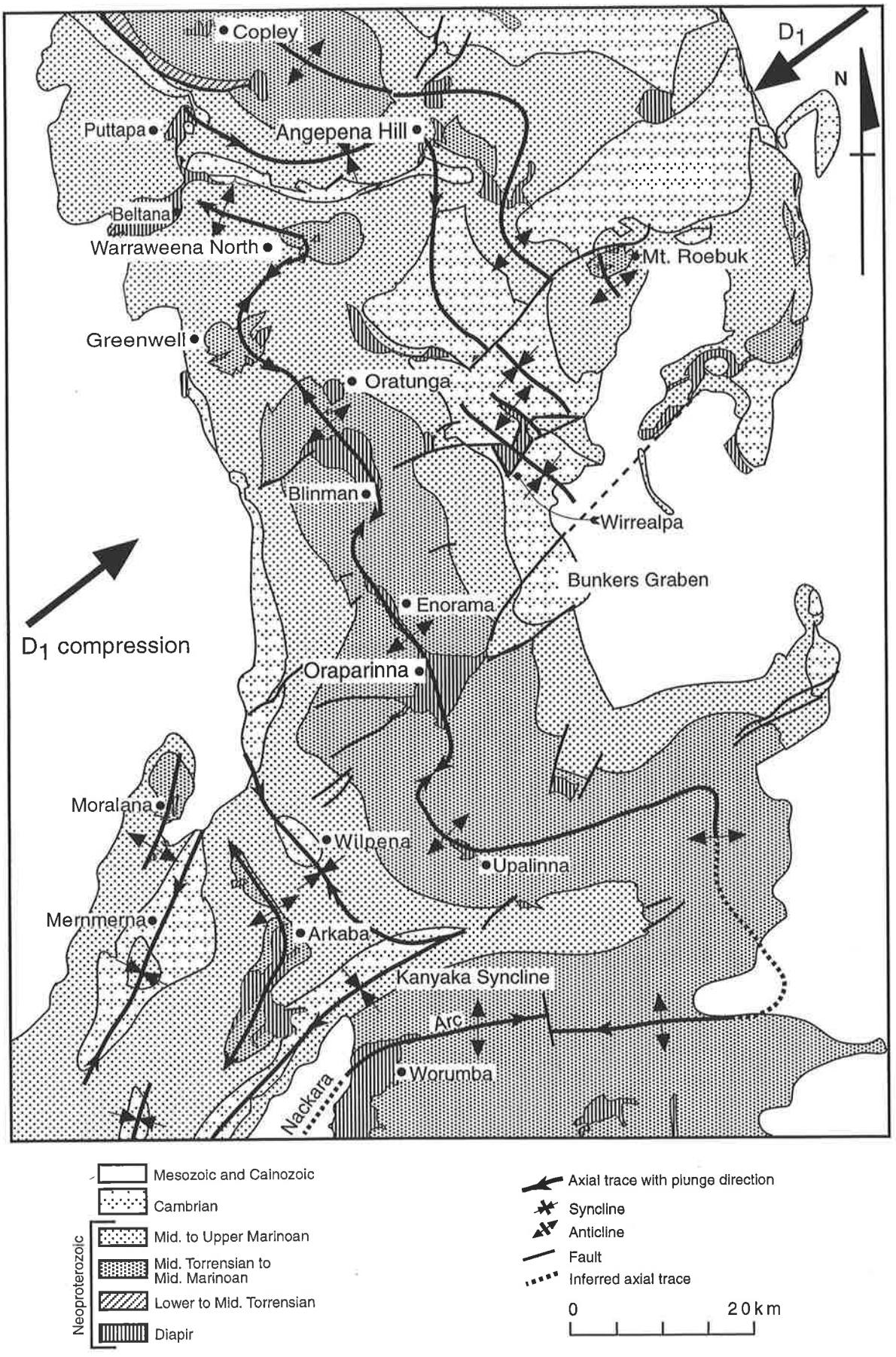

Fig. 3.2: F_1 axial traces and diapirs of the Flinders Ranges. Diapirs are commonly associated with F_1 anticlines rather than F_1 synclines.

3.3.2 F_2 folds

The F_2 axial traces in the Flinders Ranges are near parallel and dominantly oriented ENE, but vary between NE and east (Fig. 3.3). These traces can be marked by connecting the respective culminations or depressions of the F_1 folds, indicated by changes in strike orientation of the sequences. The F_2 folds, like the F_1 folds, have formed a series of alternating anticlines and synclines, similar to corrugated cardboard. The F_2 major axial traces and folds have not been previously noticed probably due to the prominence of F_1 folds. The F_2 folds suggest a dominant NNW - SSE compression, even though this also varies at times.

3.3.3 Dextral rotation of F_1 folds and the Nackara Arc

The NW trending major F_1 axial traces in the Flinders Ranges occasionally are oriented EW, as seen between the doubly plunging anticlines of Beltana and Blinman, Blinman and Enorama, Oraparinna and Upalinna, and Upalinna and Worumba (Fig. 3.2). This indicates dextral rotation of the F_1 axial traces, forming kinks or bends which possibly resulted from the NNW-SSE compression of the D_2 deformation. After rotation, the F_1 axial traces at times coincide with the easterly orientation of F_2 axial traces. The F_1 axial trace between the Upalinna and Worumba anticlines is the largest bending of some tens of kilometres scale, and forms both limbs of the Nackara Arc (Figs. 1.1, 3.2). The Wilpena - Kanyaka F_1 Synclinal axial trace to the immediate west is bent sharply, rotating to ENE and also forms part of both limbs of the Nackara Arc. The adjoining axial trace of the Arkaba F_1 Anticline to the west shows relative bending, forming part of the western limb of the Nackara Arc. Further west are the Mernmerna Syncline and the Moralana Anticline respectively, both oriented between north and NNE, showing no harmonic refolding, which also contributes to the western limb of the Nackara Arc. The sharp bend between the Wilpena - Kanyaka F_1 Synclines lessens to both the east and west across axial traces.

3.3.4 Interference of F_1 and F_2 folds

The F_1 and F_2 folds generally are nearly perpendicular to each other, even though they overlap at times, especially on the eastern continuation of the Upalinna Anticline (Fig. 3.4). O'Driscoll (1964) showed that interference between non-parallel anticlines forms domes, and that between synclines

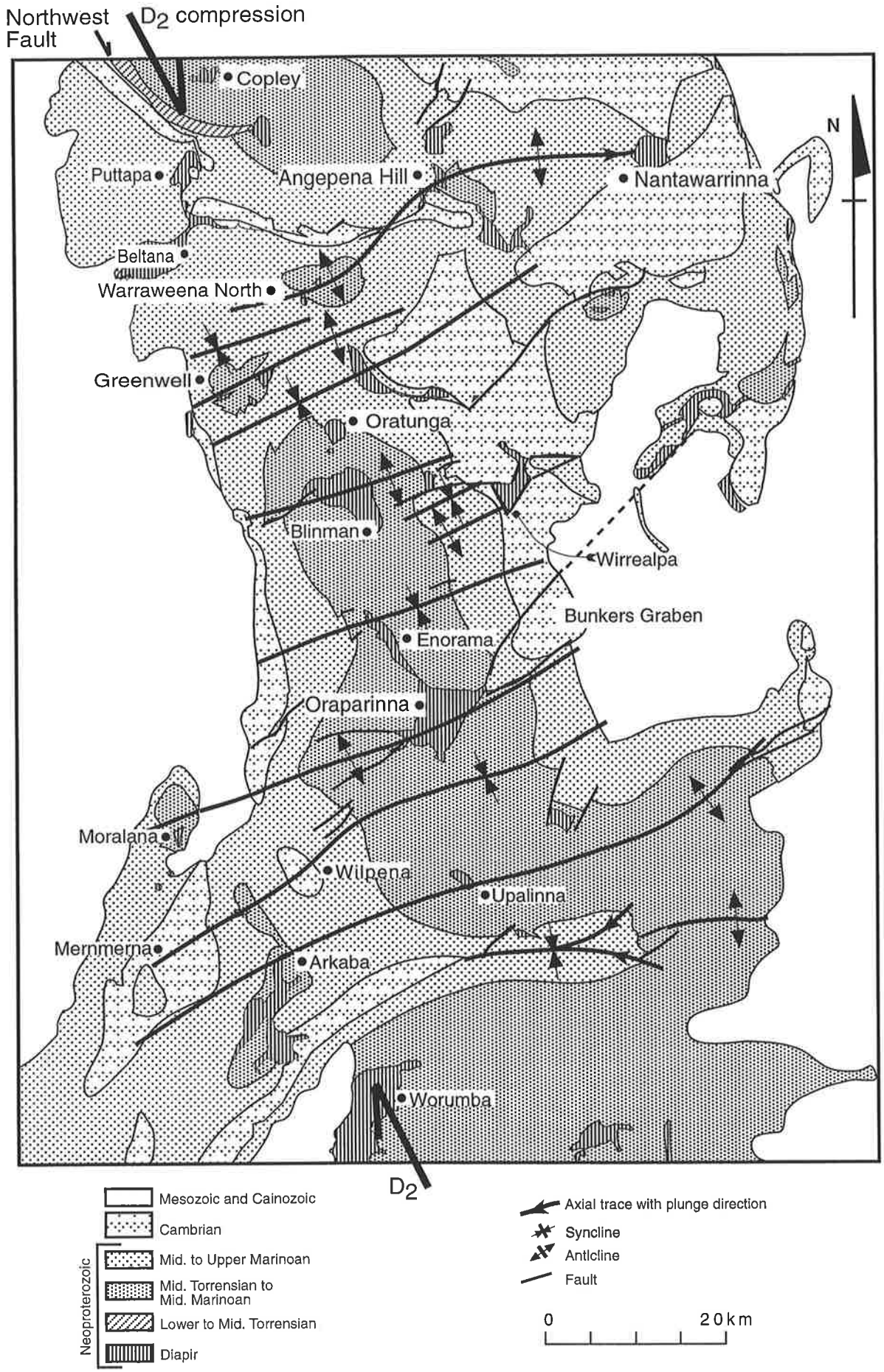

Fig. 3.3: F_2 axial traces and diapirs of the Flinders Ranges. Diapirs are commonly associated with F_2 anticlines rather than F_2 synclines.

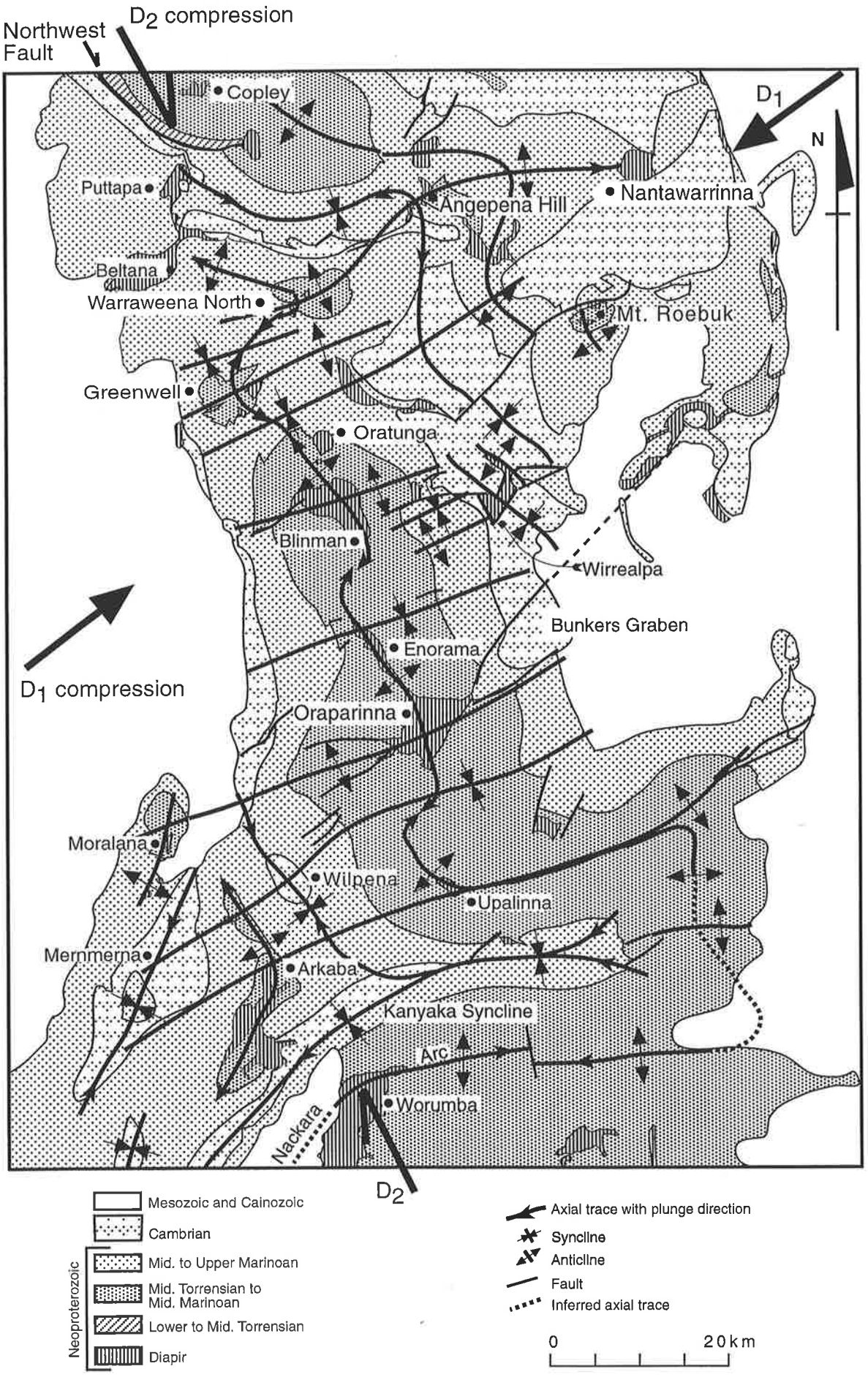

Fig. 3.4: Superimposition of F_1 and F_2 fold axial traces of the Flinders Ranges. Diapirs are largely localised on to axial traces of anticlines, expecially domes that were formed by superimposition of anticlines. Basins formed by superimposition of synclines do not host diapirs.

forms basins. Further, he showed interference between an anticline and a syncline forms a complex col or saddle structure. Interference of the Moralana and Oraparinna F_1 Anticlines with the respective F_2 anticlines has formed domes with increased respective widths (Fig. 3.4). Similarly, both the Mernmerna and Wilpena F_1 Synclines have interfered with the respective F_2 synclines, forming basins with increased widths (Fig. 3.4). These dome and basin structures somewhat resemble an egg carton structure (e.g. Ramsay and Huber, 1987).

Interference between F_1 and F_2 folds in the northern Flinders Ranges also forms similar egg carton-like structure, but here the folds are inclined (Paul *et al.*, 1999), compared to the upright folds in the southern Flinders Ranges.

The central Flinders Ranges have one major F_1 axis from the Blinman to the Oraparinna Anticlines and multiple F_2 axes. Therefore, the egg-carton structure cannot be seen at the major scale. However, the superimposition of the Blinman and Oraparinna F_1 Anticlines with the respective F_2 anticlines is indicated by the increased widths or wavelengths of F_1 anticlines (Fig. 3.4). The Enorama F_1 anticline is superimposed by the respective F_2 syncline, forming a col structure (see above), resulting in decrease in width and forming an elongated F_1 anticline. Therefore, the Blinman and Oraparinna Anticlines have been referred to as domes while the Enorama Anticline has not been called as the Enorama Dome.

Interference structures of these domes or basins show greater elongation of F_1 than of F_2, showing the dominance of D_1 deformation over the D_2.

3.4 Grabens, fractures and diapirs

The only major and well defined, significant graben structure reported to-date in the Flinders Ranges is the Bunkers Graben, which lies within the eastern limb of the Oraparinna F_1 Anticline (Figs. 1.4, 3.5, Dalgarno and Johnson, 1966; Clarke, 1986). The graben is confined by two boundary-faults, which converge to an apex within the margins in the Oraparinna Diapir. The bounding faults extend up to 3-4 km from the diapir at N15°E and N75°Etrends, and continue in a northeasterly direction for about 50 km (Dalgarno and Johnson, 1968; Map 1; Fig. 3.6). Sedimentary sequences within graben are displaced along the boundary-faults as well as by a series of approximately boundary-parallel faults within the graben (Map 1, Fig. 3.6). The displacements along these faults always increase towards the apex.

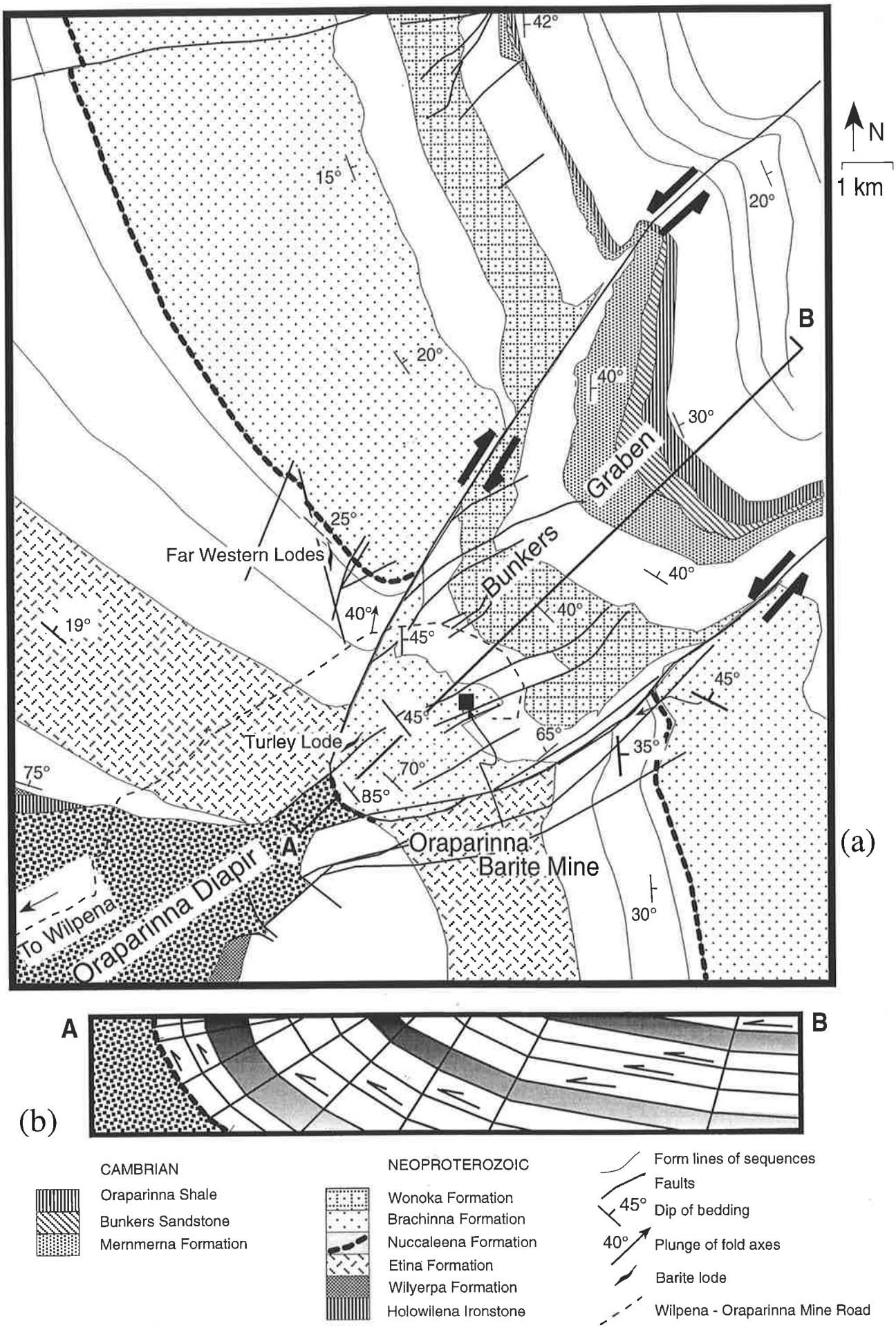

Fig. 3.5: (a) Geological map of the Bunkers Graben, showing thickening of some of the sequences within the graben. Note: Graben sequences show opposite movements along the northern fault boundary. (b) Schematic diagram explaining the mechanism of the formation of increasing dips towards the apex, resulting from SW verging bedding slip.

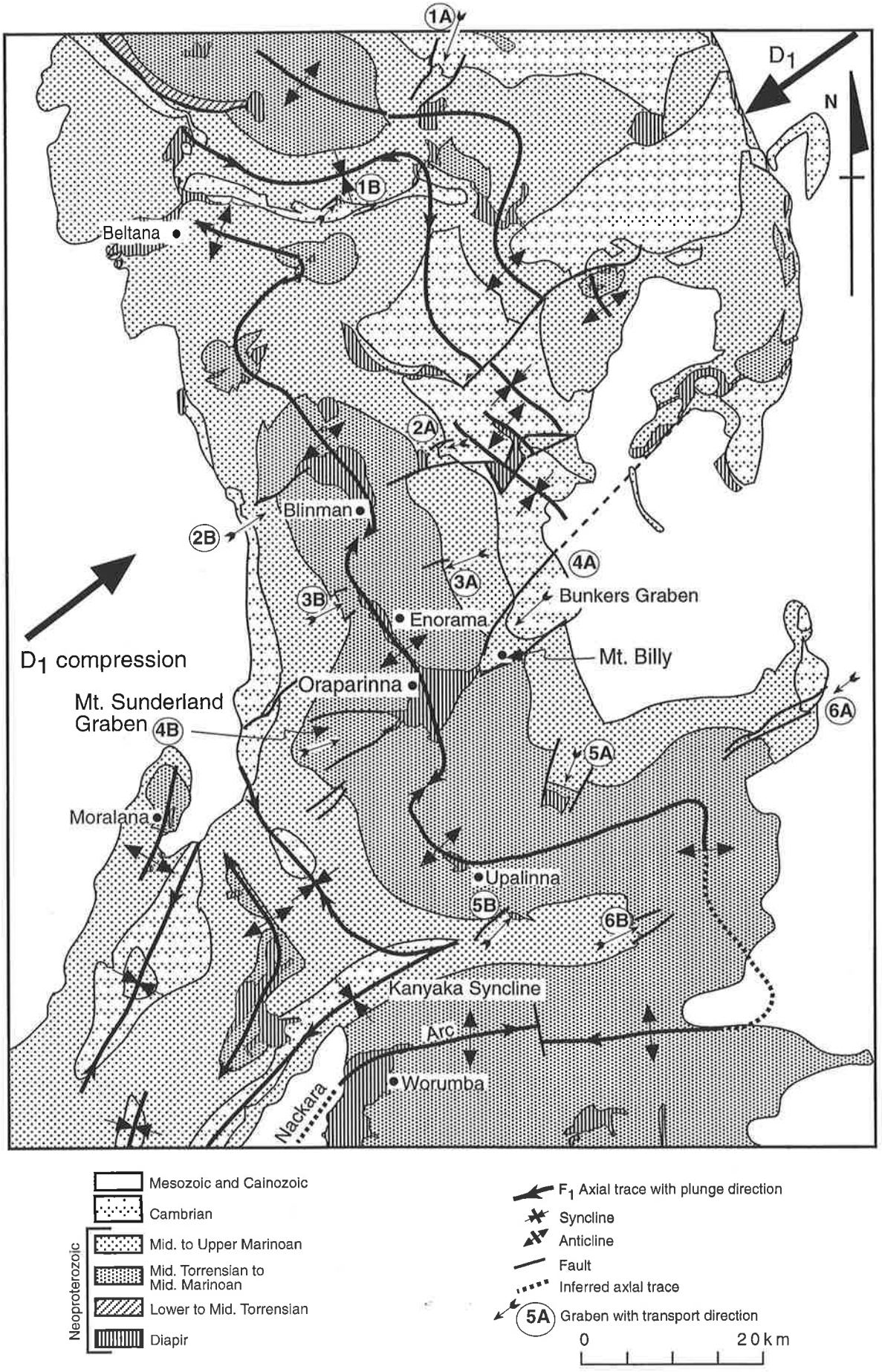

Fig. 3.6: Occurrence of pairs of grabens across the F_1 axial traces in the Flinders Ranges. Full-grabens defined by two fault boundaries are: Mucatoona (1A), Angorichina (2A), Bunkers (4A), Mt. Sunderland (4B), Yudnapunda (5A), 6A and 6B. Half-grabens defined by single fault boundary are: Mt. Goddard (1B), 2B, 3A, 3B and Mannawarra Spring (5B). Diapirs are associated with grabens, e.g. 1A, 1B, 2A, 4A, 4B, 5A and 5B grabens.

Regional fracture and fault trends (totalling 350 measurements) in the central Flinders Ranges were measured from the maps of Lemon (1988; Figs. 3.7a) and were analysed for preferred orientations. The analysis indicates three prominent fracture systems oriented NNE, NE and ENE and another two less prominent systems oriented NNW and NW (Fig. 3.7b). The sequences in the Bunkers Graben are intensely displaced along these prominent fractures.

Another two major scale bounding-faults extending for more than 13 km occur on the western limb of the Oraparinna Anticline, and converge into an apex in the Oraparinna Diapir (Maps 1, 2; Fig. 3.6). These faults are oriented between west and SW, and generally mirror those of the Bunkers Graben, on the eastern limb of the Oraparinna Anticline. Sedimentary sequences between the bounding faults on the western structure are increasingly displaced from the open-end towards the apex, showing a similarity with those of the eastern structure, i.e. the Bunkers Graben. Therefore, the western structure can be interpreted as a graben, and named here as the Mount Sunderland Graben (Fig. 3.6).

A series of graben structures were recognised in the Flinders Ranges during the structural interpretation (Fig. 3.6). The boundary-faults of these grabens generally trend between NNE-SSW and ENE-WSW. Some of the grabens are well developed, having two boundary-faults (i.e. full-grabens), while the others are less well developed and feature single faults (i.e. half-grabens). These grabens have formed as pairs on the opposite limbs of the F_1 anticlines, where each pair has been named as A and B for easy identification. Examples of full-graben structures are: the Mucatoona Graben (1A), the Angorichina Graben (2A), the Bunkers Graben (4A), the Mount Sunderland Graben (4B), the Yudnapunda Spring Graben (5A) and un-named grabens 6A and 6B (Fig. 3.6). Examples for half-grabens are: Mount Goddard Graben (1B), Mannawarra Spring Graben (5B) and un-named grabens 2B, 3A, 3B. The grabens trend nearly perpendicular to respective F_1 axial traces unless they have been otherwise rotated during later deformation. The full-grabens show boundary-faults which converge towards respective apices, and which always lie adjacent to axial traces of major F_1 anticlines. In contrast, the open ends lie always on the limbs, away from their respective axial traces. All the full- and half-grabens show increasing displacement of the contained sedimentary sequences toward their respective apices along the boundary faults and thus, conversely the displacements decrease toward the open-ends. The grabens generally show approximate mirror image patterns with opposite senses of displacement across the respective anticline axial traces.

Apices of grabens are commonly associated with breccia deposits or diapirs. Both the Bunkers and Mount Sunderland Grabens are linked to the Oraparinna Diapir, where breccia from the diapir is

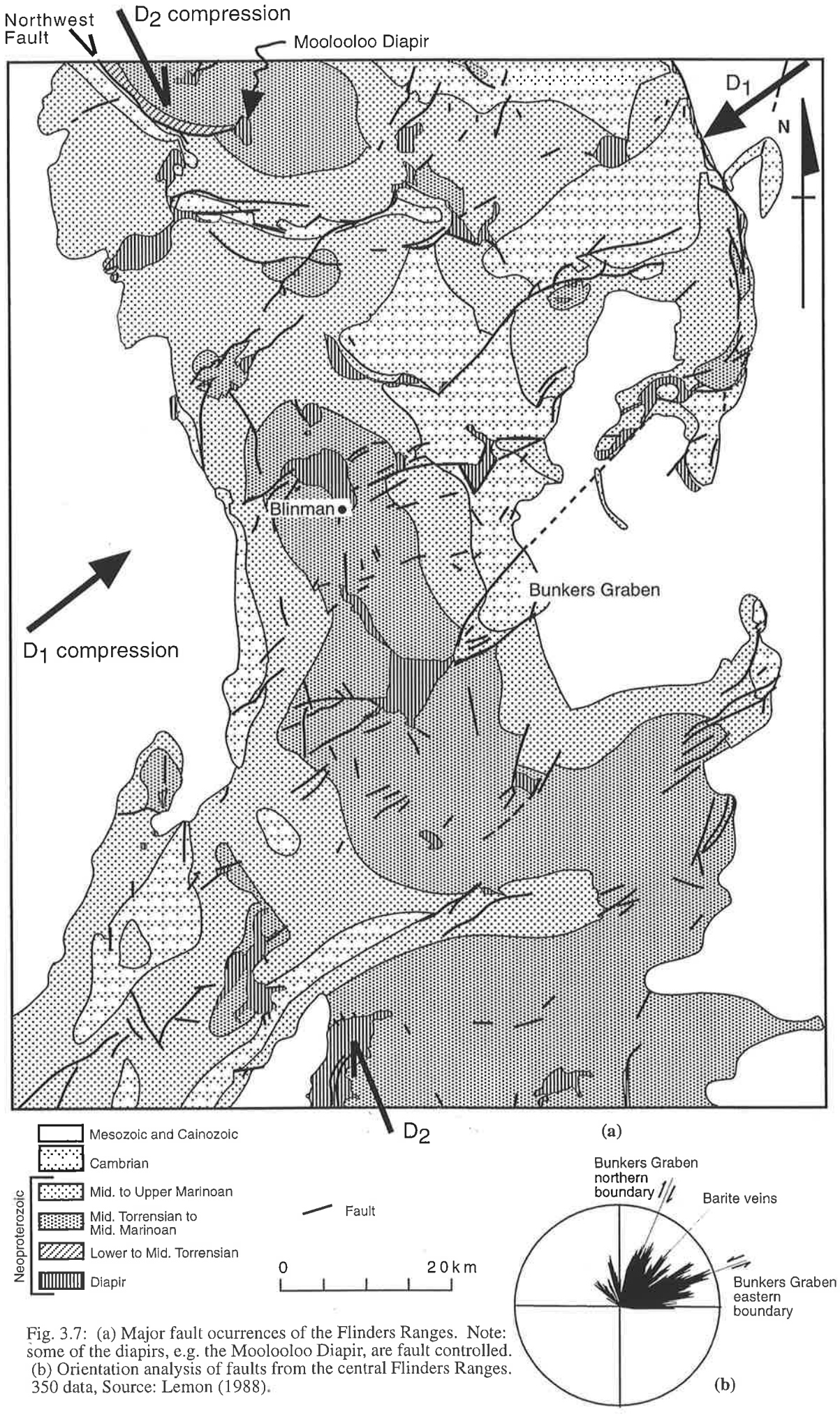

Fig. 3.7: (a) Major fault ocurrences of the Flinders Ranges. Note: some of the diapirs, e.g. the Mooloolloo Diapir, are fault controlled. (b) Orientation analysis of faults from the central Flinders Ranges. 350 data, Source: Lemon (1988).

extended into both grabens. Breccia occupies the area between the fault boundaries, up to the competent Nuccaleena Formation of the Bunkers Graben; but occurs only along the boundary-faults of the Mount Sunderland Graben (Map 2, Figs. 3.5, 3.6). Diapirs are also associated with apices of grabens at the Mucatoona Diapir (1A), the Mount Goddard Diapir (1B), the Angorichina Diapir (2A), Yudnapunda Spring Diapir (5A) and the Mannawarra Spring Diapir (5B; Fig. 3.6). These diapirs are generally more prominent on the eastern limbs of F_1 anticlines than on the respective western limbs.

The major Northwest Fault in the northern Flinders Ranges also shows displacement of lower to middle Torrensian sediments on its eastern margin, against Cambrian sediments on its western margin. This fault is associated with a breccia deposit known as the Moolooloo Diapir on its southern tip-end

3.5 Anticlines and diapirs

The Blinman, Oraparinna, Upalinna, Moralana and Warraweena North Diapirs are located within the domes formed by the intersection of respective F_1 and F_2 anticlines (Fig. 3.4). These diapirs, like their respective anticlines, are elongated along F_1 axial traces, but also increase in their widths along F_2 axial traces. The Enorama diapir shows F_1 elongation, but the superimposition of the Enorama F_1 anticline by its F_2 syncline has decreased the widths of both the anticline and diapir. Basins formed by superimposition of both F_1 and F_2 synclines show increased widths across F_2 trends, but host no diapirs, e.g. Wilpena Syncline. Diapirs are rarely found along the F_1 syncline axes (e.g. Wilpena - Kanyaka Synclines and Mernmerna Syncline). However, the Angepena Hill Diapir in the northern Flinders Ranges is formed on an F_1 syncline, but is superimposed upon by an F_2 Anticline. Thus the diapir could have formed along the F_2 anticline. Therefore, it appears that diapirs may occur on F_1 synclines if they are superimposed upon by F_2 anticlines.

A pair of F_1 anticline and syncline lies at Wirrealpa, between the major F_1 axial traces of the Blinman Anticline and the Puttapa – Angepena Hill Syncline (Fig. 3.4). The Wirrealpa Diapir lies along the axial trace of Wirrealpa F_1 Anticline and extends southwestward along a NE – SW trending wrench fault zone, across the Wirrealpa F_1 Syncline (Figs. 3.4, 3.7). In contrary to Lemon (1988), who interpreted the Wirrealpa Diapir was controlled by the Wirrealpa Syncline, it may well be that the diapir was controlled by both the anticline and the fault zone and was overlapped on to the Wilyerpa Syncline.

3.5.1 The Enorama Anticline/Diapir

The Enorama Diapir is exposed along the hinge zone of the Enorama F_1 Anticline (Fig. 3.2). Both limbs of the anticline consist of Etina Formation, Enorama Shale, Trezona Formation and Elatina Formation, as seen on the surface outcrops (Map 2). In addition, the eastern limb contains lower sequences such as the Holowilena Ironstone, Wilyerpa Formation, Tapley Hill Formation and Sunderland Formation. The western limb consists of shallow dips in contrast to steep to moderate dips on the eastern limb. A cross-section of the anticline was constructed through the lower sequences in order to explain this unusual asymmetry and its relationship to the diapir and the anticline.

The Brachina Gorge Geological Trail in the west of the Enorama Anticline to the Nanpena Spring in the east of the anticline was selected to construct the cross-section, because of the readily available access and continuous exposure. The basic geological information such as formation boundaries, and dip and strike data given on the Map of the Flinders Ranges National Park (Map 2 of Callen and Reid, 1994; 1:75,000) was used to construct the section. Additional geological data measured along the track were included in the cross-section to enhance accuracy. The area around the Enorama Anticline has been mapped in detail by Lemon (1988) as well, thus there was no necessity to produce a new geological map of the area, for the purpose of constructing a cross section.

The dips of the sequences were corrected on to the approximate profile plane of the anticline. The corrected dips decrease from 80° NE to 12° NE, from the border of the diapir to the east, accordingly. In contrast, those on the western limb dip almost constantly, between 11° SW and 8° SW. The geometry of the section was constructed using this information and the section was balanced using the techniques given by Elliot (1983).

The balanced section of the Enorama Anticline shows that the eastern limb dips decrease northeasterly from the axial surface with panels of kink bands, defined by fault-bend folds with steeper fore-limbs than back limbs, while the western limb dips gently and nearly constantly (Fig. 3.8a). Therefore, the section through the anticline reveals the geometry of a simple fault-propagation fold (Suppe, 1983 & 1985). The section was compared with the fault-propagation/detachment fold models proposed by Marrett and Bentham (1997), an improvement of Chester and Chester (1990, Fig. 3.8b). The section suggests a décollement-thrust fault underneath the eastern (back) limb that developed into a listric reverse-thrust fault adjacent to the

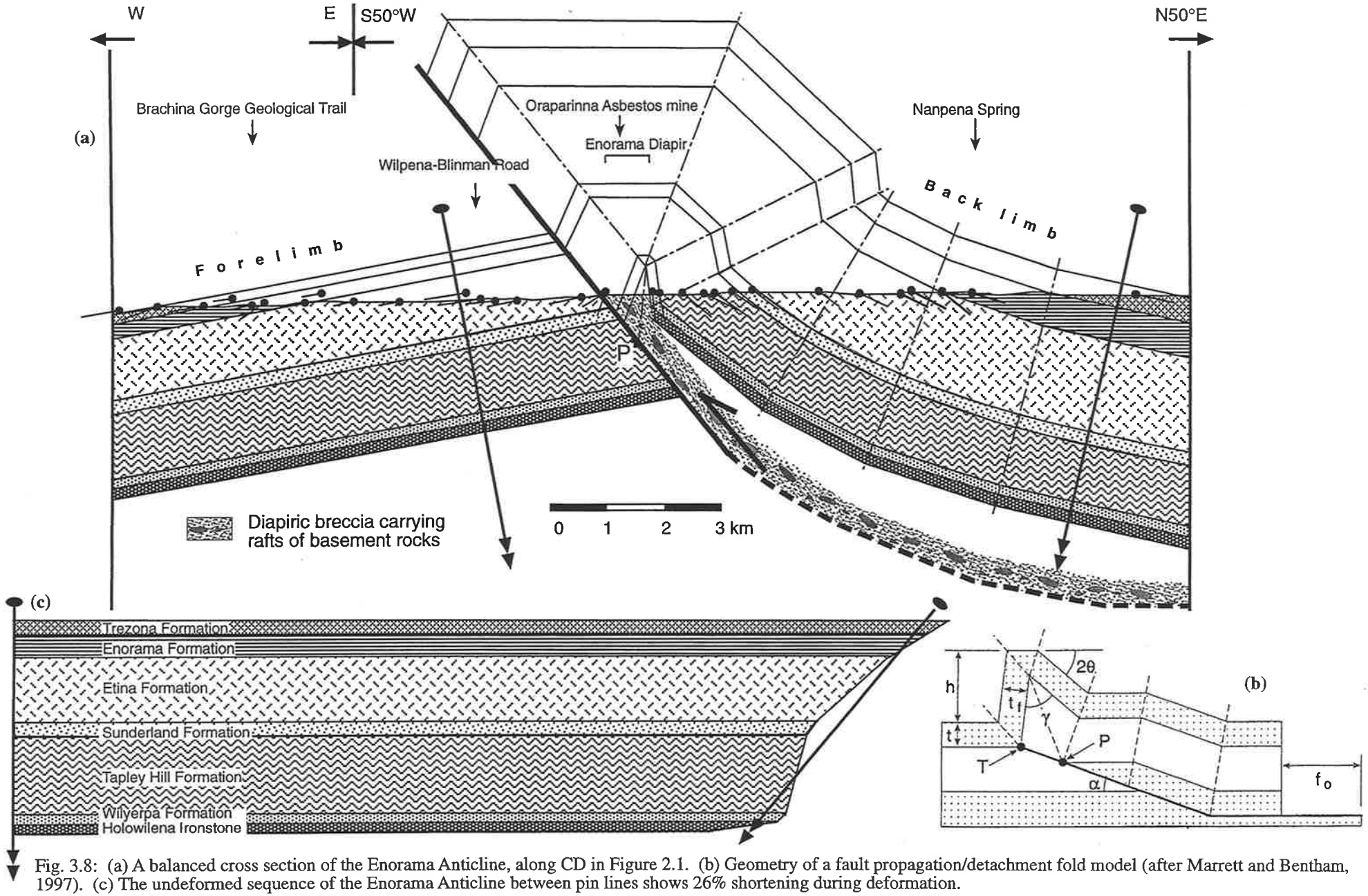

Fig. 3.8: (a) A balanced cross section of the Enorama Anticline, along CD in Figure 2.1. (b) Geometry of a fault propagation/detachment fold model (after Marrett and Bentham, 1997). (c) The undeformed sequence of the Enorama Anticline between pin lines shows 26% shortening during deformation.

hinge line of the fold. The eastern limb has initially moved on the décollement-thrust fault surface, thrusting the lower sequences of Wilyerpa Formation, Tapley Hill Formation and Sunderland Formation, over the western (fore) limb. Therefore, the Enorama fault-propagation fold verges SW.

The Marrett and Bentham (1997) method allows fault-propagation folds and many detachment folds, to be analysed using a single geometric model. The fold initiation point, P, marks the location at which displacement begins to decrease (Fig. 3.8b). The fault tip point, T, occurs where the displacement reaches zero. Fault displacement is assumed to change linearly between points P and T. The thrust ends at point 'T'; whereupon it develops into a fault-propagation fold.

The Enorama Anticline is best defined by its competent units (e.g. the Holowilena Ironstone), compared with the underlying thick horizon of incompetent breccia, detached from, and displaced relative to the underlying basement (Dalgarno and Johnson, 1966; Forbes, 1972; Preiss, 1999). Therefore, the Enorama Anticline can be considered to be best represented as a partial detachment fold (Laubscher, 1977; Wiltschko and Chapple, 1977). Both fault-propagation folds and detachment folds are thrust related structures that amplify as thrust displacement accrues near a thrust tip, or as buckle folds that develop between bounding décollements (Thorbjornsen and Dunne, 1997). The Enorama Anticline probably also has a component of formation as a mud-breccia cored detachment fold as well, with a possibility of later or simultaneous development of a reverse thrust fault into the western limb, as characteristic of fault-propagation folds in general (Mercier *et al.*, 1997). The end of the listric reverse-thrust fault, where the displacement decreases to zero (i.e. point 'T' of Fig. 3.8b) is not known for the Enorama Anticline.

The remnants of the host rocks at the margins of the Enorama Diapir are folded into steep to moderate dips. Mumme (1961) and Coats (1964a) interpreted those remnants of the Blinman Diapir as forcible emplacement of the breccia intrusion into the core. In the present interpretation, these remnants are interpreted as a component of fault-propagation folding, at which point the breccia broke through the structure (c/f. Suppe and Merwedeff, 1990; Mercier *et al.*, 1997).

The geometry of detachment folds depends on detachment depth and shortening (Dahlstrom, 1990; Groshong and Epard, 1994; Homza and Wallace, 1995, 1997; Wallace and Homza, 1998). The structural relief causes an 'excess area' during shortening (Figs. 3.8a, b). The excess area between the ground level and the upper boundary of the Etina Formation was selected for depth to detachment calculations for the Enorama Anticline (Fig. 3.8a). Deformed and undeformed lengths of 10.8 km and 14.5 km were measured respectively, between the contact points of the upper

boundary of the Etina Formation, along the ground level. Thus, the section has been shortened by 3.7 km, i.e. 26% [(14.5-10.8)/14.5x100%], which was accommodated by fault-propagation folding (cf., Jamison, 1987; Mitra and Namson, 1989 and Mitra, 1990, 1992). The 'excess area' measured is 19.7 km^2, and is equal to the 'shortened area' which is the product of the shortened distance and the depth to the detachment, below the ground level (Rowland and Duebenddorfer, 1994). Therefore, the depth to the detachment is calculated as 5.3 km (19.7km^2/3.7km). However, this depth must be treated with caution and may indicate depth to the upper surface of the thick breccia zone over the décollement. The section violates constant volume during shortening as evident by brecciation of some of the sequences during thrusting.

3.5.2 The Moralana Anticline/Diapir

The northerly trending Moralana F_1 Anticline is bisected by a northeasterly trending fault (Fig. 2.4). The northern half of the anticline is hosted by moderately dipping sequences from the Tapley Hill Formation up to the Wonoka Formation and is symmetric and plunges gently north. No diapir occurs within the northern half.

The southern half contains lower sequences from Warcowie Dolomite to Tindelpina Shale, in addition to those on the northern half. The western limb of the southern half dips moderately and approximately constantly, 45° to 50° W; while dips of the eastern limb gradually increase from moderate to steep towards the hinge zone where they overturn.

The Moralana Diapir reaches the surface along the fault that bisects the anticline and the fold hinge trace on the southern half. Breccia is more prominent along the sector of fault on the eastern limb than along that on the western limb.

The Moralana Anticline/Diapir shows similar geometric features to those of the Enorama Anticline/Diapir, i.e. (a) constantly dipping western limb, (b) increasing dips towards the hinge zone on the eastern limb, which overturns adjacent to the hinge zone, (c) a gently dipping open fold at the northern end, (d) the occurrence of a diapir in the hinge zone, and (e) more prominent occurrence of breccia on the eastern limb than the western limb as expressed along the NE trending fault with the Moralana Anticline. Therefore, the Moralana Anticline/Diapir shows a west verging detachment/fault-propagation fold geometry, similar to the Enorama Anticline/Diapir. Hence, the Moralana diapiric breccia was possibly generated on an easterly dipping décollement and

was subsequently transported into the hinge zone, similar to the mechanism of the Enorama Diapir.

If the faulting across the Moralana Anticline had not thrust up the southern half of the fault, the diapir would not have been exposed. In that case, the doubly plunging Moralana Anticline would be observed, without recognition of the occurrence of a diapir within the anticline. Thus, the Moralana Diapir may well extend into the northern half of the anticline. Therefore, it is likely that diapirs occur along many more anticlinal axial traces in the Flinders Ranges, mainly along the hinge lines and, more prominently under the eastern limbs than the respective western limbs.

3.6 Discussion

The geological structure of the Flinders Ranges has resulted from superimposition of two major deformations, the D_1 and D_2. Major D_1 structures of the Flinders Ranges are the F_1 folds trending between NW-NNW; approximately NE-SW trending grabens; and fractures orienting NW, N10°W, NNE, NE and ENE. These structures suggest a major NE-SW compression during the D_1 deformation. The F_2 folds trend ENE and thus it is suggested the D_2 compression was oriented NNW-SSE and also acted along the Northwest Fault in the northern Flinders Ranges and through the Nackara Arc in the southern Flinders Ranges. Diapirs, i.e. breccia deposits outcropping in association with (a) axial traces of anticlines (e.g. the Enorama Diapir); (b) apices of grabens (e.g. the Yudnapunda Diapir); and (c) faults (e.g. the Mooloolo Diapir at the southern tip end of the Northwest Fault, Fig. 3.7) can be explained in terms of these two deformations.

3.6.1 F_1 folds

The balanced section constructed across the Enorama F_1Anticline shows asymmetry, defined by (a) the steeper dips and occurrence of lower sequences on the eastern limbs, and (b) as a west verging detachment/fault-propagation fold with a northeastly dipping listric-thrust décollement surface (Fig. 3.8a). A series of F_1 anticlines occurs from Beltana to Worumba along a single regional axial trace, and includes the Enorama Anticline. These anticlines commonly show an asymmetry, defined by steeper dips or the occurrence of lower sequences on the eastern limbs, when compared with the respective western limbs {see Copley (Coats, 1973), Parachilna (Reid and Preiss, 1999) and Worumba (Preiss, 1985) Geological Maps by MESA}. Therefore, the F_1 anticlines along the same axial trace are also likely to be caused by a west verging fault-propagation fold mechanism, like that

of the Enorama Anticline. Other F_1 anticlines in the Flinders Ranges also indicate nearly parallel axial traces and west verging fault-propagation folds, as evidenced by the Moralana Anticline. This suggests the F_1 folds in the Ranges show a train of west verging detachment/fault- propagation folds, broadly similar in shape to corrugated cardboard. Therefore, according to the geometric and other characteristic features of the Enorama Anticline; the F_1 folds in the Ranges can be suggested to have developed on northeastly dipping décollement/listric-thrust décollement surfaces. Thus these anticlines appear to be linked with a series of west verging imbricate thrusts which subsequently developed into detachment/fault- propagation folds. Shortening is approximately 26%, as was calculated for the Enorama Anticline.

3.6.2 Diapirs

The Enorama Diapir contains clasts from both ripped-off basement rocks and the immediately overlying Callanna Group rocks (Dalgarno and Johnson, 1966). Therefore, according to the fault-propagation fold model (Figs. 3.8a,b), brecciation was initiated during gouging of the Callanna Group rocks over the basement. Breccia was brought along the detachment/décollement surfaces, through listric-thrust surfaces, into upper levels during shortening deformation. Breccia is expected to have formed along the listric-thrust surfaces as well, adding to the main stream of breccia generated along the basement. The depth calculation suggests a depth of 5.3 km to the décollement thrust surface, which then developed into a listric-thrust surface (Fig. 3.8a). As the breccia zone over the basement would probably be as much as 1-3 km thick (?), this depth will be considered to represent the depth to the upper surface of the breccia zone and not to the basement.

There are known difficulties in the identification of breccia clasts derived from different sequences within diapirs (Preiss, 1985). Moreover, most of the upper section of the Enorama Diapir and Anticline has been eroded away to its current level of surface outcrop, thus how much of the uppermost sequences contributed to the breccia formation is unknown. Therefore, the location of the end of the listric thrust fault surface or the tip line, T, is also unknown but is most likely to be formed in the Neoproterozoic or Cambrian sequences (Fig. 3.8a). In contrst, the Beltana Diapir, along the northern continuation of the axial trace of the Enorama Diapir, has been found to contain Cambrian archaeocyathid limestone, Burra and Callanna Group rocks, and crystalline basement rocks (granite and amphibolite) as xenoclasts in close proximity (C.R. Dalgarno and W.V. Preiss, unpublished field notes, South Australian Mines and Energy, 1980). This may provide a clue

that the listric-thrust fault surface in the Beltana Anticline ended at a tip-line in the Cambrian sequences thus, producing breccia from the Neoproterozoic up to the Cambrian.

A variety of detachment/fault-propagation folds may begin and end between different levels of the sedimentary sequences, comprising breccia related to those levels. If the constituents of diapirs along the axial traces of fault-propagation folds contain clasts from both the basement and the Callanna Group, those diapirs are likely to have initiated along décollement thrust surfaces over the basement. Moreover, the breccia clasts from the uppermost sequence may suggest the location of the end of the tip-line of the reverse thrust fault. Conversely, it is difficult to identify the source beds of clasts due to similarities between them and also due to the current erosion.

However, these diapirs, e.g. the Enorama Diapir etc, have been reported by Lemon (1988) and accepted by the wider geological community to be of synsedimentary origin (Figs. 2.2, 2.3). In order to provide further evidence in growth of a structural model for the formation of the diapiric breccia deposits, very detailed minor structural evidence has been examined and is presented in Chapter 6.

3.6.3 Graben Structures

Grabens were formed in pairs with apices adjacent to axial traces across F_1 anticlines, along Riedel and conjugate Riedel fractures (Harding, 1974; Hancock, 1985). In the Bunkers Graben these fractures orient NNE and ENE forming boundary-faults that generally extend along NE. The grabens show approximate mirror image features across the respective fold axial traces, and opposite senses of movement within sequences, towards their respective apices and thus can be considered as products of the D_1 deformation. However, precise mirror images of graben structures may not be seen across the respective axial traces, as the Flinders Ranges appear to have undergone a large scale dextral rotation during the D_2 deformation, which reoriented them (Chapter 4). The graben sequences show more displacement towards apices than respective open-ends, along boundary-faults and those faults parallel to the boundary-faults within the graben.

Some of the grabens have associated diapirs adjacent to the apices. These breccia deposits, including those on faults across the anticlines (e.g. the faults across the Oraparinna and Moralana Anticline), are more prominent on eastern fold limbs than on the respective western fold limbs. This is probably because the depths to the breccia zones on the eastern limbs of F_1 anticlines were less than those on respective western limbs, due to the occurrence of northeasterly dipping listric

thrust décollement surfaces. This means grabens are likely to be D_1 compressional structures formed by thrusting the fault-bound graben sequences along décollement surfaces responsible for forming the F_1 detachment/fault-propagation folds.

However, Lemon (1988) suggested that the sinking of the Bunkers Graben was related to and simultaneous with the rise of the Oraparinna Diapir, during a period of extension, where sedimentation occurred. Thickening of some of the sedimentary sequences within the Graben, as well as on the limbs of Enorama Anticline (i.e. flanks of the Enorama Diapir), was regarded as "primary thickening" related to growth of normal-faults on the crestal position of the rising Oraparinna Diapir. Therefore, in the view of a tectonic model for the Enorama Anticline that contained the Enorama Diapir, and the Bunkers Graben, these sequences have been investigated for minor structures to provide evidence of movement and thickening; to compare the likelihood of tectonic versus sedimentary origin for the structures (Chapters 4,5 & 6).

3.6.4 D_2 structures

The D_2 deformation also formed a series of corrugated cardboard-type folds similar to those of F_1 folds but oriented between ENE and NE. Cross sections across the F_2 structures were not made and thus their detailed geometry is not known. The D_2 deformation caused a dextral rotation of the F_1 axial traces, as is indicated by a series of dextral kinks along the Beltana to Worumba Anticlines as well as on the other F_1 anticlines. These kinks in the north of the Upalinna Anticline generally vary up to a few kilometres in width, and can be considered as parasitic kinks to the largest kink between the Upalinna and Worumba Anticlines, which forms the Nackara Arc (Figs. 3.2, 1.1). The Nackara Arc and the Southern Adelaide Fold Belt, both show overall 'S' shaped oroclinal bends (Marshak and Flottmann, 1996) that is also shown by the kinks between other anticlines. Therefore, the Nackara Arc was likely to have also been a product of the D_2 Deformation.

Some of the breccia deposits also were localised during the D_2 deformation, e.g. the Angepena Hill Diapir that lies along an axial trace of F_2 anticline and the Moolooloo Diapir at the southern end of the Northwest Fault (Coats, 1973). The D_2 parasitic structures have been further studied in detail in the following minor structures (Chapter 5).

3.6.5 Fold superimposition

When the angle made by two overprinting compressions related to two regional deformations is large, i.e. close to 90°, superimposed folding is expected to have occurred (Ghosh and Ramberg, 1968; Skjernaa, 1975). These authors explain that if the styles of F_1 folds are open to gentle, domes and basins are expected to be produced by the D_2 compression. The interference of these folds follows the models produced by O'Driscoll (1964) and resembles an egg carton structure. The resultant domes or anticlines are found at Moralana, Oraparinna, Upalinna and Arkaba; while the basins or synclines are found at Mernmerna and Wilpena. These superimposed folds commonly show F_1 elongation, suggesting the dominance of the D_1 phase rather than the D_2 phase.

Chapter 4

D_1 MINOR STRUCTURES OF THE CENTRAL FLINDERS RANGES

4.1 Introduction

One of the major problems in sedimentary terrains is the differentiation between sedimentary and weakly-deformed tectonic structures, because of the common similarities between them. McClay (1992a) suggested, ""Synsedimentary' folds or 'slump' folds have many geometric similarities to the shapes, wavelengths and size distributions of 'tectonic folds'. Slump folds are generally tight to isoclinal with variable shapes at low fold amplitudes. Their fold axes are commonly dispersed in the plane of the slump sheet and recumbent folds are dominant". McClay further suggested the upper boundaries of these folds may exhibit sharp erosional truncations and in general, these folds have no genetic or geometric relationship to large macroscopic folds. The central Flinders Ranges contain slump folds and stromatolites (Preiss, 1987), which can be confused with tectonic structures such as upright open to gentle folds. Differentiation of these structures is difficult but characteristics such as random orientations of slump folds rather than preferential orientations, vergence and parasitic nature to major structures of tectonic folds in the region can be used.

4.2 Parallel folds

Parallel folds show that:

- (1) Individual layers are not appreciably thickened or thinned during folding and the thickness measured perpendicular to its local dip is nearly the same at all points around the fold; and

- (2) Successive layers in the fold are conformable or harmonic (Marshak and Mitra, 1988).

Minor F_1 folds in the central Flinders Ranges have smoothly curved broad hinge zones and are commonly found on both limbs of the Enorama – Oraparinna Anticlines. They trend from NW to NNW, and plunge gently. Open folds are rare, but gentle folds commonly appear with large interlimb angles over 120°. An example of the geometry and style of these types of folds from either limb of the major anticlines is presented below.

4.2.1 Folds on the eastern limb of the Oraparinna F_1 Anticline

A series of excellent exposures of minor F_1 folds were studied at the Turley Barite Lode (McCallum and Johnson, 1981), adjacent to the apex of the Bunkers Graben, on the eastern limb of the Oraparinna Anticline (Fig. 3.5). The lode is hosted by the Mooloolloo Member of the Brachina Formation, which consists of grey to reddish brown feldspathic siltstone with fine to medium grained sandstone. The nearly vertical lode strikes NE-SW and is already mined out, exposing the folded host on the nearly vertical contact wall (Fig. 4.1a). The wavelengths and amplitudes of the folds vary up to 3m and 0.5m, respectively. The mean long limb strikes N15°E and dips 30°E, and the mean short limb strikes N45°W and dips 23°SW, showing a mean fold axis plunging 16°->168° (Fig. 4.1b). The axial planes dip steeply to moderately NE. The average interlimb angle of the folds is 134° therefore they are gentle folds. The folds are asymmetric and verge SW.

A series of micro scale asymmetric folds occur on the bedding surfaces, and are small enough to require a hand lens to observe them in detail. Their asymmetry suggests that these folds verge SW, with wavelengths and amplitudes up to 5-10 mm and 1-2 mm, respectively. The mean fold axis of these minor to micro folds plunges 26°-> 151° (Fig. 4.1c).

Both the minor and micro-scale asymmetric folds show near parallelism of fold axes. The orientation of fold axes, dip of axial planes and asymmetry of folds show a SW vergence towards the apex of Bunkers Graben and therefore are tectonic folds formed during NE–SW compression of the D_1 deformation.

4.2.2 Minor folds on the western limb of the Enorama F_1 Anticline

A series of minor F_1 folds was studied on the western limb of the Enorama Anticline, along the Brachina Gorge Geological Trail. The folds occur in the very fine-grained calcareous Trezona Formation that strikes N35°E and dips 20°W, adjacent to the boundary of the Enorama Shale (Map 2). The Trezona Formation is folded into a series of parallel, curved hinge, symmetric folds (Figs. 4.2a&b). Wavelengths of the folds vary from 1 - 3 m and amplitudes up to 1 m. Folds with more than one fold axis, i.e. polyclinal style folds (cf. Hudleston, 1973a,b), can also be seen within the sequence (Fig. 4.2c). The mean limbs strike and dip N55°W/10°E and N50°E/10°W. The inter

SW NE

(a)

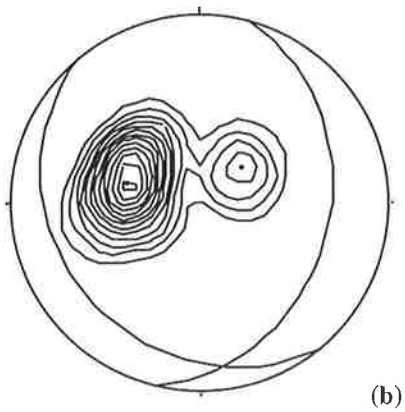

(b)

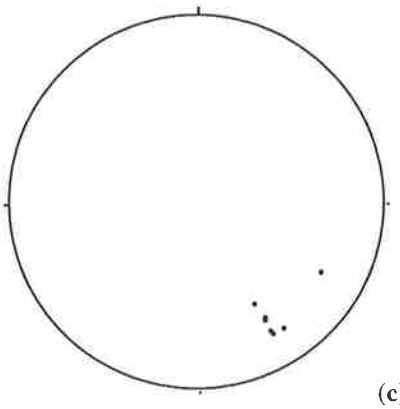

(c)

Fig. 4.1: (a) Asymmetric gentle folds adjacent to the apex of the Bunkers Graben on the contact wall of the Turley Barite Lode. Photographed facing northwest. (b) Stereogram for bedding indicating fold axis plunging 16°->168°. 26 data, contoured 1,3,.....13 times. (c) Minor parasitic fold axes showing mean plunge of 26°->151°, 7 data.

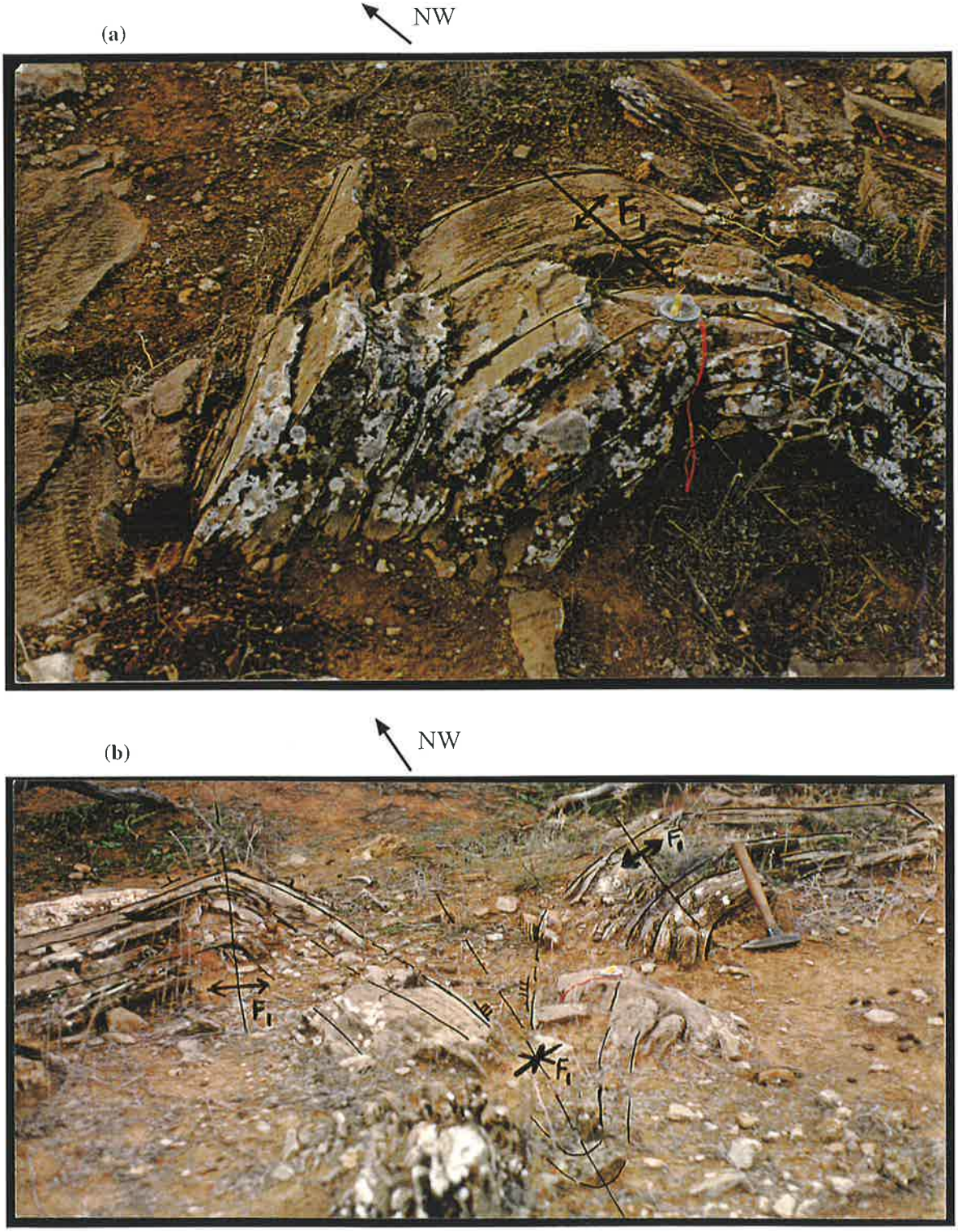

Fig. 4.2: NW-SE oriented, open to gentle, upright (F_1) folds of the calcareous, stromatolitic Trezona Formation on the western limb of the Enorama Anticline. Location: 7.5 km west of the Enorama Diapir, along the Brachina Gorge Geological Trail, along the boundary of the Enorama Shale. (a) Single fold. (b) Anticlines and a syncline. (c) & (d) See over leaf. (e) - (g) Stereograms for the F_1 folds. (e) Poles to bedding showing mean F_1 fold axis, 16^{o}->320^{o}, 13 data. (f) Measured data for the F_1 fold axes showing mean value of 19^{o}->325^{o}, 18 data. (g) L_1 striations of the slip-lineation on bedding, 11^{o}->231^{o} and 10^{o}->036^{o}, 10 data. Cont..,

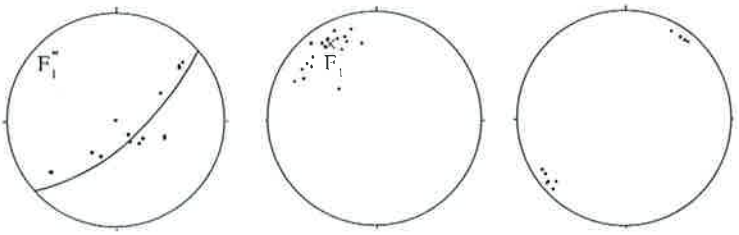

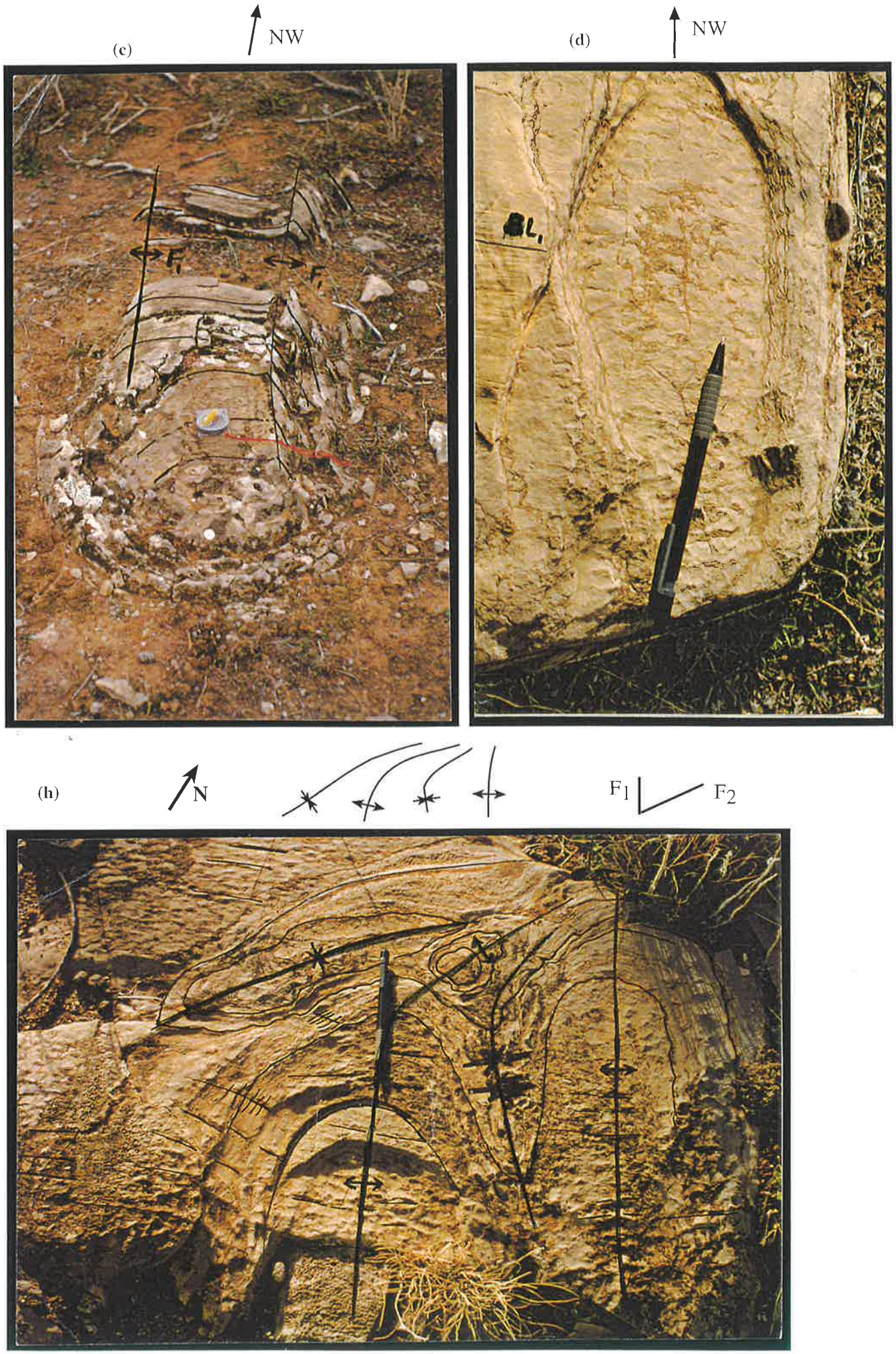

Fig. 4.2: Cont., (c) Box fold. (d) Slip-lineation (L_1) defined by striations near perpendicular to the fold axis. (h) Superimposition of folds, showing dextral rotation of F_1 axes to F_2 orientation.

limb angles vary from 70°-180°, thus are open to gentle folds with steep to upright axial planes which strike NW.

A prominent bedding-slip lineation (L_1) defined by striations appears on the limbs of the folds but disappears along the hinge (Fig. 4.2d). The striations are oriented NE and they vary in thickness from a fraction of a millimetre to a few millimetres, while spacing is from less than a millimetre to a centimetre.

The mean fold axis derived from bedding plunges 16°-> 320° (Fig. 4.2e) and that from measured plunges 19°->325° (Fig. 4.2f). The bedding-slip lineation is generally at right angles to the fold axes (Fig. 4.2g). The fine-grained texture of the calcareous Trezona Formation has possibly resulted in the formation of the fine striations during bedding-slip. Application of smoothness and roughness technique (Billings, 1972; Petit, 1987; Will and Wilson, 1989; Lin and Williams, 1992) over the lineations of both limbs show tectonic transportation towards the axial trace.

These gentle folds show NW trending axial traces and bedding-slip lineations near perpendicular to the fold axes, which suggest a tectonic origin resulting from NE-SW compression during the D_1 deformation. However, these F_1 folds do not show any vergence, unlike those studied in the Bunkers Graben.

4.3 Fault-bend folds

Parallel kink-style folds classically are known to form during fault-related folding. One of the simplest forms of such folds was described by Suppe (1983, 1985). The author explained that fault-bend folds are accommodation folds, which must form in association with the displacement of beds adjacent to non-planar faults.

Two types of basic fault-bend folds have been identified (Suppe 1985):

- A *rollover* or a *reverse drag* fold, which forms when the hanging wall tends to collapse against the footwall creating a hanging wall anticline.

- The other type is associated with stepping up of thrust faults from lower to higher décollement horizons (Fig. 4.3a&b). Here the folds are confined to the upper fault block and terminate at the fault surface. The axial surfaces of such kink folds, formed due to thrusting along ramps, terminate at the bends in the fault because the bends cause the

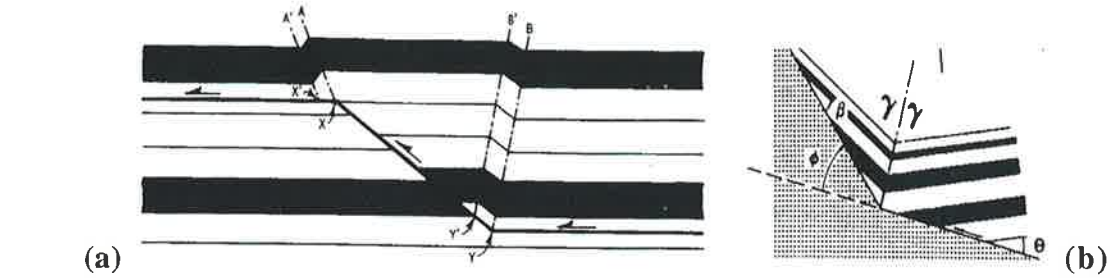

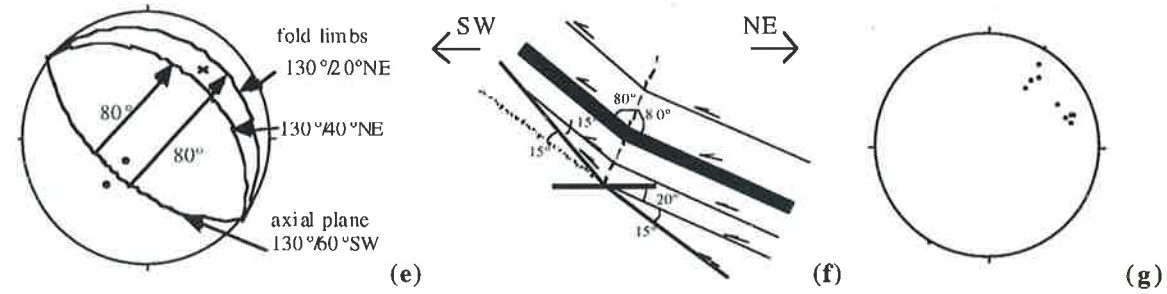

Fig. 4.3: (a) Development of fault-bend kink folds in response to a simple step décollement, (b) Fold and fault shape defining cut-off angles (after Suppe 1985). (c) Photograph of a parallel-kink style fold on the northwestern hanging wall of the 1A Lode, Level 6 of the Oraparinna Mine. Stains of white barite left on the wall belong to the 1A Lode. (d) See over leaf. (e) Stereonet for the parallel-kink style folds at (c), the 10 m mark of the section in Figure d. Dots represent poles to bedding planes while the cross represents pole to axial plane. (f) Schematic diagram of kinks with calculated detachment angles for the Oraparinna Mine area, constructed for $\theta=\phi=15°$. (g) Bedding-slip lineation (L_1) for the Oraparinna Barite Mine showing average direction of 24°->051°, 10 data.

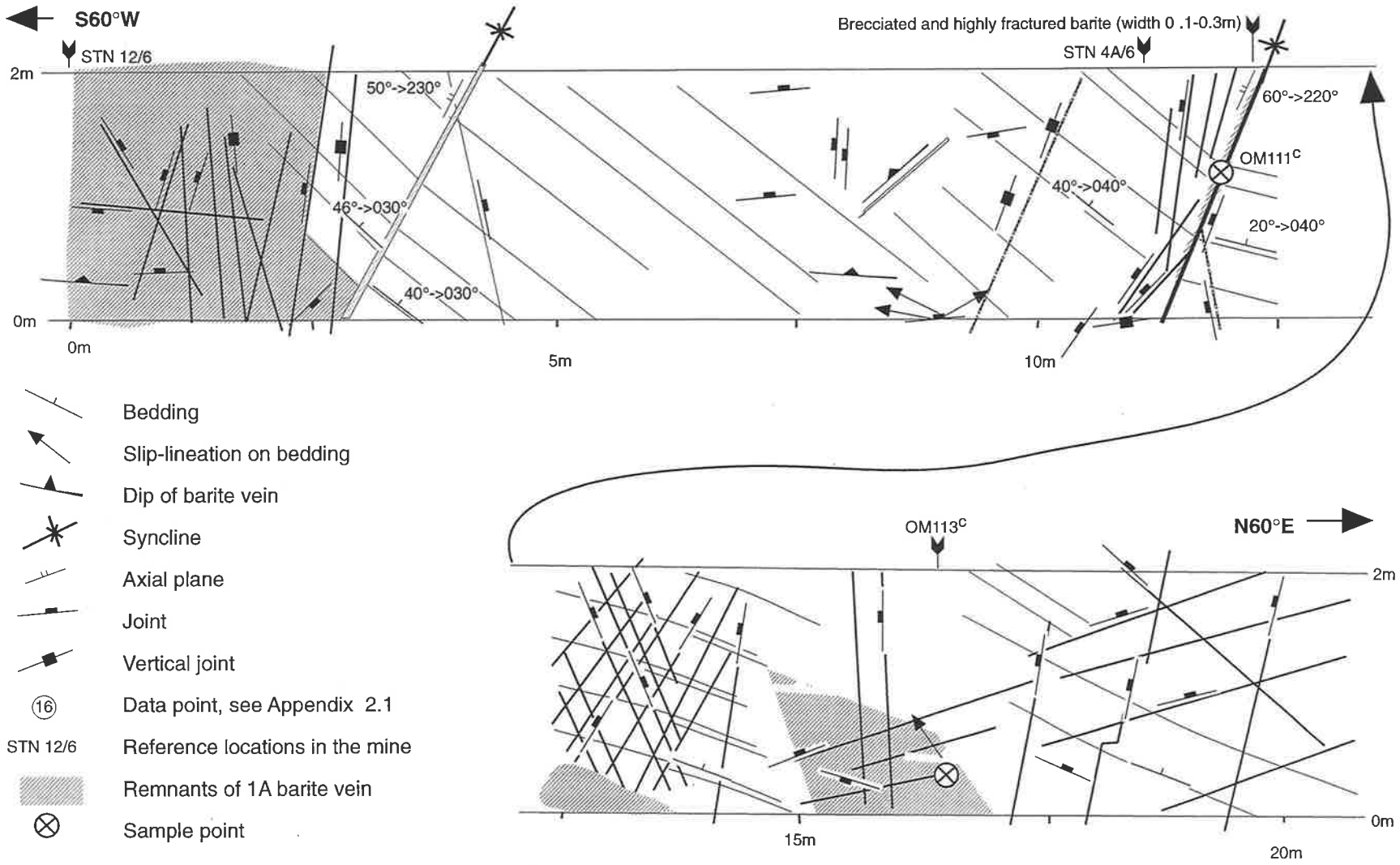

Fig. 4.3d: Parallel-kink style folds of the Brachina Formation, adjacent to the 5 m and 10 m marks (Fig. 4.3c) of the hanging wall contact of the 1A Lode, Level 6 of the Oraparinna Barite Mine. Some of the unmined barite belonging to the 1A Lode also remains.

folding (Suppe 1985). Parallel folding requires a significant amount of layer-parallel slip to accommodate the deformation while preserving layer thickness with overall deformation of simple shear style.

The Oraparinna Barite Mine exhibits some well-developed parallel kink-style folds in the thinly bedded Brachina Formation, and can be seen along NE-SW sections of its underground (Fig. 4.3c). One 20 m long section was mapped along the northern hanging-wall of the 1A Lode on Level 6 and included parallel kink-style folds (see close to the 5 m and 10 m marks of Figure 4.3d).

The parallel kink-style folds in the Barite Mine, like those described from the Pine Mountain thrust sheet in the Appalachian mountain belt (Rich 1934) or the schematic fault-bend folds of Suppe (1983, Fig. 4.3a) have well defined comparable geometric properties. They all have leading limbs with steeper dips compared to the trailing limbs, which have gentle dips, and the two axial angles are equal ($\gamma_1=\gamma_2$, Fig. 4.3b). Most natural fault-bend folds especially in fold-and-thrust belts are more complex, particularly due to multiple imbrications (Suppe, 1985; Al Saffar, 1993). Parallel folding requires that, if the bed length and the layer thickness are conserved during fault-bend folding, as occurs with the low strain examples from the Barite Mine, then according to Suppe 1983, the precise relationship between fold shape and fault geometry can be found in terms of cut-off angles, (θ= initial cut-off angle, β= final cut-off angle) and ϕ, the angle of fault bending.

The kink fold at the 10 m mark of Figure 4.3d was analysed in terms of its structural geometry. Both limbs strike N40°W but dip 20°NE and 40°NE, indicating a fold axis of F_1 generation (00°->310°, Fig. 4.3e). The axial plane strikes N40°W and dips 60°SW bisecting the obtuse interlimb angle. The angle between each limb and the axial plane is 80°.

θ, β and ϕ angles were calculated for the parallel kink-style folds using the Suppe (1983) method. Both results show the leading cut-off angle, $\phi \sim \theta \sim \beta \sim 15°$. This indicates a likely 15° cut-off angle for a subcrop décollement below the Oraparinna Mine in the Bunkers Graben. The bedding-slip movements defined by groove lineations (L_1), subjected to the smoothness and roughness technique on congruous steps (Billings, 1972; Petit, 1987; Will and Wilson, 1989; and Lin and Williams, 1992), indicate SW vergence. The L_1 lineation plunges shallowly to the NE in the mine (Fig. 4.3g).

The leading limbs with steeper dips compared to the trailing limbs of these horizontal F_1 fault-bend folds showing SW verging L_1 bedding-slip lineation suggest southwestward tectonic transportation of the Brachina Formation, during the NE-SW compression of the D_1 deformation.

4.4 Listric-thrust faults

An example of a low angle listric-thrust fault was studied on the western limb of the F_1 Enorama Anticline, 2 km SW of the Enorama Diapir, alongside the Oraparinna - Blinman road. The fault is exposed on a section of a 10 m high, steep creek bank of the thinly laminated Enorama Shale (Fig. 4.4a). It continues along strike on the surface, forming a shallow ditch that is approximately perpendicular to the section. Therefore, the section is approximately the profile plane of the fault. The fault strikes N40°W and lies nearly horizontal on the bottom of the section, and the dip increases gradually to 25° SW at the surface and suggests a listric-thrust fault. A 20 - 30 cm thick crush zone occupied by fault-breccia, composed of powdered crumbly fault rock of the Enorama Shale, occurs on the fault (Fig. 4.4b). Visible fault-breccia fragments comprise about 70% of the fault zone mass. The angular breccia clasts vary from fine grains up to 1 cm in size and are loosely bound in the shaley matrix. The fault zone exhibits gouge fabric (McClay, 1987), indicating tectonic movement verging NE (Fig. 4.4b).

The footwall block strikes N35°W and dips 12°SW, and mildly folds into a wavelength up to 4 m and amplitude up to 0.4 m (Fig. 4.4a). The fold axes are horizontal, trend 315°, and therefore are F_1 folds, while the axial planes are nearly vertical (Fig. 4.4c). The hanging-wall strikes NS, dips 10°W, and remains unfolded (Fig. 4.4a&f). A bedding-slip lineation appears on bedding and is defined by congruous steps and striations (Fig. 4.4d). The lineation is oriented NE – SW, near perpendicular to the F_1 fold axis, and is therefore recognised as L_1 (Fig. 4.4e). The smoothness and roughness technique (Billings, 1972; Petit, 1987; Will and Wilson, 1989 and Lin and Williams, 1992), applied on the congruous steps indicate a northeasterly vergence, towards the axial trace of the Enorama Anticline.

4.5 Bedding-slip lineations

Two prominent bedding-slip lineations namely L_1 and L_2 were widely formed in the central Flinders Ranges during the D_1 and D_2 deformations respectively. These can be most clearly seen on wet bedding surfaces with the aid of a hand lens. The morphology, geometry and kinematic style of L_1 bedding-slip lineations on bedding surfaces were further studied on both limbs of the Enorama-Oraparinna Anticlines.

(a)

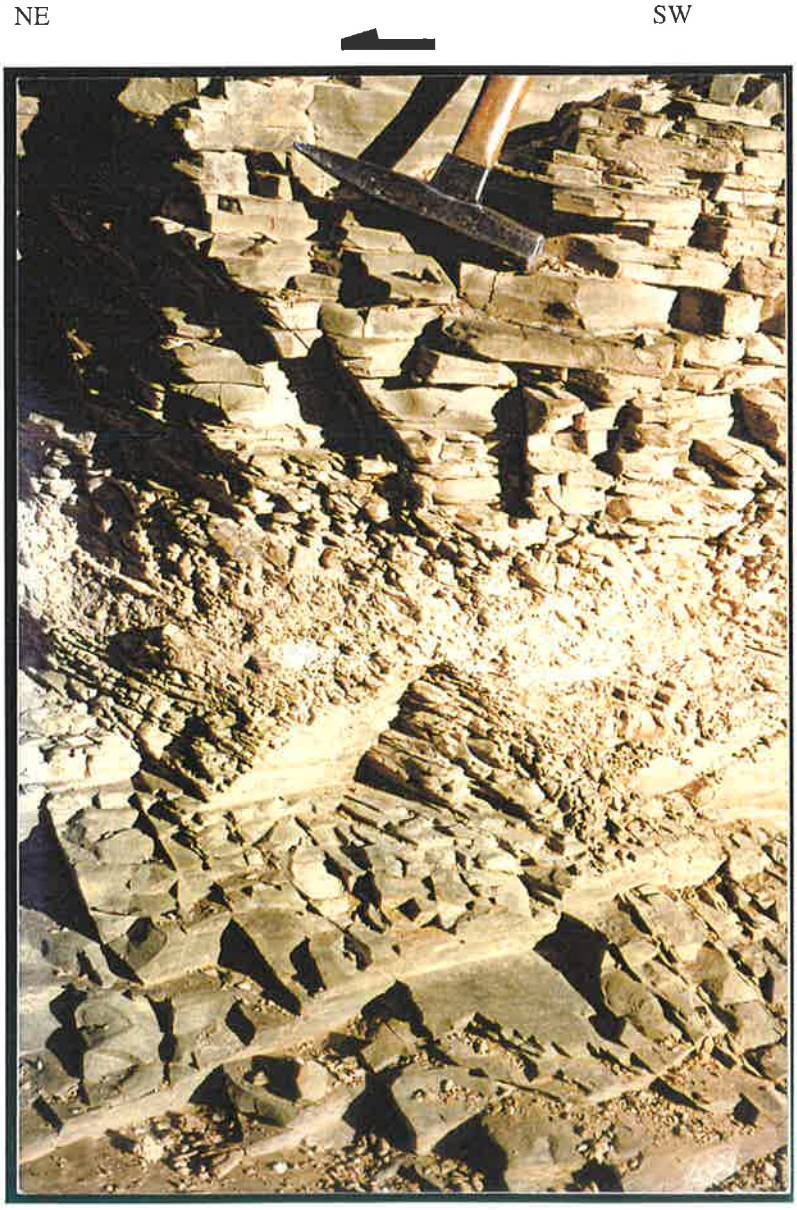

(b)

Fig. 4.4: Minor ramp thrust fault in the Enorama Shale, exposed at a crossing of a branch of the Enorama Creek and the Wilpena - Blinman Road, 2.2 km north of the turn to the Brachina Gorge Geological Trail. (a) Pale colour along the arrow of the photograph shows the brecciated decollement surface. (b) Fault zone breccia between the hanging wall and footwall showing cataclasis of the host shale. Contd....

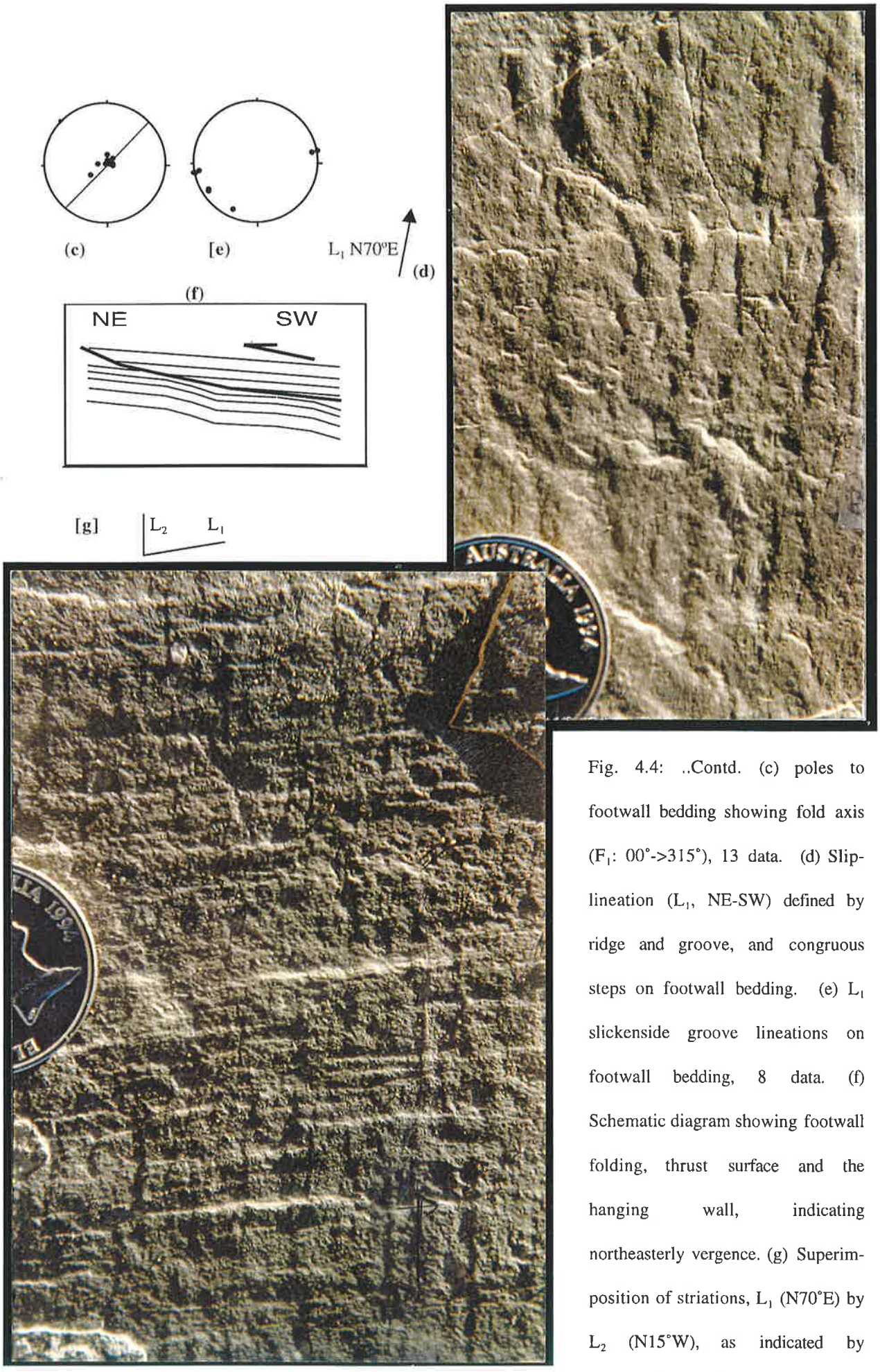

Fig. 4.4: ..Contd. (c) poles to footwall bedding showing fold axis (F_1: 00°->315°), 13 data. (d) Slip-lineation (L_1, NE-SW) defined by ridge and groove, and congruous steps on footwall bedding. (e) L_1 slickenside groove lineations on footwall bedding, 8 data. (f) Schematic diagram showing footwall folding, thrust surface and the hanging wall, indicating northeasterly vergence. (g) Superim-position of striations, L_1 (N70°E) by L_2 (N15°W), as indicated by overprinting of ridge and grooves.

The L_1 bedding-slip lineations on the western limb of the Enorama F_1 Anticline were examined on the green-grey siltstones of the Wonoka Formation, along the Brachina Gorge Geological Trail (Fig. 4.5a). These appear as ridge-in-groove type slickenlines, with the grooves varying in thickness from a fraction of a millimetre to 4-5 millimetres (Fleuty, 1975; Bates and Jackson, 1987 and Means, 1987). The grooves commonly have formed due to dragging of broken pieces between bedding surfaces therefore, groove thicknesses usually depend on the size of the broken pieces dragged during gouging. The bedding surfaces also contain polished thin flakes, formed during gouging. Bedding strikes N-S and dips 30°W, and shows an average L_1 lineation, plunging 30°->260°. Use of the smoothness and roughness technique (Billings, 1972; Petit, 1987; Will and Wilson, 1989; Lin and Williams, 1992) indicates movement in a direction of N80°E, towards the axial trace of the Enorama Anticline.

The L_1 bedding-slip lineations on the eastern limb of the Enorama F_1 Anticline were also studied. The boundary between Etina Formation and overlying Enorama Shale on the eastern limb of the Enorama Anticline was studied along the Nanpena Spring Track (Map2; Fig. 4.5b). The weak Enorama Shale is eroded on the competent and siliceous Etina Formation, leaving a rough and uneven boundary surface produced due to gouging. The boundary is parallel to bedding of the Etina Formation, which strikes N45°W and dips 40°NE. This surface contains angular to well-rounded clasts of gouge material including breccia, gravel and cobbles up to 10 cm in diameter, dominantly of the Etina Formation (Fig. 4.5b). Some of the well-rounded gravels appear like golf balls with uneven surfaces. The gravels are attached intact onto the boundary surface by a ground shaley matrix of the Enorama Shale. Occurrence of angular to well-rounded gravel between the two formations indicates extensive gouging with simultaneous breaking of new clasts. The groove lineations on the surface plunge 30°->N20°E. Use of smoothness and roughness technique (Billings, 1972; Petit, 1987; Will and Wilson, 1989; Lin and Williams, 1992) on the ridge-in-grooves indicates the upper surfaces moving up along the bedding surfaces in a direction of S20°W, towards the axial trace of the Enorama Anticline.

The L_1 bedding-slip lineation data collected from all over the central Flinders Ranges were contoured on stereograms (Fig. 4.6a). The L_1 ranges from NNE to east and the mean L_1 plunges 24°->033° on the eastern limb of the Enorama - Oraparinna F_1 Anticlines and 31°->255° on the western limb. This lineation is extremely common on both limbs of these major anticlines, showing vergence towards the major axial trace but disappears on the hinge zone, as examined between the Blinman and Enorama Anticlines, suggesting the flexural slip nature of folding.

(a)

(b)

Fig. 4.5: L_1 Slip-lineation on bedding surfaces of (a) western and (b) eastern limbs of the Enorama Anticline. (a) Ridge and grooves (X10) on the very fine grained siltstones of the Wonoka Formation along the Brachina Gorge. The arrow shows the movement direcion of the upper layer, N80^{o}E. (b) Upper boundary of the Etina Formaton, 5.3 km NE of the Enorama Diapir, along the Nanpena Spring Track. Well rounded gravel (see to the left of the black arrow) derived from the same formation is attached to the rough bedding surface, which contains striations, showing movement direction of the upper layer is S20^{o}W.

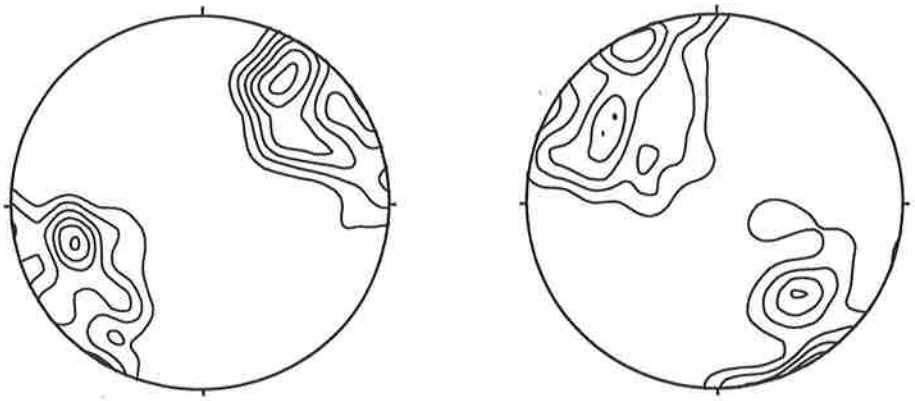

(a) (b)

Fig. 4.6: Slip lineation (L_1 and L_2) data for the central Flinders Ranges. (a) Mean directions of L_1 on the western and eastern limbs of the F_1 Enorama - Oraparinna Anticline plunge 30°->254° and 23°->032°, respectively. 65 data, contoured at 1,2,3,..,5 times uniform. (b) Mean L_2 plunges 30° ->310° and 36° ->139°. 59 data, contoured at 1,2,3,..,5 times uniform.

4.6 Discussion

4.6.1 Vergence of the Bunkers Graben

The minor structures within the Bunkers Graben indicate vergence towards the apex, as indicated by the occurrence of:

(a) NW to NNW trending fault-bend folds in the Oraparinna Mine, with steeper fore limbs than back limbs,

(b) asymmetric minor to micro-scale gentle folds adjacent to the apex, and

(c) L_1 bedding-slip lineations within the graben.

Therefore, a southwestward tectonic transportation of the graben sequences towards the apex is evident. Further, these structures suggest tectonic thickening of graben sequences during southwestward thrusting of the D_1 deformation. The analysis of fault-bend folds suggests the tectonic movement of sequences along a low-angle décollement surface, dipping 15°NE. This is in agreement with the fault-propagation fold model suggested for the Enorama F_1 Anticline, indicating a low angle décollement beneath the eastern limb (Fig. 3.8a). Therefore, both the Bunkers Graben and the eastern limbs of the Enorama – Oraparinna Anticlines, suggest low-angle décollements, on which the sequences moved towards the axial trace. Thus, a working model can be suggested for the Bunkers Graben, showing the increase of dips from gentle, on the open-end, to steep on the apex, as a result of fault-bend folding and extensive bedding-parallel shear (Fig. 3.5b). However, detailed mapping in the graben would be required to produce a comprehensive section. The model suggests syntectonic thickening rather than synsedimentary thickening, speculated by Lemon (1988) for the Bunkers Graben sequences.

4.6.2 Relevance of minor structures to the major F_1 Anticlines

The minor structures on the western limb of the Enorama F_1 Anticline include:

(a) symmetric folds,

(b) listric-thrust faults producing breccia and showing gouge fabric (McClay, 1987), and

(c) bedding-slip lineation.

Those on the eastern limb of the Enorama – Oraparinna F_1 Anticlines include:

(a) asymmetric, minor to micro folds adjacent to the apex of the Bunkers Graben,

(b) fault-bend folds in the Oraparinna Mine, and

(c) bedding-slip lineation.

All the minor structures on both limbs, except bedding-slip lineation, show prominent orientation between NW-NNW, parallel to that of the Blinman – Enorama - Oraparinna F_1 Anticlines. Except for the symmetric folds on the western limb; all the others show vergence towards the major axial trace. The L_1 bedding-slip lineations disappear over the major fold hinge, as observed between the Blinman and Enorama Anticlines. Therefore, these minor structures are parasitic to the major F_1 anticlines from Blinman to Oraparinna and suggest tectonic transportation of sequences towards the major axial trace. They also suggest tectonic thickening of the sequences on the limbs of the F_1 Anticlines, even though Lemon (1988) interpreted synsedimentary thickening during rise of the diapirs. Therefore, a fault-propagation fold model explaining all these characters including symmetric folds on fore limbs and asymmetric folds on back limbs, as well as tectonic thickening, is put forward in Chapter 6.

The symmetric gentle folds within the Trezona Formation have been previously identified as primary stromatolite structures by Preiss (1987). Evidence for a tectonic origin of these folds is discussed in Chapter 5.

D_2 MINOR STRUCTURES OF THE FLINDERS RANGES

5.1 Introduction

This chapter examines minor D_2 structures formed by the NNW - SSE compression of the D_2 deformation (see Chapter 3). Recognition of minor D_2 structures is difficult, because of the low intensity of the deformation in the Ranges, which leads to some confusion with primary sedimentary structures (see Chapter 4). The D_2 tectonic structures studied include parallel folds, kink folds and bedding-slip lineations. F_2 fault-propagation/detachment folds were also studied but are considered separately in Chapter 6 in relation to the formation of the diapirs.

5.2 F_2 Parallel folds

F_2 minor parallel folds are wide-spread in the central Flinders Ranges. Their fold axes predominantly trend between NNE and NE, but show a wide range in orientation, varying from NNE to ESE (Table 5.1, Figs. 5.1a, b, c, d). These folds generally plunge gently but increase their plunge angles to moderate adjacent to diapirs or apices of graben structures.

Table 5.1: Examples of minor parallel F_2 folds from the central Flinders Ranges.

Location	Host formation	Strike and dip of host formation	Plunge and plunge direction of fold axis(F_2)	Fig. no.
1.6km NE of Enorama Diapir, along the Nanpena Spring Track	Tapley Hill Formation	N70°W/40°N	40°->020°	5.1a
750m NE of the apex of the Bunkers Graben	Brachina Formation	N30°W/60°E	60°->030°	5.1b
Turley Lode, adjacent to the apex of the Bunkers Graben	Brachina Formation	N45°W/35°S	59°->036°	5.1c
1.5km NE of Oraparinna Diapir, along the Little Patterton Spring Track	Sunderland Formation	N30°W/40°N	33°->106°	5.1d

5.2.1 F_2 parallel folds in the Oraparinna Mine

A large number of parallel folds hosted by the thinly bedded Brachina Formation were studied in the Oraparinna Mine. The wavelengths of the folds vary from 1 m to 10 m, while the amplitudes vary from 0.5 m to 5 m. The fold intensity, defined by wavelength and amplitude, commonly

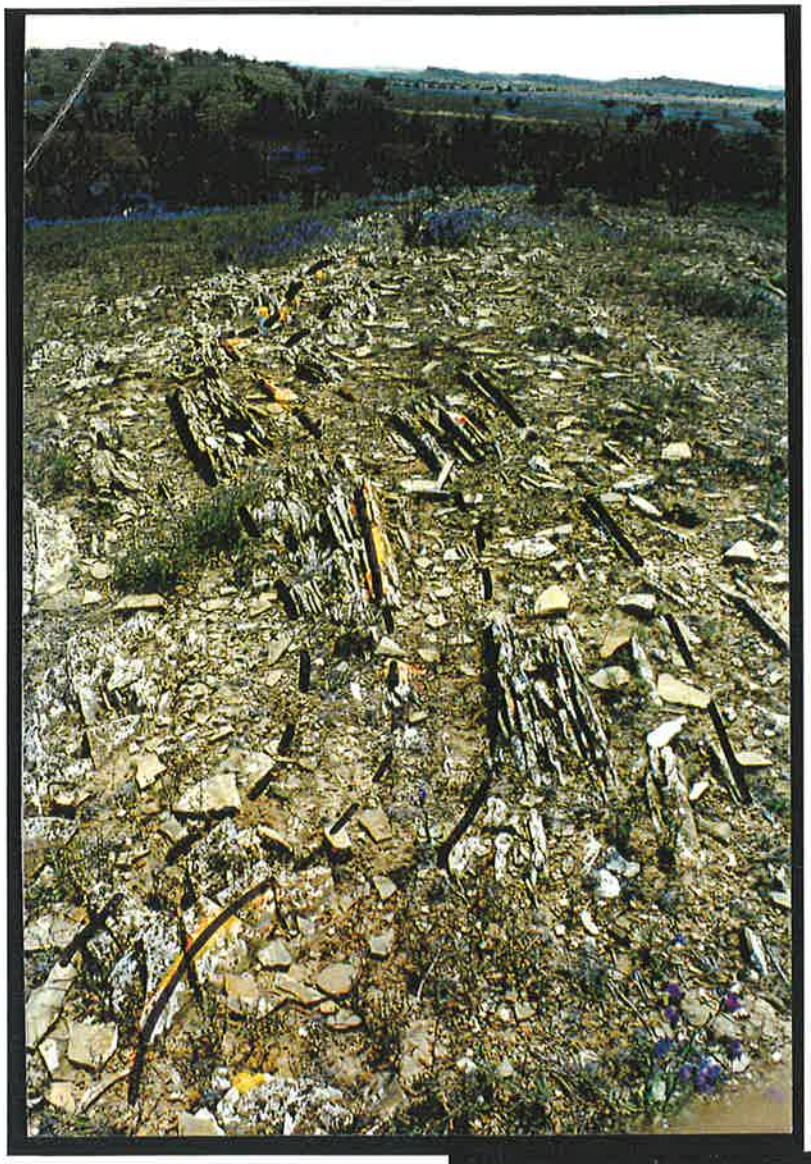

(a)

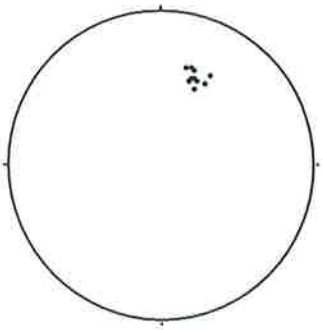

Fig. 5.1: Photographs and stereograms for the F_2 gentle folds of the central Flinders Ranges. (a&b) fold axes data; (c&d) bedding data. (a) 2 km east of the Enorama Diapir, along Nanpena Spring Track. Fold axis plunges 40°->020°, 10 data. (b) 750 m NE of the apex of the Bunkers Graben. Fold axis plunges 60°->030°, 6 data. Both a&b were photographed looking SE. Cont..

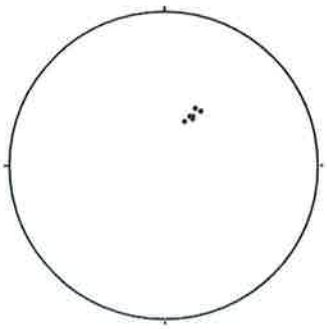

(b)

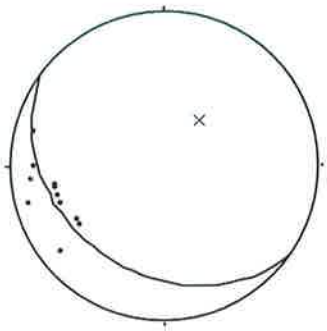

(c)

Fig. 5.1: Cont.., (c) Stereogram for the bedding at the Turley Lode, apex of the Bunkers Graben. Fold axis plunges 59°->036°, 12 data. (d) Photograph and stereogram for the F_2 gentle folds. 1.5 km NE of Oraparinna Diapir along Little Patterton Spring Track. Fold axis plunges 33°->106°, 48 data. Photographed looking NW.

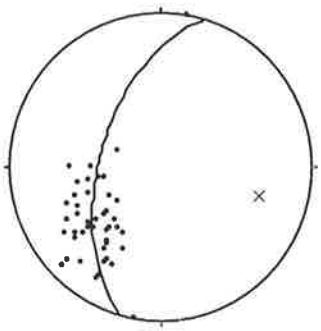

(d)

increases towards steeply dipping and northeasterly striking thick barite veins in the mine. The gentle folds commonly consist of asymmetrical, long and short limbs and at times take the shape of curvy-hinged, kink-style folds (Fig. 5.2a,b).

Bedding generally strikes EW and dips 40°N in the mine. The mean long limb of the folds strikes N83°W and dips 38°N, while the mean short limb strikes N3°W and dips 40°E, with an interlimb angle of 132°, indicating gentle folds (Fig. 5.2c). The mean fold axis plunges 33°->054°, thus these are F_2 folds. The mean axial plane strikes N45°E and dips steeply to NW. An average angle of 61° between the axial plane and bedding outside the kink fold band (α), and of 68° between the axial plane and bedding inside the fold band (β, Fig. 5.2d&e) was measured. This satisfies the criteria of $\alpha \leq \beta < 90°$, developed for the contraction mechanism of formation of kink bands (Ramsay and Huber, 1987). Thus, these folds have formed as a result of contraction.

A strongly developed bedding-slip lineation (L_2), defined by striations and congruent steps (Fleuty, 1975; Bates and Jackson, 1987; Means, 1987) occur more prominently on limbs than on hinges of these folds (Fig. 5.2f). These lineations are oriented NW and are near perpendicular to the F_2 fold axes (Fig. 5.2g).

5.2.2 F_2 folds of the barite mines around the Oraparinna Mine

Geological maps prepared by the Mines Department (Plan No. 80-241), detailing the barite lode systems and hosts adjacent to the Oraparinna Mine were studied for their F_2 folds (Fig. 2.5). These folds essentially are gentle and parallel folds, as was evident in the field. Bedding data collected during the present investigations were also included in the analyses. Stereograms were plotted for the host bedding data of the Belsen Lode, Western Lodes, Oraparinna Mine, Bainbridge Lodes and Roberts Lode. These are located on the northern hanging wall of the ENE trending major fault zone in the area. The area immediately south of the fault zone does not contain major barite lodes but the bedding from that area was also plotted on a stereogram for comparison. The lodes show decreasing distances of 700, 600, 350, 300, and 150 m respectively, from the fault zone. The host F_2 fold axes are oriented at 021°, 037°, 044°, 044°, 040° respectively, and the trend of the fault zone is oriented at 064°, while that of the area south of the fault zone is oriented 033° (Fig. 5.3, Table 5.2). These data probably show a dextral rotation of the F_2 fold axes on the northern hanging-wall, as it approaches the fault zone. Maximum rotation is achieved at the fault zone, whilist the south of the fault zone shows little relative rotation.

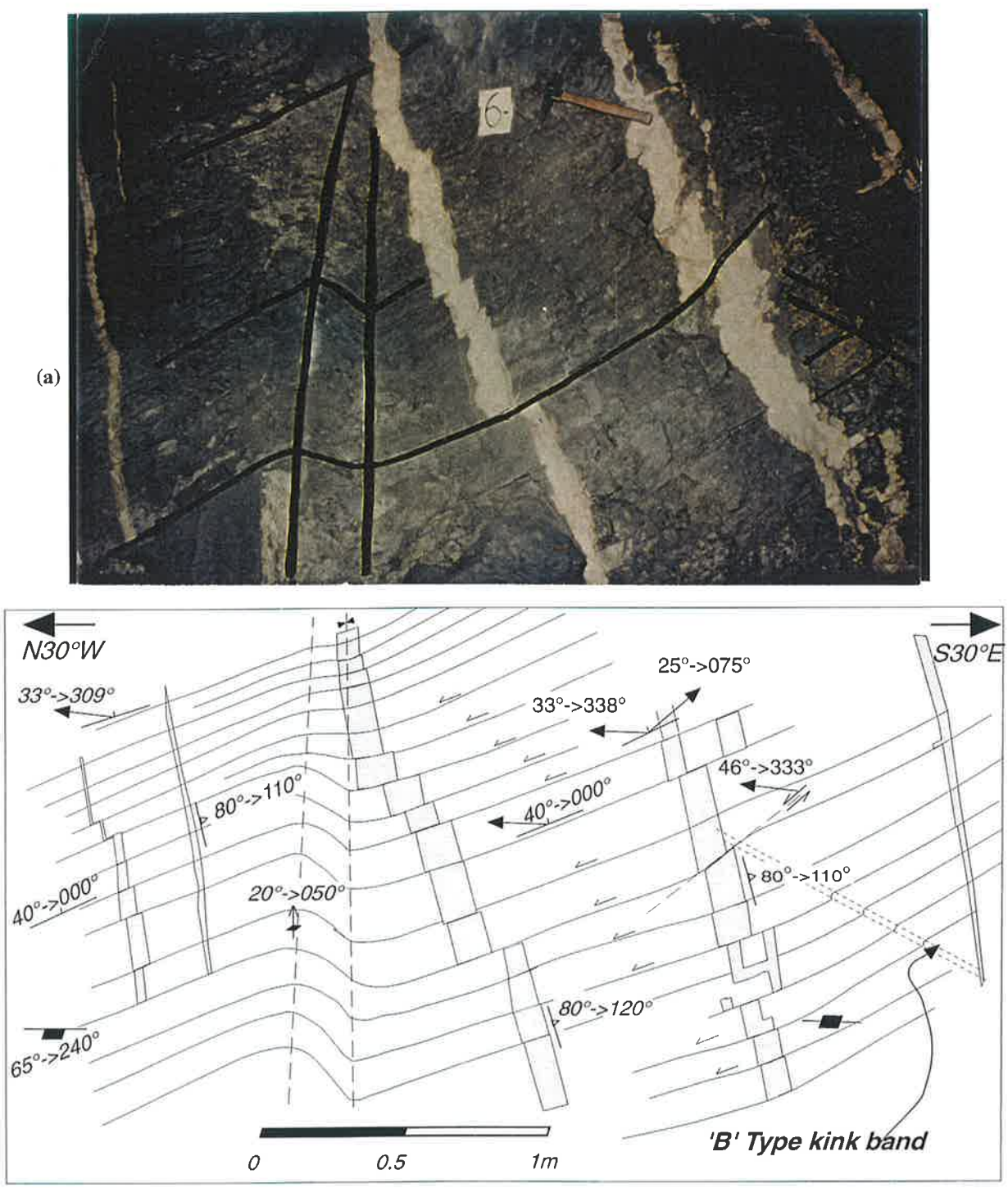

Fig. 5.2: (a) Photograph and (b) sketch of an underground vertical tunnel wall of the Brachina Formation, 15 m east of the 1A Lode at level 6 of the Oraparinna Mine, showing an upright asymmetric fold, thin barite veins of 1D Type sheared along bedding and a 'B' Type kink band with axial plane striking N10°W and dipping 50°E. (c) A stereogram of the section showing the northerly dipping long limb, easterly dipping short limb and the fold axis plunging 33°->054°. 34 data; contoured at 1,3,5,.. times. Cont..,

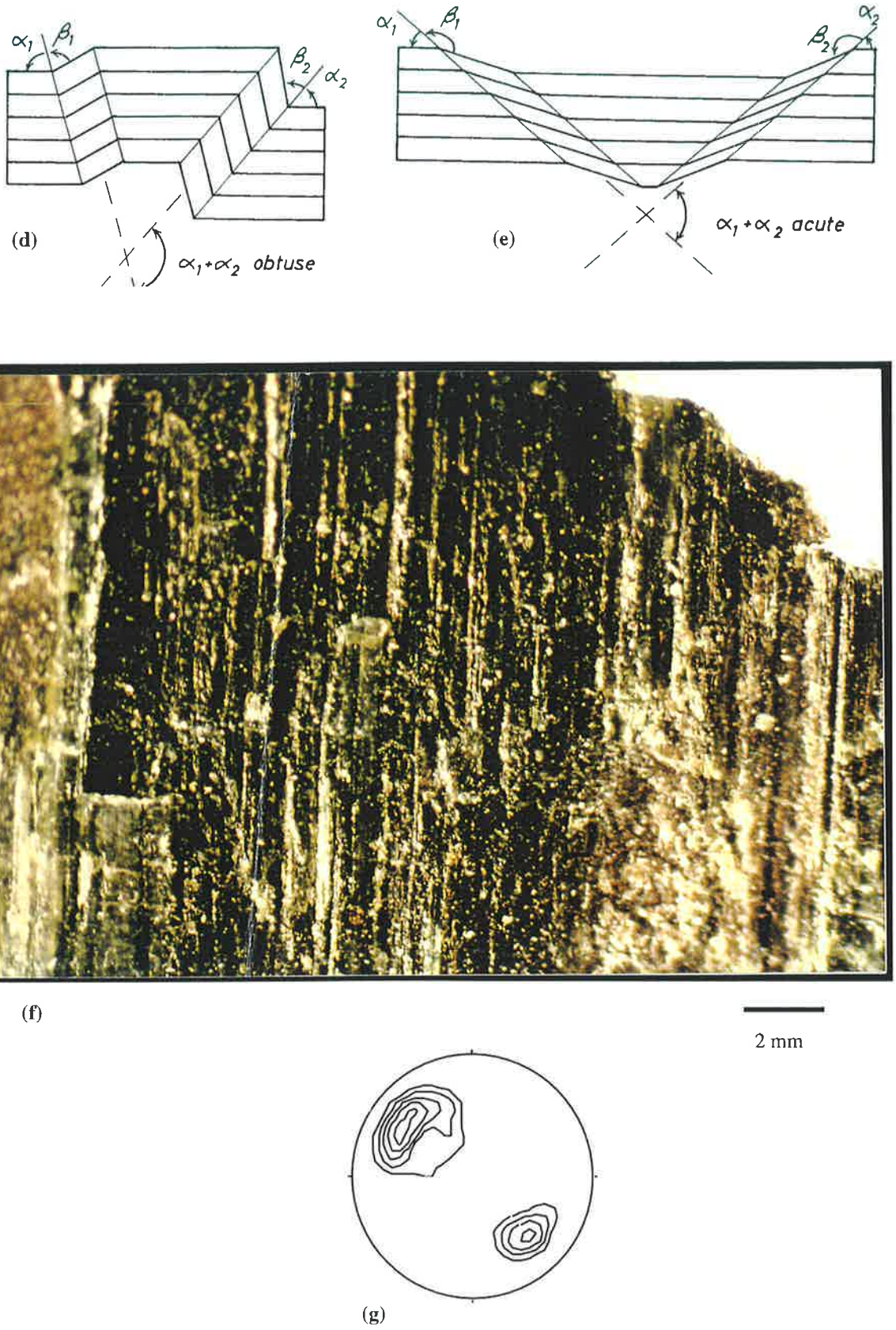

Fig. 5.2: Cont.., Geometric features of (d) contractional and (e) extensional kink bands (after Ramsay and Huber, 1987). (f) Striations and congruous steps of the bedding slip-lineations (L_2) of the mine, indicating (g) mean plunge and orientaions of 31°->309° and 33°->127°. 37 data, contoured at 2,3,4,5 times uniform.

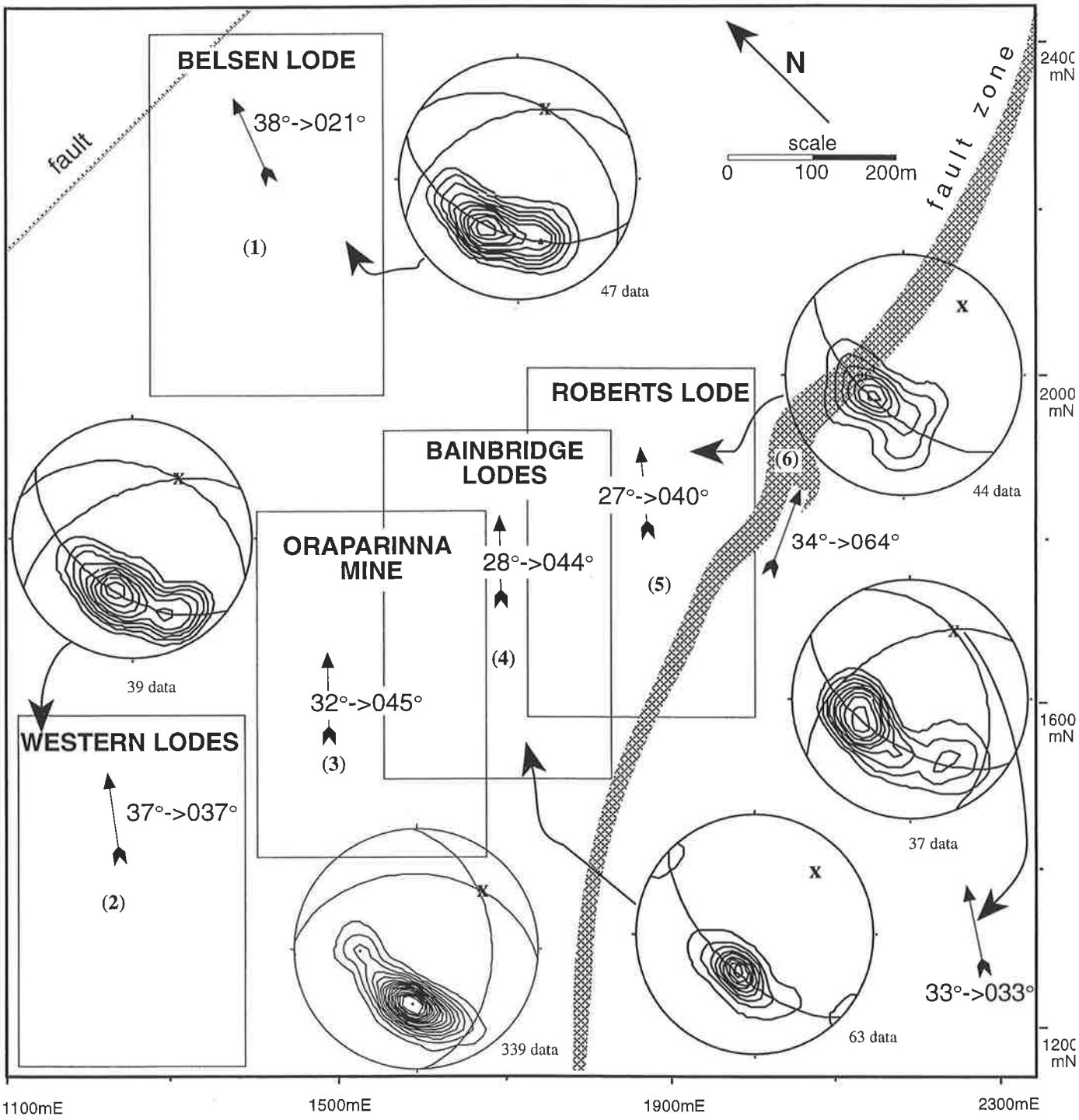

Fig. 5.3: (a) Stereograms for the bedding of the host Brachina Formation at satellite barite vein systems of Oraparinna. F_2 fold axis denoted by (**x**) in the stereograms are marked with an arrow in the rectangle area defined for each vein system. All the data were contoured uniformly: (**1**) Belson Lode, 1,3,5,7 times;(**2**) Western Lodes, 1,2,3,...,7 times; (**3**) Oraparinna Mine 1,2,3,...,8 times; (**4**) Bainbridge Lodes, 1,4,7,..,19 times; (**5**) Roberts lode 2,3,4,..,8 times and south of fault zone, 1,2,3,...,7 times. The great circles for long and short limbs of the folds are also marked where possible. Base map modified from plan No. 80-241, Department of Mines, SA. (b) NE quarter of a stereogram showing dextral rotation of host fold axes (**x**) towards (**6**) the fault zone; except that of the Roberts Lode (**5**).

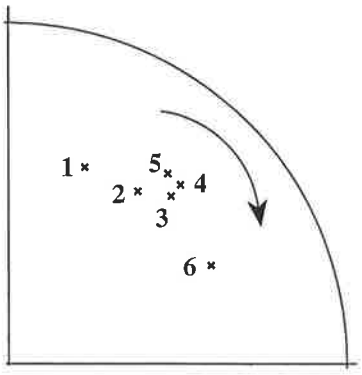

(b)

Table 5.2: The F_2 gentle fold axes of the Oraparinna Mine and associated areas.

Lode name	Distance to the fault zone (m)	Mean plunge and plunge direction of the host fold axis(F_2)	No. of data
Belson Lode	700	38°->021°	24
Western Lodes	600	37°->037°	19
Oraparinna Mine	350	32°->044°	339
Bainbridge Lodes	300	28°->044°	63
Roberts Lode	150	28°->040°	44
Fault zone	0	34°->064°	5
South of Fault zone		33°->033°	17

Source of data: McCallum (1982).

5.3 Conjugate kink folds

Two main types of conjugate arrays of kinks have been defined by Ramsay and Huber (1987), known as contractional and extensional kink bands. The contractional type is generated by overall regional shortening of a planar fabric ($\alpha \cong \beta$, $\alpha \leq \beta < 90°$), while the extensional type forms due to layer parallel stretching of the pre-existing fabric (Figs. 5.2d&e). The sum of the angles $\alpha_1 + \alpha_2$ is obtuse for overall shortening and is acute for overall stretching.

Conjugate kink bands are sparse in the central Flinders Ranges. However, these kink bands found in the Ranges are sharp angular folds, bounded by planar surfaces. Two types of kink bands are common in the area, both dipping moderately to steeply, one approximately to NW (Type 'A') and the other to SE (Type 'B').

A good exposure of conjugate kink bands, hosted by thinly bedded Brachina Formation, was studied at the hilltop of the Oraparinna Mine (Fig. 5.4a). The kink bands are spread over a 4x2 m^2 area of the partially exposed outcrop. 'B' Type kink bands (K_1 to K_6) are common with axial planes dipping moderately to the east (Fig. 5.4b). 'A' Type bands (K_7) are uncommon with axial planes dipping steeply to the NW. Kink bands show a conjugate relationship when truncating each other. Average bedding (S_o) outside the kink bands strikes N76°W and dips 37°N (Fig. 5.4c). Bedding inside the Type 'A' (S_oA) kink bands strikes N3°E and dips 39°E while the same in the Type 'B' (S_oB) strikes N66°E and dips 69°N. The intersection of the kink bands with the bedding i.e., the kink axis plunges 31°->053°, thus demonstrates that these are F_2 folds.

The average Type 'A' axial plane at this location strikes N50°E and is vertical, while the same data for the 'B' Type kinks strike N10°E and dips 43°E (Fig. 5.4d). The angle between the axial planes, $\alpha_1 + \alpha_2$ is 118°, showing an obtuse angle, therefore, kinking has formed due to shortening (Fig.

(a)

Fig. 5.4: (a) Kink band occurrences hosted by the Brachina Formation at the hill top of the Oraparinna Mine, adjacent to the Bainbridge No. 2 Vein. Red paint along kink bands. (b) Sketch of the outcrop showing the 'A and B' Types of kink bands. Cont..,

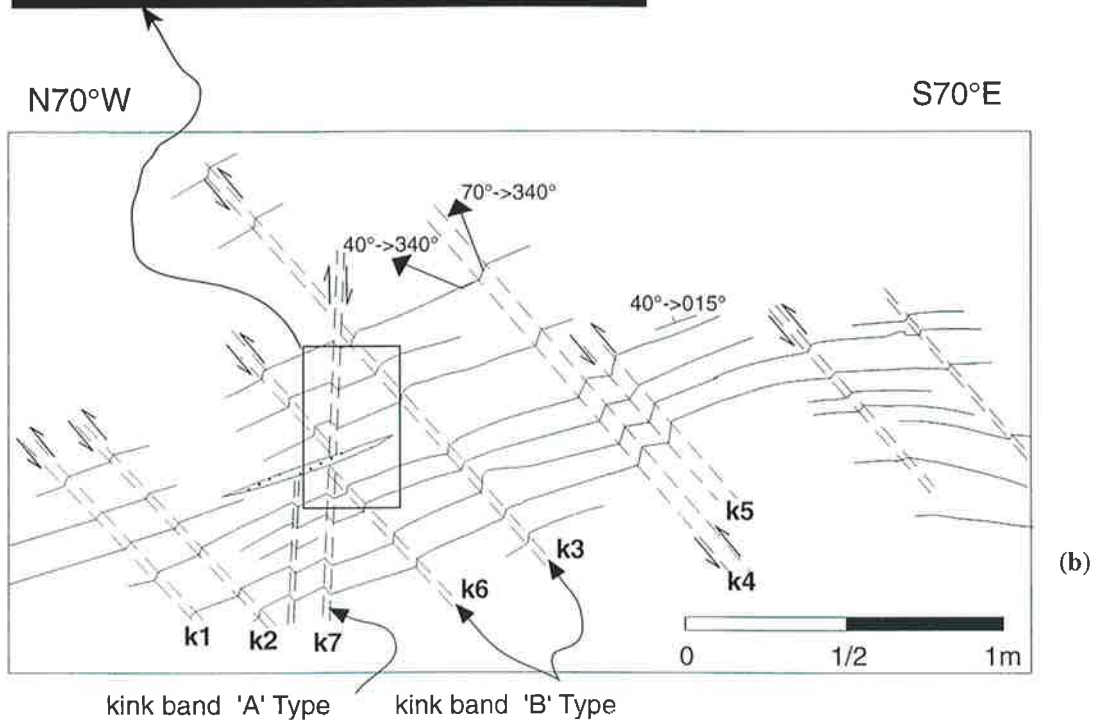

(b)

40°->015° Dip and dip direction of bedding

40-340 Plunge and plunge direction of bedding-slip lineation

Competent siliceous band

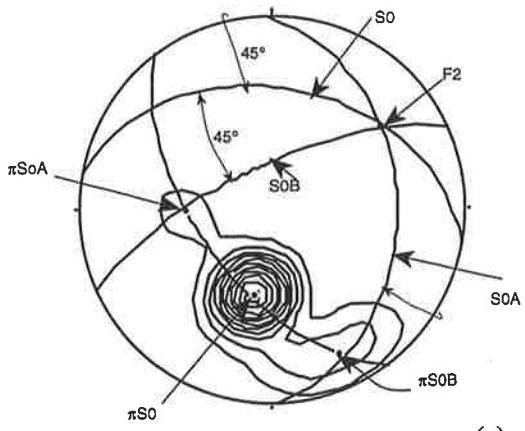

(c)

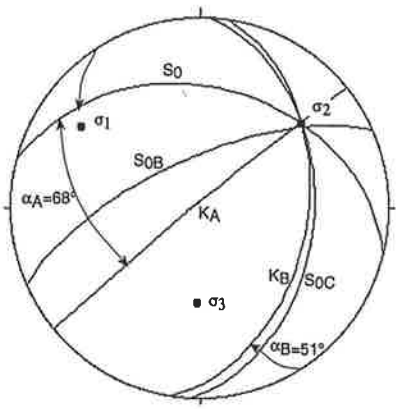

(d)

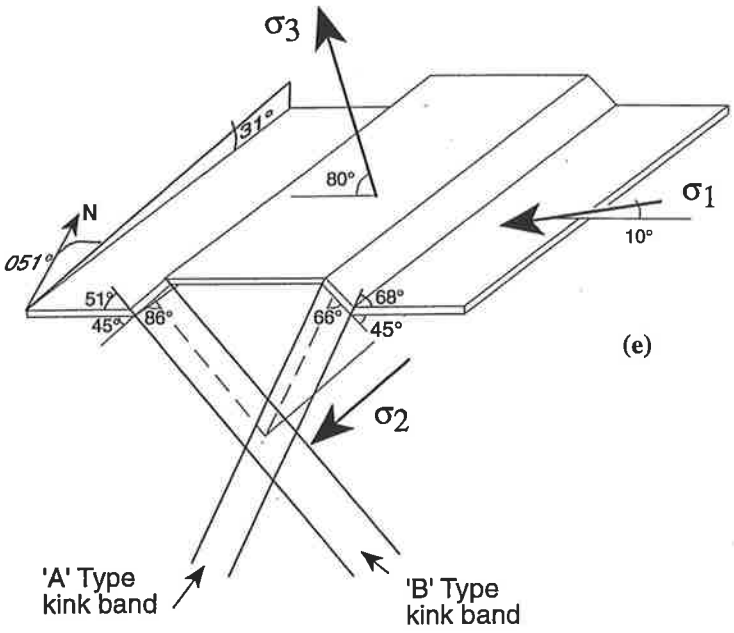

(e)

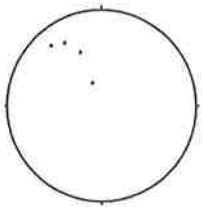

(f)

Fig. 5.4: Cont.., (c) Stereogram showing bedding (S_0), bedding within kink bands A and B, S_0A and S_0B respectively, indicating fold axis plunging 31°->053°. 37 data, contoured at 1,3,5,...x times uniform. (d) Axial planes of the kink bands (K_A and K_B) and respective angles (α_A and α_B) with bedding. Major compression directions are σ_1 (max.) 25°->304°, σ_2 (int.) 31°->051° and σ_3 (min.) 48°->182°. (e) The conjugate kink band geometry and the directions of principal stresses producing them at the hill top of the Oraparinna Barite Mine (Modified after Ramsay and Huber, 1987). (f) Bedding-slip lineation (L_2) directed northwesterly.

5.2d and Ramsay and Huber, 1987). The conjugate kink bands intersect along the kink-intersection axis which plunges 31°->053°, forming the intermediate compression axis (σ_2, Fig. 5.4d). The maximum compression axis (σ_1) is at the bisector of the obtuse angle of the kink axial planes and trends at 25°->304°. The minimum compression (σ_3) axis is at the bisector of the acute angle, and trends at 48°->182°. The σ_2 axis lies along the bedding while σ_1 and σ_3 axes make 10° and 80° angles, respectively, with bedding (S_o) at this location. Bedding shows an average angle of 68° (α_A) with 'A' Type kink axial planes and 51° (α_B) with the 'B' Type. Hence, these are asymmetric conjugate folds formed when the principle compressive stress direction is obliquely inclined to the folded surfaces (Fig. 5.4e; Ramsay and Huber, 1987).

Bedding surfaces display a prominent bedding slip lineation (L_2) oriented NW - SE, near perpendicular to the fold axes at this location (Fig. 5.4f).

Thus, the F_2 conjugate kink folds found in the Oraparinna Mine are compressional structures, indicating WNW - ESE major compression. Other F_2 conjugate kink folds studied in many other locations in the central Flinders Ranges also show compressional structures with similar orientations.

5.4 Conjugate reverse thrust faults

Excellent subcrops of reverse-thrust faults were mapped on Level 6 of the Oraparinna Mine (Figs. 5.5a&b). The faults were exposed on a 4 x 2m NW – SE vertical section, hosted by the Brachina Formation. The section contains thin barite veins striking 025° and moderately dipping SE (1D Type veins; Chapter 7), and steeply NW dipping offshoots striking 050° (1A Type veins; Chapter 7). The host is folded into gentle F_2 folds, which intensify between thick barite veins in the section. The fold axes plunge 32°->037°, which is nearly parallel to the intersection axes of barite veins in the mine (Fig. 5.5c, Chapter 7).

The whole section is sheared along reverse-thrust faults, comprising flat- and link- types. The flat-faults strike N75°E and dip 35°N and are approximately parallel to bedding or the long limbs of gentle F_2 folds (Fig. 5.5d). The link-faults strike N10°W and dip 40°E and truncate bedding at shallow conjugate angles. Both types of faults intersect along an axis plunging 26°->023°, therefore, belong to the D_2 deformation. The mapped section here is nearly perpendicular to the intersection axes of the reverse-thrust faults as well as barite veins and the axes of F_2 folds. The link-faults

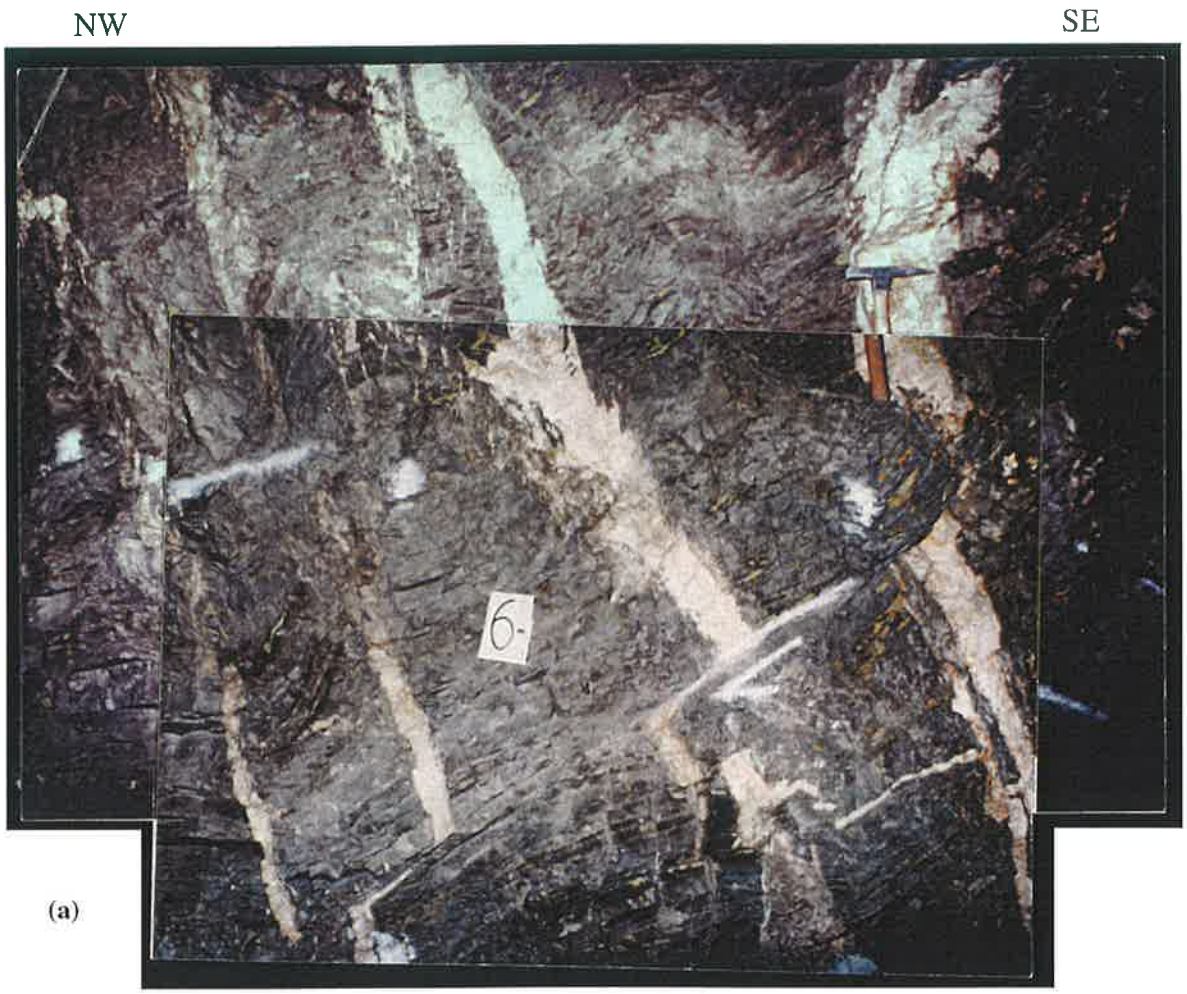

Fig. 5.5a: Reverse thrust faults on Level 6 of the Oraparinna Barite Mine showing displacement of steeply dipping, 1D Type barite veins.

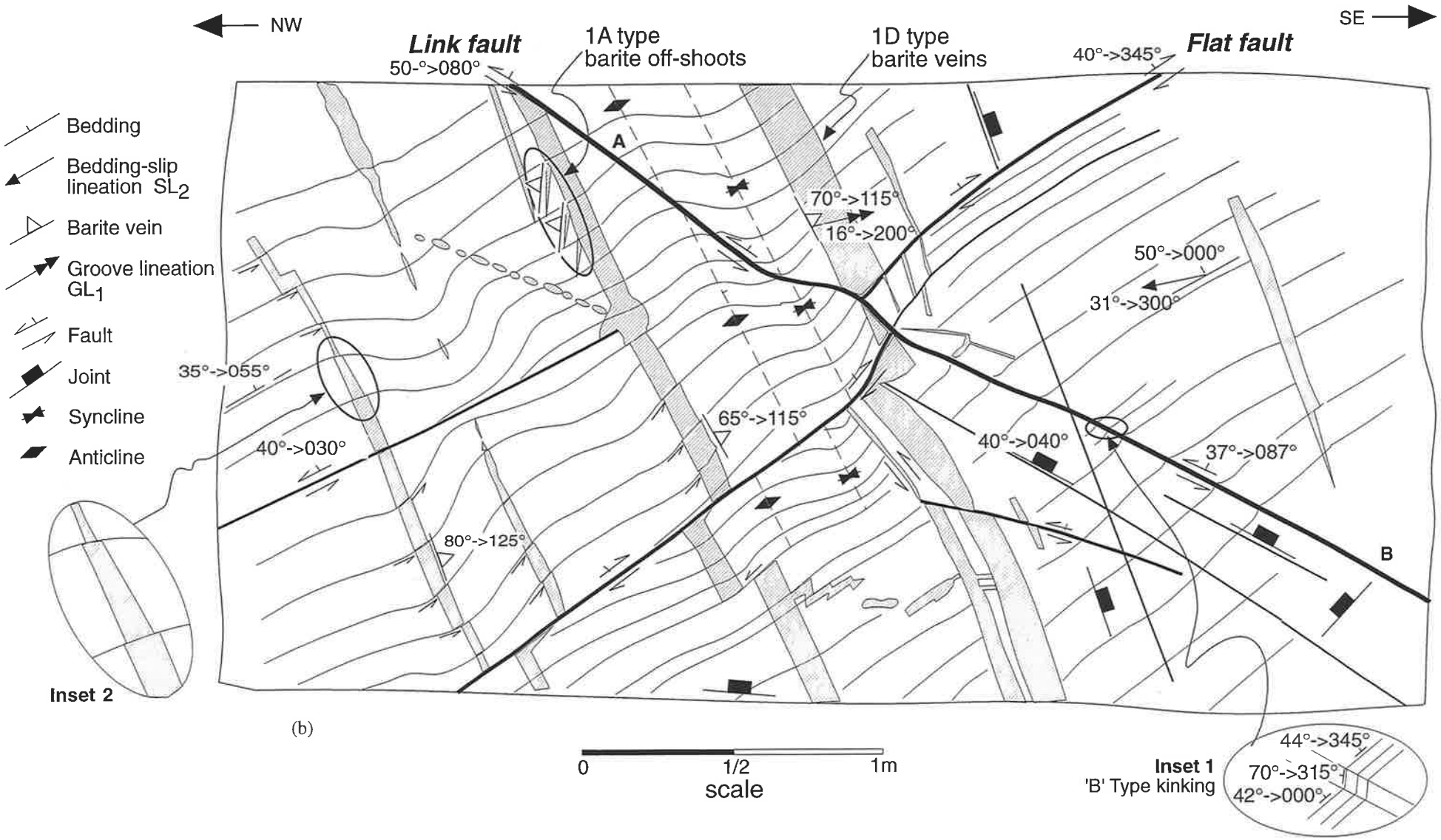

Fig. 5.5b: Field sketch of Figure 5.5a, a section nearly perpendicular to the barite veins striking NE-SW. The reverse thrust faults (both Link and Flat faults) displace 1D Type barite veins. 'B' Type kink bands are formed along the continuation of the Link fault (Inset 1). Veins are sheared NE-SW (Inset 2) and NW-SE as well.

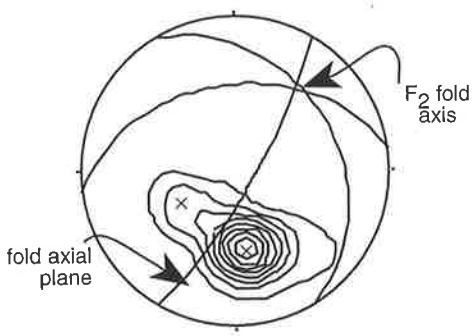

(c)

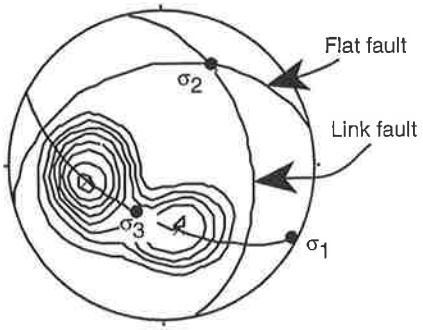

(d)

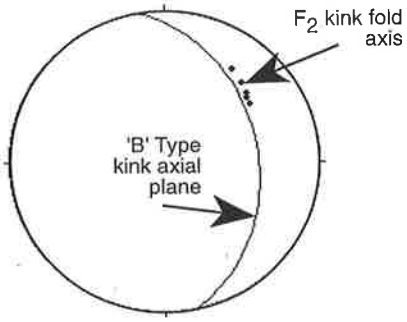

(e)

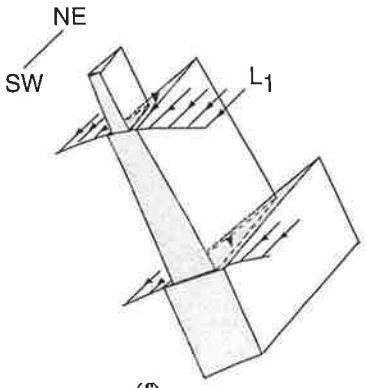

(f)

Fig. 5.5c-f: (c) Poles to bedding showing northerly dipping long limb, northeasterly dipping short limb, steep axial plane and the fold axis plunging 32°->037°; 39 data, 1,3,5,...times contoured uniform. (d) Poles to reverse - thrust fault planes showing the maximum, intermediate and minimum compression directions; σ_1, σ_2, and σ_3, plunging 3°->113°, 26°->023° and 64°->212° respectively; 42 data, contoured at 1,3,5,....times uniform. (e) The 'B' Type kink axial plane dipping 40°->080° and the average kink fold axis plunging 29°->045°, 5 data. (f) Schematic diagram showing displacement of a 1D Type barite vein during the D_1 Deformation, forming L_1 bedding-slip lineation.

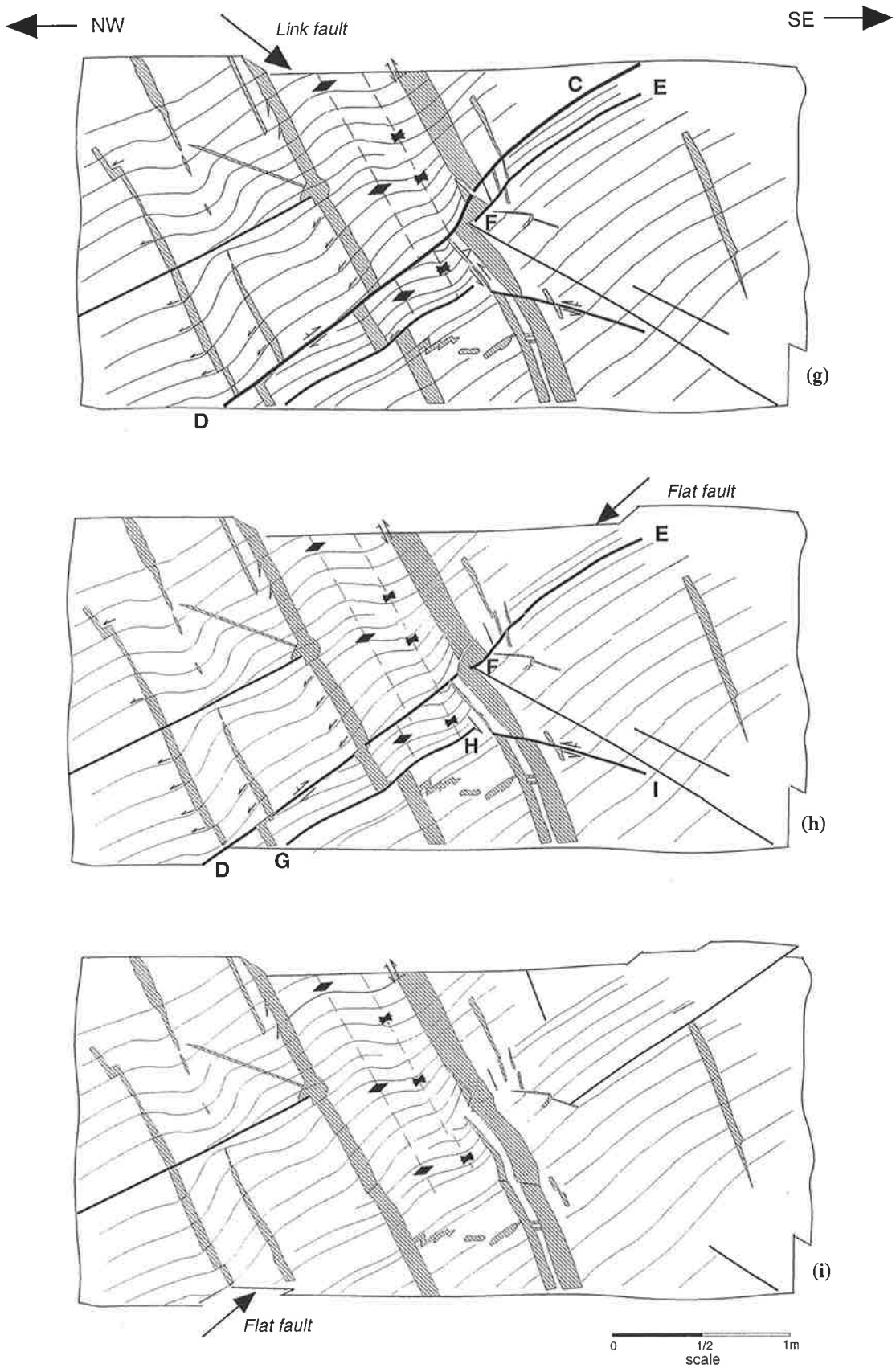

5.5g-i: Restoration of the section by moving along reverse-thrust faults.

continue as 'B' Type kink bands which strike N3°W and dip 37°E, with a kink axis plunging 29°->045° (Inset 1 of Fig. 5.5b, Fig. 5.5e). Therefore link-faults have formed simultaneously with 'B' Type kink bands.

Barite veins generally form lenses, and have sheared off along bedding surfaces (Fig. 5.5b). The thin veins have commonly been displaced during bedding parallel shearing and faulting. Some of the veins show symmetrical change of thicknesses by steps, across adjoining bedding surfaces (Inset 2 of Fig. 5.5b). A NE – SW oriented bedding-slip lineation occurs in the mine (L_1, Chapter 4), including this section. Thus the bedding parallel shear along strike of the veins apparently has resulted in formation of symmetric change of thickness by steps (Fig. 5.5f). Nevertheless, differential expansion rates of adjoining packets of bedding during the fracture dilation also could have contributed to this scenario.

The deformational sequence of the section was restored in order to understand the chronological sequence of events. The link-fault, which acted last and sheared off the barite veins, was restored first by sliding the upper-right block down along the link-fault AB (Figs. 5.5b, g). This restores the continuity of the anticlinal and synclinal axial planes as well as part of the main 1D Type vein. The next two restorations were carried out along the flat-faults. Firstly, the upper-left block was slid-down along the major flat-fault CD (Figs. 5.5g, h). Secondly, the thin block between the two major flat-faults, DF and GH was thrust-up through the section, bringing the axial planes of folds, and 1D Type veins to their original positions (Figs. 5.5h,i). This shows that the flat- and link- faults possibly were conjugate faults, with shallow conjugate angles, and thus are considered to represent a system of conjugate reverse-thrust faults (Anderson, 1971, 1974). As the 'B' Type kink folds were simultaneous with the link-faults (see above), the conjugate reverse thrust faults were also simultaneous with the conjugate kink folds. Therefore, both the conjugate reverse thrust-faults and conjugate kink folds postdated the 1D Type barite veins as well as F_2 gentle folds.

The conjugate reverse-thrust faults can be used to find the likely principal compression directions. The maximum compressive stress (σ_1, 3°->113°, i.e. WNW - ESE) occurs as the bisector of the acute angle between the conjugate faults, while the minimum stress (σ_3, 64°->212°) occurs on the bisector of the obtuse angle, and the intermediate stress (σ_2, 26°->023°) occurs at the intersection of two fault planes (Fig. 5.5d). The σ_2 closely agrees with the F_2 fold axis plunging 32°->033°.

5.5 Bedding-slip lineations (L_2)

The L_2 bedding-slip lineations show ridge and groove, and congruous steps; and are widespread in the central Flinders Ranges (Fig. 5.2f). Both the L_1 and L_2 show similar characteristics, but the latter is more prominent than the former (Chapter 4.5). The L_2 ranges from WNW to NNW (Fig. 4.6b). The mean L_2 plunges 30°->310° and 36°->139°, on the limbs of the F_2 folds, thus indicating an approximate NW – SE movement.

5.6 Interference of structures

Two minor scale fold interference examples were recorded. One was on a bedding surface of the Etina Formation, on the eastern limb of the Oraparinna Anticline, 2.6 km NE of the Oraparinna Diapir (Fig. 5.6). The outcrop was found in a creek bed and consists of two fold axes, oriented NW – SE (F_1) and NE – SW (F_2), where the earlier is more prominent and elongated than the latter. The interference pattern shows domes and basins arranged in an egg carton structure, as defined by O'Driscoll (1964).

The other example of fold interference was found in the calcareous Trezona Formation, on the western limb of the Enorama Anticline. Here, like the previous example, NW – SE elongated, F_1 anticlines and synclines have been overprinted by NE – SW oriented F_2 folds, resulting in domes and basins (Fig. 4.2a, b, c & d). The F_1 folds are more prominent than the F_2 folds, forming F_1 elongated domes and basins. The F_1 axes have been rotated into F_2 elongation (Fig. 4.2h).

Interference of bedding-slip lineations is also common in the central Flinders Ranges. These were observed 2 km west of the Enorama Diapir at the minor décollement thrust previously studied (Fig. 4.4a). Here, the outcrop shows two lineations L_1 (5°->250°) and L_2 (3°->165°; Fig. 4.4g). The L_2 lineations show ridge and groove striations, identical to L_1 except orientation. The L_2 striations have grooved into those of L_1, suggesting L_2 post-dated L_1.

5.7 Discussion

The mean long limbs of gentle F_2 folds and fault-propagation folds (see Chapter 6); and the flat faults in the mine strike between 075° and 097° and dip between 35°N and 40°N. The mean short limbs of both types of folds, link faults and 'B' Type kink bands strike between N10°W and N10°E

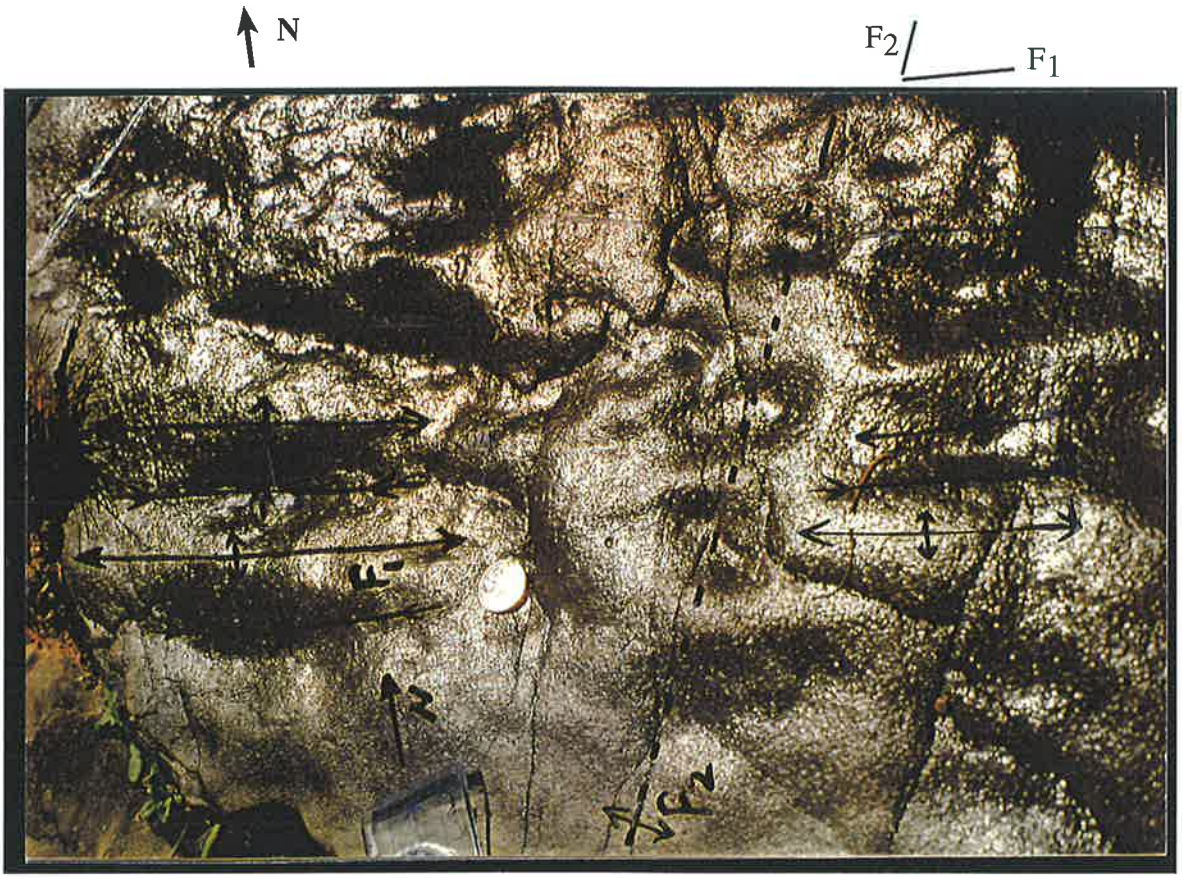

Fig. 5.6: A possible superimposition pattern of F_1 and F_2 folds of the Etina Formation in the eastern limb of the Oraparinna Anticline, 2.6 km NE of the Diapir along Oraparinna - Little Patterton Spring Track. The Formation strikes N65°W and dips 20°N. A series of F_1 folds is superimposed on F_2 folds forming domes and basins, resembling egg cartoon structure (cf., O'Driscoll, 1964).

and dip between 40°E and 45°E. The fold axes of gentle folds and fault-propagation folds as well as the intersection axes of both conjugate faults and kink folds are dominantly oriented between NE and E, even though some vary between NNE and ESE. These axes commonly plunge gently to either side. The F_2 minor structures adjacent to the axial trace of major folds, or diapirs, plunge steeply to moderately, because the relevant limbs also dip steeply. The L_2 ridge and groove bedding-slip lineation shows an approximate NW – SE orientation and is nearly perpendicular to the F_2 fold axes.

The F_2 structures of gentle folds, fault-propagation folds, kink folds and reverse-thrust faults are contractional structures. Orientation of the minor F_2 fold axes including the intersection axes of conjugate structures and the L_2 bedding-slip lineations suggest an approximate NW to NNW major compression for the central Flinders Ranges.

5.7.1 Sequence of events

The gentle F_2 folds in the mine increase in intensity:

(a) towards thick major 1D Type veins described in Chapter 7,

(b) between veins (Fig. 5.5b), and

(c) disappear at the intersections of the veins (Fig. 5.2a&b).

Therefore, gentle F_2 folds postdate 1D Type veins. The conjugate reverse-thrust faults cross-cut both the 1D Type Lodes and F_2 gentle folds, thus those faults postdate both the lodes and folds. The reverse-thrust faults were simultaneous with the 'B' Type kink bands and therefore the conjugate kink bands. Therefore, the sequence of events from older to younger is: (a) 1D Type veins, (b) F_2 gentle folds, and (c) conjugate reverse-thrust faults and conjugate kink bands.

5.7.2 Dextral rotation

The gentle F_2 folds on the hanging wall of the major fault zone adjacent to the Oraparinna Mine show a dextral rotation, compared to the footwall structure. The NW - SE trending minor F_1 fold

axes in the Trezona Formation have also rotated to the NE - SW trending F_2 axes, along the Brachina Gorge Geological Trail.

The inhomogeneous dextral rotation of structures during D_2 deformation apparently has resulted in a wide range of orientations between NNE and ESE for both the F_2 fold axes and intersection axes of conjugate structures. In contrast, the early-formed F_1 minor folds show a narrow range of orientations between NW and NNW. Correspondingly, the L_2 bedding-slip lineation shows a narrower range of orientation, varying from WNW to NNW, compared to a wider range of the L_1 varying from NNE to east. This is possibly because the D_2 compression was applied along the F_1 fold axes as well as along the L_2 lineation, and was perpendicular to both the F_2 fold axes and the L_1 lineation, thereby resulting in more rotation along the axes perpendicular to the compression direction than parallel to it.

5.7.3 Superimposition of folds

Evidence of interference between F_1 and F_2 folds was found in:

(a) the Etina Formation on the eastern limb and

(b) the calcareous Trezona Formation on the western limb of the Enorama - Oraparinna F_1 Anticlines.

However, Preiss (1987) reported a variety of microorganisms of cyanobacteria in the Trezona Formation from the same location (Fig. 4.2a-g). Preiss suggested the general appearance of these structures was similar to those of present day stromatolite mounds in Shark Bay of Western Australia. Therefore, he presumed these structures were synsedimentary stromatolite mounds, grown in the direction of the Sun. In contrast, these structures show:

(a) Formation of doubly plunging domes and anticlines with F_1 prominency in elongation (McClay, 1992b), similar to those of the adjacent Blinman, Enorama and Oraparinna Anticlines.

(b) Occurrence of NE-SW oriented L_1 bedding-slip lineation on the limbs, nearly perpendicular to the F_1 fold axes. These lineations show tectonic transportation towards the axial trace and disappear along the hinge line (Fig. 4.2).

(c) Symmetrical nature, similar to those below the ramp thrust faults on the forelimb of the Enorama Anticline (Figs. 4.4a, f) or those on the forelimbs of fault-propagation folds (Fig. 6.1f-i),

(d) Formation of fold superimposition patterns similar to the dome and basin, egg-carton like structures produced by O'Driscoll (1964), which has been interpreted as the mechanism of the major structure of the Flinders Ranges (e.g. the southern Flinders Ranges, Chapter 3).

(e) Evidence of dextral rotation of F_1 fold axis towards F_2

Therefore, the current research in this thesis suggests that the Trezona Formation, like the other formations in the Ranges, has been subjected to both the deformations, forming fold interference patterns of dome, basin and col structures (c.f. O'Driscoll, 1964). The parasitic nature of these structures to the major fold structure of the Flinders Ranges more strongly suggests a tectonic origin, than a synsedimentary - stromatolite mound origin suggested by Preiss (1987).

Chapter 6

USE OF MINOR FAULT-PROPAGATION/DETACHMENT FOLDS FOR MODELLING OF DIAPIR FORMATION

6.1 Introduction

Flow of breccia into diapirs has been considered forcible emplacement because of folding the host rocks into steep to moderate dips at the margins of the Enorama Diapir (Mumme, 1961 and Coats, 1964a). Accordingly, Mount (1975) demonstrated the importance of source bed mobility to the intrusive process, implying that the material need not be less dense than the host for invasion to occur. Therefore, Mount suggested tectonic enforcement of mud breccia into relatively brittle overburden, moving aside the flanking host-rock mass. He proposed décollement at the source-layer and breccia movement on faults to be essential and presumed the 'geostatic load' as the prime driving force. Lemon (1988) assumed that breccia was produced during differential loading and raised due to its lesser density than the host rocks, similar to salt deposits (Seni and Jackson, 1983a,b). In any of these views, geostatic load (Mount, 1975), or differential loading (Lemon, 1988), mud breccia had moved on the basement under compression and therefore had most likely risen through the sedimentary column under compression. Therefore, the deviatoric pressures of the moving breccia deposit containing rock mass and fluids expected would be outwards.

In Lemon's (1988) experiments, the presumed shapes of diapirs from pillows to overturned waterdrops were produced by upward pulling of a thread attached to the centre of a stiff rubber membrane (Figs. 1.4, 1.5). These shapes were a function of both the stiffness of the rubber membrane and the partial vacuum that was created under the membrane. Therefore, the shapes were created under inward deviatoric pressures, in contrary to the outward deviatoric pressures of diapirs in nature. In recognition of similarities between his models and field observations, Lemon suggested a general synsedimentary origin for diapirs. His model has been widely accepted so far by the geological community in South Australia and remains unchallenged.

Weaknesses in Lemon's (1988) model are:

- Because the diapirs were modelled under inward deviatoric pressures, any lateral diapiric breccia extrusions into the host could not be observed. Furthermore, the rubber diaphragm used in the experiment is not likely to be true to nature and leads to an overconfidence on the part of the observer about the lack of intrusion of breccia into the host.

- The sandbox experiment was conducted under a special condition of 'non-continuous breccia flow' into the diapir-model, resulting collapse of the rubber membrane into an overturned waterdrop (Fig. 1.4). The overlying sediments on the flanks followed collapsing, thus formed 'inward dipping peripheral sinks around the diapir'. These sinks have not been documented around any diapir in the Adelaide Fold Belt, therefore the experimental result remains unjustified.

- No profile of a diapir has been documented from the Adelaide Fold Belt thus; the experimental shapes from pillow to overturned water-drop shapes remain unjustified as well.

Therefore, material used in the sandbox experiments such as the rubber membrane and the partial vacuum, poorly represented the parameters of diapirs. Even though Lemon's model could be repeated, these parameters and the experimental procedure, i.e. replacement of compression by tension, was contradictory to that of the natural course of diapir formation. For these reasons, Lemon's sandbox models did not represent the true processes of diapir formation. Therefore, the Flinders Ranges were examined for natural models which might best represent diapirs.

Minor detachment/fault-propagation folds have not been previously reported from the Flinders Ranges. These structures have probably been overlooked as slump folds or tepee structures of sedimentary origin, possibly because of the characteristically very low intensity of deformation in the area. A few good exposures were documented from the Ranges during the fieldwork and the relevance to diapirs was examined. Microstructures were also studied under the optical microscope and under the microprobe at the University of Adelaide.

6.2 Fault-propagation folds on the eastern limb of the Oraparinna Anticline

An asymmetric gentle fold was studied in a road cutting at the hilltop of the Oraparinna Mine, hosted by the Brachina Formation (Fig. 6.1a,b). The fold was located on a nearly vertical road cutting of the contact wall of the Bainbridge no. 3 Lode that was almost mined out. The lode strikes NE and dips nearly vertical. The fold begins on a flat basal layer and dies out at the ground level within a 2 m height (Figs. 6.1c). It shows a mean long limb that strikes N88°E and dips 40°N, and a mean short limb that strikes N7°E and dips 45°E (Fig. 6.1d). The fold axis plunges 30°->042°, and is thus an F_2 fold and is parallel to the strike of the lode. The axial plane of the fold strikes NE and dips 64°NW, thus indicating SE vergence. Each layer in the section has not moved

(a)

(b)

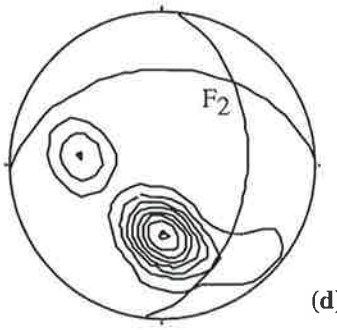

(d)

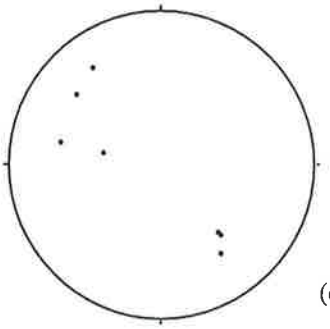

(e)

Fig. 6.1: (a) The excavated Bainbridge No. 3 Lode at the hill top of the Oraparinna Mine, showing remnants of the mined vein on the wall rock. (b) The wall rock of the Brachina Formation is folded and is exposed on the road cut. (c) See over leaf. (d) Bedding data showing the F_2 fold axis plunging 30°->042°. 36 data, contoured at 1,3,5,....,x times uniform. (e) Bedding-slip lineation (L_2) showing NW-SE orientation. 9 data. Cont..,

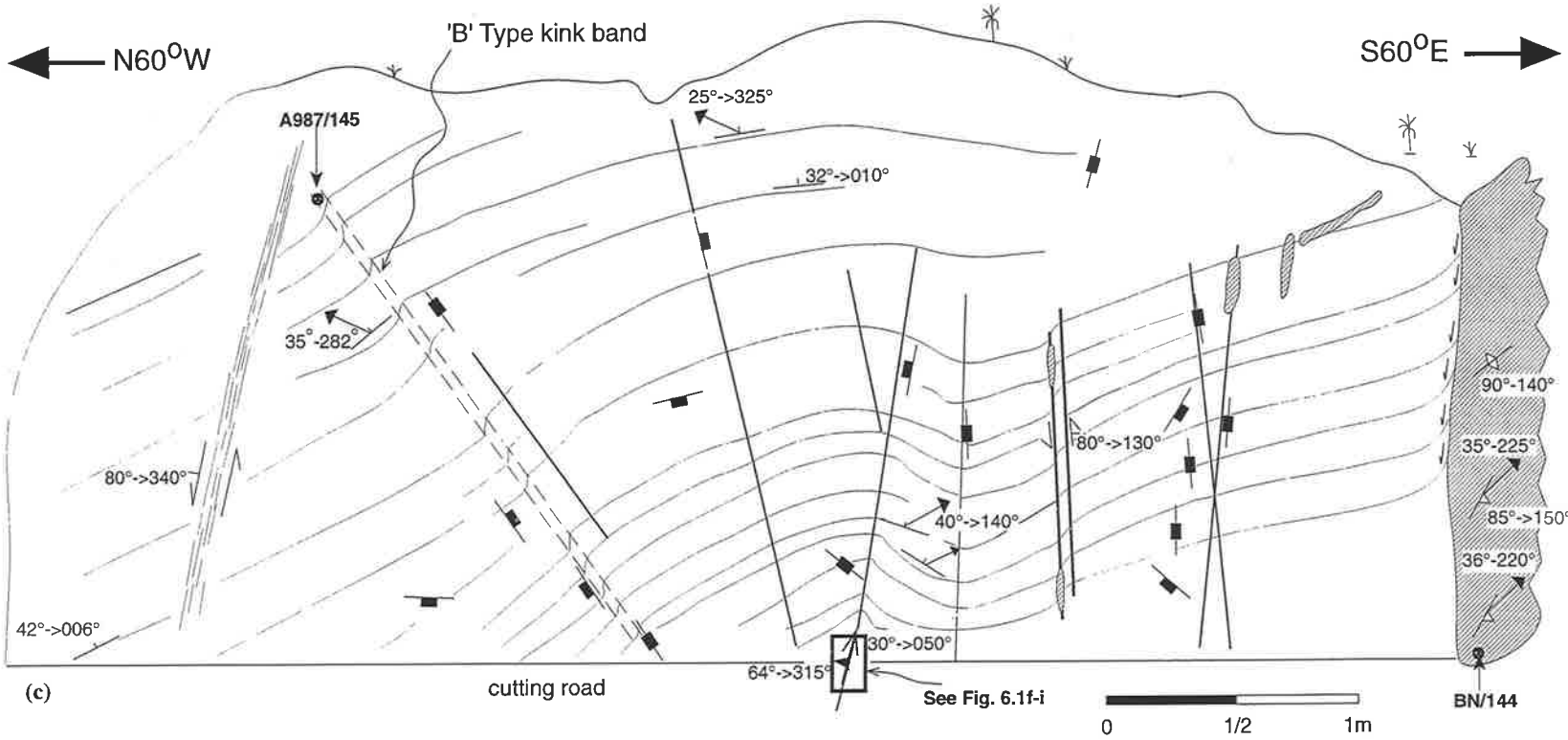

Fig 6.1: (c) Skech section of the western contact wall of the Bainbridge No 3 Lode, showing a detachment/fault-propagation fold (See Fig. 6.1f-i). The remnants of the mined vein occur at the southeastern end of the section. Cont..,

32°->010° Dip and dip direction of bedding

25°->325° Plunge and plunge direction of bedding slip lineation (L_2)

80°->130° Dip and dip direction of fault plane

30°->050° plunge and plunge direction of F_2 fold with dip and dip dip direction of axial plane

70°->150° Dip and dip direction of barite vein

Joint/fracture

Barite

BN/144 Sample

by the same proportion during propagation, forming bedding parallel shear within packets of beds, thereby creating a bedding-slip lineation (L_2), defined by NW-SE oriented ridge and groove striations (Fig. 6.1e; cf. McClay, 1987).

6.2.1 Geometry of folds

A 15 cm long piece of the core of the fold was cut into four serial sections, normal to the fold axis, and analysed in thin sections (Figs. 6.1f, g, h, i). Each section comprises a forelimb syncline and a back limb anticline pair moved on a thrust surface, which therefore indicates a fault-propagation fold (Figs. 6.1f^, g^, h^, i^; Suppe, 1983, 1985). The sections contain low angle, gently dipping décollement thrust surfaces AP, which further developed into moderately dipping reverse thrust faults PT, ending at tip line T (Figs. 3.8b, 6.1h^). The fold has sheared along the BC level on the back limb resulting in translational movement of the axial surface further into the forelimb.

The geometry of the folds was analysed separately for both the upper and lower halves which sheared off the axial plane along BC, by using the detachment/fault-propagation fold models put forward by Marrett and Bentham (1997), an improvement of Chester and Chester (1990, Fig. 3.8b). The sections were balanced using the basic assumption that the rock volume was conserved during deformation; therefore, deformation approximates plane strain and simply distributes rock volume in the two dimensional cross section profiles (Elliot, 1983). In contrast, the rock volume of the sections is unlikely to be constant, due to (a) brecciation of the host along the detachment surfaces, and (b) intrusion of breccia into the adjacent hosts. Therefore, constant volume may not have been achieved during folding. However, due to admissibility, deformability and viability, the balanced sections were assumed to be reasonable for shortening calculations.

Parameters for the lower half of BC in Figure 6.1f^ are: a back limb dip (2θ) of 29°, measured relative to the regional inclination of bedding below the detachment; an interlimb angle (γ) of 75°; and thickness of the forelimb (t_f) of 10 mm and that of the back limb (t) of 8 mm. The forelimb shows thickening compared to the back limb. A structural relief (h) of 47 mm was measured orthogonal to the regional. The data are consistent with a thrust ramp dip (α) of 22°, TP distance of 34 mm and a shortening (f_o) of 38 mm (Table 6.1). The calculation shows a shortening of 38 mm. However, measurement between two pin lines in either limb of the section shows a length of 210 mm, shortened to 180 mm, thus indicating a shortening of only 30 mm. This difference between the calculated and measured shortening is due to thickening of the forelimb during

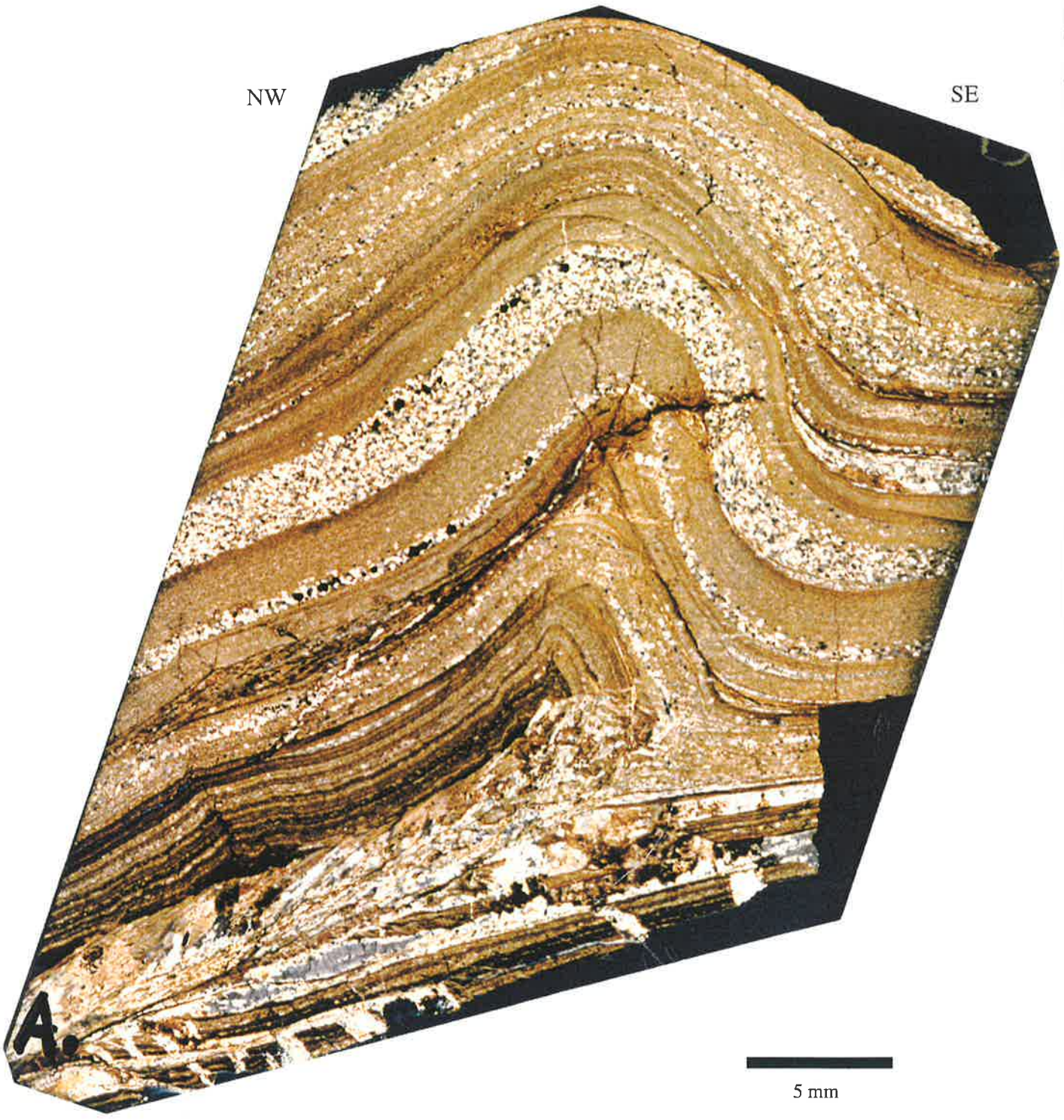

[f]

Fig. 6.1: (f-i) Thin sections cut perpendicular to the fold axis of the core of the fold shown in Figure 6.1c, showing that the fold resulted from a thrust-related detachment/fault-propagation fold. Breccia has formed along the decollement and core zones up to the tip-line in the forelimb syncline. A variety of dilational fractures have formed below the decollement, resulting in mineralisation. (f) A series of gentle parasitic folds appear along the backlimb above the detachment zone. Breccia has formed along layers of backlimb at a mid level of the fold. Cont..,

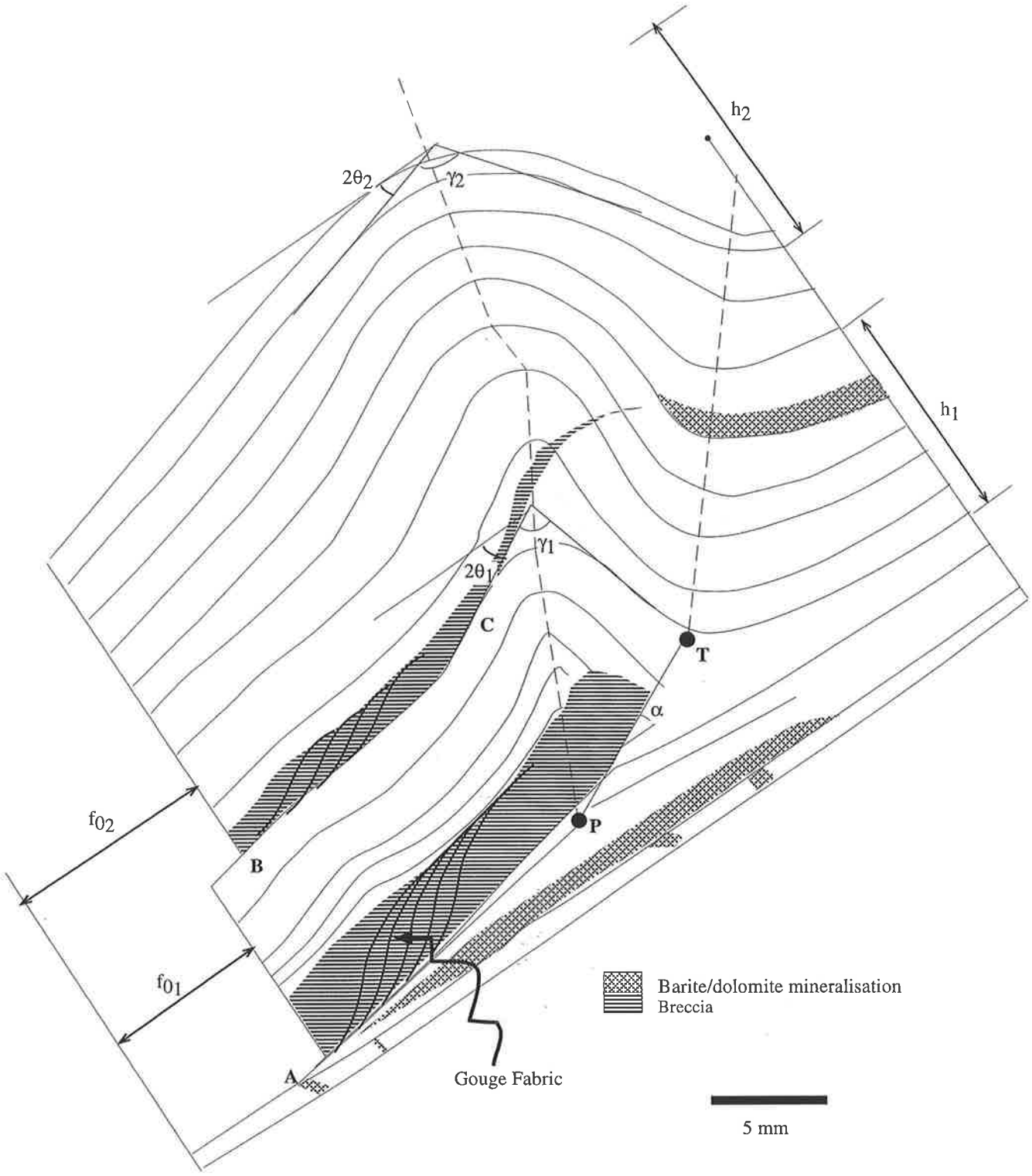

Fig. 6.1f^*: Balanced section of Figure 6.1f. Note: Breccia has formed along the decollement surfacet and concentrated in the core, and on the BC level as well. Barite/dolomite minralisations have formed in the basement and forelimb syncline.

* The ^ symbol denotes cartoon figures constructed from photographs of serial sections.

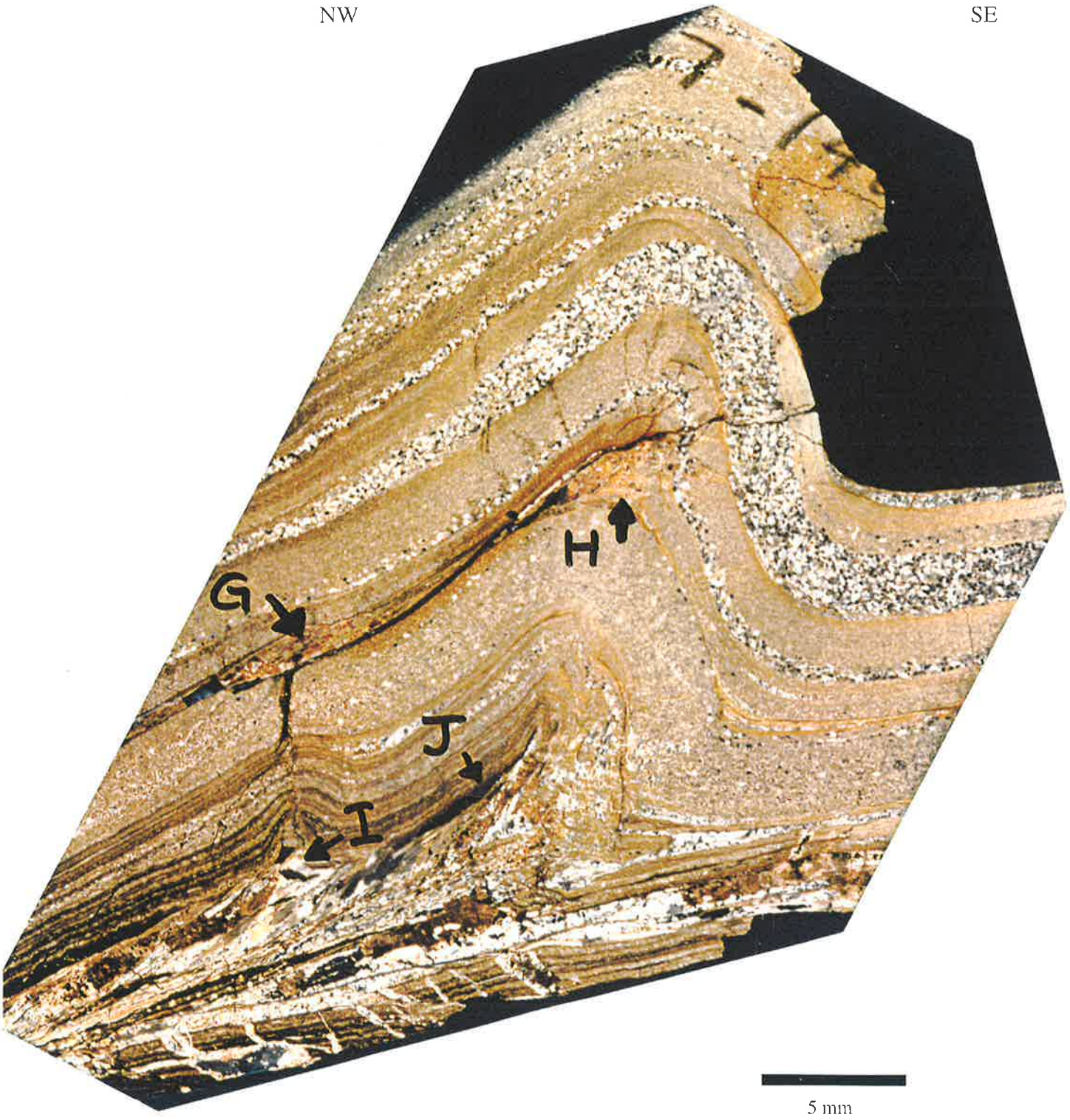

(g)

Fig. 6.1g Parasitic folds on the backlimb have developed from open to gentle folds. Breccia has formed along the hinge zone at a mid level of the fold (GH) and concentrated on the respective hinge zone. Cont..,

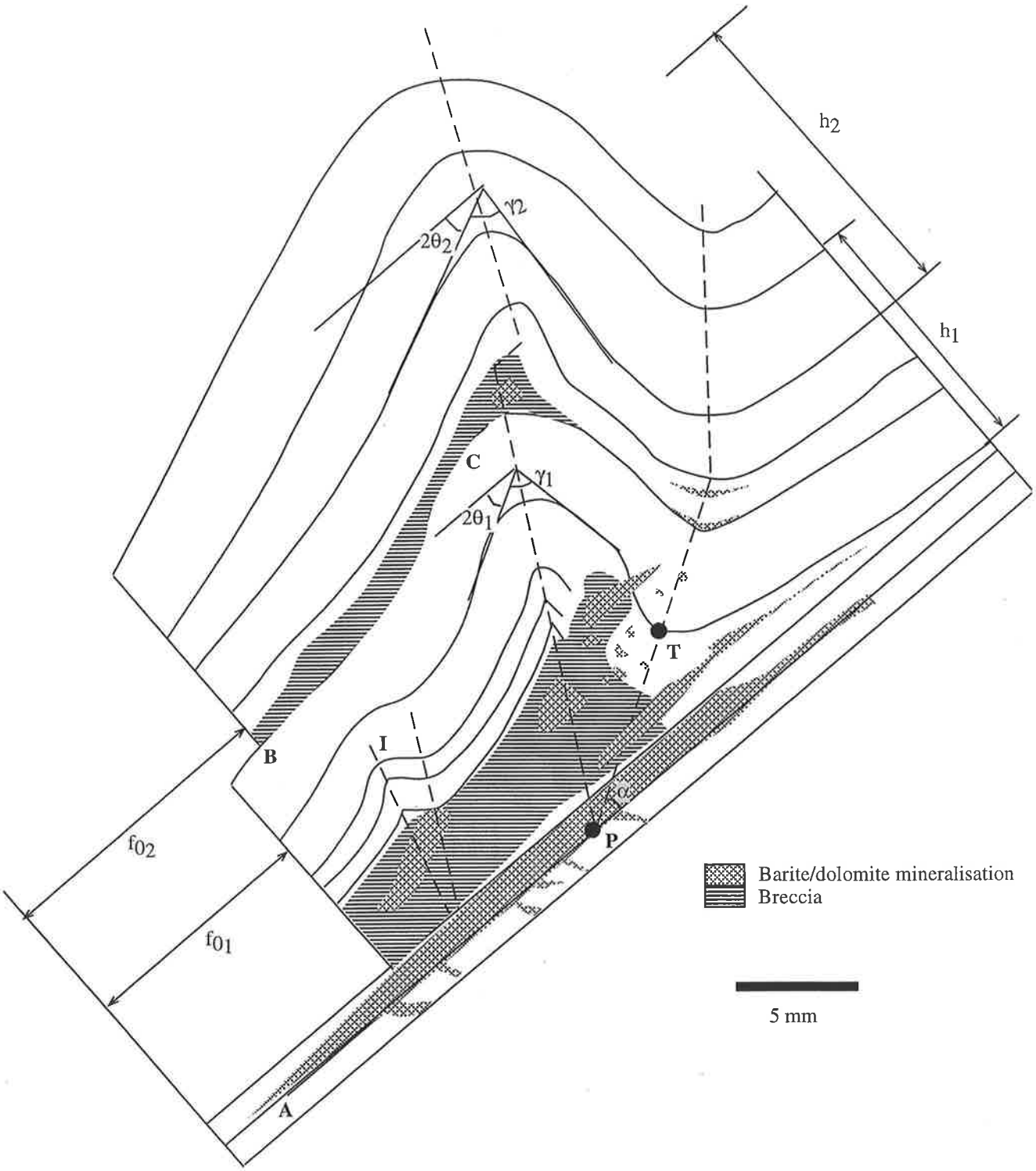

Fig. 6.1g^: Balanced section of Figure 6.1g. Note: The upper part of the fold is translationally moved on a layer of breccia towards the fore limb. Parasitic folds appear on the back limb. The fold is tilted compared to the original position, to show upward continuation of the forelimb, resulting in formation of downward dips on both limbs of the forelimb syncline. Disseminated dolomite deposits have formed on the forelimb, adjacent to the main breccia deposit.

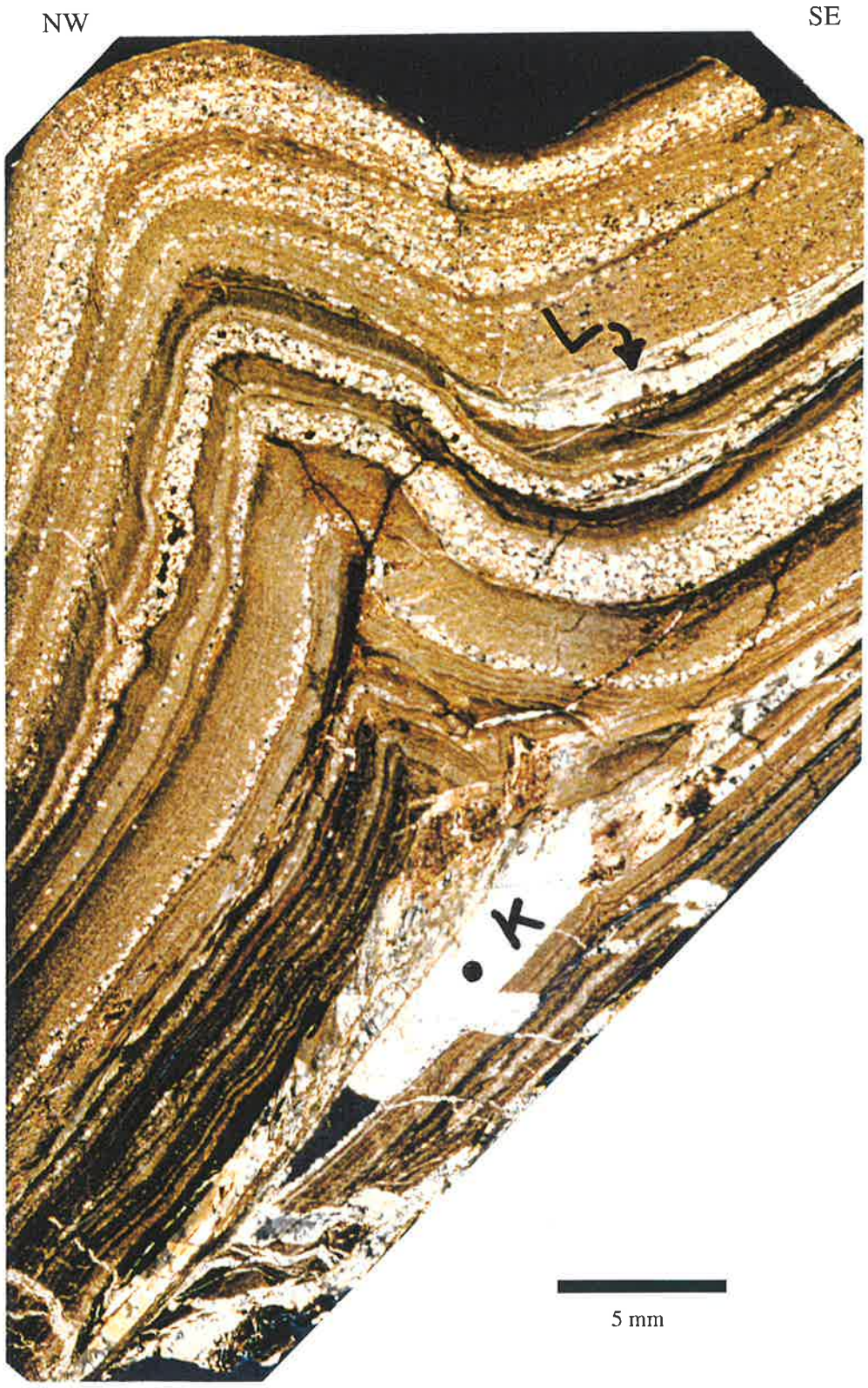

(h)

Fig. 6.1h: Parasitic folds on the back limb disappear into the shape of asymmetric drag folds while new parasitic folds appear within the forelimb syncline, adjacent to the major breccia deposit in the core. Occasional dilational fractures have formed on the back limb, emanating from the major breccia deposit on the decollement, in extreme left of the photograph. Cont..,

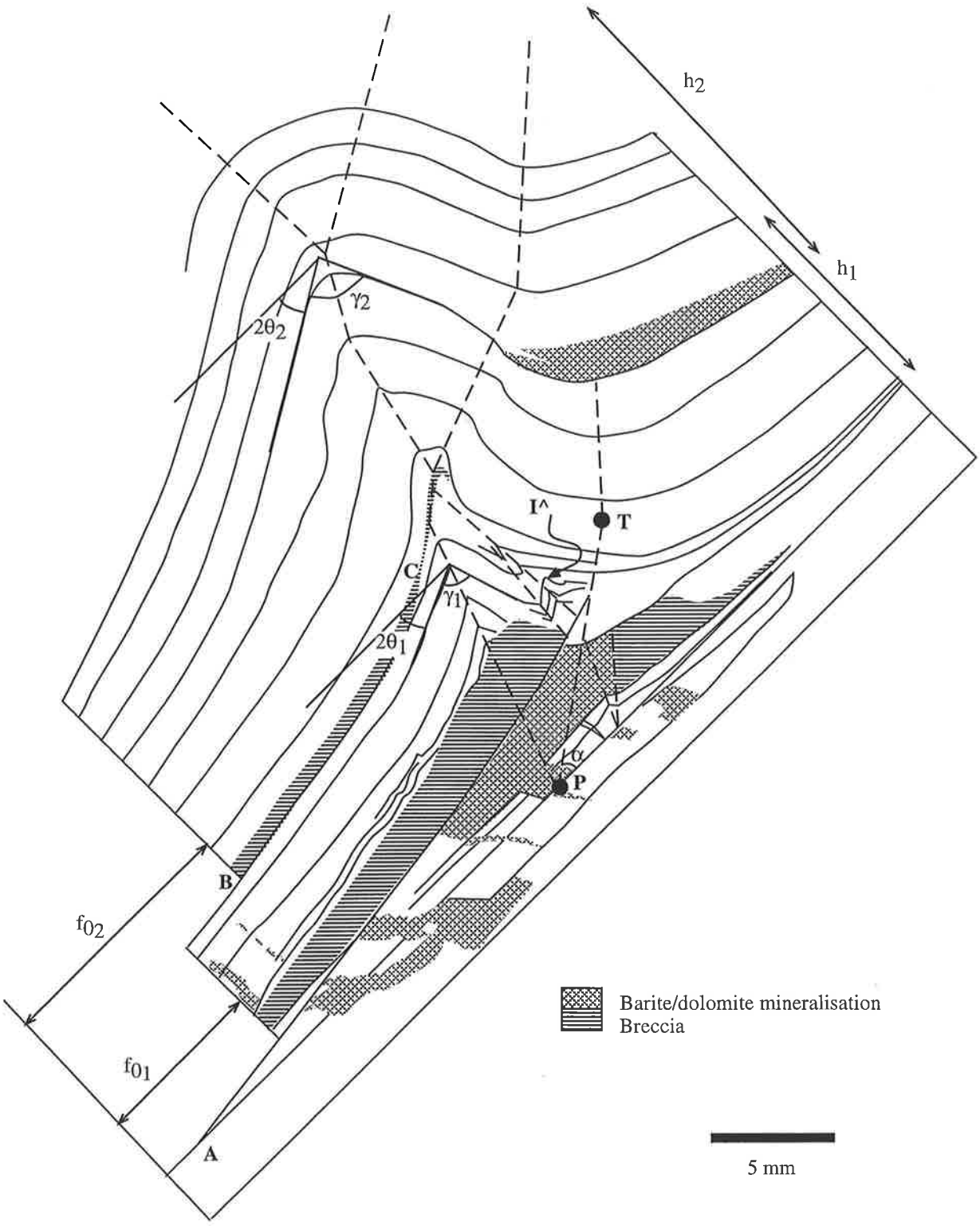

Fig. 6.1h^: Balanced section of Figure 6.1h. Note: Formation of parasitic folds on the forelimb, adjacent to the breccia deposit in the core.

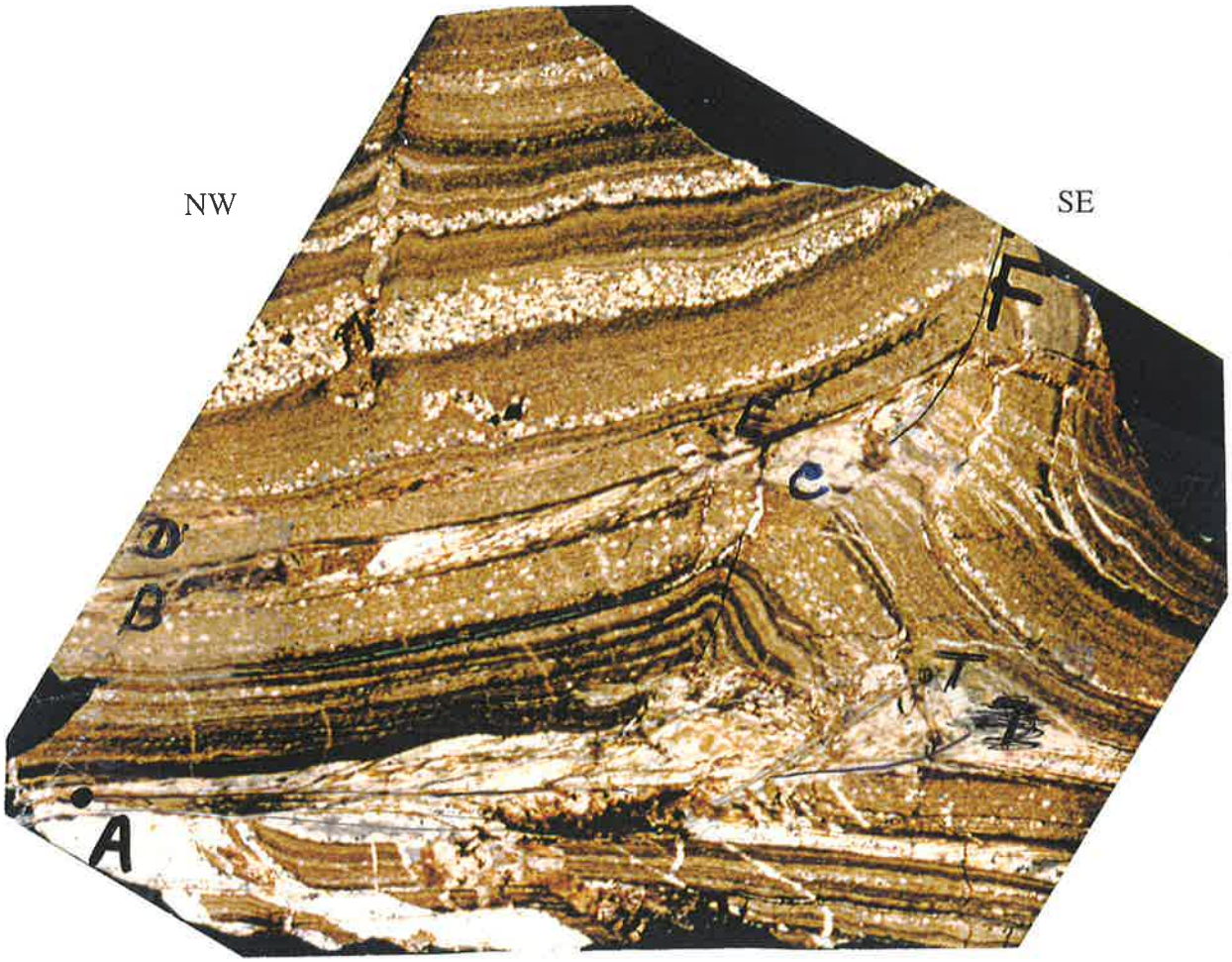

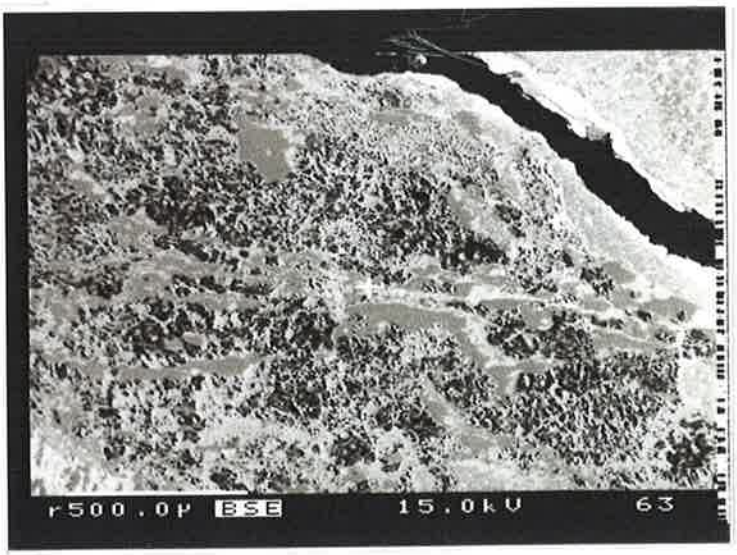

Fig. 6.1: (i) Parasitic folds in the backlimb are in near extinction. Upper part of the fold has further advanced into the forelimb, forming a series of wedge shaped tongues of dilational fractures synchronously filled with breccia or barite/ dolomite mineralisation. (j) A back scattered image of breccia of the core zone of the fold obtained from the microprobe indicating cavities [black], quartz [white] and feldspar [grey].

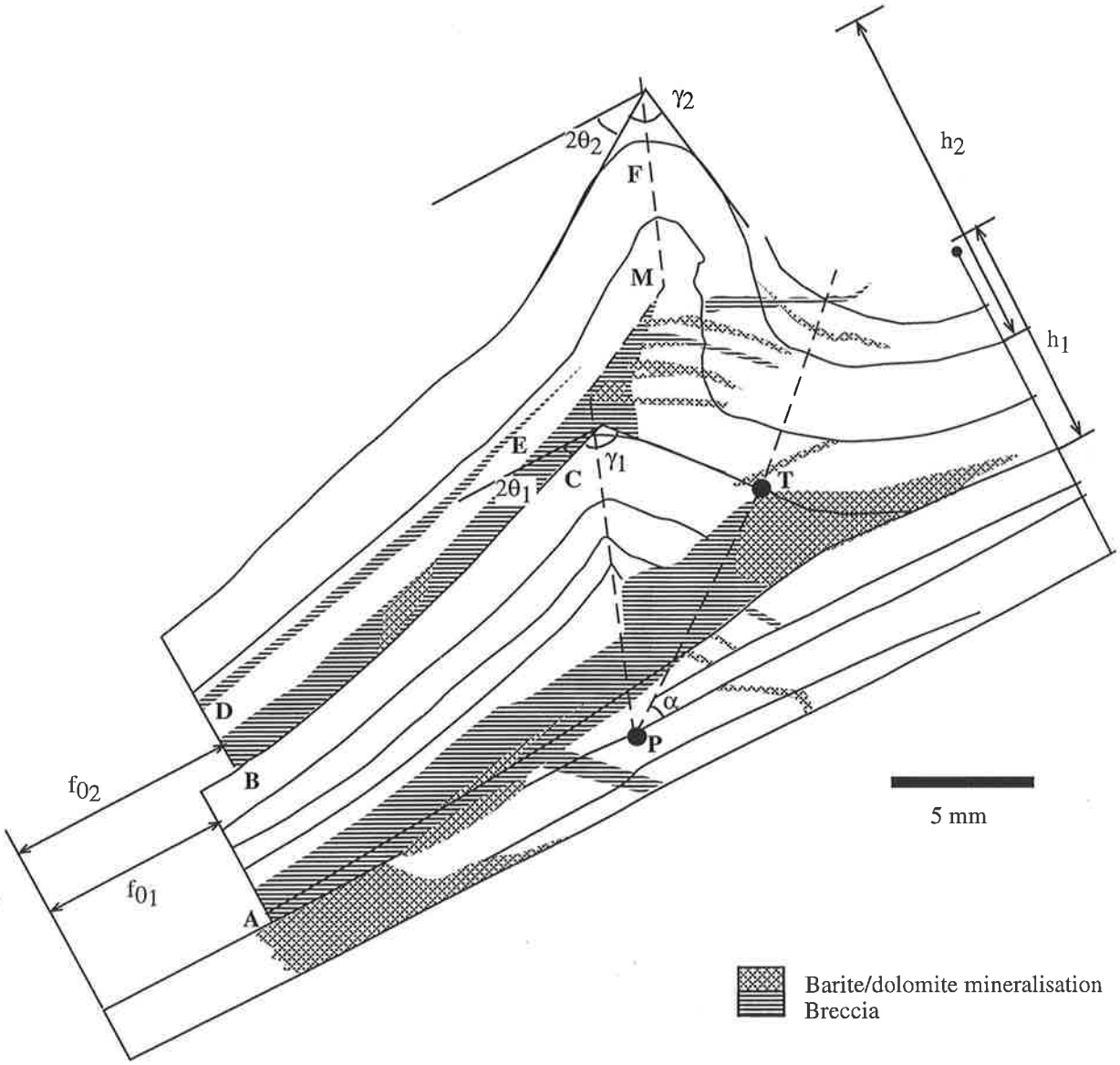

Fig. 6.1i^: Balanced section of Figure 6.1i. Breccia has formed on the DE level of the back limb as well. The wedge shaped tongues emanating from the breccia deposits are commonly limited to the fore limb or below the decollment surface.

shortening, while thinning does the opposite (Marrett and Bentham, 1997). Therefore, the actual shortening was assumed to be 38 mm, thus indicating a shortening of 18% {(38/210) x100%}.

The displacement transportation along BC has reduced the interlimb angle from 75° to 51°, from the lower half to the upper half of the fold, immediately after transportation (Fig 6.1f^, cf. Jamison, 1987). The angle of the upper half has then increased up to 110° with the increasing height. The upper section of the fold shows shortening of 47 mm, i.e. a shortening of 22% (Marrett and Bentham, 1997 method), indicating more shortening than the lower section (Table 6.1). The interlimb angle (γ) of the fold in all the sections ranges from 60° to 112°, varying from open to gentle folds. Therefore, the fold has grown from an open fold adjacent to the detachment surface, to a gentle fold with the increasing height. The interlimb angle further increases with the increasing height, until folding disappears (Fig. 6.1c). The shortening of all the sections varies from 18 - 29%.

Table 6.1: Parameters for the four sections of the fault-propagation fold (Figs 6.1f-i), cut perpendicular to the fold axis in the contact wall of the Bainbridge no. 3 Lode, hilltop of the Oraparinna Mine. Method of analyses: Marrett and Bentham (1997).

Parameter	Fig. 6.1f		Fig. 6.1g		Fig. 6.1h		Fig. 6.1i	
	*1	*2	*1	*2	*1	*2	*1	*2
2θ	29°	15°	30°	25°	25°	32°	20°	37°
γ	75°	110°	69°	60°	80°	82°	112°	65°
t_f (mm)	10	6	14	16	4	8	10	9
t (mm)	8	9	15	17	4	8	8	12
h (mm)	47	59	53	64	47	74	40	58
α	22°	74°	60°	24°	35°	36°	36°	38°
TP (mm)	34	219	50	47.5	62.5	88	45	96
f_o (mm)	38	47	50	61	40	59	34	43
Shortening (%)	18	22	24	29	17	25	20	27

*1 – lower half and *2 – upper half of each section, below and above the bedding parallel shear, BC, respectively.

Open to gentle parasitic folds have developed on both limbs of the fold. Those on the back limb are asymmetric and verge towards the main axial trace of the fold (I of Fig. 6.1g^), while those on the forelimb have formed next to the breccia deposit and are symmetric and upright, showing no vergence (I^ of Fig. 6.1h^).

6.2.2 Origin of breccia deposits in relation to folds

The folds show that breccia has been produced on different levels on the back limb (Figs. 6.1f-i^). The thickest breccia deposit is developed on the décollement and reverse thrust fault surface, AT, and is concentrated in the core of the fold (Figs. 6.1i, i^). Two other perched deposits are also

developed on upper levels of BC and DE on the back limb, and the latter deposit on the DE level is not extended up to the hinge. These breccia deposits show:

(a) gouge fabric (McClay, 1987; Fig. 6.1f^),

(b) repeated brecciation while mixing with breccia that was added during progressive deformation,

(c) perched breccia deposits on the hinge zone of the main fold and different levels, that were not stoped from the main breccia deposit on the décollement, and

(d) the composition mainly of silica and feldspar, similar to that of the host, and loosely compacted and full of cavities (Fig. 6.1j).

Therefore, these deposits consist of clasts ripped off during gouging, which indicates a syntectonic and insitu origin, instead of an intrusive origin from external sources. The main breccia deposit on the décollement includes clasts from:

(a) the basal layers below the décollement,

(b) the lowermost layers above the décollement, and

(c) the upper layers, which are brecciated up to the end of the tip line, T, along the reverse thrust décollement surface.

Breccia has been continuously mixed during thrusting, leaving a thick deposit on the décollement as well as in the core.

Dilational fractures or fissures have been formed in the host sequences of these folds:

- At a 45° or 135° angle below the décollement surface and
- Onto the forelimb, especially emanating from the core (perched) breccia deposit that is advanced on to the fore limb during progressive deformation (Fig. 6.1i, i^).

These fissures have commonly formed as wedges or tongues emanating from the bordering breccia deposit and taper into the host and occur both bedding-parallel and across bedding. These tongues contain breccia, barite or dolomite, which have formed synchronously during dilation (Section 7.3).

Some rare breccia offshoots have been intruded into the back limb from the décollement zone, along fissures or dilational fractures (bottom left of Fig. 6.1h).

6.3 Fault-propagation folds on the eastern limb of the Enorama Anticline

An example of a minor fault-propagation/detachment fold was studied in the eastern limb of the Enorama Anticline, 12 km NE of the Enorama Diapir, on the western bank of the Second Plain Creek. The fold is hosted by the Brachina Formation and can be seen in a 5 m high section, at a road-track crossing (Fig. 6.2a). The fold axis plunges 21°->084°, and therefore is an F_2 fold. The axial plane dips moderately to the north, and shows a southerly vergence, similar to that of the previous example.

The competence of layers varies depending on the silica and shale contents and the thicknesses vary from millimetres to tens of centimetres. The basal layer of the fold consists of a competent siliceous layer on the creek bed and is slightly folded with an interlimb angle of 160°. This competent layer has acted as the décollement and the overlying shaly layer has folded into a detachment fold. The asymmetry of the fold suggests later development into a fault-propagation fold. The shaly layer has been ground to breccia that has concentrated in the core of the fold, similar to the previous example (Figs. 6.2b; 6.1f-i). Displaced rafts of competent layers, varying up to 50 cm long, occur within breccia in the core. Some of the weak layers on the limbs have been brecciated and have partly contributed to the breccia deposit in the core and vice-versa; breccia has flown from the core to adjacent limbs, especially into the forelimb. Some of the weak layers have increased thicknesses on the limbs adjacent to the fold hinge, while the competent layers show no change in thicknesses.

6.4 Fault-propagation folds on the western limb of the Enorama Anticline

An example of a fault-propagation/detachment folds was studied on the western limb of the Enorama Anticline, 11 km SW of the Enorama Diapir. The outcrop was in the ABC Range Quartzite, along the Brachina Gorge Geological Trail (Fig. 6.3). The long limb strikes N45°E and dips 10°W, and the short limb strikes N55°E and dips 75°W. The fold axis plunges gently SW (4°->235°), and is an F_2 fold. The axial plane dips moderately to the SE, and shows a northwestern vergence, in contrast to both previous examples from the eastern limb.

S N

(a)

S N

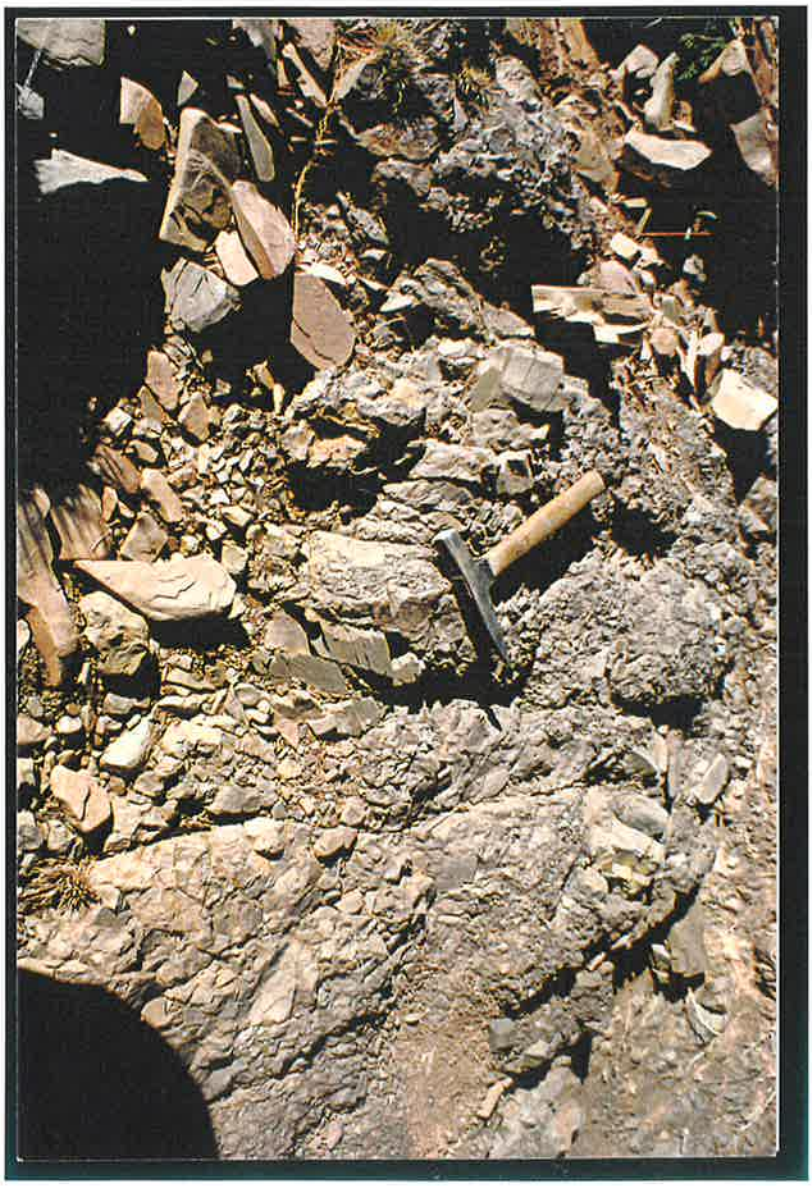

(b)

Fig. 6.2: (a) A southerly verging, F_2 detachment/ fault-propagation fold on the eastern limb of the Enorama Anticline. Location: 12 km NE of the Enorama Diapir, on a branch of the Second Plain Creek. The track follows the long, northern limb of the anticline. The fold is hosted by the Brachina Formation. (b) Brecciated Brachina Formation with varying sizes of clasts in the core of the fold.

SE NW

Fig. 6.3: A NW verging detachment/ fault-propagation fold on the western limb of the Enorama Anticline. The fold is located 11 km southwest of the Enorama Diapir, along the Brachina Gorge Geological Trail and is hosted by the ABC Range Quartzite. The stereogram shows gently dipping long limb and moderately dipping short limb, both towards NW, and a moderately SE dipping axial plane (thick line). The fold axis plunges 4°->235°.

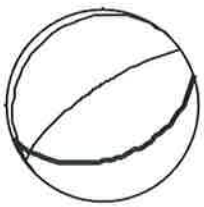

The quartzite contains thick and competent siliceous layers as well as thin and weak feldspathic layers. Extensive bedding parallel shearing has occurred on the limbs, thickening some of the weak layers. In situ breccia occupies the core and is also along bedding on limbs, similar to previous examples.

6.5 Model of a detachment fold

A doubly plunging and elongated dome hosted by the Wonoka Formation and consisting of a flat base with a curved hinge was found 13 km SW of the Enorama Diapir, along the Brachina Gorge Geological Trail. The dome culminates at the centre and gently plunges down to flatten on the base at either end, along the fold hinge. The height of the fold increases as slope of the limbs increases. The angle between the limbs and the base varies from shallow to steep, depending on the asymmetry. A ridge and groove bedding-slip lineation occurs more prominently on the limbs than on the hinge, and is nearly perpendicular to the fold axis. Use of smoothness and roughness technique (Billings, 1972; Petit, 1987; Will and Wilson, 1989; Lin and Williams, 1992) on the lineations indicates flexural-slip movement of bedding (Tanner, 1989) towards the hinge.

The fold was displaced within the formation and the orientation and the phase of folding are unknown. It was studied in detail because of the character it showed in relation to the mechanism of detachment folds and breccia formation. The sample was 10 cm wide and 20 cm long and was cut into three sections orthogonal to the elongated fold axis (Fig. 6.4a-c). The sections show a competent basal layer, the limbs, and a mud breccia core, similar to the previous examples. The size of angular clasts in the breccia vary from fine, to rafts as large as 1/3 of the width of the core (Fig. 6.4c).

The fold in Section (b) shows approximate symmetry while the other two sections show some asymmetry, possibly indicating that the fold moves into the foreland as the fold becomes too tight to accommodate further shortening (Twiss and Moores, 1991).

The flexural-slip lineation on bedding and increasing vergence of the fold suggest a detachment fold. Composition and the nature and preferred orientation of breccia clasts parallel to adjacent limbs suggest that the breccia in the core of the fold was formed syntectonically during faulting on the harder bed and not intruded from an outside source. The weak, argillaceous layers were broken into clasts and squeezed into the space left in the core of the fold. The larger clasts of 1/3 of the width of the core of the fold appear to have detached from the roof of the core during folding.

(a)

(b)

Fig. 6.4: Core of an elongated, doubly plunging detachment/ fault-propagation fold of the Wonoka Formation, cut normal to the fold axis. Sample collected 13 km southwest of the Enorama Diapir, along the Brachina Gorge Geological Trail. (a) Formation of breccia from a weak incompetent layer between two competent layers during folding. (b) Enlargement of carbonate crust including cavities, as the fold grows. Fluids have escaped through conduits from the core into the limb sequences during fold growth, altering chemistry of the host. Contd.

Fig. 6.4: Contd., (c) Rafts broken from competent layers up to a width of 1/3 of the detachment fold occur within breccia. A dolomite cap has developed on the top of the breccia deposit during the growth stages of the fold in Figures 6.4a and b, but has crumpled during the last compression stage in Figure 6.4c. The white rectangular or square type mineralisations in the core are disseminated carbonates or dolomites.

Therefore, the sample represents a tectonic fold and not a primary structure like an intraformational slump fold, stromatolite or tepee structure and it is unlikely that this breccia either had a synsedimentary intraformational or stromatolitic origin.

Porous dolomite caps have been formed on the top of the breccia body in the core. These caps have grown during the growth in amptitude of the fold from small to large (Figs. 6.4a,b&c). Disseminated carbonates, anhydrite and barite mineralisation, including rectangular to cubic shapes, have been transferred randomly within the breccia deposit. 'Tilted-mushroom' shape fluid extrusions have been conduited from the core to the limbs through fissure openings and spread in a large area similar to the cap of a mushroom (Figs. 6.4a&b). These fluid extrusions have changed chemical composition of limb sequences in the affected areas.

6.6 Discussion

The minor to micro fault-propagation folds examined in this chapter are F_2 folds, parasitic to the major F_2 folds, thus the latter are considered to be fault-propagation folds as well, similar to the major F_1 folds (Fig. 3.3). These minor F_2 fault-propagation folds on the eastern limb of the Enorama – Oraparinna F_1 Anticlines show a southeasterly vergence and those on the western limb show northwesterly vergence, agreeing with the dextral rotation of structures along the major F_1 axial trace from Beltana to Worumba Anticlines (Chapter 3).

Detachment/fault-propagation folds are known to have generated breccia during thrusting (Fig. 6.5; Morley, 1994). These folds of centimetres to tens of metres scale from the central Flinders Ranges, documented in this chapter, show evidence of syntectonic breccia generation on a décollement that is extended as a listric thrust fault on to upper levels of the sedimentary sequence. Breccia has been localised mainly in the core and also formed on different levels of fold limbs and corresponding levels of core as well, and presumably has flown into wedge shaped tongues emanating from the breccia deposits. The wedges on limbs have mainly formed onto the forelimb adjacent to the core breccia deposit that is further advanced onto the forelimb over a bedding level. Wedges also have formed into the basal layers below the décollement but unlikely on back limbs. There is no evidence to suggest that the breccia on different levels of limbs, or that in the tongues emanating from the main breccia deposit in the core, was deposited synsedimentarily due to erosion of the main deposit by any means.

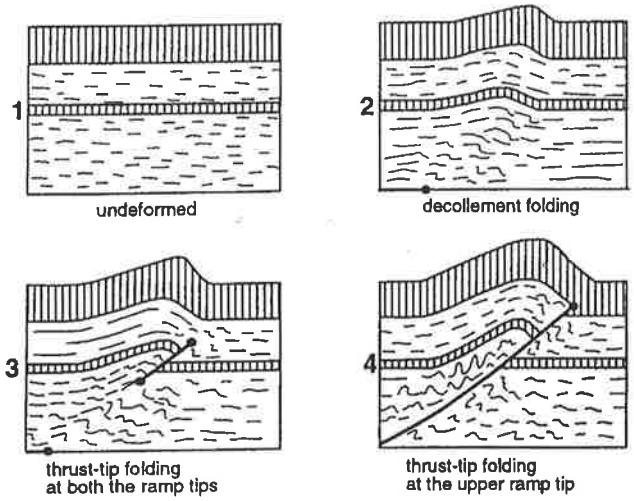

Fig. 6.5: Evolutionary model for thrust-related folds in the Osen-Rea thrust sheet, Norway (after Moley, 1994).

The natural detachment/fault-propagation fold examples show the following characteristics in relation to the diapirs in the Flinders Ranges that are confined into anticlines:

(a) Asymmetry and vergence of anticlines (e.g. Enorama and Moralana Anticline, Chapter 3).

(b) Steeper or overturned dips on the back limb, compared to moderate or gentle dips on the forelimb (e.g. Enorama and Moralana Anticlines, Fig. 3.8a).

(c) Occurrence of lower sequences on the back limb rather than on the forelimb (Fig. 3.8a).

(d) Occurrence of a well-defined forelimb syncline and an ill-defined or half-developed back limb syncline (Fig. 3.8a).

(e) Thickening or thinning of limb sequences adjacent to the hinge as has been recorded adjacent to the Enorama Diapir by Lemon (1988).

(f) Formation of parasitic folds on both limbs, i.e. asymmetric folds verging towards the axial trace on the back limb (Fig. 4.1a), and non-verging upright folds on the forelimb (Figs. 4.2a-d, 4.4f, Section 5.7.3c).

(g) Well-defined bedding-slip lineations on the limbs, nearly perpendicular to the fold axes (Figs. 4.6a,b), that are ill-defined on the hinge zone.

(h) Shortening of the fault-propagation fold models between 17-29%, compared to that of the Enorama Anticline of 26% (Fig. 3.8c).

(i) Formation of breccia along a low angle décollement fault by gouging of a weak layer on a competent detachment surface, which developed into a listric thrust fault (Fig. 3.8a).

(j) Breccia comprises clasts from the sequences in contact with the décollement and up to those at the end of the tip line, T, on the listric thrust fault surface. In comparison, breccia in the Beltana Diapir contains clasts from the basement, the lowest Adelaidean of Callanna Beds and the Cambrian sequences (C.R. Dalgarno and W.V. Preiss, unpublished field notes, South Australian Mines and Energy, 1980), thus suggesting extension of the listric thrust surface up to the Cambrian sequences.

(k) Possible formation of perched breccia deposits on different levels of the hinge zone and on limbs. This is evident by the occurrence of breccia layers between the Enorama Shale and Etina Formation, east of the Enorama Diapir (Section 4.5, Fig. 4.5).

(l) Translational movement of the axial plane of the fold towards the forelimb (fault-propagation fold models only), leaving the major breccia deposit under the back limb and a perched breccia deposit on the forelimb. This is evident by the shifting of both magnetic and Bouguer gravity anomalies to the east of the Blinman – Oraparinna Diapirs, as indicated on the Parachilna 1:250,000 geological map of Reid and Preiss (1999).

(m) Flow of breccia and fluids through fissures into the limbs, causing temporal changes in composition of host sequences adjacent to the diapirs; as reported by Lemon (1988) adjacent to the Enorama Diapir.

(n) Formation of wedge shaped tensional fractures emanating from the breccia deposits, on to the forelimb and under the décollement surface, and synchronous filling of these tongues with breccia, barite or dolomite. Wedges emanating from the Enorama – Oraparinna Diapirs to the western (fore) limbs containing breccia clasts have been reported by Dalgarno and Johnson (1968). Barite deposits, e.g. the Dunbar Lodes (Scott, 1979) occur on the western limb of the Oraparinna Anticline.

(o) Carving of breccia into weak sequences adjacent to main breccia deposits.

(p) Floating of rafts as wide as 1/3 width of the breccia deposit, in the core of the fold. Rafts up to 3 km long occur in the Blinman Diapir (Coats, 1964a; Chapter 2).

(q) Formation of dolomite in breccia deposits and dolomite caps at the top of the diapir. These were documented by Lemon (1988).

(r) Formation of breccia in the cores of fault-propagation folds/detachment folds, but uncommon in synclines. This is indicated on the major structure interpreted in Chapter 3, showing the structural control of breccia deposits, mainly into anticlines and not synclines.

In comparison to Lemon's (1988) laboratory sandbox models, these detachment/fault-propagation fold models show:

a. That the folds have been formed in the nature thus materials in the models and processes involved are compatible with the natural phenomenon and further, are parasitic to the major structures.

b. Breccia is represented by breccia while no artificial membrane is wrapped around the diapir and breccia is free to interact with the host or flow into dilating wedges during progressive deformation.

c. Breccia deposits within these folds were formed during compressional deformation. The main breccia flow was derived and transported along décollement and listric thrust faults during thrusting, therefore breccias possibly had outward deviatoric pressures. The thrust models agree with: (1) forcible emplacement of breccia as noted by folded remnants of the host rocks into steep to moderate dips at the margins of the Enorama Diapir (Mumme, 1961 and Coats, 1964a), and (2) the host formations are rarely brecciated and contact metamorphism is particularly absent, showing the passive nature of intrusions while the source bed mobility, instead of density, was paramount to the intrusive process (Mount, 1975).

d. The models show occurrence of breccia on the hinge and limbs of anticlines but is unlikely to form in synclines unless controlled by other factors.

e. The examples show a continuous supply and formation of breccia on the main décollement, during progressive deformation. Deposits that initially formed in detachment folds apparently have formed into fault-propagation folds during progressive deformation (Figs. 6.4, 6.5). Therefore, the diapirs that formed in the fault-propagation folds show a shape of "upside down plunging cucumber", instead of "pillow to overturned water-drops of Lemon's (1988)".

Therefore, these natural detachment/fault-propagation fold examples from the Flinders Ranges show that breccia flows have been driven by compression and raised through the sedimentary column during thrusting, thus forming diapirs. These thrust models, including the major Enorama Diapir (Fig. 3.8a), do not show inward dipping peripheral sinks around the diapirs, as modelled by Lemon (1988) in the synsedimentary model. This is further discussed in the final Discussion (Chapter 13).

Chapter 7

BARITE VEIN STRUCTURE AND MECHANISM OF FORMATION

7.1 Introduction

The relationship between the orientation of principal stress and strain axes and vein formation has been investigated by many researchers in the past (Shainin, 1950; Durney and Ramsay, 1973; Durney, 1979, 1985; Pollard and Segall, 1987; Ramsay and Huber, 1987; Rothery, 1988; Smith, 1996; Becker and Gross, 1999; and Srivastava, 2000). Two major extensional fracture systems have been identified to most commonly occur during both pure and simple shear. In pure shear, the extensional fractures are generally oriented parallel to the principal (incremental) compression axis (Fig. 7.1a) and in simple shear they are generally oriented at 45° or 135° to the shear boundaries (Fig. 7.1b). Progressive deformation in simple shear may cause fracture propagation concurrent with shear displacement resulting in sigmoidal veins (Fig. 7.1c, Durney and Ramsay, 1973). During pure shear or simple shear, complex patterns of vein arrays can also be formed. As well as the extensional fractures oriented parallel to the principal incremental compressive axis, two conjugate shear zones also may form during compression, forming two arrays of en échelon veins (Fig. 7.1d,e). These veins are either parallel in orientation (Fig. 7.1d; Type A of Beach, 1975) or converge towards the acute bisector of the conjugate arrays (Fig. 7.1e; Type B of Beach, 1975). Smith (1996) included the parallel and convergent conjugate arrays of Beach (1975) as two sub-configurations in his vein-array configuration (Fig. 7.1f). Smith's (1996) analysis classifies vein-array geometries of all types, and includes parallel, convergent or divergent vein-arrays towards the acute bisector of the conjugate arrays. Srivastava (2000) added zone-parallel pairs of veins that require opposite sense of shearing on two arrays that are conjugate and yet parallel to each other. The author suggested that this is a geometrical-type end-member and cannot form in rocks due to mechanical constraints. This theoretical framework is considered in this chapter, in relation to barite vein formation in the central Flinders Ranges.

Thousands of barite vein occurrences have been reported from the Adelaide Fold Belt. Vein descriptions and inspection reports from the Mines Department (SA) geologists and field officers, including mineral tenure, production, mining operations, geological setting, quality and reserves, are presented in the 'Mining Resources Review, Quarterly Geological Notes and Mineral Resources Review journals published by Primary Industries and Resources, SA. McCallum (1992) summarised all these occurrences, including vein orientation and dip data. Three BSc (Honours) theses also have been produced on Australian barites (Reid, 1969), Artipena Lodes (Robertson, 1981), and

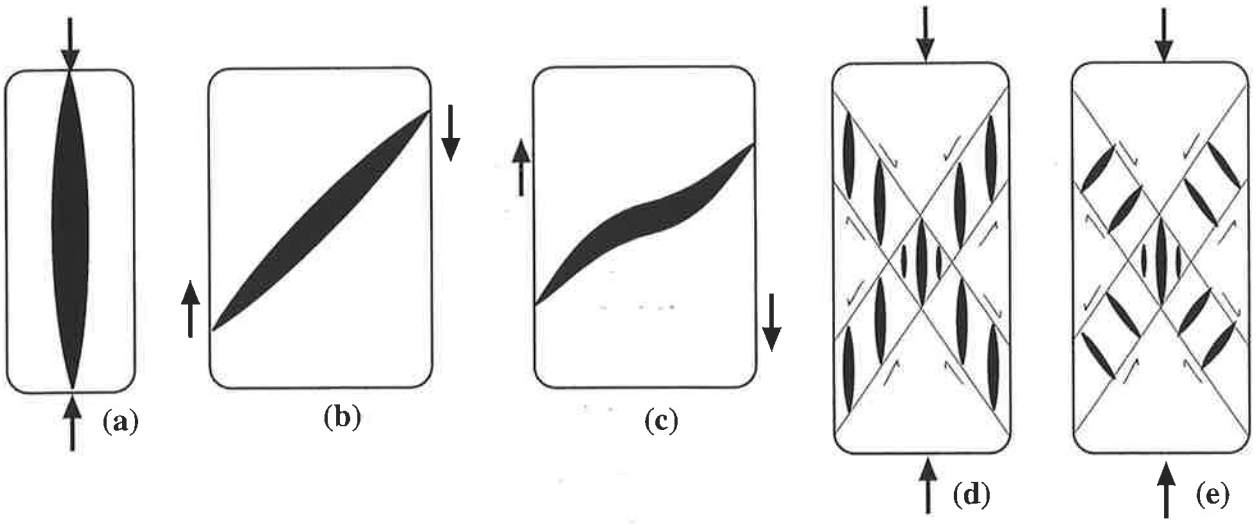

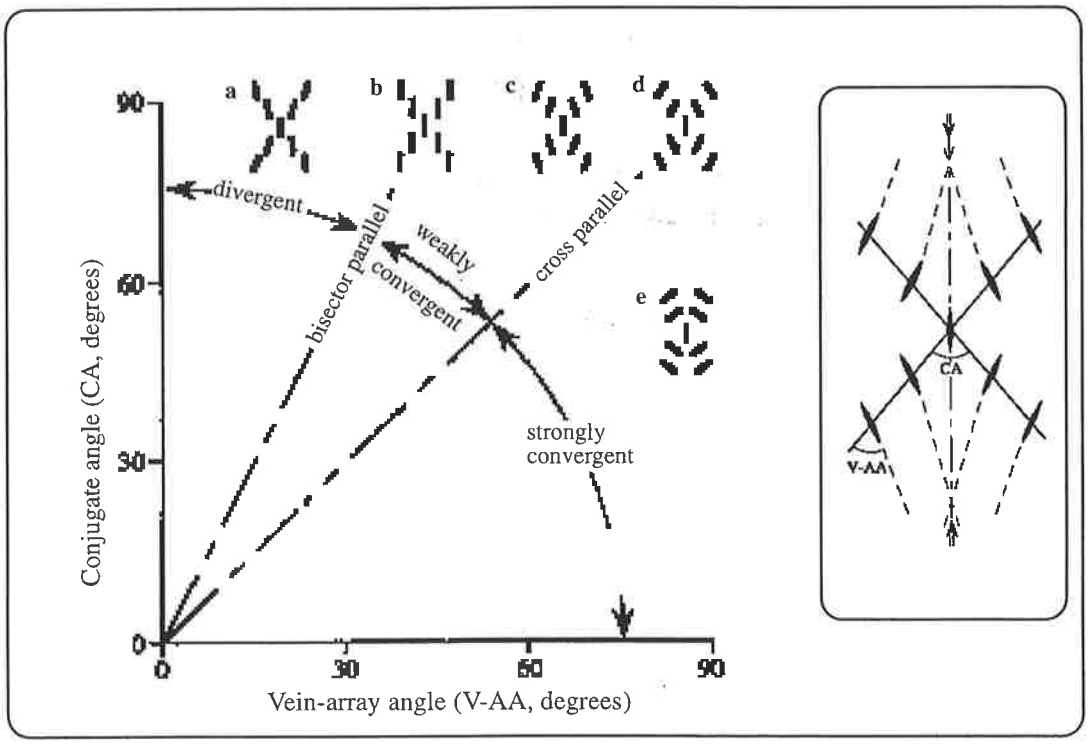

(f)

Conjugate angle (CA, degrees)

Fig. 7.1a-e: Different geometric types of vein formation in extensional fractures. (a) Veins oriented parallel to the principal (incremental) axis in pure shear. (b) Veins oriented 45° to the shear boundaries in simple shear (c) Formation of sigmoidal veins in progressive simple shear deformation. (d-f) Vein formation in conjugate shear zones. (d) All veins are parallel to the bisector of the conjugate array, Type A of Beach (1975). (e) The veins of one array are parallel to the trend of the conjugate array, Type B of Beach (1975). (f) Geometry of all types of vein arrays, indicating conjugate-angle (CA) versus vein-array angle (V-AA, see inset), after Smith (1996).

Oraparinna barite deposits (Cawley, 1983), all from the Department of Geology and Geophysics of the University of Adelaide.

Barite veins generally range from 1-3 m in width and 100-300 m in length, and cut across Neoproterozoic to Cambrian strata of the gently dipping sequences in the Adelaide Fold Belt. These veins commonly dip steeply to moderately (e.g. Carey Hill Lodes (Figs. 1.2, 7.2a)), but bedding parallel veins are found at Noarlunga (Fig. 1.1). Barite veins are also hosted by the diapirs, e.g. the Mount Frome Diapir (Figs. 1.2, 7.2b).

Many barite deposits have been commonly found comprising several major lodes and numerous subparallel and en échelon veins, stringers and pods (e.g. Artipena Lodes; Barnes and Robertson, 1985). Furthermore, lodes are generally parallel to adjacent fault or fracture systems (e.g. Patawarta Barite Deposits; Townsend, 1985). Lodes may shear off along faults or bedding planes as in the Oraparinna Mine, between keels and crowns (McCallum, 1982). Elongated rafts of continuous or discontinuous host rock inclusions commonly occur parallel to the vein borders, as seen at the Carey Hill Deposits (Fig. 7.2a; McCallum, 1990). The veins that form within diapirs contain layers of discontinuous host-breccia clast inclusions, arranged parallel to the vein borders (e.g. the Mount Frome Diapir, Fig. 7.2b). The hosts on either side of veins may shear against the lode or show unequal patterns of folding across the lodes, as shown by the 1A Lode in the Oraparinna Mine.

Olliver and Scott (1978) considered that the barite deposits were formed by migration of barium sulphate from the nearby Adelaidean sediments, with redeposition in open fracture zones. Robertson (1981) suggested a fluid-mixing model for barite veins, following the generalised model for vein formation by Boyle (1972). According to this model, Ba rich brines migrated upwards within the opened-up fractures to meet sulphate rich waters migrating downwards along the same fractures, which thus formed barite at the meeting of the two fluids. Cawley (1983) also considered that Ba rich brines, further enriched with Ba released by sericitisation of K-feldspars of the Brachina Formation, were circulated through fractures while mixing with sea/connate waters, to form barite veins.

The mechanism of barite vein formation in the Adelaide Fold Belt, structural control, and the internal texture/microstructure of the veins are however, still poorly understood. A comprehensive analysis is yet to be done. Thus, the major barite vein deposits from the central Flinders Ranges, and in particularly those of Oraparinna and Dunbar Mines, were subject to detailed investigation of their vein texture, propagation and the structural control of vein formation in the context of previously described Delamerian deformation history of the Adelaide Fold Belt.

(a)

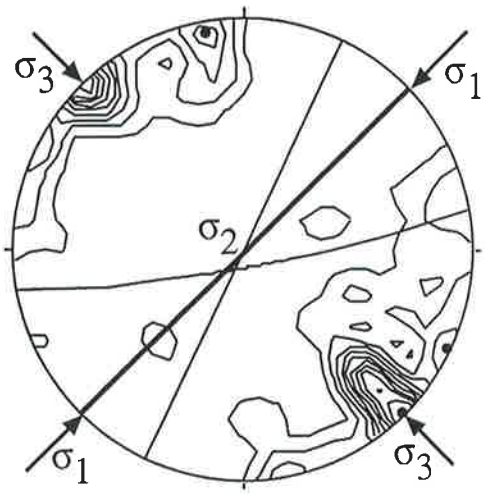

(c)

(b)

Fig. 7.2a-c: Barite lodes in the Flinders Ranges and their orientations. (a) Remnants of the mined out Carey Hill deposits. The vein strikes east and dips 80°N while the host strikes N70°W and dips 50°NE. Photographed facing east. (b) Mount Frome deposits hosted by the Mount Frome Diapir. The vein strikes east and dips 75°S. Photographed facing west. (c) Stereographic analysis of major barite veins with production and reserves of more than 2000 tonnes in the central Flinders Ranges. The major type is vertical and NE-SW orientated (thick line). Two subtypes occur in acute angles to the major type, with an interlimb angle of 54°. 140 data, contoured at 1,2,3,...,7 times uniform. Source of data: McCallum (1992).

7.2 Analysis: Major Barite Deposits

Barite veins in the major vein deposits, defined by total production and reserves of more than 2000 tonnes from the Flinders Ranges, were analysed stereographically in order to investigate principal stress orientation in relation to the structure. These data indicate three sets of veins are prominent; (a) strike N45°E and dip 88°NW are dominant, while two are subordinate (b) strike N26°E and vertical, and (c) strike N80°E and dip 84°S (140 data, Fig. 7.2c). The mutual intersection axis of these three sets is nearly vertical and the approximate acute angle between the two subordinate types is 54°. The dominant set lies at the bisector of the acute angle between the two subordinate types and makes an angle of 19° with the northerly trending subordinate type (b; see above); and 35° with the easterly trending subordinate type (c).

7.2.1 Oraparinna Barite Mine

A complex system of barite veins is hosted by the siltstones of the Brachina Formation in the Oraparinna Barite Mine. Mine working occurs mainly on five major lodes namely, 1A, 1B, 1C, 1D and Link Lodes (Figs. 7.3a). The 1A Lode is in contact with the 1B and 1C Lodes, while the 1D Lode is isolated at the southeastern end of the mine. The 1A Lode generally dips moderately to steeply to the NW, while the 1B, 1C and 1D Lodes also dip the same to the SE (Figs. 7.3a,b,c). Both the 1A and 1C Lodes are in contact at the northeastern end of the mine on Level 6 (Fig. 7.3d). The contact zone is somewhat fractured, but shows a continuity of barite from one vein to the other, indicating that the veins formed simultaneously. The intersection of these two lodes at near-surface levels plunges 45° NE (McCallum, 1982). The 1A Lode above No.2 level dips to the east, and below the same level and north of 1A-1C Lode the junction dips steeply to the west (McCallum, 1982). McCallum further noted that on some cross sections, the 1A Lode north of the 1A-1C Lode junction appears to be more aligned with the 1C Lode than with 1A Lode. Therefore, a vein may dip to both the NW and SE, forming both the 1A and 1D Types.

Barite vein orientation data were collected from the surface and also from levels 5, 6 and 7 of the mine. Levels 1 to 4 were not accessible due to back filling, but the data for these levels were obtained from the maps produced by the Department of Mines and Energy of South Australia (McCallum, 1982). Additional data for levels 5, 6 and 7 were also obtained from the maps produced by Commercial Minerals Limited (McCallum, 1982). All of the orientation data for major

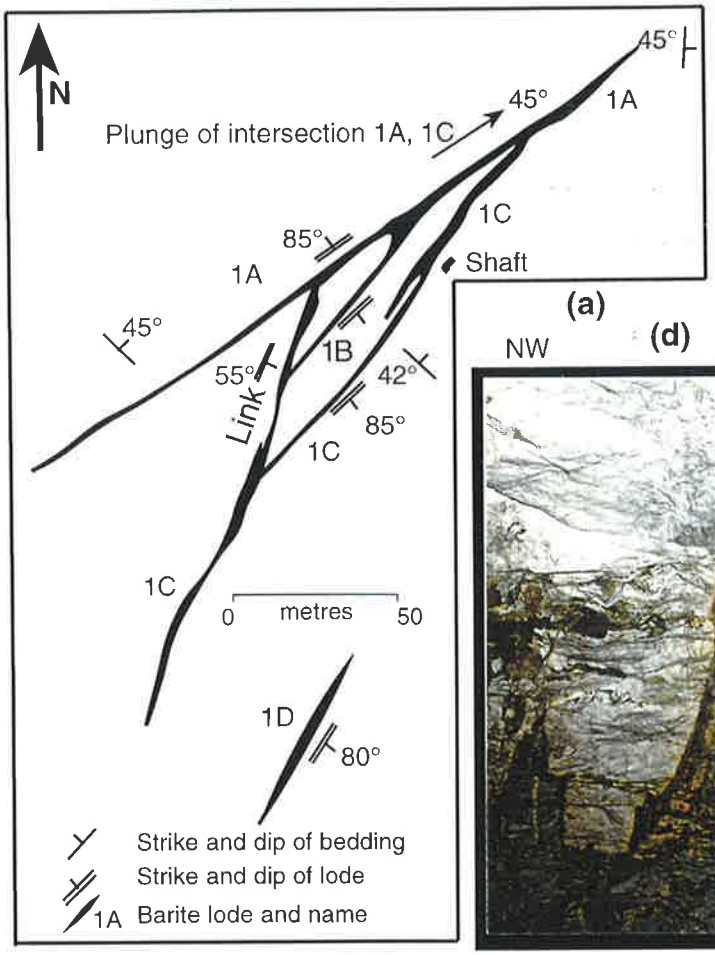

(a)

(d)

(b)

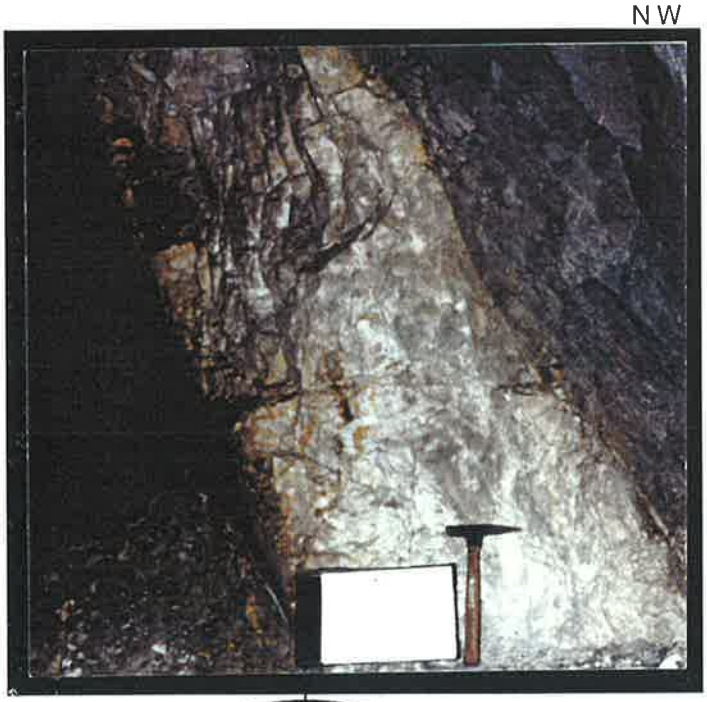

(c)

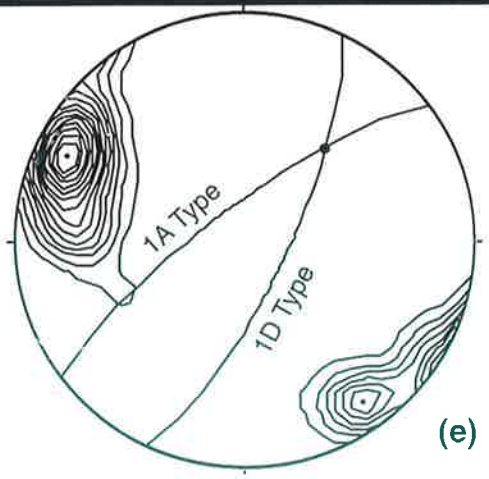

(e)

Fig. 7.3a-e: (a) Generalised, near surface plan of the major barite lodes (1A, 1B, 1C, 1D and Link Lode) distribution at the Oraparinna Barite Mine (Modified after McCallum, 1980). (b&c) The 1D and 1A Lodes at Level 6 of the mine, dipping steeply to SE and NW respectively. (d) The NE tunnel face at Level 7 of the mine showing the intersection of 1A and 1C Lodes dipping NW and SE respectively. Horizontal edge is 5m. (e) Stereogram showing the 1A and 1D Types striking N53°E and N27°E and dipping 77°NW and 77°SE respectively. The vein intersection axis plunges 45°->041°. 287 data, contoured at 1,3,..,11 times uniform.

and minor barite veins (287 total data; field collection 95, Commercial Minerals Ltd 122 and MESA 70) were plotted on one stereogram (Fig. 7.3e). This shows clearly that two types of veins dominate, (a) strike N26°E and dip 77°SE (a dominant type), and (b) strike N53°E and dip 77°NW (a subordinate type). These two types correspond to the 1D (SE dipping) and the 1A (NW dipping) Lodes, which were therefore named as '1D' and '1A' Types, respectively. The acute interlimb angle between these two types is 37°. The 1B and 1C Lodes strike and dip similarly to the 1D Lode, and thus belong to the 1D Type. The continuity of barite between the 1A and 1C Lodes and the average acute angle between the two types of 37° suggest these lodes are conjugate and formed at the same time under the influence of the same stress field.

Both the 1D and Link Lodes are lens shaped with sharp ends, while most of the other lodes either thin out laterally or end abruptly (Figs. 7.3a, 7.4a). The Link Lode dips moderately to the east and is connected to the 1C Lode, but lenses out before the 1A Lode on both the surface and the No.2 level, and they intersect at the No 3 & 4 levels (McCallum, 1982). A series of veins oriented near parallel to the Link Lode, strike between NNW and NNE, and dip moderately to the east (Fig. 7.4b). These veins, which are sub parallel to the Link Lode, were named 'Link Type Lodes', with mean strikes of N15°E and dips 61°E (Fig. 7.4c).

Thus in summary, the Oraparinna Mine contains three sets of barite veins, the 1D (dominant) Type, and Link and 1A (subordinate) Types. These veins intersect adjacent to a common axis, plunging 45° ->041° (Fig. 7.4d). The two subordinate types, Link and 1A, make an acute angle of 56° with each other. The 1D (dominant) Type lies between the two subordinate types and makes an angle of 19° with the northerly trending, Link subordinate Type and 37° with the easterly trending 1A subordinate Type.

7.2.2 Vein deposits adjacent to the Oraparinna Mine

The area around the Oraparinna Barite Mine is rich in barite vein deposits namely: the Belsen, Western, Bainbridge and Roberts Lodes (Fig. 7.5a). These veins have been worked out and abandoned at shallow depths. Maps produced by the Mines Department (SA), contain data for the Belsen, Western and Bainbridge Lodes surface levels, while the Robert's Lode also contains data for levels 2&3 (McCallum, 1982). Stereographic analyses of data for each lode show sets of vein occurrences related to those in the Oraparinna Mine. The 1D Type is prominent in the Western Lode, Bainbridge and Roberts Lodes, and both 1A and Link Types in the Belsen Lode. The plunge of the intersection axes of individual lodes varies between 27° and 50°, and trends between N21°E

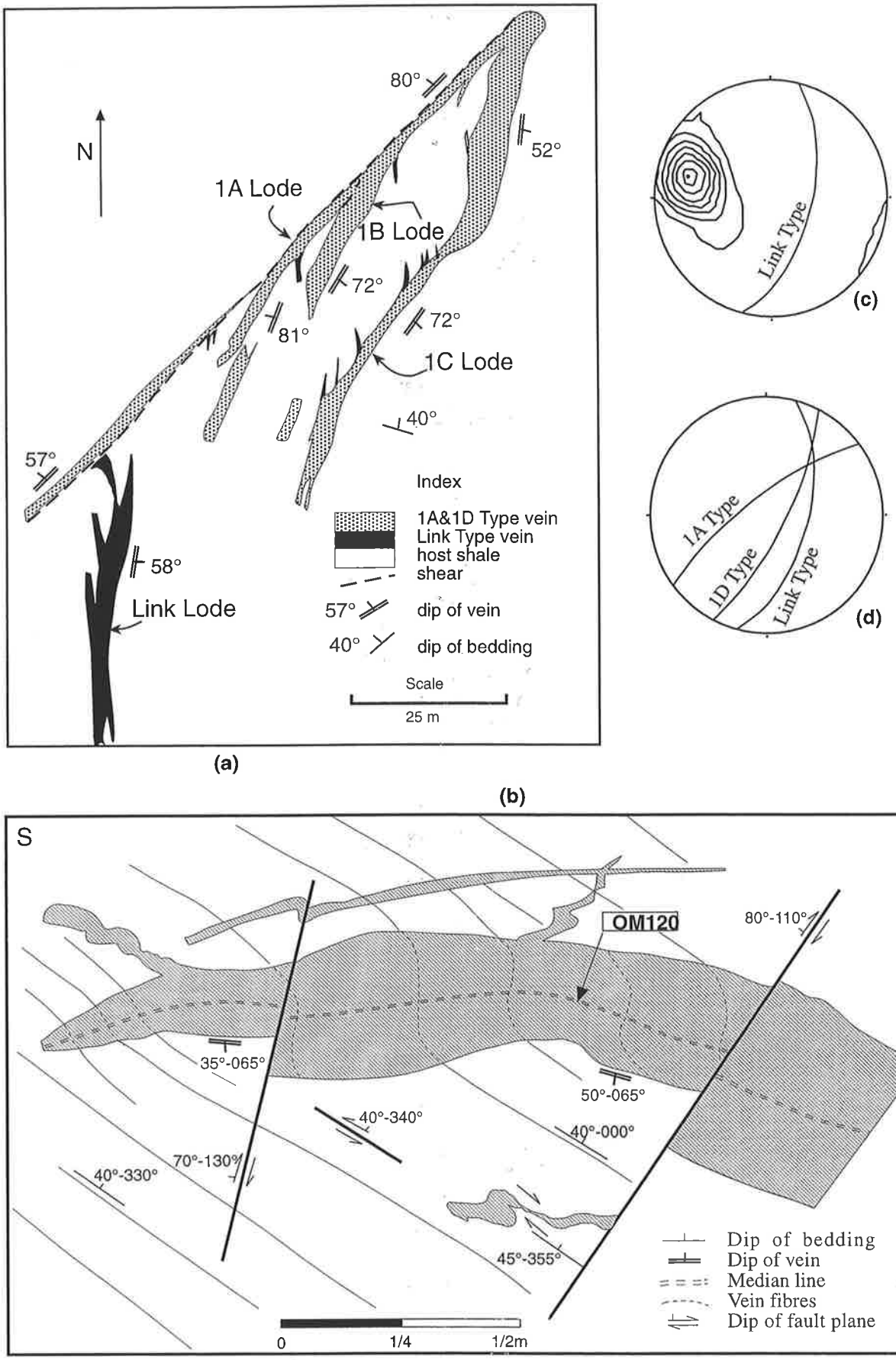

Fig. 7.4a-d: (a) Mine plan on Level 5 of the Oraparinna Barite Mine showing major 1A, 1B, 1C and Link Lodes. A shear plane occurs along the border of 1A Lode. Plan modified after Commercial Minerals Ltd., 1985. (b) Map of a sub-Link vein on Level 6, adjacent to the 1A Lode. The median line of the vein is denoted by two parallel dashed lines. (c) Stereogram for the Link Type veins showing average strike of N15°E and dip of 61°E, 18 data, contoured at 1,3,5,..,11 times uniform. (d) The three major types of veins of the mine, showing the mutual axis plunging 45°->041°.

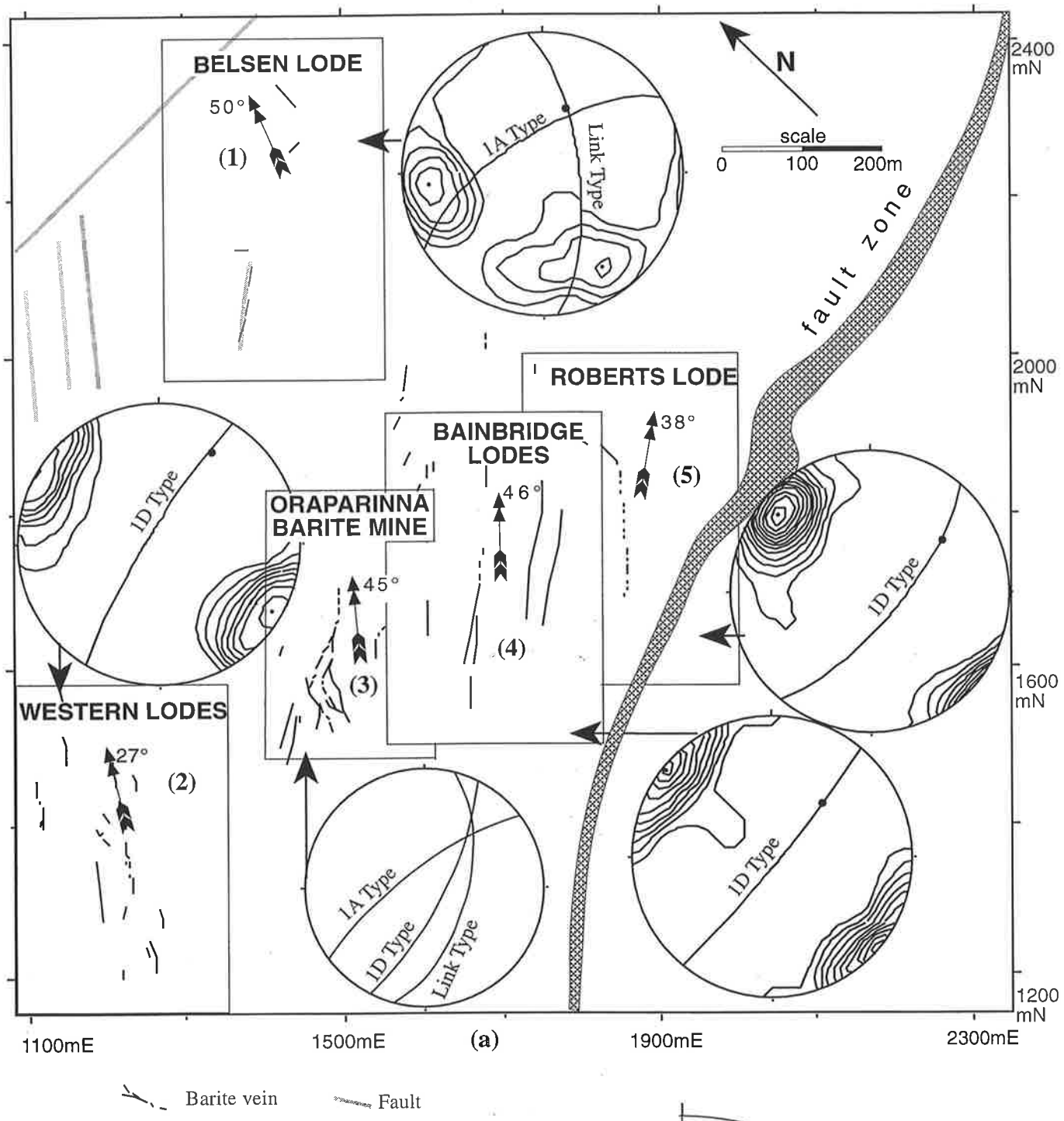

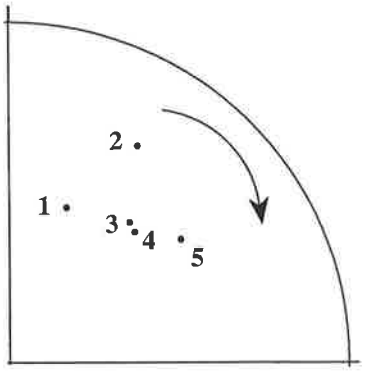

(b)

Fig. 7.5: (a) Barite lode systems adjacent to the Oraparinna Mine and their stereograms showing major vein types. Vein intersection axes are marked by dots (•) on the stereograms and by arrows on relevant lode systems. **(1)** Belson Lode, 35 data: contoured at 1,2,3,4 times uniform; followed by **(2)** Western Lode, 38: 1,2,..,5; **(3)** Oraparinna Mine (adopted from Fig. 7.4d); **(4)** Bainbridge Lode, 29: 1,2,3,...,9; and **(5)** Robert Lode, 36: 1,2,3,...,9. Data includes that from Mines Department, SA. (b) NE quarter of a stereogram showing dextral rotation of the vein intersection axes (•) towards fault zone.

and N55°E (Fig. 7.5b). The Belsen Lode, Western Lode, Oraparinna Mine, Bainbridge Lodes and Robert's Lode are located at 700, 600, 400, 300 and 150 m north of the major fault zone adjacent to the mine and the orientations of vein intersection axes trend 021°, 031°, 041°, 044° and 055°, respectively (Table 7.1). Thus the vein intersection axes indicate that a dextral rotation has occurred from NNE to ENE, towards the nearby major fault zone.

Table 7.1: Comparison of orientation of the barite vein intersection axes of the satellite vein systems adjacent to the Oraparinna Barite Mine, with respect to the decreasing distance to the southeastern major fault zone (see Fig. 7.5a).

Vein system	**Distance to fault zone**	**Strike and dip of the prominent vein Type**			**Plunge and orientation of the intersection axes**
		1A Type	1D Type	Link Type	
Belsen Lode	700m	N56°E/66 °W		N6°W/69°E	50°->**021°**
Western Lode	600m	N33°E/85 °W			27°->**031°**
Oraparinna Mine	400m	N53°E/77 °W	N27°E/77°E	N15°E/61°E	45°->**041°**
Bainbridge Lodes	300m		N40°E/86°E		46°->**044°**
Robert's Lode	150m		N40°E/73°E		38°->**055°**

7.2.3 Dunbar Lodes

The Dunbar Lodes (also known as Linke's Lodes) are hosted by thinly bedded siltstones of the Tapley Hill Formation on the western footwall of the Oraparinna thrust-related Anticline (Fig. 1.3). Thicknesses of the lodes vary up to 5 m and the lodes have been mined out by open-pit mining (Fig. 7.6a,b). All the veins commonly show thinning towards the ground surface from the bottom of the pit. Some of the veins thin out and continue as fractures towards the upper ground level without vein filling. Some veins show siderite crusting of up to 2 cm thickness along both borders, (McCallum, 1982). Thin siderite veins up to 5 cm thick also occur with no apparent association of barite. Diapiric breccia offshoots from the nearby Oraparinna Diapir have intruded both the host and the barite veins (Fig. 7.6a).

Most of the barite veins dip moderately to steeply to the south, and a few dip steeply to the north. Stereographic data analysis of the veins indicates an average strike of N80°E and a dip of 67°S with a vein intersection axis plunging at 54°->113° (Fig. 7.6c). There is not enough data to differentiate any subordinate types. General bedding strikes N10°W and dips gently, 4° to 15°W. The host is folded at the borders of the veins, showing higher dips of 20°W to 30°W, probably indicating some

Fig. 7.6a-d: (a) Vein distribution of the western pit-wall, Dunbar open mine. (b) A barite vein on the pit-wall showing inclusions along the median line. (c) Stereogram for barite veins showing average strike N82°E and dip 71°S with the vein intersection axis (thick dot) plunging 54°->113°. (d) Poles to bedding showing fold axis plunging 5°->279°. (c&d) 31 and 22 data, contoured at 1,2,..,9 and 1,4,..,16 times uniform, respectively.

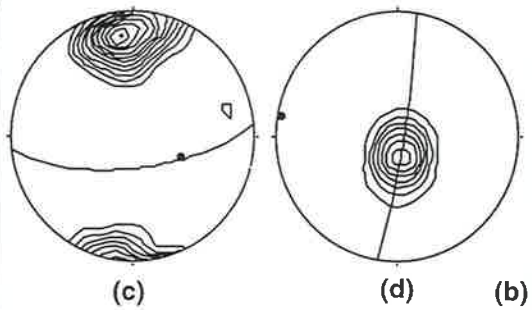

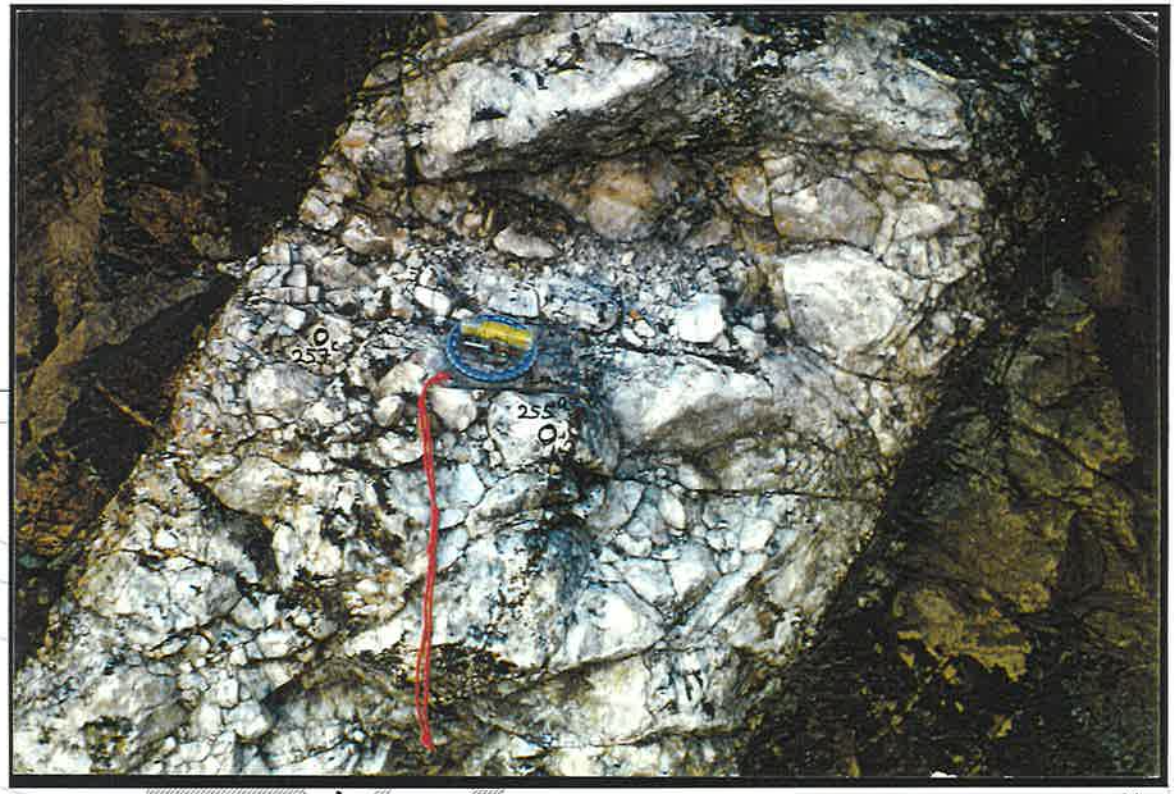

(a)

rotation of the sequences after vein formation (Hudleston, 1989; Gayer *et al.*, 1978). The fold axes of the host plunge 5°->279° (Fig. 4.6d).

7.3 Minor Barite Deposits

Disseminated minor barite occurs within host formations (Figs. 9.2, 9.6), and may be associated with minor detachment/fault-propagation folds as well. The latter were studied in detail from previous examples (Figs. 6.1f-i^). The folds show that breccia has been produced at different levels on the back limb and on the décollement-thrust surfaces that continued as reverse-thrust faults into the forelimb. Barite and dolomite mineralisation has formed within these breccia deposits and repeatedly brecciated, while mixing with breccia that was added during progressive deformation (Figs. 7.7a,b). Dilational fractures or fissures have formed in the host sequences of these folds, commonly as wedges or tongues emanating from the breccia deposit that taper into the host and occur both bedding-parallel and across bedding (Section 6.2.2). The tongues contain breccia, barite or dolomite. A series of bedding-parallel veins containing barite and dolomite has also formed in the hinge zones of the forelimb synclines, and thinned into respective limbs (Fig. 7.7d). These mineralisations show border parallel host rock inclusions, and thus have been formed synchronously during incremental fracture dilation (Ramsay, 1980; Ramsay and Huber, 1987; Fig. 7.7c). Therefore the mineralisations are of syntectonic origin.

The main mineral deposits around these detachment/fault-propagation folds fold have been formed below the décollement and in the forelimb syncline (Fig. 6.1h). In contrast, the thinly bedded hosts on the back limbs are unlikely to produce prominent extensional fractures due to absorption of thrust movements by bedding-slip, even though such rare fractures were also observed (Figs. 6.1h). Furthermore, disseminated dolomite deposits have also formed in minor quantities on the stretching forelimb immediately adjacent to the main breccia deposit in the core (Figs. 6.1g,g^).

7.4 Evolution of barite veins

Thin sections of barite veins from the Oraparinna Mine were studied under the microscope and electron microprobe. These veins commonly comprise both barite and calcite grains which essentially show an elongated fibrous nature (Fig. 7.8a,b). The grains occur near perpendicularly to

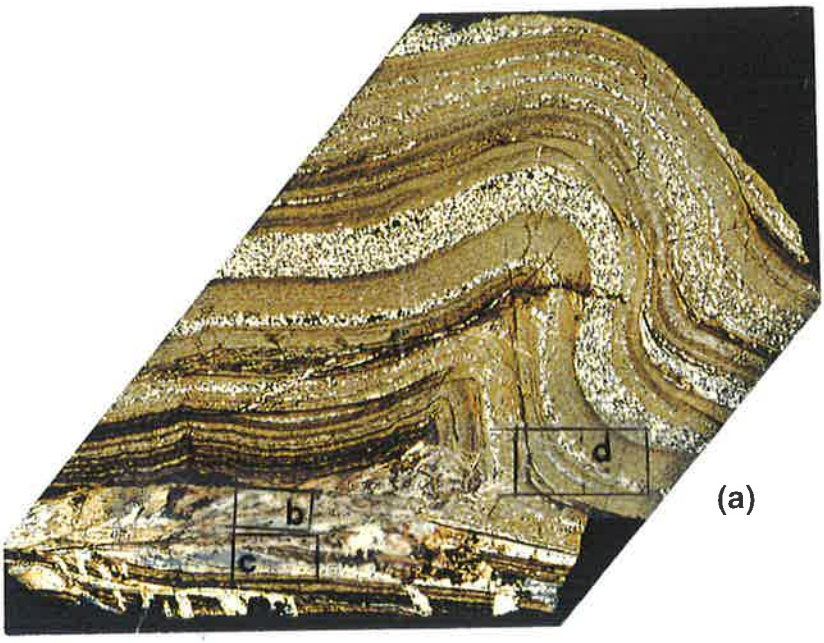

(a)

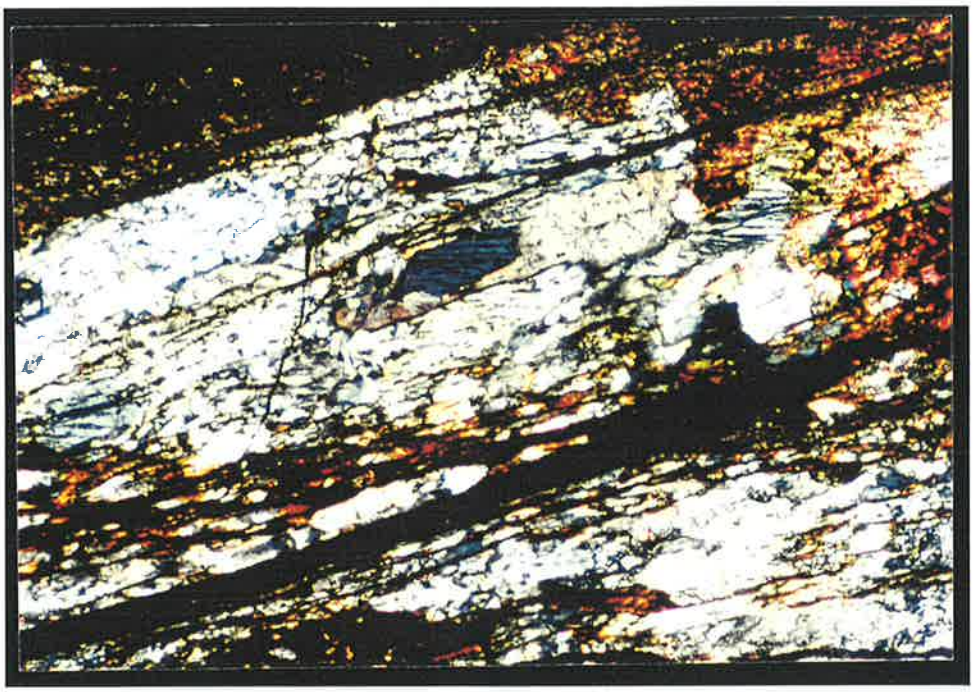

(b)

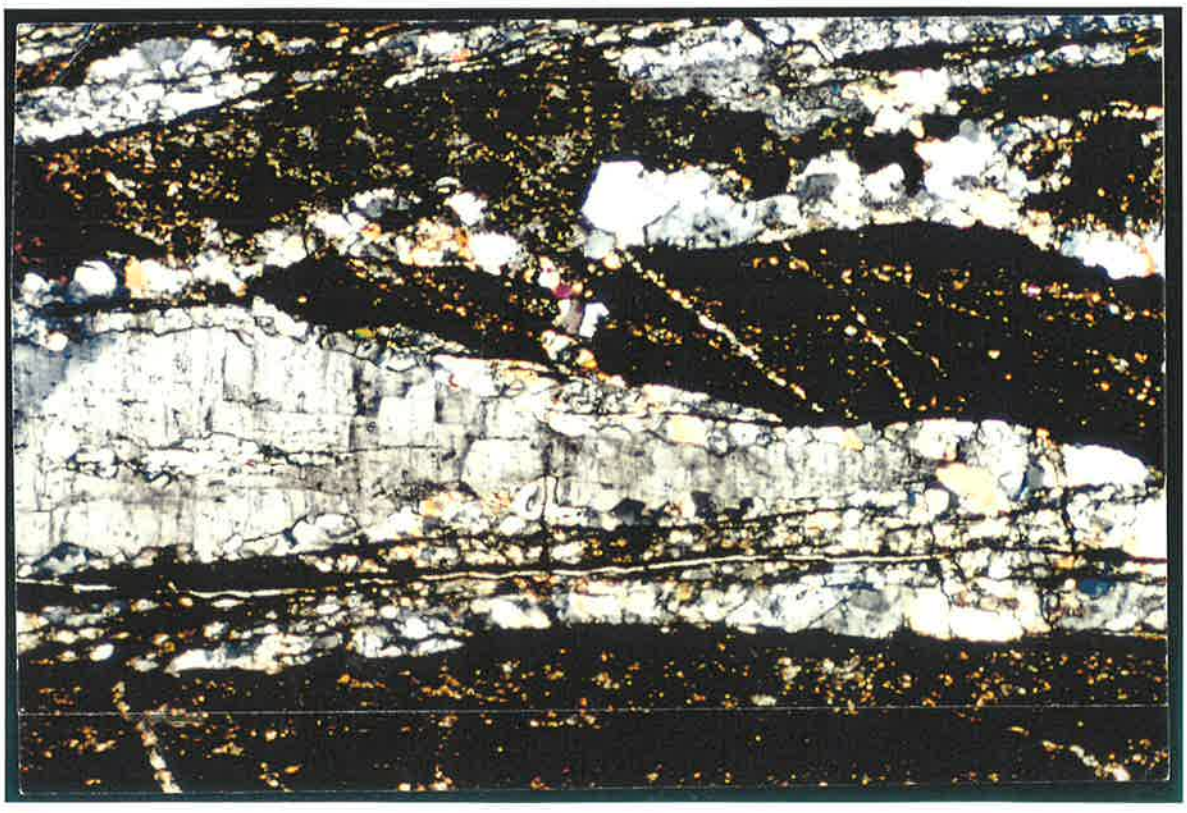

(c)

Fig. 7.7a-d: (a) Photomicrograph of the fault propagation fold at the western border of the Bainbridge No3 Lode (cf. Fig. 6.1f-i). Width of the section is 2.5 cm. (b) Barite (blue) associates with dolomite (white) in the brecciated fault-thrust zone above the decollement surface. Horizontal edge 3.5 mm. (c) Same mineralisation below the decollement along dilated tensional fractures. Horizontal edge 4 mm. Cont...

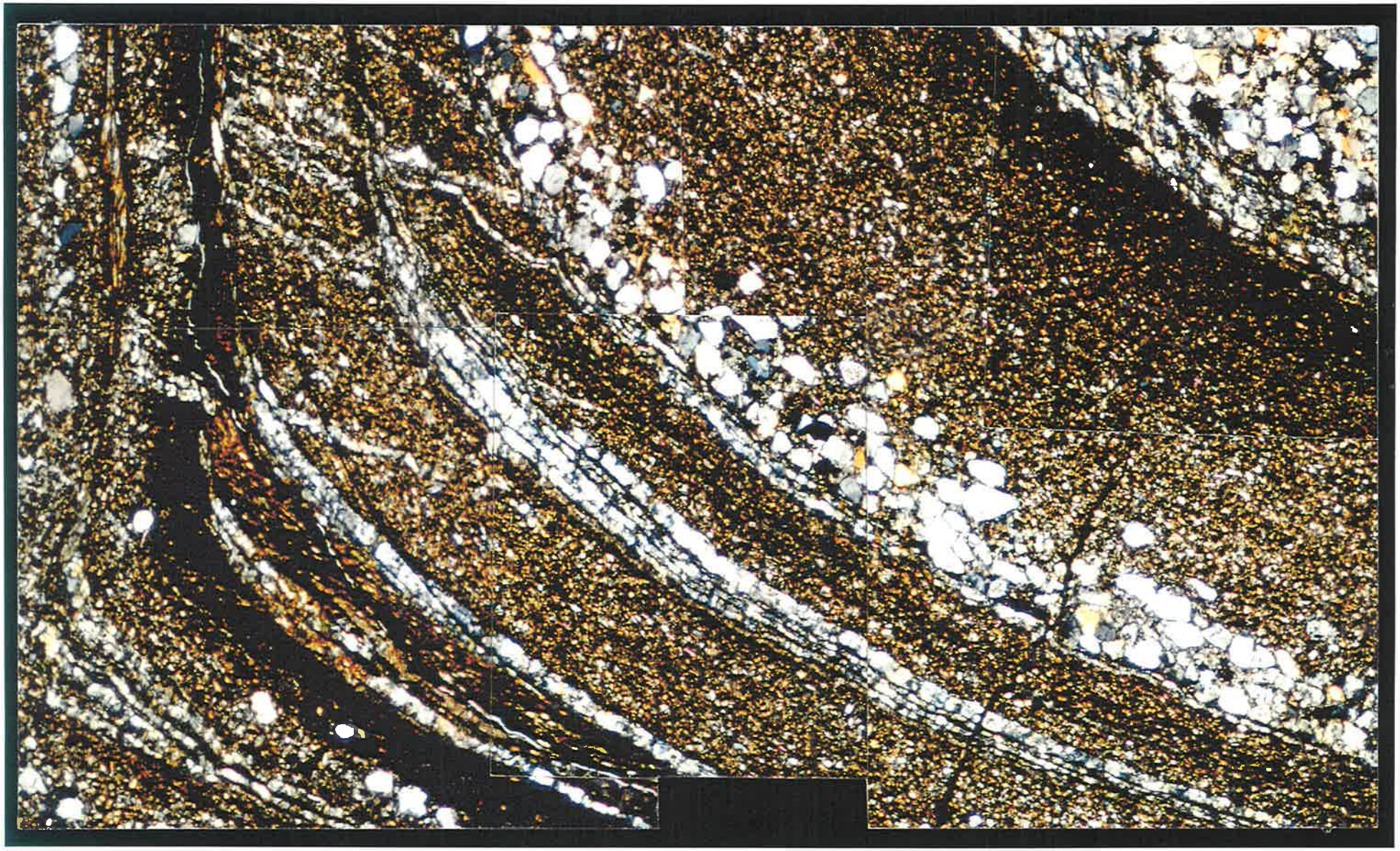

Fig. 7.7d: Cont... Barite (blue) and dolomite (white) in veins associated with the forelimb syncline. The bedding parallel veins are limited to the hinge zone, while the extensional veins in the top left quarter of the photograph make approximately 45^{o} angle with bedding. Horizontal edge 7 mm.

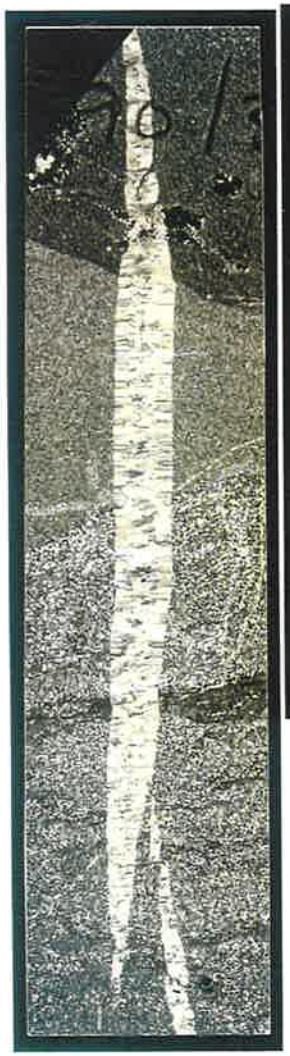

(a)

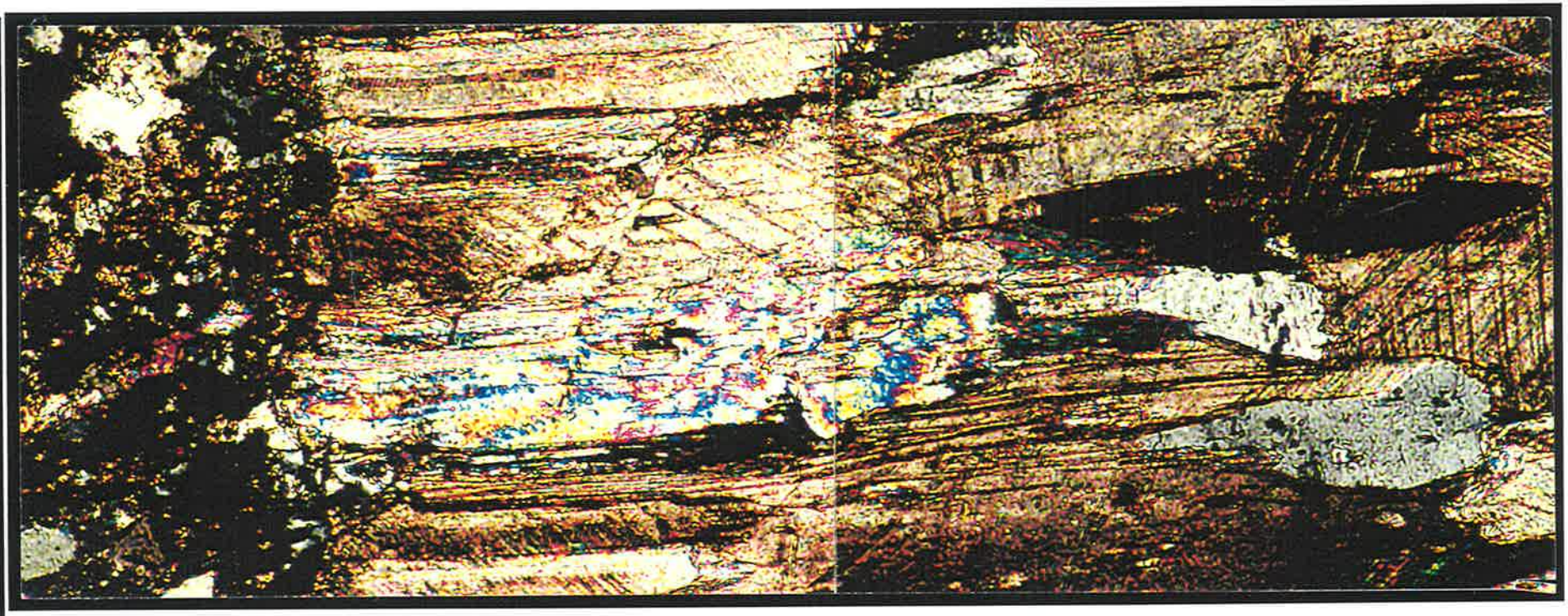

(b)

Fig. 7.8a&b: Thin section of a calcite/barite vein from the Oraparinna Barite Mine. Sample No. A987/2/90/38. (a) Under ppl light. Note the faint median line along the centre of the vein. Horizontal edge is 2.5 cm. (b) Under crossed polars, showing barite (grey); the rest of the pale colours of the vein are calcite. Horizontal edge 5 mm.

vein walls and essentially continue across a median line structure that is defined by a trail of fluid inclusions at the centre of veins (Figs. 7.9a,b,c,d; Ramsay and Huber, 1987). Fibres die out within the vein probably because the fibre long axis is not exactly parallel to the thin section plane, or the rate of fracture dilation was higher than the supply of ingredient material to form barite and therefore the grains ceased forming (Fig. 7.8b). In some of the occurrences, quartz is associated with elongated ends of barite grains (Fig. 7.9a&c). Occasionally the median line may contain host-rock inclusions, as is seen at Dunbar, but the elongated grains continue near perpendicularly across the median line (Fig. 7.6b). Adjoining fibre grains sometimes show colour contrast between them.

7.5 Post vein deformation

Post-vein shearing of the veins has been noted by previous authors, as for example the 1A Lode of the mine is cross cut by a shear plane near-parallel to the vein border (Fig. 7.4a; McCallum, 1982). At the grain scale, the undeformed barite grains generally show plumose textures (Fig. 7.10), even though this texture was found to be deformed in many sections.

7.5.1 Cataclasis

Cataclasis is a product of cataclastic flow which is a process of deformation that involves continuous brittle fracturing of grains in a rock, with attendant frictional sliding and possibly rolling of the fractured particles passing one another (Twiss and Moores, 1991). Most of the barite grains show microstructural features of cataclastic flow zones of varying thickness (Fig. 7.11a-c). The barite samples collected from isolated occurrences of the major fault zone near the Oraparinna Mine indicate extensive cataclastic flow, more than those of any other vein investigated, possibly suggesting the fault movements occurred or continued after vein formation (Fig. 7.11c). Shattering and rotation of these fragments suggest that dynamic fragmentation is the process causing grain size reduction. Grains with broken edges, as well as rounded edges, occur within barite veins where the former is a result of cataclasis, while the latter is a result of dissolution assisted by cataclasis (Agar, 1990). These cataclasts within the barite veins commonly show a preferred grain orientation indicating an aseismic slip, rather than a seismic slip, where such preferred orientation is unlikely to develop (Sibson, 1986). However, such preferred orientation in barites does not lead to any schistosity or foliation. The cataclastic flow has partly or in some cases completely destroyed the original fibrous nature of barite grains during post-vein deformation.

(a)

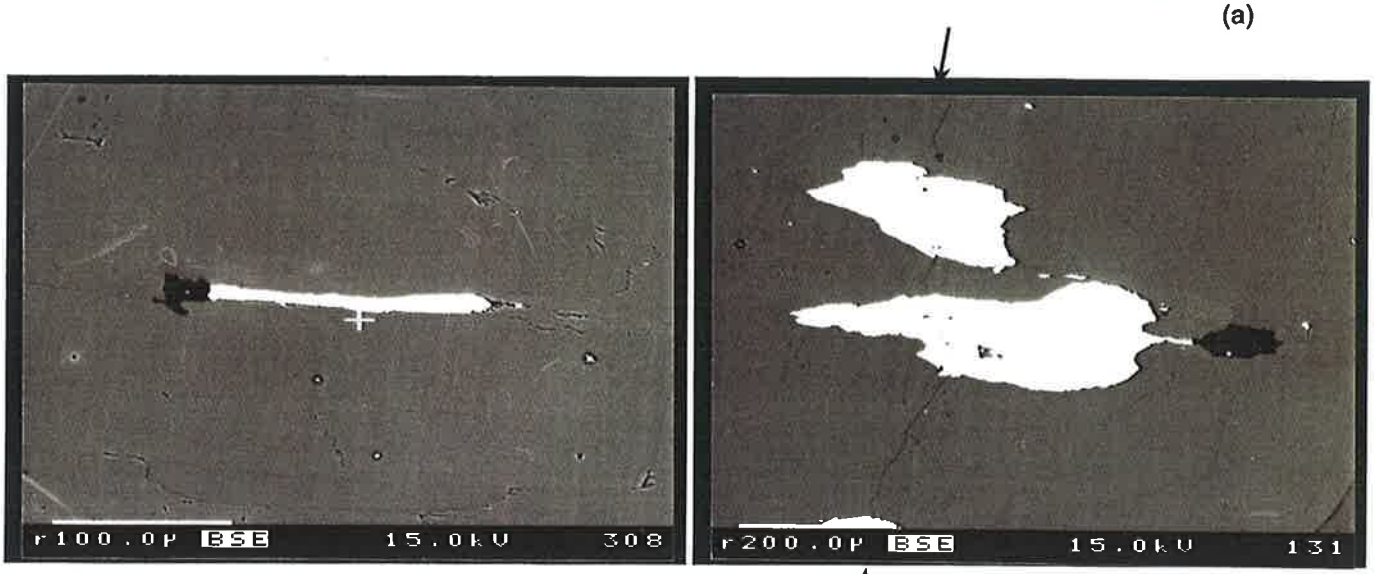

(b) (c) Median line defined by fluid inclusions

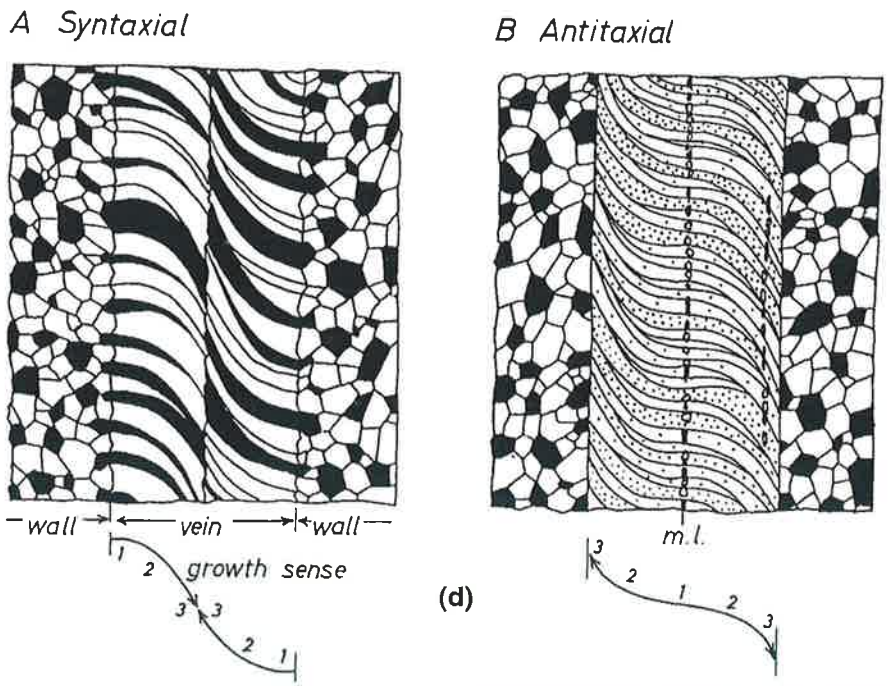

(d)

Fig. 7.9a-d: (a-c) Electron microprobe image of the vein shown in Figure 7.8b. (a) Barite (white) and calcite (grey) in the vein. (b) Top left barite grain of (a) shows extreme length to width ratio. (c) Barite grains continue across the inclusions of the median line. Black at the ends of barite (white) grains of (b&c) denotes quartz. White scale bars on the botton left of (a), (b) and (c) are 0.5, 0.1 and 0.2 mm, respectively. (d) Schematic diagram showing mechanism of antitaxial and syntaxial vein formation (Ramsay and Huber, 1987).

Fig. 7.10: Undeformed Plumrose texture of barite grains adjacent to the median line of the 1D Lode, Level 5 of the Oraparinna Barite Mine. Sample No. OM128[a]. Horizontal edge 3.5 mm.

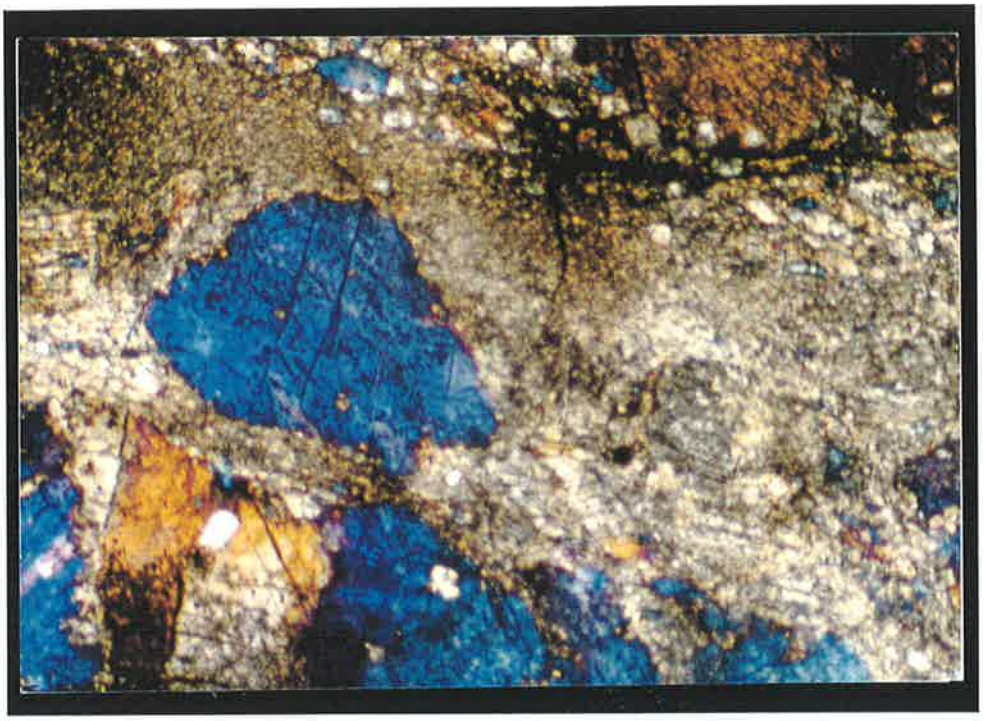

(a)

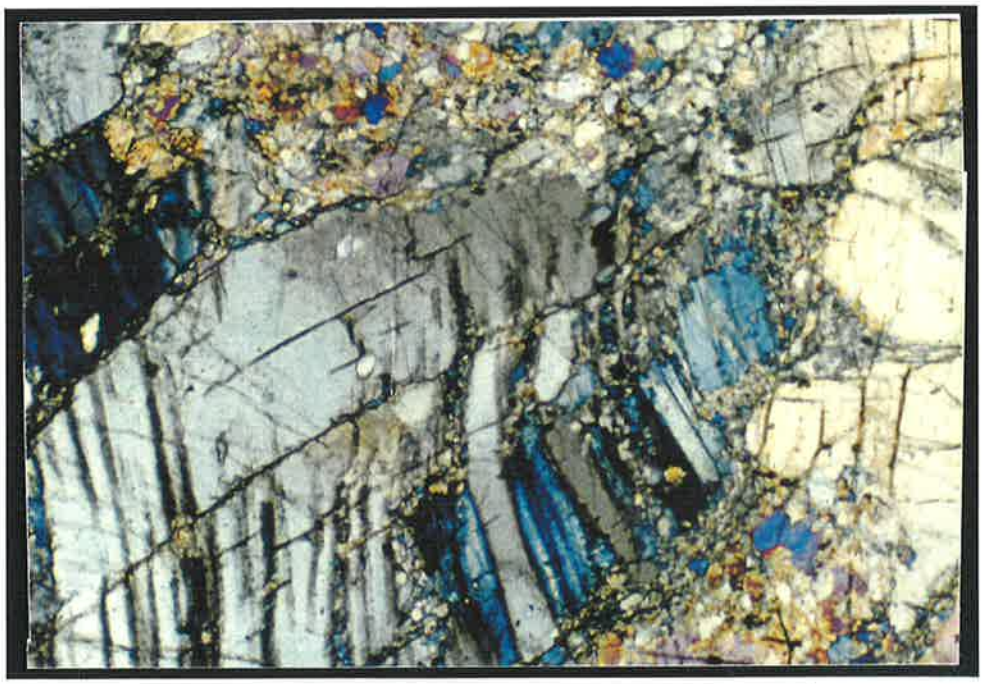

(b)

(c)

Fig. 7.11a-c: Deformational structures of barite grains. 1D Lode on the Level 5 of the Oraparinna Mine showing; (a) cataclasis, on the border of the Lode (Sample No. OM127) and (b) glide twinning, adjacent to the median line (Sample No. A OM108). (c) Both cataclasis and glide twinning lamellae in barite samples collected from the NE-SW fault zone adjacent to the mine. Horizontal edges a&b: 3.5 mm and c: 2 mm.

7.5.2 Grain boundary sliding

Grain boundary sliding is indicated by the dislocation movements in grains (Etheridge and Wilkie, 1979). Fine-grained mortar texture developed around large grains is common in barite veins (Fig. 7.12a). Undulose extinction is frequent in these old grains, indicating high strain, but is rare in younger grains. Increased strain has lead to the development of deformation lamellae, i.e. glide twinning, in old grains (Fig. 7.11b,c). The lamellar twins mostly develop at a high angle to the grain boundaries. New barite grains have developed along deformation lamellae possibly due to accommodation of grain boundary sliding and migration as a result of transfer of material through lattice defects, defined as diffusional accommodation by Ashby and Verrall (1973, Fig. 7.11b).

7.5.3 Annealing

Barite in the Adelaide Fold Belt has semi-transparent colourless mottling in grains which are dominantly translucent white. The mottles are randomly distributed, irregular and vary in size from a few millimetres to centimetre scale (Fig. 7.12b). Grains in the mottles commonly show dihedral angles of 120°, indicating low energy grain boundaries (Fig. 7.12c). These grains are relatively free from inclusions as well as fractures under the microscope, compared to intense fracturing and inclusions in surrounding grains. The boundaries between these two varieties indicate grain boundary migration from semi-transparent strain-free grains to translucent and strained grains (Fig. 7.13). This is known as a *static recovery* process, which decreases the elastic energy of the system, eliminates dislocations into stable arrays by migrating into old grain boundaries, and also modifies into more stable grain structure and boundaries, thus decreasing the surface energy (Barker, 1990).

Static recovery and static recrystallisation are collectively referred to as *annealing*, that has been driven by an associated decrease in the internal strain energy per unit volume of the material (Twiss and Moores, 1991). Such recrystallisation has reduced the internal strain energy of barite grains by replacing the deformed grains that have a high dislocation density with new grains that are essentially strain-free (Figs. 7.12a,c). Therefore, new grain boundaries have become straight with triple junctions of 120°.

During continuing deformation, some of the annealed triple junction and straight grain boundaries have also become destabilised into non-straight grain boundaries. This has resulted from further

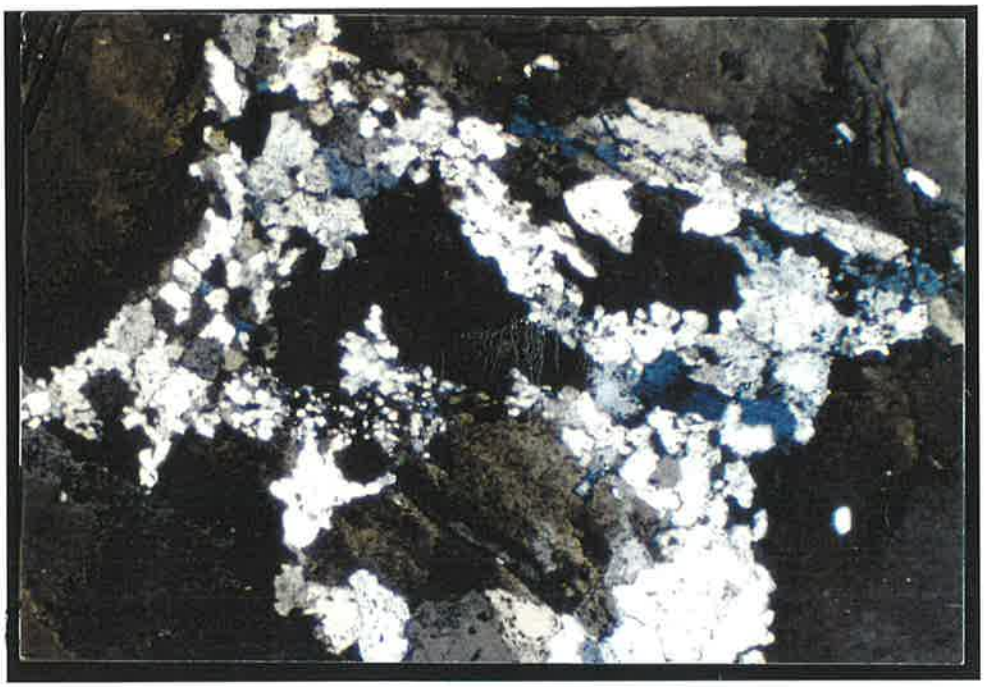

(a)

(b)

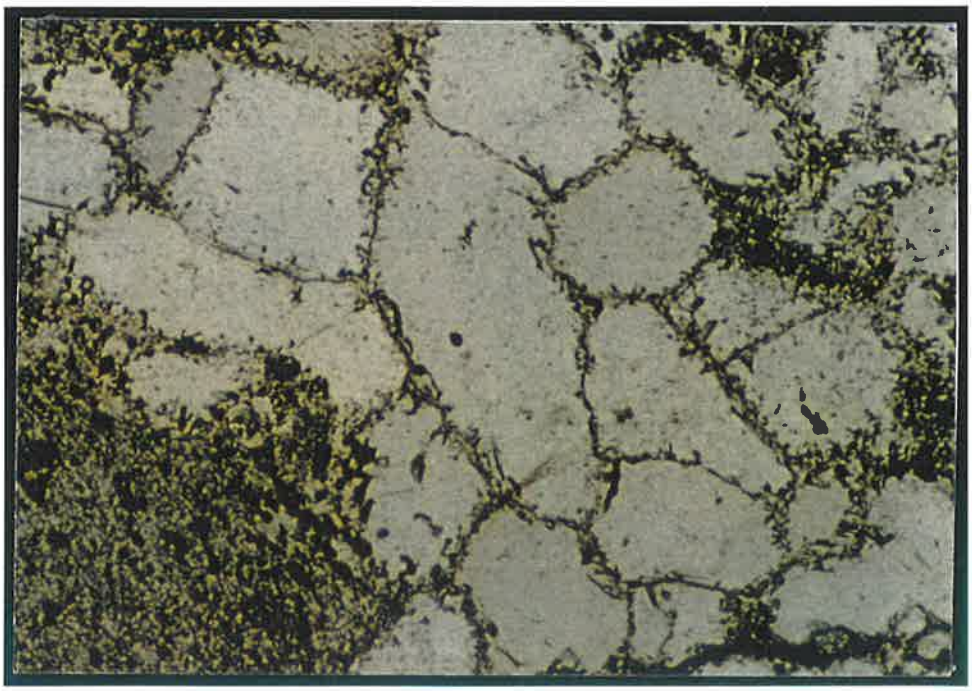

(c)

Fig. 7.12a-c: Annealing textures of barite. (a) Mortar texture developed around large barite grains showing undulose extinction in old grains. Horizontal edge 3.5mm. Sample No. NL50, Noarlunga. (b) Colourless, semi-transparant mottling in white barite grains from the border of the Bainbridge No 3 Lode, Oraparinna. Sample No. BN144. (c) Semi-transparent and colourless younger grains with 120° low energy dihedral boundary angles at the middle of the section compared to that of older grains full of inclusions at the SW quarter. Horizontal edge 2.2mm. Sample No. NL50, Noarlunga.

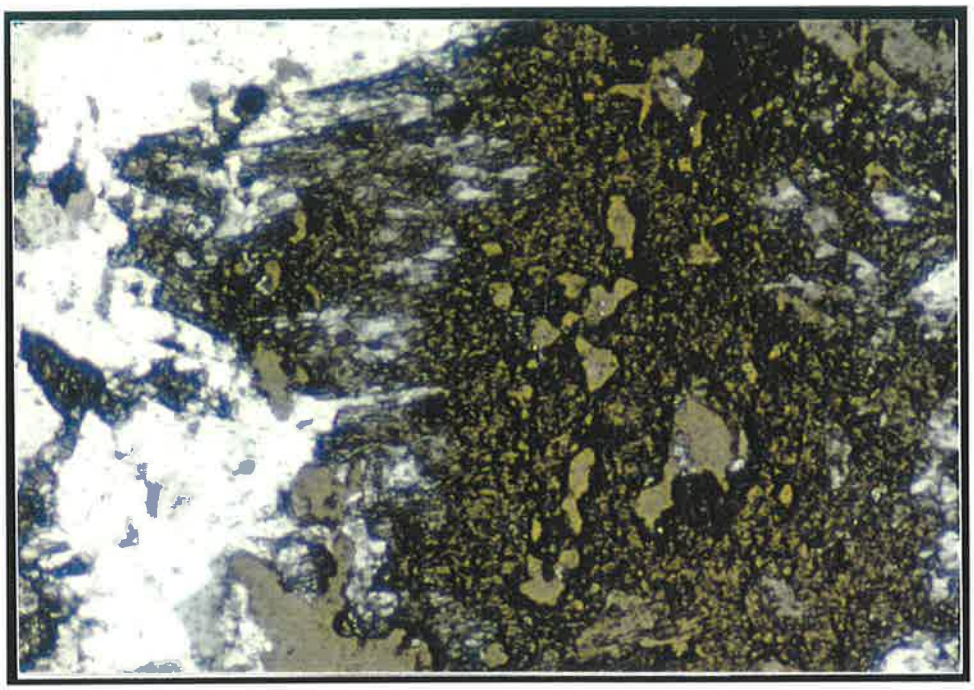

Fig. 7.13: Grain boundary migration from semi-transparent strain free (white) to translucent and strained grains. Horizontal edge 2.2 mm. Sample No NL50, Noarlunga.

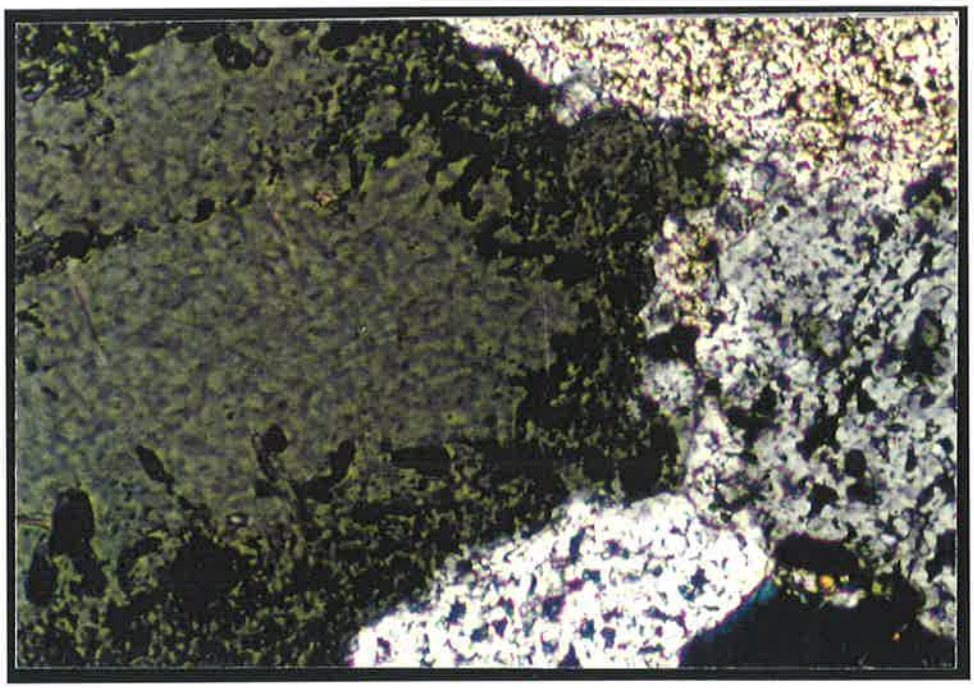

Fig. 7.14: Stable grain boundaries become unstable during further grain boundary sliding in continuing deformation. Horizontal edge 0.6 mm. Sample No NL50, Noarlunga.

grain boundary sliding, indicated by the occurrence of trails of inclusions and fracture propagation from the grain boundaries towards the interior of the grain (Fig. 7.14).

7.6 Discussion

7.6.1 Mechanisms of barite vein formation and deformation

Barite veins in the Adelaide Fold Belt show evidence of the crack-seal mechanism of vein dilation. These veins contain boundary-wall parallel trails of country rock inclusions that ripped from the host, which can be seen at all scales. The Carey Hill Lodes and Mount Frome Lodes show major scale examples (Figs. 7.2a,b). The minor fault-propagation folds on the wall-rock of the Bainbridge no.3 Lode show similar occurrences, even though those veins are parallel to bedding on the forelimb syncline (Fig. 7.7d). These boundary-wall parallel inclusions suggest periodic opening of dilational fractures. Therefore, the mineralisation was synchronous with successive opening of bedding-parallel fissures that formed during progressive deformation, leaving trails of host inclusions along each incremental opening. Thus, veins have accreted by the crack-seal mechanism; where tectonically induced elastic strains reached a critical level and then fractures occurred, adding new barite to the vein-walls of the initial vein (Ramsay, 1980; Ramsay and Huber, 1987). Therefore, barite veins in the Adelaide Fold Belt have dilated during progressive, non-continuous deformation; as indicated by the crack-seal mechanism.

Barite veins in the Fold Belt show a well-defined internal structure. This includes a median line structure defined by fluid inclusions or country rock inclusions (Figs. 7.4b, 7.6b, 7.8a, 7.9c) and a fibrous and elongated grain nature (Figs. 7.4b, 7.8a,b, 7.9a). The continuity of fibrous grains nearly perpendicularly across the median line and occurrence of vein border parallel host-rock inclusion bands within the veins (see above) suggest the veins have been formed following an antitaxial growth mechanism (Fig. 7.9d; Durney and Ramsay, 1973; Durney, 1979; Ramsay and Huber, 1987). In contrast, grains in syntectonic veins do not continue across the median line and are not necessarily perpendicular to the median line as well (Fig. 7.9d). Therefore, barite veins in the Adelaide Fold Belt follow the antitaxial mechanism of vein formation and not the syntaxial mechanism.

The fibres link points that were once in contact and thus (a) reveal the displacement vector across the vein, and (b) grow in the direction of displacement. At times the veins also show a 'sigmoidal type' of fibres indicating original growth directions as seen in the central Flinders Ranges (Fig.

7.15a; Passchier and Trouw, 1996; Urai *et al.*, 1991). However, the ability of fibre growth to track the incremental separation history of crack walls depends on details of the nucleation and growth mechanisms (Cox and Etheridge, 1983), as the crack-seal process can lead to the development of both irregular and laminated vein microstructures, as well as fibrous microstructures (Cox, 1987). Thus, an investigation into displacement paths of barite veins requires great caution, as most of the veins also show recrystallisation.

Barite veins show evidence of internal deformation. The continuing intragrain and intergrain deformation was accompanied with grain boundary sliding, cataclastic flow and recrystallisation, indicating post-vein movements. Comparison of vein textures indicates the barite samples collected from the fault zone adjacent to the Oraparinna Barite Mine have suffered extensive cataclasis. Veins have undergone a varying degree of deformation depending on timing of vein formation and the location of the vein, especially in a post-vein tectonically active area.

7.6.2 Vein types, orientations and rotations

Orientation analyses suggest three major types of barite veins for both the Flinders Ranges and the Oraparinna Mine. The dominant type is oriented NE, while the other two types make 19° and about 36° angles towards NNE and ENE, respectively (Figs. 7.2c, 7.4d, Table 7.2). These types are nearly vertical in the Ranges and in comparison, except the dominant 1D Type (NE-SW), both the other two types of Link (NNE-SSW) and 1A (ENE-WSW) dip moderately to steeply in the mine, respectively to east and north. Plunge of the mutual vein intersection axis varies from nearly vertical in the Ranges to 45°->041° in the mine (Figs. 7.2c, 7.4d, 7.16a,c). In both occurrences, dip and orientation of the dominant type as well as the angles between dominant and subordinate types remain unchanged. Furthermore, rotation of the vein system in the Oraparinna Mine by 45° clockwise around a horizontal axis orienting 315° (NW) yields a vein setup similar to that of the Ranges, showing nearly vertical mutual vein intersection axis (Fig. 7.16d). Therefore, it can be suggested that the veins in the Mine were initially formed nearly vertically, similar to that of the Ranges, but lately rotated anticlockwise by 45° around a horizontal axis orienting 315° (NW). Hence, the vein type classification given for the mine can be applied to the Flinders Ranges, thus the vein type occurrences in the Ranges can be named as 1D, Link and 1A Types.

The Bunkers Graben shows evidence of vein rotation. The F_1 fault-bend folds in the mine and F_1 asymmetric gentle folds elsewhere in the graben, as well as the L_1 bedding parallel shear, suggest SW verged thrusting of graben sequences during the D_1 deformation (Figs. 4.1a, 4.3c, g). These

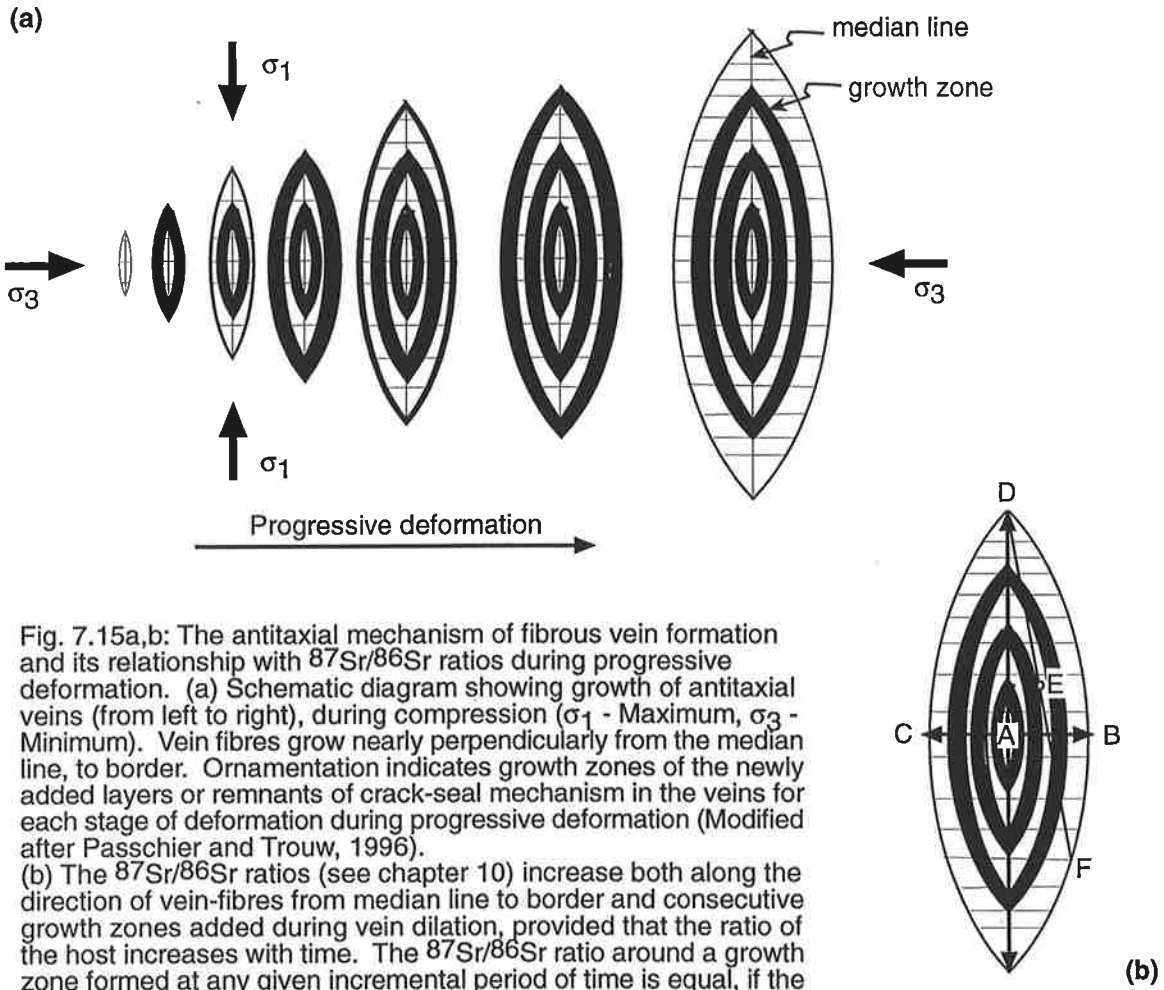

Fig. 7.15a,b: The antitaxial mechanism of fibrous vein formation and its relationship with $^{87}Sr/^{86}Sr$ ratios during progressive deformation. (a) Schematic diagram showing growth of antitaxial veins (from left to right), during compression (σ_1 - Maximum, σ_3 - Minimum). Vein fibres grow nearly perpendicularly from the median line, to border. Ornamentation indicates growth zones of the newly added layers or remnants of crack-seal mechanism in the veins for each stage of deformation during progressive deformation (Modified after Passchier and Trouw, 1996).
(b) The $^{87}Sr/^{86}Sr$ ratios (see chapter 10) increase both along the direction of vein-fibres from median line to border and consecutive growth zones added during vein dilation, provided that the ratio of the host increases with time. The $^{87}Sr/^{86}Sr$ ratio around a growth zone formed at any given incremental period of time is equal, if the isotopic ratio of the host is uniform during that period of time. Therefore, $^{87}Sr/^{86}Sr$ ratios increase along AB, AD, ED and EF, where E is the contact point of the respective tangent to a growth zone.

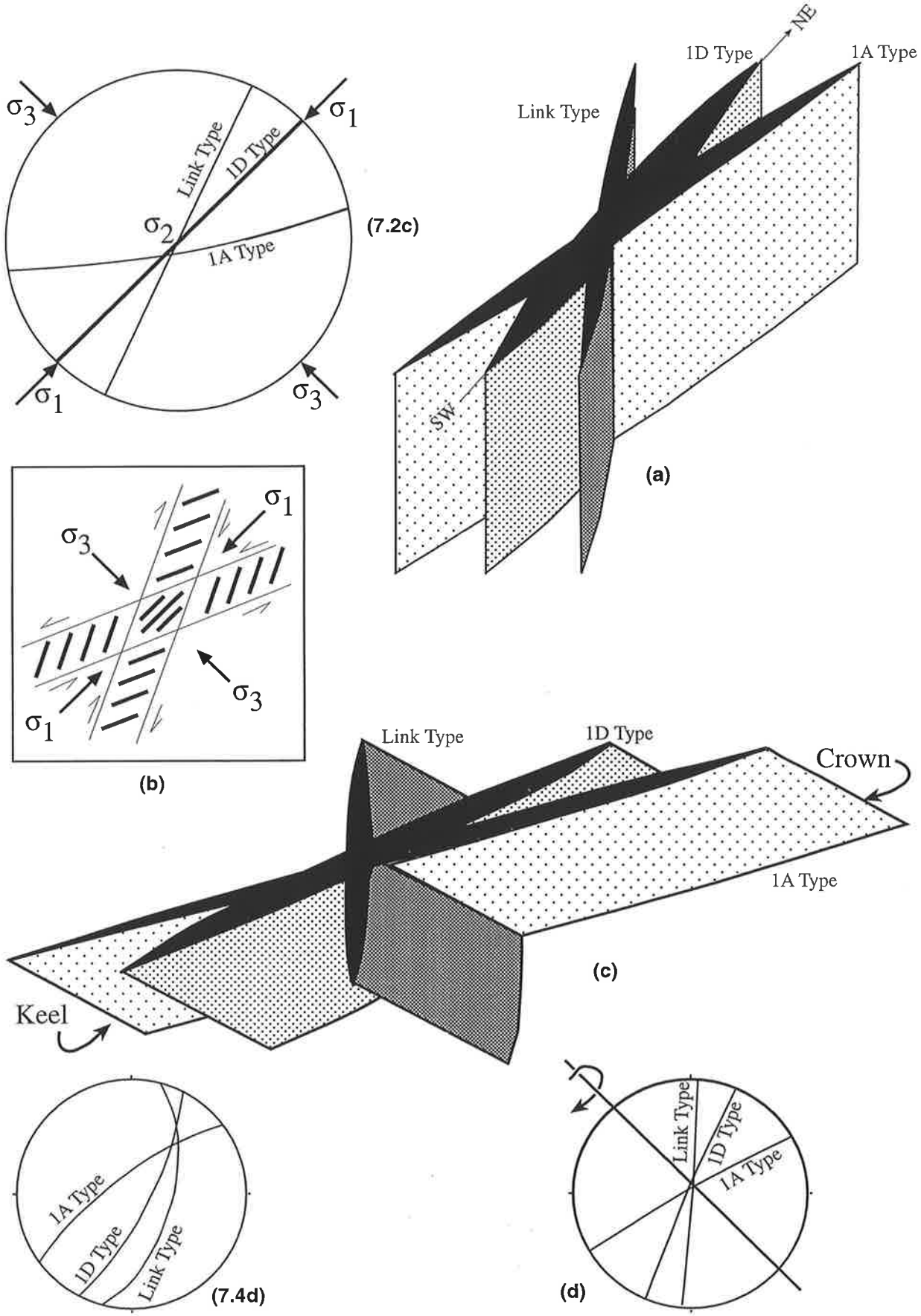

Fig.7.16: Stereographic analysis of barite veins in the Flinders Ranges (Fig. 7.2c) and the schematic diagram (a) showing an approximately vertical mutual vein intersection axis. The major type is that of the 1D Type of the Oraparinna Mine, and the subtypes are those of 1A and Link Types of the mine. (b) Possible geometry of barite veins showing en-echelon vein arrays after conjugate shear zones (modified after Beach, 1975). The stereographic analysis of barite veins in the mine (Fig. 7.4d) and its schematic diagram (c) showing mutual intersection axis plunging 45°->041°. (d) The vein types in the mine, after rotating clockwise by 45° around an horizontal axis orienting 315°, showing the relationship with those in the Flinders Ranges.

folding mechanisms require the upper sequences to undergo more southwesterly verging bedding-parallel shear movements than the lower sequences, in order to create the fold geometry. If the major barite vein types in the mine predated the graben formation, the veins also could have been rotated during the SW verging graben movement. Therefore, rotation of the vein intersection axis can be explained by southwestward bedding-parallel shear movements of the graben sequences that occurred increasingly towards upper sequences rather than lower sequences. The bedding parallel shear has also affected the other barite vein deposits adjacent to the Oraparinna Mine, as indicated by plunging of their intersection axes between 50° to 27° in northeasterly directions (Fig. 7.5).

Table 7.2: Summary of the barite vein types in the Flinders Ranges.

Parameter	Flinders Ranges	Oraparinna Mine	Dunbar Lodes
Dominant type (strike/dip)	N45°E/88°NW	N26°E/77°SE (1D Type)	N80°E/67°S
Subordinate type (1) (strike/dip)	N26°E/vertical	N15°E/61°E (Link Type)	
Subordinate type (2) (strike/dip)	N80°E/84°S	N53°E/77°NW (1A Type)	
Plunge of intersection axis	vertical	45°->041°	54°->113°
Acute angle between subordinate types	54°	56°	
Acute angle between subordinate type (1) and dominant type	19°	19°	
Acute angle between dominant type and subordinate type (2)	35°	37°	

The Brachina Formation in the mine area shows a sinistral rotation of bedding strike from NW to EW. The mine is situated between two northeasterly oriented major faults that are parallel to the fault boundaries of the graben (Map 2). The southerly lying fault shows a major displacement of 1.4 km of the overlying Bunyeroo Formation, and the displacement decreases gradually towards NE. Therefore, the sinistral rotation of bedding in the mine area between the adjacent faults has very likely been associated with faulting, simultaneously with sinking of the graben.

Barite veins in the Flinders Ranges have undergone complex rotations. Rotated back to the original position, the three types of barite veins in the mine show that all of them have rotated sinistrally by 10° to 20° (Figs. 7.2c, 7.16d). This rotation indicates that the vein types predated the associated faulting, thus the graben formation. However, orientation of the vein intersection axes of the deposits adjacent to the mine vary from 021° to 055° (Table 7.1), thus their host fold axes (021° to 064°, Table 5.2) suggest both the hosts and the deposits have subsequently undergone a dextral

rotation towards the southern fault zone adjacent to the mine, during the D_2 deformation. On the contrary, the vein intersection axis of the Dunbar Lodes on the western limb of the Oraparinna Anticline plunges southeasterly, 54°->113°. The southeastern plunge of the intersection axis may agree with a northwestward verging thrust on the western limb of the Enorama – Oraparinna Anticlines during the dextral rotation of the D_2 deformation, while the veins adjacent to the Oraparinna Mine also have responded to the same dextral rotation. Therefore, the three types of veins either predated or formed simultaneously with the D_1 deformation and, thus predated the D_2 deformation as well.

The three nearly vertical vein types of the Flinders Ranges agree with a maximum horizontal compression (σ_1) of NE-SW orientation, a vertical intermediate compression (σ_2), and horizontal minimum compression (σ_3) of NW-SE orientation (Fig. 7.2c). Therefore, it can be suggested that the veins were formed during the NE-SW major compression during the D_1 deformation in the Cambro-Ordovician Delamerian Orogeny.

7.6.3 Geometry of vein types

Barite vein types in the Flinders Ranges can be modelled. However, minor en échelon and conjugate barite vein exposures are rare in the central Flinders Ranges, and were not found during fieldwork. Therefore, vein arrays in the Flinders Ranges (Figs. 7.2c), the Oraparinna Mine (Fig. 7.16d), and the vein deposits around the mine (Fig. 7.5a), were used to suggest the vein geometry. The large data set of the Oraparinna Mine indicates occurrence of all the three types, while the limited data sets of the adjacent deposits indicate occurrences of limited types, i.e. the Belsen Lode (Link and 1A Types), and all other deposits i.e. the Western, Bainbridge and Roberts Lodes indicate only the 1D Type (Fig. 7.5). The acute angle (approximately 55°) between subordinate types suggests convergent configurations, e.g. Beach (1975) Type B (Fig. 7.1e) or weakly convergent to divergent configurations of Smith (1996, Fig. 7.1f), which are a combination of both pure and simple shear for the Flinders Ranges. The 1D (dominant) Type is suggested to have formed in extensional fractures during pure shear resulting from NE-SW compression of the D_1 deformation. Both the Link and 1A (subordinate) Types also have formed in extensional fractures in subsequent conjugate shear-zones associated with the same compression (Figs. 7.1e, f).

Barite veins have formed in association with fault-propagation folds as well (Figs. 6.1f-i, 7.7a-d). These occurrences can be found repeatedly brecciated and mixed with breccia associated with such

folds. Bedding-slip movement around the folds may form dilational tensional fractures at 45° and 135° angles to the bedding surfaces, forming barite veins (Fig. 6.1i). However, the veins below the décollement surfaces could be the most prominent, because of accommodating large slip movements along the décollements (Figs. 6.1h, 7.7c). Bedding parallel crack-seal veins may form along the hinge of the forelimb syncline or back limb anticline, hence shall not be misinterpreted as synsedimentary deposits (Fig. 7.7d). Even though these examples of minor vein formation in association with fault-propagation folds were formed during the D_2 deformation, the principles may be applied to the major fault-propagation folds, i.e. the Enorama Anticline/Diapir (Fig. 3.8a). The barite veins that form in association with fault-propagation folds do not follow the three major types.

In conclusion, barite veins in the Adelaide Fold Belt were formed syntectonically, following the antitaxial growth. Veins were dominantly formed during the D_1 deformation, prior to or simultaneous with graben formation, and there is evidence of minor vein formation during the D_2 deformation as well. The majority of veins have formed in association with (a) pure shear (1D 'dominant' Type) and (b) simple shear (1A and Link 'subordinate' Types in conjugate shear zones), during the D_1 deformation. Veins that formed during the early stages of the D_1 deformation have been subjected to both the D_1 and D_2 Deformations. The veins show complex occurrences, but the majority belong to the three main types that formed during the D_1 deformation in the Cambro-Ordovician Delamerian Orogeny.

The antitaxial texture of barite veins defined by fibres growing perpendicular to and from median line to border, within the essentially unconnected tensional-gashes, suggests occurrence of source constituents such as Ba in minor quantities within a short distance, as proposed by Ramsay and Huber (1987). This principal of vein growth may agree with the suggestion of migration and redeposition theory imagined by Olliver and Scott (1978) but does not support the theory of mixing of two fluids within opened fractures, by downward percolating connate waters with upward moving Ba rich brines from the basement, suggested by Robertson (1981) and Cawley (1983).

Chapter 8

GEOCHEMISTRY OF BARITE VEINS

8.1 Introduction

Barite ($BaSO_4$) and celestite ($SrSO_4$) are end members of a continuous solid solution series (Starke, 1962). However, in nature, most barites contain only a few mole percent $SrSO_4$ and most celestites contain only a few mole percent $BaSO_4$ (Leach, 1980). The intermediate compositions are rare. Hundreds of barite samples from the veins in the Adelaide Fold Belt have been chemically analysed by PIRSA and have been summarised by McCallum (1992). $BaSO_4$ contents up to 96.9 wt % and $SrSO_4$ contents up to 9.2 wt % have been reported in these samples. The impurities include SiO_2 and Fe_2O_3 in minute quantities.

Cawley (1983) carried out 119 microprobe analyses on barite grains from samples of the Oraparinna Mine. The Ba content varied from 52.62 to 61.09 wt % and Sr content varied from 0.34 to 4.28 wt %. Cawley also carried out XRF and AAS analyses of barite samples from the mine. He concluded that there was some variation across the 1A Lode of the mine on levels 4 and 7 but that there were no consistent chemical variations of Ba or Sr concentrations of veins horizontally along strike or vertically. Previously, Robertson (1981) made similar observations for the Artipena Lodes.

8.2 Sampling of barite veins

Barite veins were sampled from the Flinders Ranges and the southern Adelaide Fold Belt. Samples were collected from defined positions within the veins, (a) the central median layer, (b) between the median layer and border, and (c) adjacent to the border. The sample numbers were identified by the suffixes "a", "b" and "c" respectively.

Samples from the Oraparinna Mine were collected from all the major veins including 1A, 1B, 1C, 1D and Link Lodes from levels 5, 6 and 7 (Fig. 8.1). Both 1A and 1D Lodes have mean dips of 73° to NW and SE, respectively, on these levels. The 1B Lode dips nearly vertically and the 1C Lode dips vary from 75°SE to nearly vertical. The Link Lode dips 58°E. The 1D Lode was sampled on Level 5 at the centre (OM128[a]) and border (OM127[c]), perpendicular to the vein border, with a distance of 1 m between the two samples. 1A Lode on Level 6, having a thickness of 1 m, was

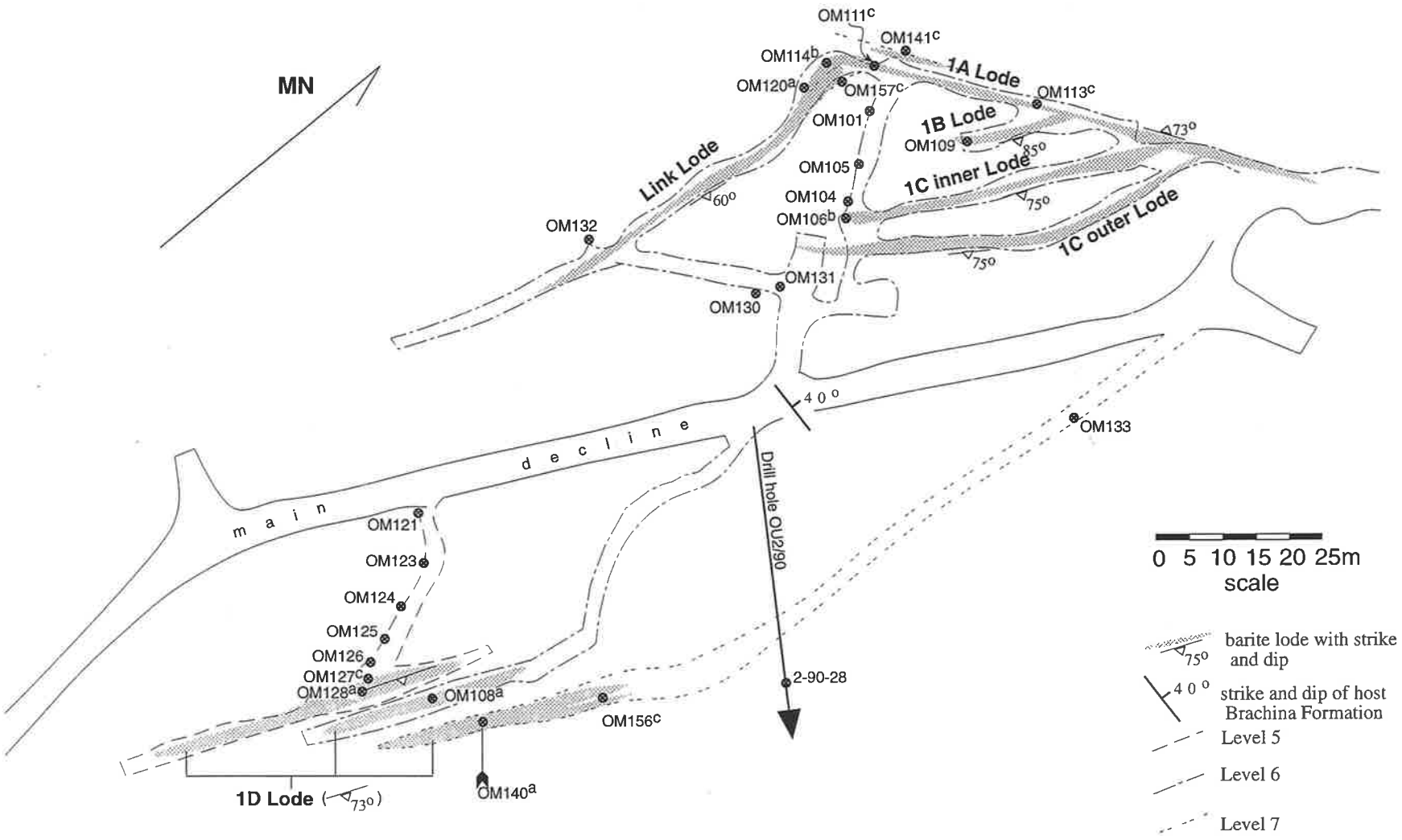

Fig. 8.1: Barite lode distribution and sample locations at the Oraparinna Barite Mine, showing underground levels 5,6 &7. Base map from Commercial Minerals Ltd.

sampled along a horizontal line inclined to the vein borders, with a distance of 32 m between OM114[b] and OM113[c] samples. Other barite samples collected from major lodes in the mine were: 1A Lode (OM111[c] - Level 6 (Figs. 4.3d), OM141[c] - Level 7), 1B Lode (OM109 - Level 6), 1C Lode (OM106[b] - Level 6), 1D Lode (OM108[a] - Level 6 and OM140[a] - Level 7) and Link Lode (OM120[a] - Level 6 and OM157[c] - Level 7). A few minor veins were also sampled; OM130 (barite mixed with localised breccia - Level 6), and OM131, OM132 and OM133 (levels 6, 6 and 7, respectively), in which barite was mixed with high amounts of carbonate.

Barite veins near the Oraparinna Mine were also sampled. Bainbridge No3 Lode at the hilltop above the mine was sampled adjacent to vein border (BN143[c]), in the open-pit (Fig. 6.1a). Isolated minor barite occurrences from the NE-SW trending fault zone (Fig. 7.5a) in the mine were also sampled. Two samples (OF158 and OF159) were collected from the fault zone, with a distance of 2 km between them.

Barite veins in the open pit at Dunbar near the western margin of the Oraparinna Diapir (Fig. 1.3) were sampled in two batches (Fig. 7.6a,b). Samples D251[c], D252 and D253[b] were collected in an early batch from three different veins. Samples D255[a] and D257[c] were collected later from one vein with a distance of 60 cm between samples, along a line perpendicular to the vein border.

Hall Lode (H301) at the southern end of the Oraparinna Diapir and Bowering Lode (BW200) at the southeastern margin of the Diapir (Fig. 1.3) and veins from the southern Adelaide Fold Belt at Noarlunga (NL50, NL51B (B Lode), NL51D (D Lode), NL52 and NL53; Fig. 2.7) were also sampled.

The samples from 1D Lode in the Oraparinna Mine (Level 5; OM128[a] and OM127[c]), and Dunbar vein (D255[a] and D257[c]) were collected *along the direction of vein fibres.*

8.3 Analyses

Barite samples collected from the veins generally weighed from 100 - 500 g. About 20 - 50 g were powdered for the use in XRD (1-2 g) and XRF (1 g for fused discs for major element analyses, 5-8 g for pressed pellets for trace element analyses). The uncrushed remainder was used for petrological and electron microprobe investigations. (See Appendix 8.1 for methods of sample preparation and analysis).

8.4 Results

Ba is the major element in barite, hence the pressed pellet (trace element) method did not yield highly accurate values for Ba by the XRF, but the precision was sufficient for comparison between samples to define trends of composition. Samples D255[a] and D257[c] from Dunbar were analysed in a second batch where the instrument calibration settings differed from those used in the earlier Ba analyses. Therefore, values for Ba of the two batches were not compared.

8.4.1 Ba and Sr contents of barite ore samples

XRF analyses show the Ba content of barite ore samples collected from deposits in the Adelaide Fold Belt varies from 21.4 wt % in the quartz-mixed Hall Lode to 41.7 wt % in the Noarlunga Lodes (Table 8.1 and Appendix 8.2). Hall Lode contains high amounts of quartz and was therefore excluded from the following comparison with other lodes. The highest mean Ba content of 40.75 wt % (39.5 wt % - 41.7 wt % for 5 analyses) was obtained from the Noarlunga Lodes, while the lowest mean of 39.10 wt % (37.7 wt % - 39.7 wt % for 11 analyses) was obtained from the Oraparinna Mine (Table 8.1). Conversely, the highest mean Sr content of 3.32 wt % (2.19 wt % to 3.87 wt % for 11 analyses) was obtained from the Oraparinna Mine and the lowest of mean 0.67 wt % (0.62 wt % to 1.11 wt % for 5 analyses) was obtained from the Noarlunga Lodes. Furthermore, the lowest Ba content of an individual sample was obtained from the Oraparinna Mine (37.7 wt %) and the highest was obtained from the Noarlunga Lodes (41.7 wt %).

Table 8.1: Ba and Sr contents of ore samples from barite veins in the Adelaide Fold Belt. (See Appendix 8.2 for details.)

Deposit	Ba analyses			Sr analyses		
	No. of samples	Mean (wt %)	Range (wt %)	No. of samples	Mean (wt %)	Range (wt %)
Noarlunga Lodes	5	40.75	39.5 - 41.7	5	0.67	0.62 - 1.11
Bainbridge Lodes	1	40.48	40.48	1	2.0	2.0
Bowering Lode	1	40.2	40.2	1	1.31	1.31
Dunbar Lodes	3	39.87	39.5 - 40.2	5	1.74	1.37 - 2.78
Fault zone 2 km NE of Oraparinna Mine	2	39.85	39.4 - 40.3	2	2.91	2.64 - 3.19
Oraparinna Mine	11	39.1	37.7 - 39.7	11	3.32	2.19 - 3.87
Hall Lode	1	21.4	21.4	1	0.24	0.24

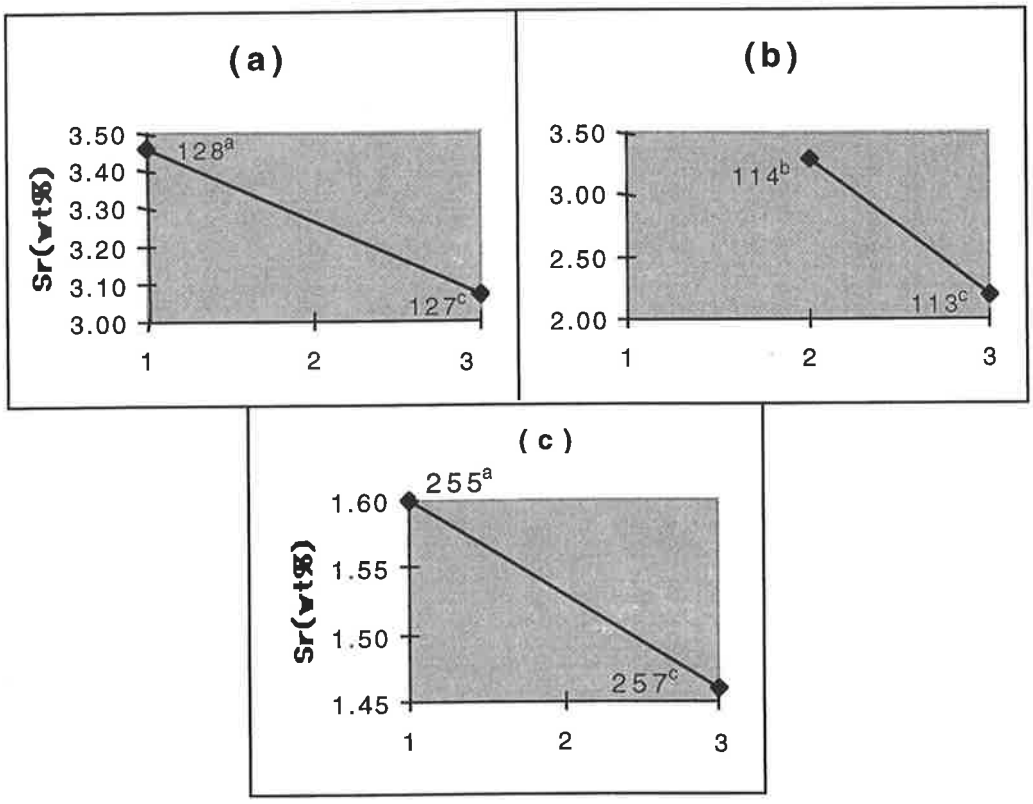

Fig. 8.2a-c: Variation in Sr (wt. %) content across barite veins. (a) and (b), 1D and 1A Lodes, respectively of the Oraparinna Mine and (c) Dunbar Lodes. Sample positions are defined by median layer (1), between median layer and border (2), and border (3).

8.4.2 Geochemical variation within veins

The barite veins examined are commonly white, although the central median layers are light grey to colourless and appear somewhat glassy. Barite in the veins can be easily broken along cleavages by a geological hammer, except the barite along median layers, which is more resistant to breaking. However, the XRD analyses of various samples from the median layer and elsewhere indicated no difference in mineralogy.

XRF analyses of samples from the veins on different levels of the Oraparinna Mine show a decrease of mean values of Sr from 3.56 wt % of the median layers, to 2.86 wt % adjacent to the borders (Table 8.2). Individual samples collected perpendicular to the vein borders across 1D Lode on Level 5 of the Oraparinna Mine and from a Dunbar vein, both show a decrease in Sr content from the median layers to vein borders by 0.4 wt % and 0.14 wt %, respectively (Fig. 8.2a,c, Appendix 8.2). The 1A Lode in the Oraparinna Mine also shows a decrease in Sr of 1.2 wt % from halfway between median line and border (114^{b}) to border (113^{c}, Fig. 8.2b). These samples show a corresponding increase in Ba of 0.4 wt %, 0.3 wt % and 0.2 wt % respectively, for 1D Lode, 1A Lode, and Dunbar Lode in the direction of median layer to border. The other elements analysed (Cu, Zn, Co, Sc, Ce and Na) do not show significant differences between median line and border layers (Table 8.2).

Table 8.2: Comparison of chemistry of ore from the median layers and adjacent to borders of barite veins in the Oraparinna Mine.

Sample No.	Lode	Ba wt %	Sr wt %	Cu ppm	Zn ppm	Co ppm	Sc ppm	Ce ppm	Nd ppm
Median layer									
OM108[a]	1D	39.33	3.46	780	16	9.5	3.6	272	346
OM120[a]	Link	38.95	3.64	751	15	7.9	2.4	273	334
OM128[a]	1D	39.29	3.46	728	13	8.6	2.2	274	334
OM140[a]	1D	39.20	3.67	745	12	9.9	2.9	271	335
Mean		39.19	**3.56**	751	14	9.0	2.8	273	337
Border									
OM113[c]	1A	39.68	2.19	680	13	8	3.1	274	324
OM127[c]	1D	39.67	3.07	724	12	8.6	3.3	280	336
OM141[c]	1A	38.96	3.39	907	13	9.1	2	274	351
OM157[c]	Link	38.37	2.8	711	14	8.7	3.3	267	332
Mean		39.17	**2.86**	755	13	8.6	3	274	336

The median layer and border samples from 1D Lode, Level 5 ($OM128^{a}$ and $OM127^{c}$ respectively) were further analysed by electron microprobe (Table 8.3). The data agree with the XRF results in that the mean values show a decrease in Sr from 3.23 wt % to 3.01 wt % from median layer to border, and a corresponding increase in Ba from 55.87 wt % to 55.98 wt %.

Table 8.3: Comparison of electron microprobe analyses of barite from the median layer (a) and border (c) samples from 1D Lode, Level 5 of the Oraparinna Mine.

Sample	No. of analyses	Sr (wt.%) mean [range]	Ba (wt.%) mean [range]
OM128[a]	6	3.23 [2.60-3.94]	55.87 [54.94-56.99]
OM127[c]	16	3.01 [2.44-3.74]	55.98 [55.12-57.34]

Thin barite veins in the Oraparinna Mine commonly contain intergrown calcite grains. The thin vein shown in Figure 7.8a,b was studied by electron microprobe for the chemistry of barite fibres (Fig. 7.9a). The vein consists dominantly of calcite, including elongate and discontinuous micro-fibres from 10 to 500 μm in length. The median layer is defined by a series of fluid inclusions, nearly parallel to the border. Barite grains were analysed from the median layer to the border of the vein (distance = 1.26 mm), and further into the wall rock where scattered barite grains of non-fibre shape occur (Fig. 8.3a). The electron microprobe results show a decrease in Sr content from near the median line (3.28 wt %) to border (2.50 wt %), with a corresponding increase in Ba from 57.59 wt % to 58.8 wt %, except for some spike values at 0 and 0.95 mm, corresponding to high Ca values of 1.27 wt % and 1.54 wt %, respectively (Table 8.4 and Fig. 8.3b). The trend to lower Sr and higher Ba away from the median line of the vein also continues in grains in the wall rock. Overall, the traverse shows a decrease of Sr from 3.28 wt % to 0.55 wt %, and an increase of Ba from 57.59 wt % to 60.22 wt %, from near the median line in the minor vein into the host rock, over a distance of less than 2 mm.

Table 8.4: Sr and Ba chemistry (wt.%) of barite with respect to the perpendicular distance from the median line of a minor calcite-barite vein towards, and into, the wall rock at the Oraparinna Mine (sample 2/90/38, Fig. 8.1).

Distance from median line (mm)	Sr (wt.%)	Ba (wt.%)	Ca (wt.%)	Remarks
0.00	2.92	57.34	1.27	Barite
0.17	3.28	57.59	0.02	fibres
0.92	2.65	58.40	0.06	in
0.95	2.88	55.84	1.54	vein.
1.02	2.71	57.86	0.94	
1.22	2.50	58.80	0.35	Vein border
1.45	1.81	59.24	0.57	Barite grains
1.55	0.89	60.13	0.03	in wall-
1.84	0.55	60.22	0.02	rock.

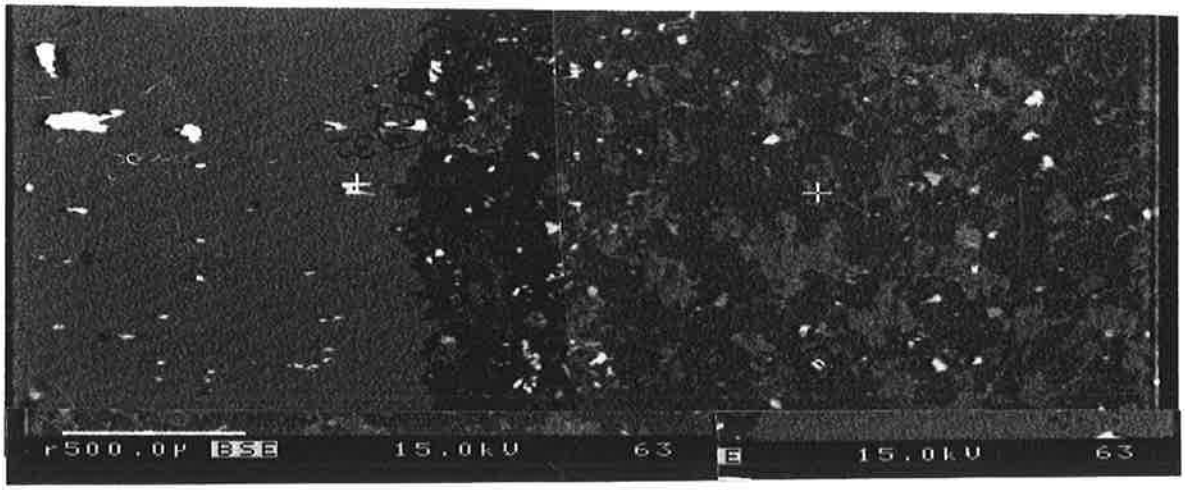

Fig. 8.3a: Back scattered electron image of sample 2/90/38 showing a section of the vein (left) and the host Brachina Formation (right). The vein consists of barite (white) and calcite (grey). The host rock consists of barite (white spots), K-feldspar (black) and quartz (grey). A few white spots in the host denote Fe2CO3 as well. White bar scale (bottom left of photograph) is 0.5 mm.

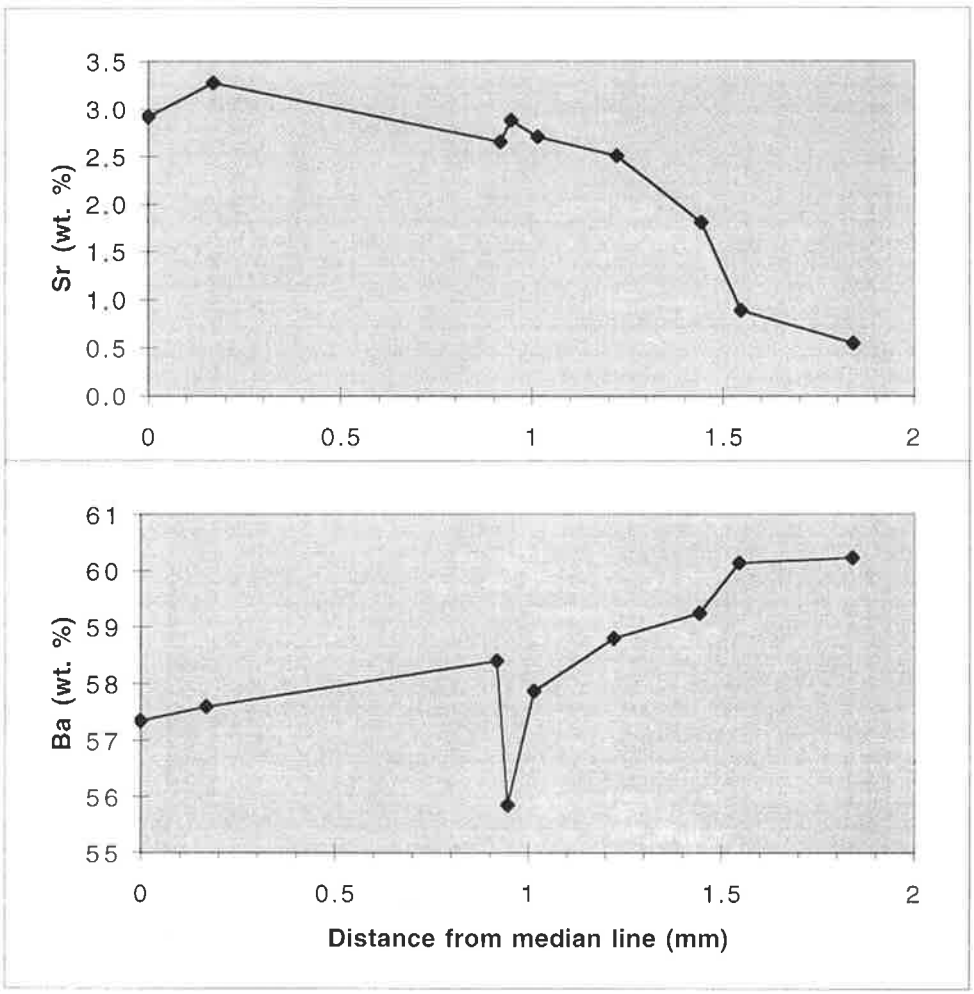

Fig. 8.3b: Sr and Ba content of barite grains of the above sample, with respect to the perpendicular distance from median line of vein.
Note: Vein border is at 1.26 mm, with Brachina Formation wall rock to the right.

8.4.3 Geochemistry of recrystallised barite grains

The barite veins studied commonly show recrystallisation in any part of a vein because of post-vein deformation (Chapter 7). Recrystallised samples analysed are identified by the suffix 'r', and the non-recrystallised by 'n'. Sample NL50 from Noarlunga contains randomly distributed patchy occurrences of recrystallised grains ($NL50^r$), surrounded by non-recrystallised grains ($NL50^n$), that were analysed by electron microprobe for their composition (Figs. 2.7, 7.12c; Table 8.5). The results show higher Sr contents in recrystallised grains (mean 2.50 wt %) than non-recrystallised grains (mean 0.53 wt %). The corresponding mean Ba contents are 57.03 wt % and 59.38 wt %, respectively.

Table 8.5: Sr and Ba (wt %) analyses of barite by electron microprobe of recrystallised grains (r) and non-recrystallised grains (n) from Noarlunga (sample NL50).

Sample	No. of analyses	Sr (wt %) mean [range]	Ba (wt %) mean [range]
$NL50^r$	6	2.50 [2.38-2.75]	57.03 [56.75-57.33]
$NL50^n$	9	0.53 [0.21-1.34]	59.38 [58.09-60.19]

8.4.4 Other minerals associated with the barite veins

The lens shaped 1D Lode in the Oraparinna Mine splits into two sub-lenses near parallel to each other at the northeastern end on Level 7 (Fig. 8.1). The mineralisation between the sub-lenses adjacent to their junction mainly consists of a colourless and semi-transparent mineral with minor white barite (Fig 8.4a, Sample OM156). X-ray diffraction (Fig. 8.4b) shows the colourless material to be strontianite ($SrCO_3$), which had not been previously reported in South Australia (pers. comm. Alan Pring, SA Museum). Calcite ($CaCO_3$) is also common on the border of barite veins in the Oraparinna Mine.

Fig. 8.4a: Strontianite (colourless) deposited between the sub-lenses emanating from northeastern end of 1D Lode on level 7 of the Oraparinna Mine. Barite (white) is also present as a minor constituent. Sample OM156.

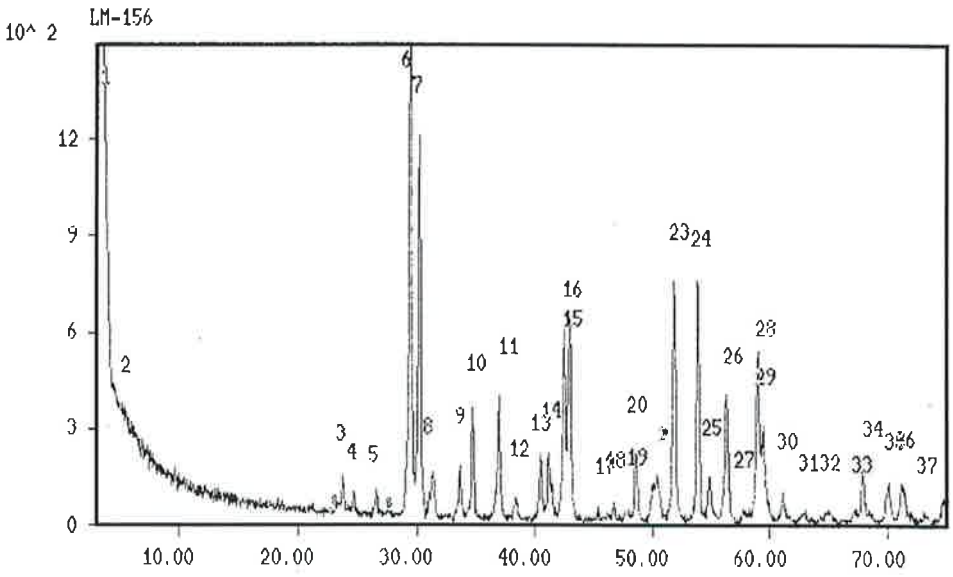

Fig. 8.4b: XRD chart (with 2θ angles) of strontianite and barite in sample OM156. Peaks 6,10,16, 23 and 24 are strontianite while 5,8 and 9 are barite. Peak 7 coincides with both minerals.

8.5 Discussion

The Sr contents of barite show a well-defined decrease from median layer to border of barite veins, and further into the host, while Ba shows the opposite trend (Table 8.6). Since the veins were formed from median layer to border, following the antitaxial mechanism (Chapter 7), this trend suggests the supply of Sr was being depleted while Ba was being increased during formation. This could be due to:

(a) a closed system, so that Sr precipitated preferentially with respect to Ba, and hence the Sr/Ba ratio of the barite decreased with time;

(b) the fracture opening rate, so that the demand for Sr was faster than Sr migration to the depositional site, suggesting lack of connection of these fractures to a network directly connected to any major source such as seawater that could supply Sr.

In either of these situations, decreasing gradients of Sr contents from median layer to border indicate that there was not a massive quantity of fluids flowing through fractures and supplying Sr on a large scale. Instead, barite veins were formed as fibres in relatively unconnected fractures. These findings disagree with vein formation by mixing of Sr rich seawater or connate water flowing downwards through fractures and basement fluids flowing upward through the same fractures, as suggested by Robertson (1981) and Cawley (1983).

The Ba-Sr gradient continue from the vein into the host rock in sample 2/90/38, with lower Sr and higher Ba in isolated barite grains than in the vein. This relationship is compatible with the isolated Noarlunga Lodes, which have lower Sr contents and higher Ba contents than the vein complex in the Oraparinna Mine. This may be a clue to participation of host formations in the barite forming process. However, this matter is further discussed in the next chapter, using geochemistry of the host rocks.

Table 8.6: Summary of comparison of Sr and Ba contents of median line and border samples.

Source	Analysis	Mean Sr (wt %)		Mean Ba (wt.%)		Reference
		Median line	Border	Median line	Border	
Oraparinna Mine	XRF	3.56	2.86	39.19	39.17	Table 8.2
1D Lode	Microprobe	3.23	3.01	55.87	55.98	Table 8.3
Micro vein	Microprobe	3.28	2.50	57.59	58.80	Table 8.4
Dunbar	XRF	1.60	1.46	52.52	52.79	D255[a], D257[c], Appendix 8.2

The recrystallised grains show higher Sr contents and lower Ba contents than adjacent non-recrystallised grains (Table 8.5). Recrystallisation involved grain boundary migration, thus releasing strain and forming new grains, due to the strains caused by post-vein deformation (Chapter 7). During this process, Sr apparently migrated from the parent grains into the recrystallising grains.

Chapter 9

GEOCHEMISTRY OF BARITE HOST ROCKS AND SOURCE OF BARIUM FOR BARITE MINERALISATION

9.1 Introduction

Barite veins in South Australia are hosted in a range of rock types and formations representing a long interval of geological time. The ages of the host rocks range from pre-Adelaidean Hiltaba Suite Granites (1595 Ma, Mortimer *et al.*, 1988; Wawryk, 1989) at the Olympic Dam Cu-U-Au deposit to post-Adelaidean, early Cambrian Parara Limestone at the Potato Patch barite deposit (Olliver and Scott, 1978) in the Parachilna 1:250,000 sheet. As described in section 1.2, the close association of barite veins with diapirs (e.g. the Oraparinna Diapir, Fig. 1.3) has been interpreted as indicating that barite veins were genetically related to the diapirism (e.g. McCallum, 1998, 1990). It was generally believed that Ba-rich brines derived from the Adelaidean basement through diapirism or fractures (Robertson, 1981), in addition to Ba derived from the host formations, were the major sources of Ba for barite vein formation (Cawley, 1983). However, barite veins also occur without any close association of diapirs, e.g. Noarlunga barite lodes (Mansfield, 1956). Previously, there has been some emphasis on the Brachina Formation that contains relatively high Ba (Horwitz, 1962), and hosts extensive barite vein deposits in the Flinders Ranges (Olliver *et al.*, 1979). These authors considered that Ba had been derived from the Brachina Formation by a process of lateral secretion and subsequently deposited as barite from low temperature solutions in open fissures, during diapiric emplacement. The purpose of this chapter is to investigate the source of Ba by studying the geochemistry of host rocks.

9.2 Background

The combined production + reserves of all barite deposits in the Adelaide Fold Belt estimated to have more than 2000 tonnes amounts to 824,000 tonnes of barites (Appendix 9.1; McCallum, 1992). Classification of these deposits in terms of the host formations demonstrates that the Brachina Formation is by far the most important host to barite occurrences, with total production + reserves of nearly 486,600 tonnes (59 % of the total), followed by the Wilyerpa Formation and the Tapley Hill Formation with production + reserves of 61,400 tonnes (7 %), and 51,800 tonnes (6 %), respectively (Table 9.1 and Fig. 9.1). The diapirs host only low amounts of barite, 9500 tonnes (1 %, Table 9.1).

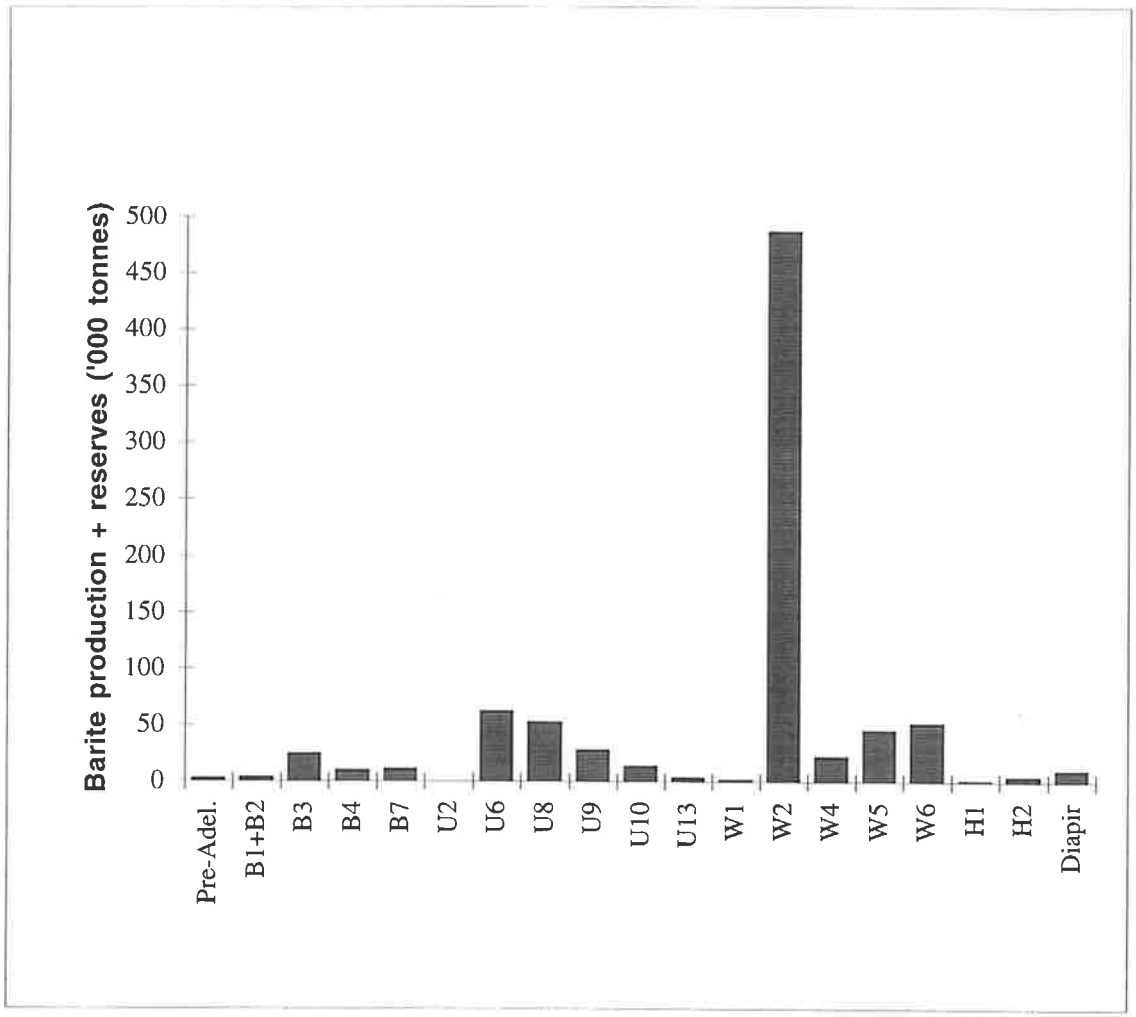

Fig. 9.1: Adelaide Fold Belt host formations and barite production + reserves. Data and formation abbreviations are as in Table 9.1.

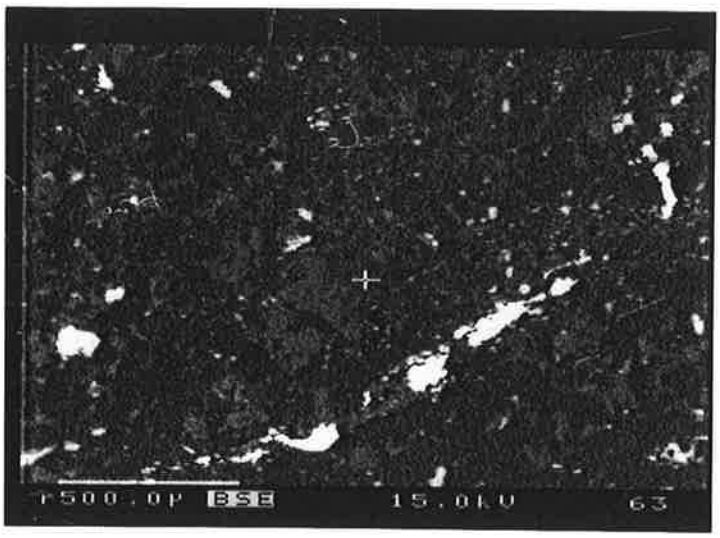

Fig. 9.2: A back scattered electron image showing minor barite occurrence in the host Brachina Formation in the Oraparinna Mine. K-feldspar (black) and quartz (grey) are the main constituents while barite (white) has deposited along minor fractures and in pore spaces. Sample No. OM123, 16.9 m from the 1D Lode. Bar scale (bottom left) is 0.5 mm.

Classification of these deposits in terms of host lithology shows that the most important lithology is siltstone, hosting 471,200 tonnes of barite (57 %) of the total of 824,200 tonnes (Appendix 9.1; Table 9.2). Other significant lithologies are siltstone + shale (72,930 tonnes, 9 %), siltstone + sandstone (33,500 tonnes, 4 %), sandstone (29,440 tonnes, 4 %) and shale (28,230, 3 %). Siltstone combined with other lithologies hosts 123640 tonnes (15 %) of barite (Appendix 9.1). Therefore, siltstones, both alone and combined with other lithologies host a total of 72 % of barite of the Adelaide Fold Belt.

Table 9.1: Barite production + reserves in host formations in the Adelaide Fold Belt. Data from Appendix 9.1

Host Formation (with abbreviation)	Barite production + reserves ('000 tonnes)	%
Pre-Adelaidean	2.5	0.30
Rhynie Sandstone (B1)+ River Wakefield Subgroup (B2)	3.0	0.36
Aldgate Sandstone (B3)	23.9	2.90
Woolshed Flat Shale (B4)	9.1	1.10
Saddleworth Formation (B7)	10.0	1.21
Holowilena Ironstone (U2)	0.1	0.01
Wilyerpa Formation (U6)	61.4	7.45
Tapley Hill Formation (U8)	51.8	6.28
Etina Formation (U9)	13.0	1.58
Enorama Shale (U10)	27.2	3.30
Elatina Formation (U13)	2.9	0.35
Nuccaleena Formation (W1)	1.0	0.12
Brachina Formation (W2)	486.6	59.04
ABC Range Quartzite (W4)	21.6	2.62
Bunyeroo Formation (W5)	44.9	5.45
Wonoka Formation (W6)	51.1	6.20
Wilkawillina Limestone (H1)	0.7	0.08
Parara Limestone (H2)	3.9	0.47
Diapirs	9.5	1.15
Total	824.2	100

A compilation of geochemical data by the South Australian Department of Mines and Energy and Turner *et al.* (1993) for various Adelaide Fold Belt stratigraphic units and lithologies shows mean Ba values in decreasing order as: Brachina Formation (1011 ppm), Callanna Group (635 ppm), Skillogalee Dolomite (610 ppm), Holowilena Ironstone (607 ppm), Tapley Hill Formation (522 ppm) and Umberatana Group (517 ppm), and a lowest value of 164 ppm for the ABC Range Quartzite (Table 9.3A). Thus, a mean Ba content of 419 ppm was obtained for the Adelaide Fold Belt (162 samples). Siltstone alone shows a mean Ba content of 546 ppm, siltstone mixed with shale and clay has a mean of 433 ppm, and shale alone has a mean of 414 ppm (Table 9.3B). All these mean values are higher than the overall mean value for the Adelaide Fold Belt.

The Brachina Formation as stratigraphic unit and siltstone as a lithology stand out in terms of high Ba contents compared to other formations and lithologies, and these are clearly important factors to be considered in the origin of the barite deposits.

Table 9.2: Lithology of the host formations and barite combined production + reserves in the Adelaide Fold Belt*.

Host lithology	Barite (tonnes)	%
Siltstone	471200	57.17
Siltstone, Shale	72930	8.85
Siltstone, Sandstone	33500	4.06
Sandstone	29440	3.57
Shale	28230	3.43
Sandstone + Slate	23900	2.90
Shale, Sandstone, Quartzite	18000	2.18
Siltstone + Limestone	11710	1.42
Shale, Dolomite	10000	1.21
Diapirs (mixed lithologies/breccia)	9500	1.15
Slate, Phyllite, Dolomite	9200	1.12
Limestone, Shale, Sandstone	7380	0.90
Slate, Siltstone, Dolomite	5500	0.67
Shale, Sandstone	4200	0.51
Siltstone, Quartzite	3000	0.36
Sandstone, Conglomerate	2200	0.27
Sandstone, Quartzite	1000	0.12
Slate	40	0.00

* Data obtained after tabulation of Appendix 9.1. Contributions from a variety of mixed lithologies were omitted, as such individual contributions were quite small compared to that of the siltstone. Percentages were calculated for total of 824,200 tonnes, see Table 9.1).

Wedepohl (1969) reported the Ba content of a variety of lithologies on a global scale, from Africa, Asia, Europe, USA and the Pacific Islands, with individual samples ranging from 10 to 5,000 ppm Ba. Siltstones were not listed separately from shale in Wedepohl's compilation. A maximum mean Ba content of 628 ppm was reported for 404 shale samples and 316 ppm and 90 ppm were obtained for 1309 sandstone samples and 1068 carbonate samples, respectively. These findings are in general agreement with the data on lithologies in the Adelaide Fold Belt (Table 9.2).

Mean Sr contents of stratigraphic units in the formations associated with Adelaide Fold Belt vary from 272 ppm for the Glen Osmond Slate to 15 ppm for the Pepuarta Tillite, and Rb contents vary from 255 ppm for the Skillogalee Dolomite to 23 ppm for the ABC Range Quartzite (Table 9.3A).

Table 9.3: (A) Ba, Sr and Rb mean concentrations of various Adelaide Fold Belt formations (Source of data: Department of Mines and Energy, 1996 and Turner *et al.*, 1993). (B) Summary of Ba contents in siltstone, shale and clay (from data in A).

(A)

Stratigraphic unit	Rock type analysed	No. of analyses	Mean values (ppm)		
			Ba	Sr	Rb
Skillogalee Dolomite	Phyllite, slate	3	610	-	255
Woolshed Flat Shale	Shale	1	230	-	98
Saddleworth Formation	Siltstone, meta siltstone, phyllite, sandstone	11	303	-	98
Glen Osmond Slate	Clay, siltstone, soil	34	333	272	79
Tarcowie Siltstone	Siltstone, sandstone	9	462	86	96
Pepuarta Tillite	Diamictite, siltstone	2	367	15	91
Umberatana Group	Siltstone	7	517	60	194
Brachina Formation*#	Siltstone	2	1011	87	149
Uroonda Member	Siltstone, sandstone	2	351	38	85
Ulupa Siltstone	Siltstone	7	482	63	147
Belair Subgroup	Slate, phyllite, clay	4	375	93	149
Bunyeroo Formation*	Shale	4	446	76	170
ABC Range Quartzite	Sandstone	1	164	35	23
Enorama Shale*#	Shale	1	498	114	115
Etina Formation*#	Shale	1	384	106	122
Tapley Hill Formation*#	Siltstone, shale	12	522	101	115
Wilyerpa Formation#	Siltstone, conglomerate	6	407	118	87
Tindelpina Shale Member	Siltstone	5	492	84	110
River Wakefield Subgroup	Siltstone, sandstone	11	452	87	99
Callana Group*	Siltstone, shale	3	635	48	181
Yudnamutana Subgroup	Claystone, siltstone	4	525	43	120
Holowilena Ironstone	Siltstone	1	607	51	136
Burra Group*	Siltstone, clay	12	299	125	89
Appila Tillite*	Conglomerate, diamictite, siltstone	7	499	86	113
Yerelina Subgroup	Dolomite, schist, carbonatite, siltstone	9	320	77	86
Waukaringa Siltstone	Siltstone	3	520	48	140
Mean concentrations (Total no. of analyses)			419 (162)	128 (147)	101 (162)
# Mean concentrations of the formations common in both Tables 9.3 and 9.4		22	528	105	111

*Includes data from Turner *et al.* (1993).

(B)

Rock type	No. of analyses	Mean Ba values (ppm)
Siltstone	25	546
Siltstone, shale, clay	32	433
Shale	7	414

9.3 Sampling and analyses

Cawley (1983) analysed the host Brachina Formation in the Oraparinna Mine for a variety of major and trace elements adjacent to barite veins (Fig. 8.1). Cawley's samples were on two sections out from 1C Lode on Level 4: (a) 25 m SE along the crib room drive and (b) along the main decline on an oblique angle to 1C Lode. Sampling in the present research included two sections out from 1D Lode: (a) five samples on Level 5 (OM121 and OM123 to OM126), within 25 m from the Lode; and (b) 14 samples from drill hole OU2/90 drilled from Level 6 of the main decline, to meet 1D Lode below the Level 7 (Fig. 8.1; see Appendix 9.2 for the geological log). Whole rock analyses of the samples were carried out by XRF (Appendix 8.1). The Level 5 samples were analysed for 11 major and 20 trace elements by XRF (Appendix 9.3). The drill hole samples were analysed for the same trace elements as Level 5 samples, but were not analysed for major elements (Appendix 9.3).

The Oraparinna Mine area contains a complex vein system, with veins from micro to major scale. It is impossible to sample a lengthy section of host rocks free of small scale barite veins, either because of the interference from other veins, or lack of outcrop near the mine area. Therefore, the Far Western Lode (Reid, 1969, 1970; Harris, 1979), an isolated barite vein with considerably lower minor vein occurrences in the Third Plain area, 2.8 km NNW of the mine, was selected for sampling (Figs. 1.3, 3.5). These samples were also analysed for major and minor elements by XRF.

In order to have a better understanding of the background Ba contents, a variety of formations in the central Flinders Ranges were sampled from different locations, away from the barite-mineralised areas. Brachina Formation sample no. 769 was collected 17.5 km NNW of the Oraparinna Mine and nos. 771 and 772 were collected from locations within 2 km of each other, at 11 km NNW of the Oraparinna Mine. Sample no. 829 was collected 30 km SW of the Oraparinna Mine, from the same formation. The samples were analysed by XRF for whole rock Ba concentrations.

The Brachina Formation from the Flinders Ranges as well as the Southern Adelaide Fold Belt was further subjected to electron microprobe analyses for grain scale concentration. A range of samples from the Brachina Formation in the Oraparinna Mine, and away from the barite-mineralised areas was analysed. The latter included samples nos. 769, 771, 772 and 829 from the central Flinders Ranges as well as 91/536 (Pichi Richi, courtesy P. James) from the southern Flinders Ranges, and A987/W1 (Wirinna) and 6/8/80-1 (Hallet Cove, courtesy P. James) from the southern Adelaide Fold Belt

9.4 Results: Ba content of the host rocks adjacent to barite veins

Whole rock Ba contents of 50 host rock samples from the Brachina Formation in the Oraparinna Mine and the Elatina Formation at the Far Western Lode vary from 155ppm to 3.3 wt % (Appendixes 9.3, 9.4). The high Ba contents such as 3.3 wt % are due to the occurrence of barite in minor and micro fractures, as well as grain scale, in the host rock (Fig. 9.2). Thus, those samples do not truly represent the geochemistry of the Brachina Formation, and were excluded from comparison with the rest of the samples.

Cawley (1983) found an increase in SiO_2 and Na_2O away from the 1C Lode in the mine. His work showed that Al_2O_3 and K_2O also increase within 5 - 10 m of the vein, followed by a decrease, and that Ba and Sr decrease away from the vein. He did not, however, record whether any of the samples contained micro-veins or grains of barite.

9.4.1 Level 5, Oraparinna Mine

Five samples of the host Brachina Formation up to 25 m distance from the 1D Lode on Level 5 of the Oraparinna Mine show Ba contents from 996 ppm to 3.3 wt % (Appendix 9.3). The samples at 4.2 m and 16.9 m from the vein show abnormally high Ba values of 3.3 wt % and 2.5 wt % respectively, therefore were excluded from comparison with others (Section 9.4). The samples at 1.1 m, 10.2 m and 24.8 m were clear of any visible veinlets of barite and have Ba contents of 1566 ppm, 996 ppm, and 765 ppm, respectively, and thus were used in the comparison.

The major element analyses show increasing trends for SiO_2, Al_2O_3, MgO, Na_2O, K_2O and TiO_2 and decreasing trends for MnO, CaO and P_2O_5 away from the vein (Fig. 9.3a-j). Fe_2O_3 shows an inconsistent trend (Fig. 9.3c). Trace elements Rb, Ni, Co, V, Ce, Nd, La, Ga, Cr, Nb and Pb show increasing trends away from the vein and Ba, Sr, Cu and Y show decreasing trends (Fig. 9.3k-ac). Zn, Sc, Zr, Th and U show inconsistent trends.

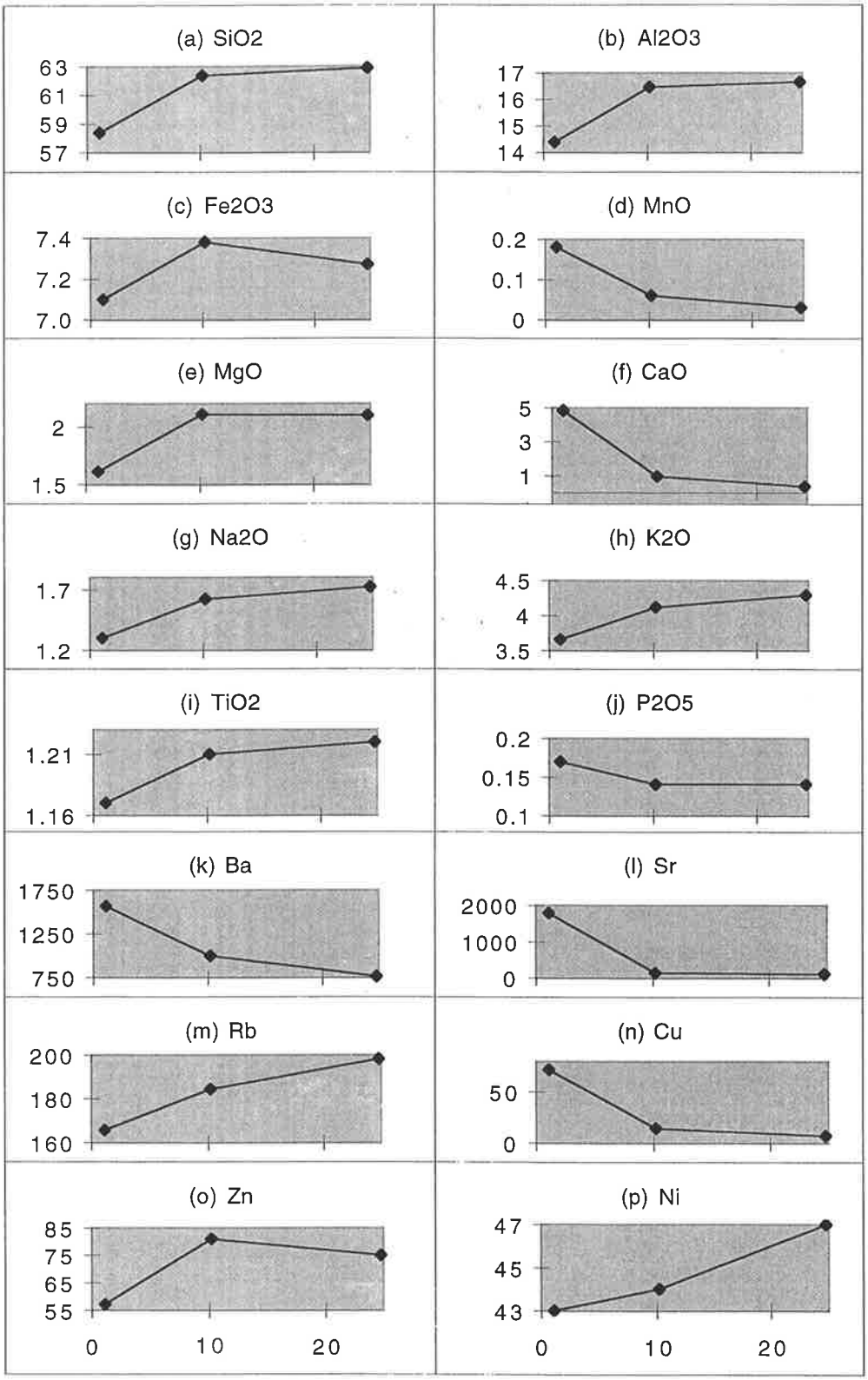

Fig. 9.3a-ad: Geochemistry of samples OM126, 124 and 121 of Brachina Formation with respect to distance (m) from 1D Lode, Level 5, Oraparinna Barite Mine. Major elemets (a-j) are in wt % oxide, trace elements (k-ad) are in ppm element.

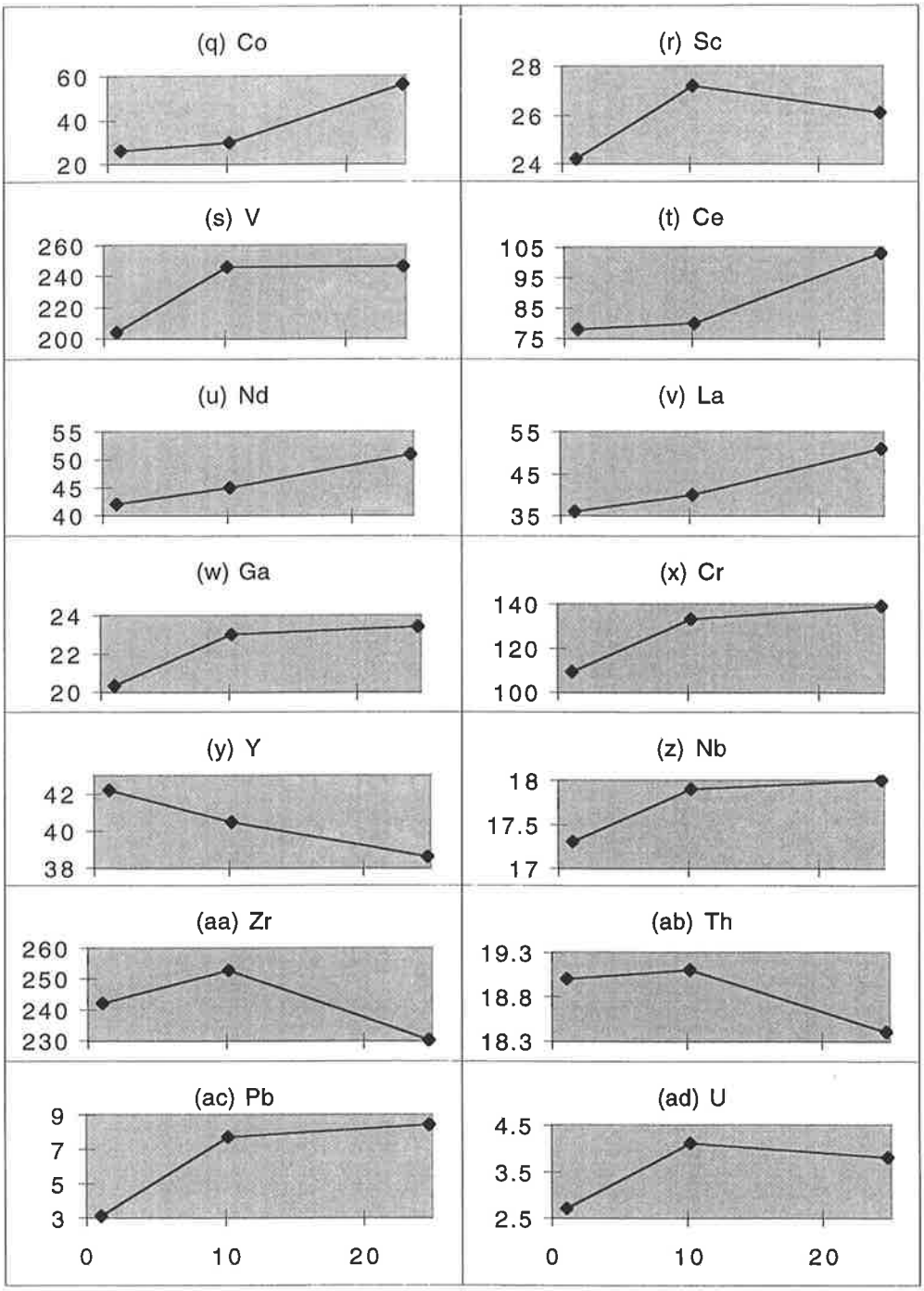
(q) Co
60
40
20
(r) Sc
28
26
24
(s) V
260
240
220
200
(t) Ce
105
95
85
75
(u) Nd
55
50
45
40
(v) La
55
45
35
(w) Ga
24
22
20
(x) Cr
140
120
100
(y) Y
42
40
38
(z) Nb
18
17.5
17
(aa) Zr
260
250
240
230
(ab) Th
19.3
18.8
18.3
(ac) Pb
9
7
5
3
0
10
20
(ad) U
4.5
3.5
2.5
0
10
20

Fig. 9.3q-ad

9.4.2 Drill Hole OU2/90, Oraparinna Mine

Both 1C and 1D Lodes of the mine strike NE with steep to moderate dips to SE (Fig. 8.1). On Level 6 of the mine, 1C Lode is 75 m north of 1D Lode. Samples were selected from drill hole OU2/90, on either side of 1D Lode, up to 45.8 m NW and 9.1m SE of the lode. Ba contents measured from the drill hole samples vary from 155 ppm to 7064 ppm (Appendix 9.3). Even though the pattern of element concentrations to the SE of the vein is not identical to that to the NW, both sides generally show similar ranges of concentrations, except for Rb, Zr, Ce, Nd and La, for which the ranges for the SE samples slightly exceed those for the NW samples (Appendix 9.3). The number of samples on the SE side of 1D Lode is less than that on the NW due to the limit of the drill hole. Hence, only the samples NW of 1D Lode, towards 1C Lode, were used in interpreting the trends of element concentrations (Fig. 9.4). "Spikes" in the data (i.e. particularly high values representing single samples) were ignored in the following discussion, which examined general trends. Such "spikes" were probably due to variations in the accessory mineral contents of the samples.

Ba shows a decreasing trend away from the 1D Lode, with the lowest value of 155 ppm at 41.8 m from the vein (Fig. 9.4a). Sr, Rb, V, Y, Sc, Ga, Nb, Th, Pb, Co and Zn show general trends of decreasing values approximately to 10 m from the vein, but thereupon increase (Figs. 9.4c-n). Sr shows the lowest value of 102 ppm at 22.7 m and increases to 211 ppm at the edge of the vein. Pb shows the lowest value of 1.2 ppm at 8.5 m and increases to 8.2 ppm at the edge of the vein. The sample at 42 m shows values inconsistent with the general trends for most elements. Cu shows an increasing trend away from the vein (Fig. 9.4m), U shows a decreasing trend (Fig. 9.4b), while Zr and Nd show flat trends (Figs. 9.4q, s). Cr shows an increasing trend within 10 m from the vein, but thereupon a decrease (Figs. 9.4p). Ni although more variable, shows a similar overall trend (Fig. 9.4o). Ce and La show inconsistent trends (Fig. 9.4r, t). However, the patterns of element concentration are strongly dependent on host rock sample "contamination" by barite in micro-cracks and variations in accessory mineral contents.

9.4.3 Host rock samples from the Far Western Lode

The lode strikes north and dips 52° W with a maximum exposed width of 1.1 m and extends for about 80 m (Harris, 1979). The host rocks strike NW, dip 30°NE, and consist of sandy siltstones of the Elatina Formation. The host rock was sampled on the surface along strike, for about 400 m SE from the vein, where a change in facies was noted between 110-275 m along strike, with a more

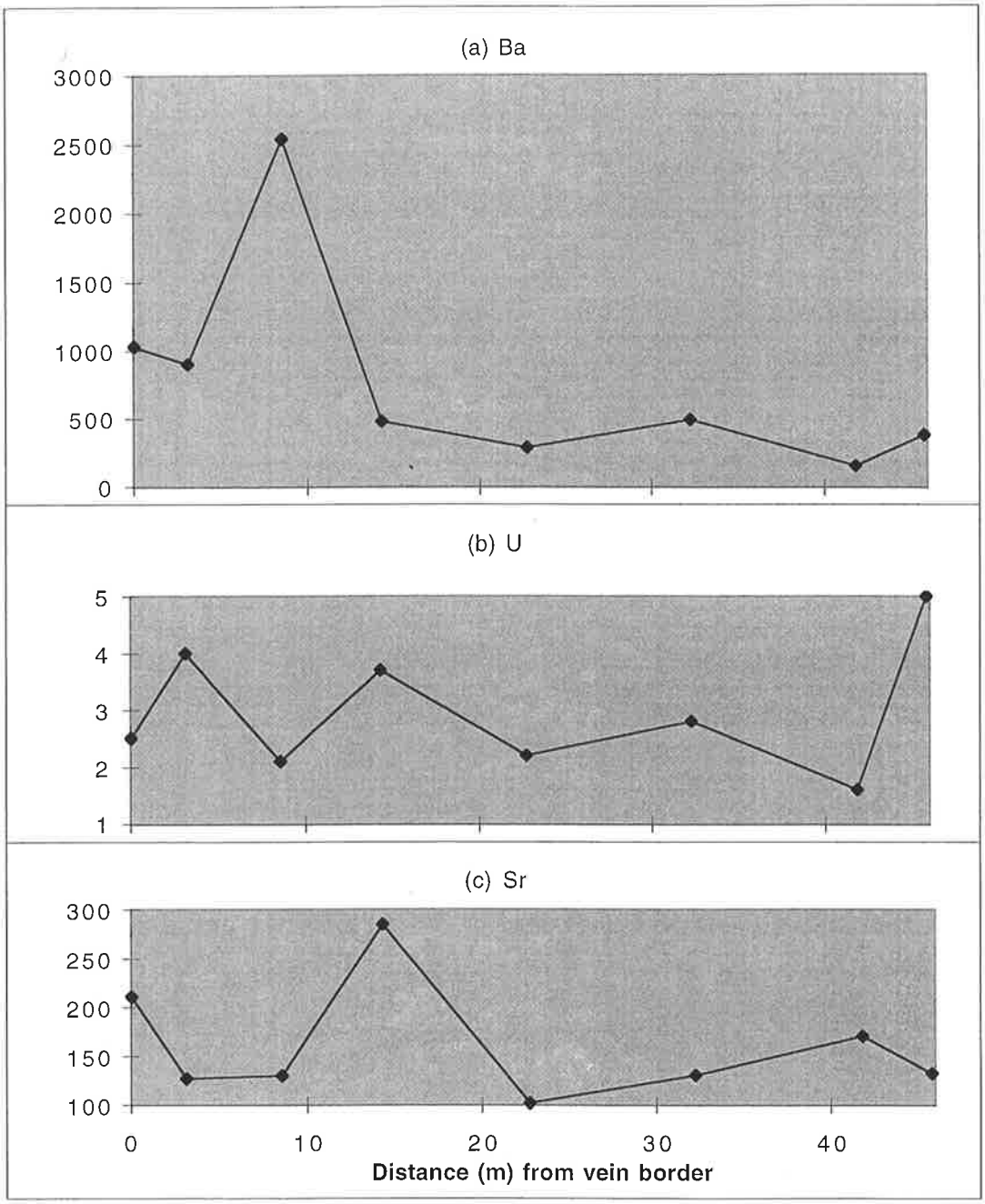

Fig. 9.4a-t: Geochemistry of drill hole OU2/90 samples of the Brachina Formation with respect to distance to the NW from 1D Lode, between Levels 7 and 8, Oraparinna Barite Mine. All the elements are in ppm concentration.

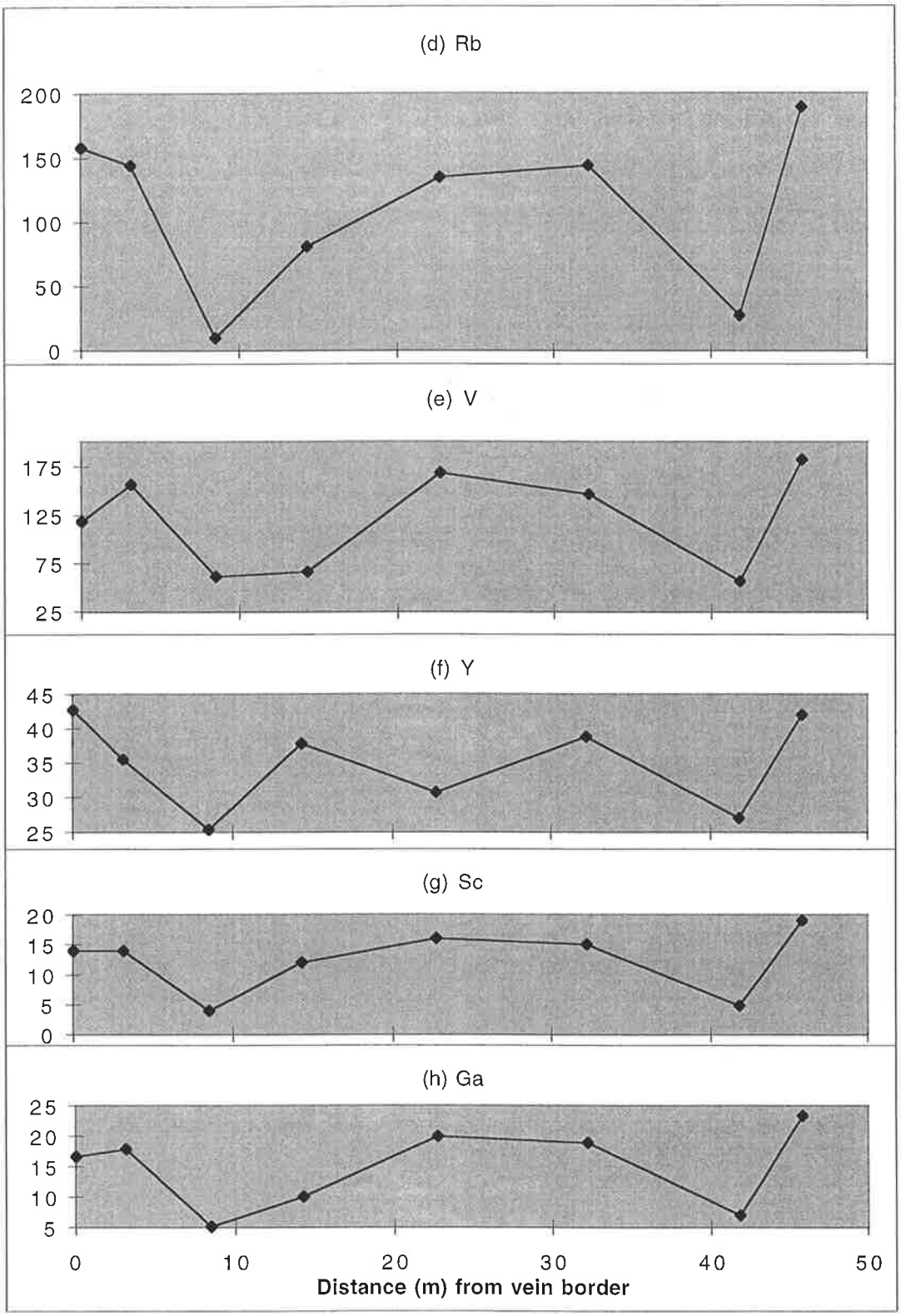
(d) Rb
200
150
100
50
0
(e) V
175
125
75
25
(f) Y
45
40
35
30
25
(g) Sc
20
15
10
5
0
(h) Ga
25
20
15
10
5
0
10
20
30
40
50
Distance (m) from vein border

Fig. 9.4d-h

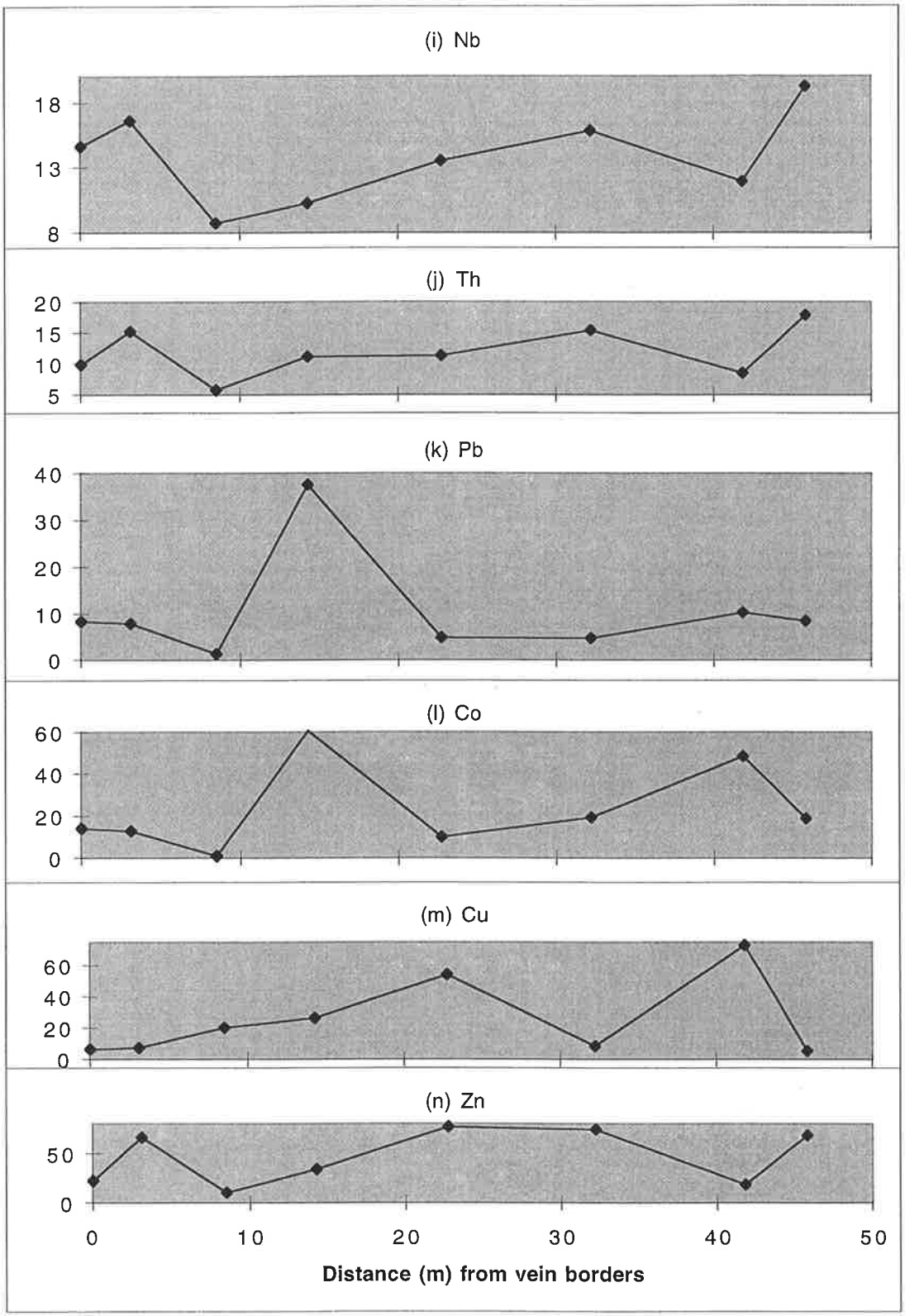
(i) Nb
18
13
8
(j) Th
20
15
10
5
(k) Pb
40
30
20
10
0
(l) Co
60
40
20
0
(m) Cu
60
40
20
0
(n) Zn
50
0
0
10
20
30
40
50
Distance (m) from vein borders

Fig. 9.4i-n

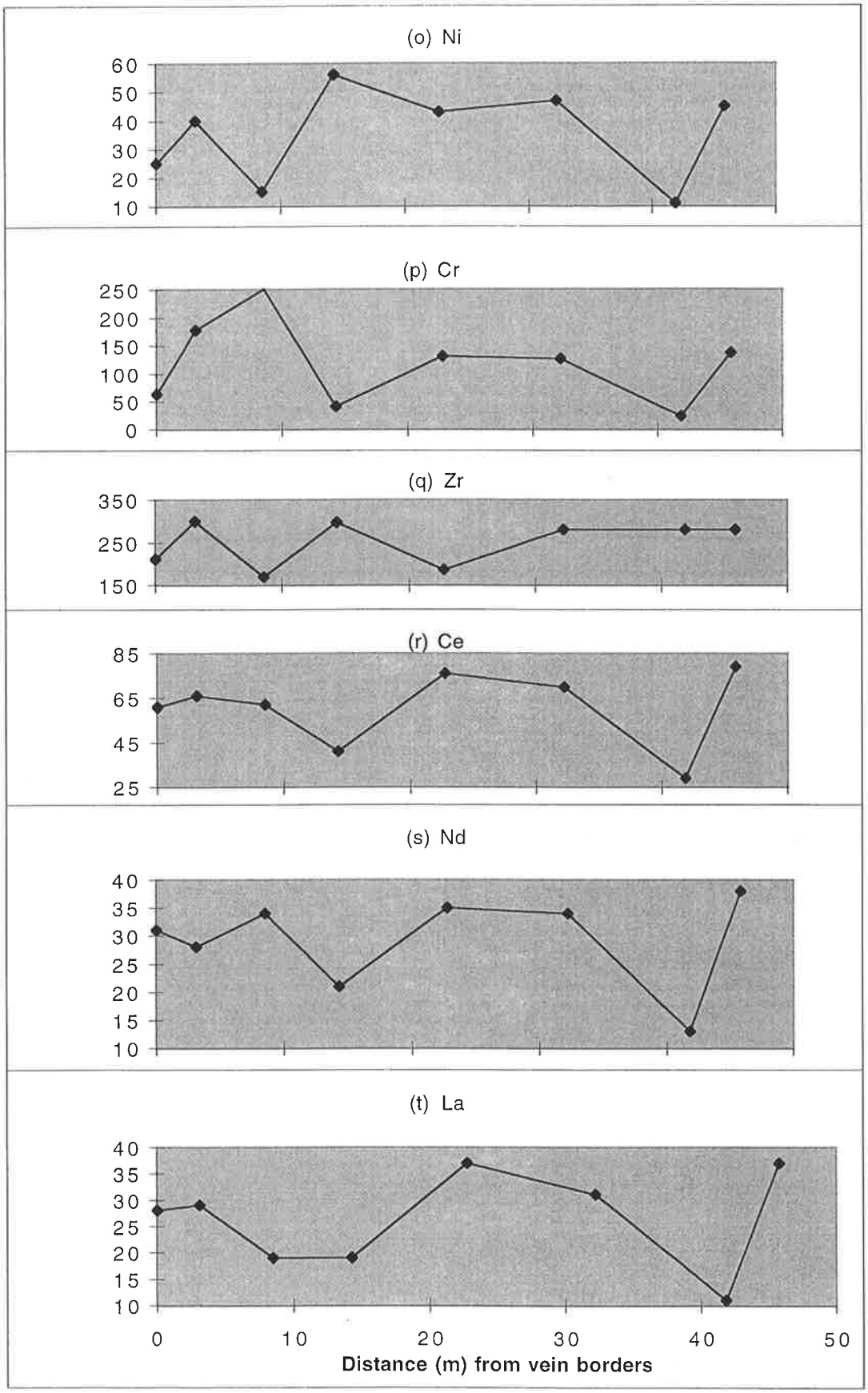
(o) Ni
60
50
40
30
20
10
(p) Cr
250
200
150
100
50
0
(q) Zr
350
250
150
(r) Ce
85
65
45
25
(s) Nd
40
35
30
25
20
15
10
(t) La
40
35
30
25
20
15
10
0
10
20
30
40
50
Distance (m) from vein borders

Fig. 9.4o-t.

pelitic nature than the rest of the section. All the samples were slightly weathered compared to the samples from the two underground sections in the Oraparinna Mine.

XRF analyses of the samples of most of the elements show elevated concentrations between 110 m and 275 m, compared to the other samples of the traverse (Fig. 9.5 and Appendix 9.4). This interval shows relative enrichment of Al, Fe, Mg, Ca, Na, Ti, P, Mn, Sc, Nb, Ce, Zr, V, Y, La, Cr, Nd, Th, Ga and U, and relative depletion of Si and Ba (Fig. 9.5a-ac). The Al_2O_3 content increases from average 5 wt % to 8.5 wt % while SiO_2 content decreases from an average of 87 wt % to 65 wt % within this interval, in accordance with the more pelitic nature (sandy siltstone) than the rest of the samples (sandstone).

If the interval between 110-275 m is excluded, the 400 m long section shows SiO_2 decreases away from the vein by 7 wt % (Fig. 9.5a). It further shows a generally increasing trend for Al_2O_3, Fe_2O_3, MgO, Na_2O, K_2O, TiO_2, P_2O_5 and CaO, although the latter's increase is minimal (Fig. 9.5b-i). MnO shows a flat trend, again excluding the interval between 110-275 m (Fig. 9.5j). However, Al_2O_3, Na_2O and K_2O show an increase in concentration within 10 m from the vein.

Ba content varies from 241 ppm to 5071 ppm over the whole section (Fig. 9.5k). Minor barite veins of 0.1-0.3 m length were observed at 15 m and between 18-21 m from the main lode and would account for high Ba values. If the pelitic interval between 110-275 m is excluded, Ba and Co are the only trace elements that show an overall decreasing trend away from the vein (Fig. 9.5k, l), although both elements show an increasing trend up to 25m from the vein. Zn, Sr, Rb, Sc, Nb, Pb, Ce, Zr, V, Y, La, Cr, Nd, Th and Ga show increasing trends away from the vein (Fig. 9.5m-aa). The elements from Zn to Pb (i.e. Figs. 9.5m-r) show a decreasing trend away from the vein, to within 25 m from the vein. Cu content varies between 5-20 ppm showing a flat trend (Fig. 9.5ab). U shows very low concentrations of less than 3 ppm and an inconsistent trend (Fig. 9.5ac).

9.5 Background Ba contents of formations in the central Flinders Ranges

Rock samples from widely distributed locations in the central Flinders Ranges, with no close proximity to known barite veins, were analysed by XRF, in order to obtain background geochemical information (Table 9.4). The samples represent nine major formations, including the Brachina Formation, and rocks from the Oraparinna Diapir. The results show Ba contents range from 26 ppm for the Trezona Formation to 2981 ppm for the Brachina Formation. Dolomite, calcareous shale and siltstone from the Oraparinna Diapir recorded 42, 207 and 270 ppm Ba

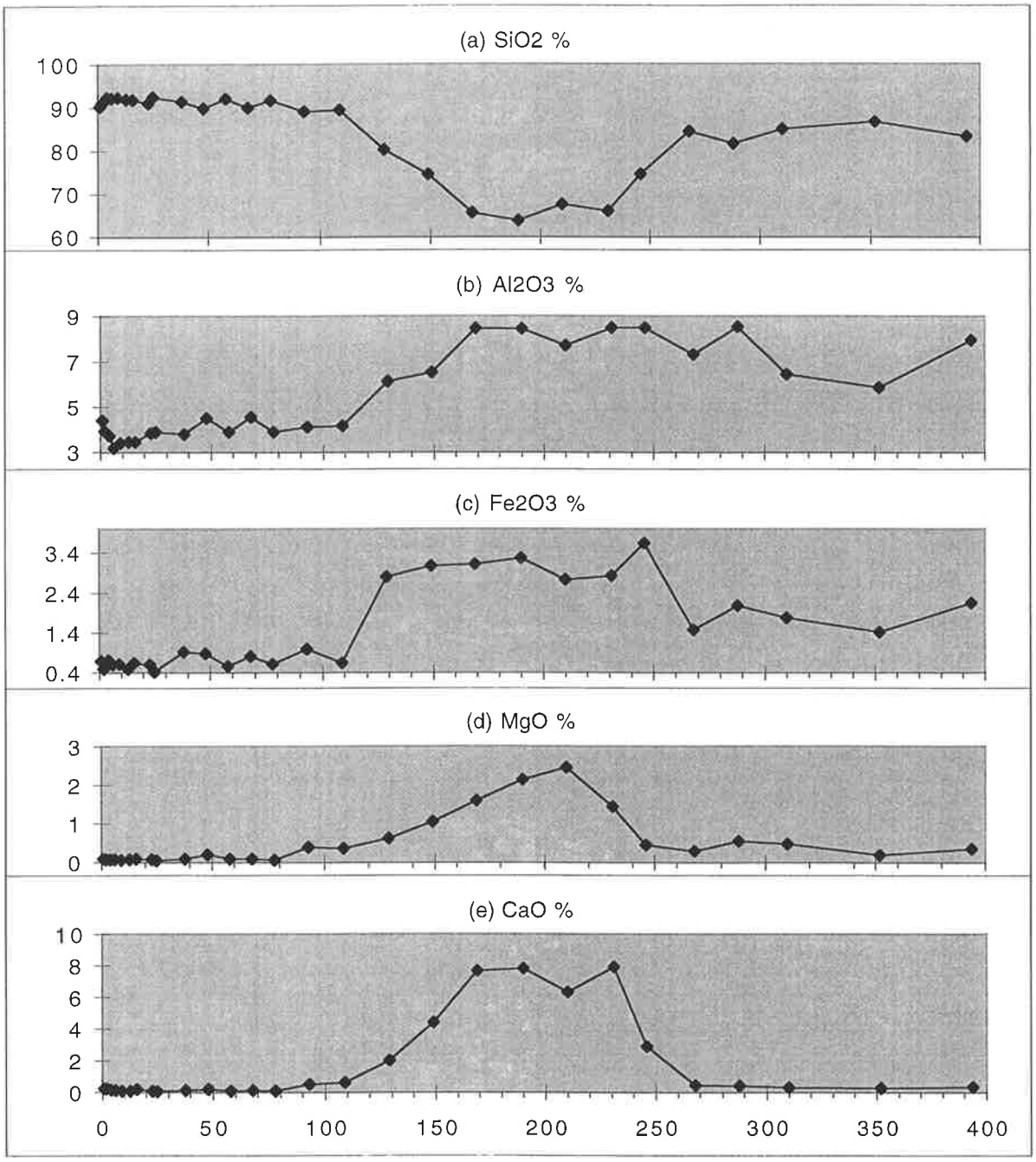

Fig. 9.5a-ac: Geochemistry of samples of Elatina Formation with respect to distance (m) from Far Western Lode in the Third Plain area, northwest of Bunkers Graben. Major elements (a-j) are wt % oxide, trace element (k-ac) are in ppm element.

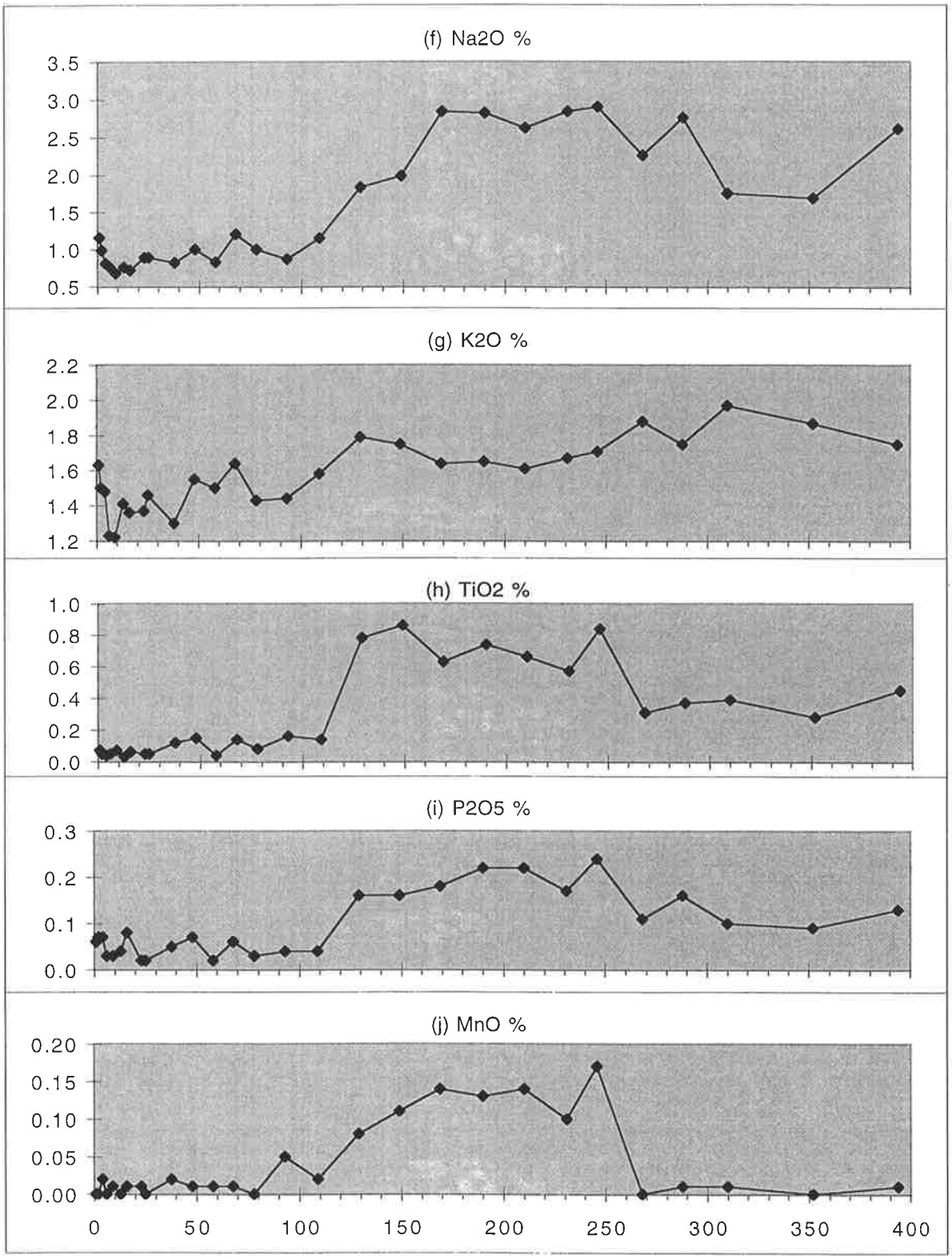
(f) Na2O %
3.5
3.0
2.5
2.0
1.5
1.0
0.5
(g) K2O %
2.2
2.0
1.8
1.6
1.4
1.2
(h) TiO2 %
1.0
0.8
0.6
0.4
0.2
0.0
(i) P2O5 %
0.3
0.2
0.1
0.0
(j) MnO %
0.20
0.15
0.10
0.05
0.00
0
50
100
150
200
250
300
350
400

Fig. 9.5f-j

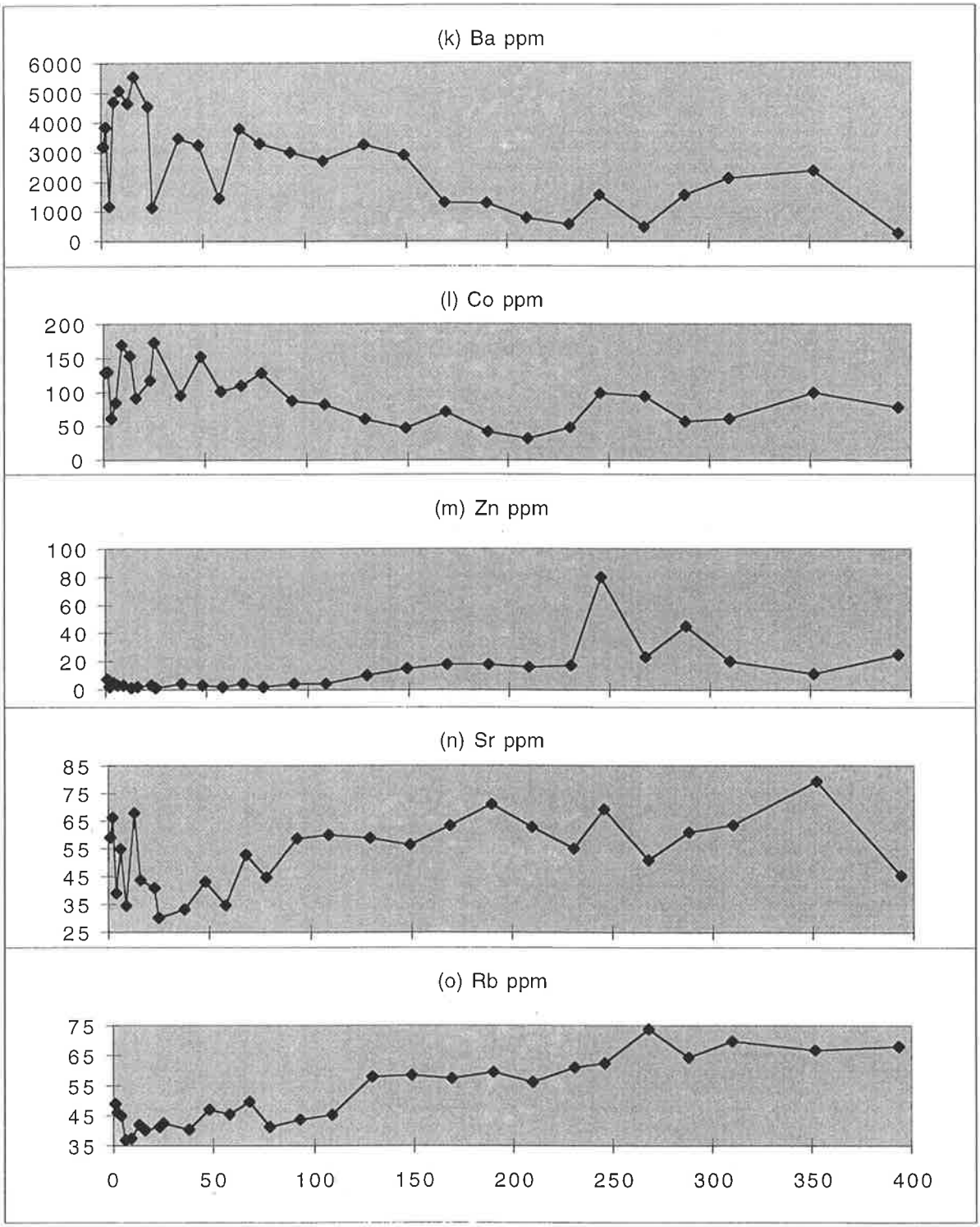
(k) Ba ppm
6000
5000
4000
3000
2000
1000
0
(l) Co ppm
200
150
100
50
0
(m) Zn ppm
100
80
60
40
20
0
(n) Sr ppm
85
75
65
55
45
35
25
(o) Rb ppm
75
65
55
45
35
0
50
100
150
200
250
300
350
400

Fig. 9.5k-0

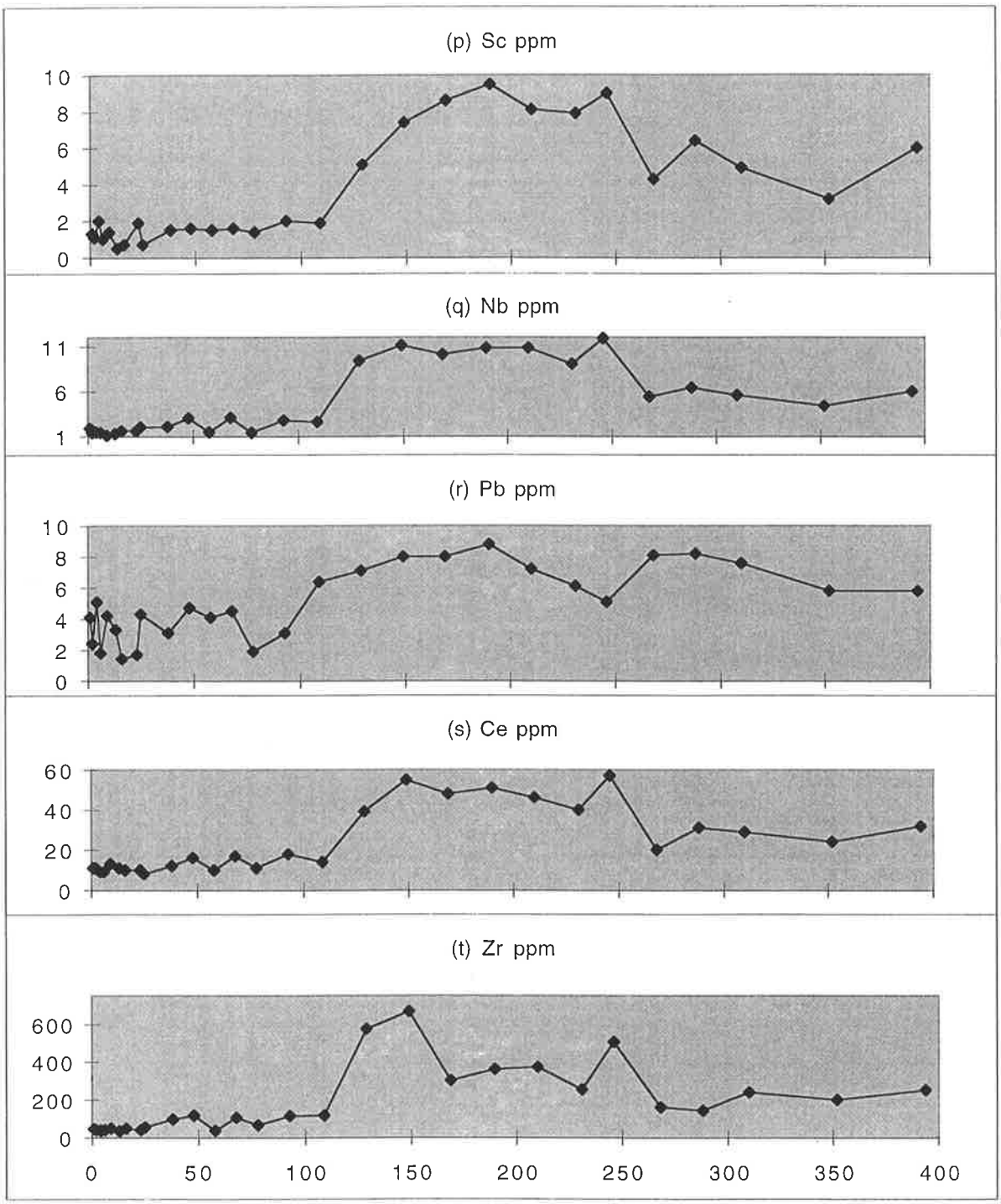
(p) Sc ppm
10
8
6
4
2
0
(q) Nb ppm
11
6
1
(r) Pb ppm
10
8
6
4
2
0
(s) Ce ppm
60
40
20
0
(t) Zr ppm
600
400
200
0
0
50
100
150
200
250
300
350
400

Fig. 9.5p-t

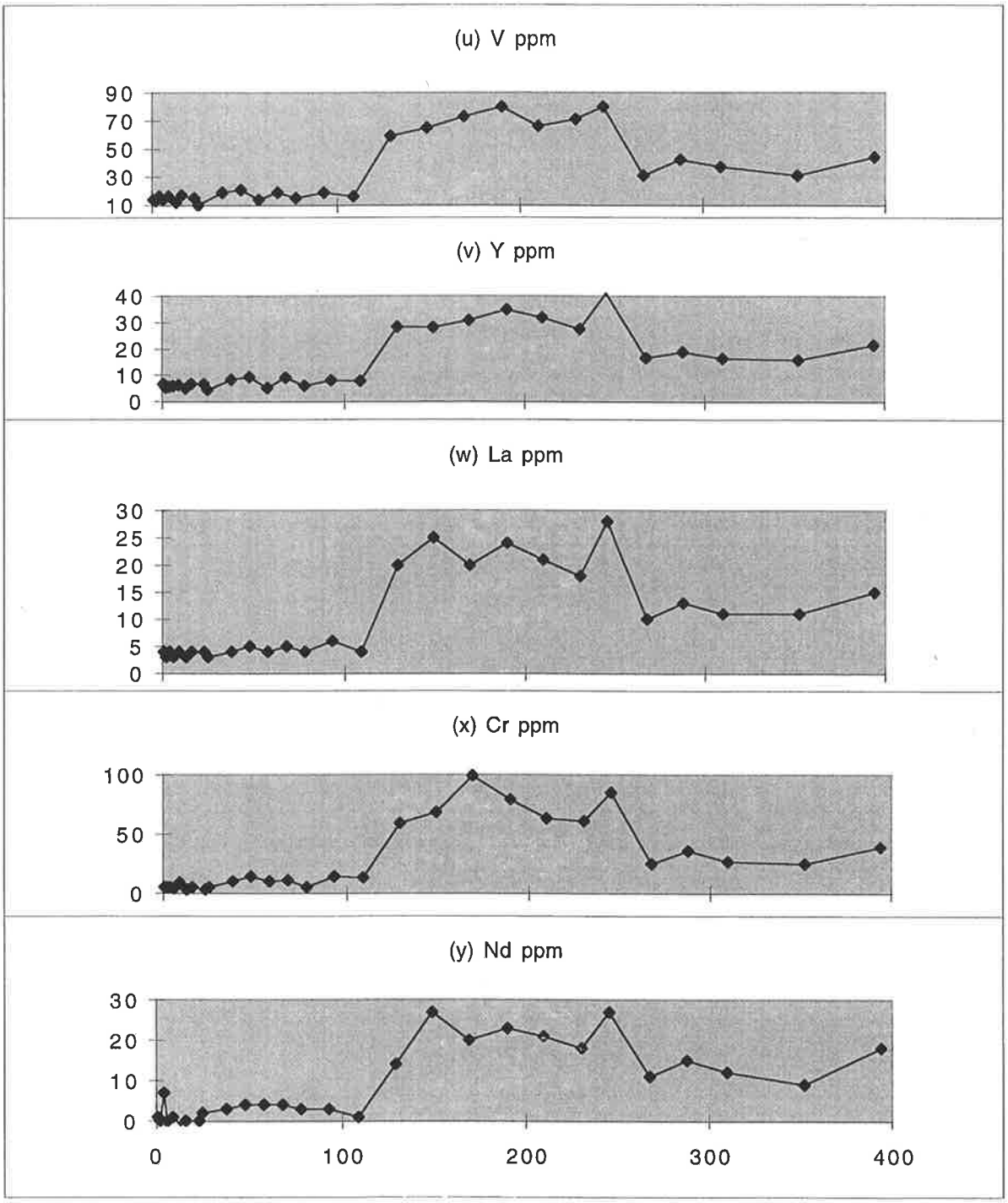
(u) V ppm
90
70
50
30
10
(v) Y ppm
40
30
20
10
0
(w) La ppm
30
25
20
15
10
5
0
(x) Cr ppm
100
50
0
(y) Nd ppm
30
20
10
0
0
100
200
300
400

Fig. 9.5u-y

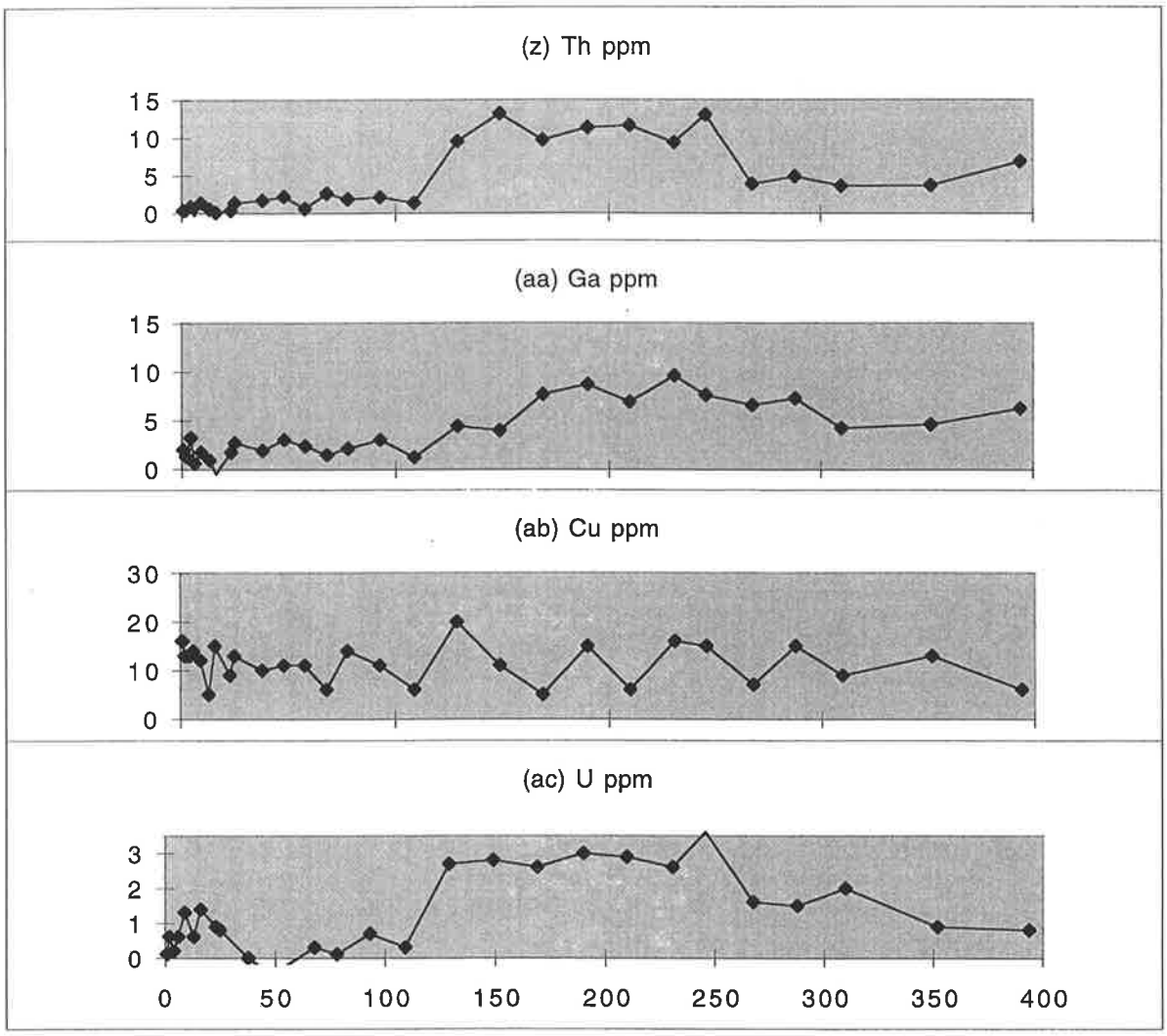
(z) Th ppm
15
10
5
0
(aa) Ga ppm
15
10
5
0
(ab) Cu ppm
30
20
10
0
(ac) U ppm
3
2
1
0
0
50
100
150
200
250
300
350
400

Fig. 9.5z-ac.

respectively, with a mean value of 173 ppm. The Ba content of the Brachina Formation ranges from 293 to 2981 ppm (5 analyses). The highest value of 2981 ppm was shown by sample 769, collected 17.5 km NNW of the Oraparinna Mine. An electron microprobe back-scattered image of the sample shows barite present in the pore spaces and triple junctions of the grains (Fig. 9.6). Therefore, the sample is not considered representative of the Brachina Formation, and was excluded from the exercise. The Ba contents of the other four samples of the Brachina Formation vary from 293-409 ppm (4 analyses) with a mean value of 359 ppm. Samples other than those from the diapir and the Brachina Formation show a mean value of 325 ppm (8 analyses). The Sr and Rb contents show mean values of 207 and 90 ppm, respectively, for these 8 analyses. Therefore, the analyses suggest that the Brachina Formation in the central Flinders Ranges may have a higher background Ba content (359 ppm) than (a) all other formations investigated (325 ppm) and (b) the Oraparinna Diapir (173 ppm).

Table 9.4: Analyses of a variety of regional rock samples away from barite veins in the central and southern Flinders Ranges.

Formation	Description	Sample no.	Ba ppm	Sr ppm	Rb ppm
Oraparinna Diapir	Shale in calcareous matrix	715	207	95.0	127.0
Oraparinna Diapir	Dolomite	722	42	256.5	5.8
Oraparinna Diapir	Siltstone	823	270	45.0	140.7
Wilyerpa Formation#	200 m E of Enorama Diapir	788	221	105.5	59.2
Tapley Hill Formation#	5 km SW of Dunbar Lodes	783	356	108.9	87.2
Sunderland Formation	9.5 km SW of Dunbar Lodes	828	345	161.0	84.9
Etina Formation#	11 km SW of Dunbar Lodes	780	620	144.8	134.0
Etina Formation#	4.2 km E of Enorama Diapir	802	407	63.9	154.9
Enorama Shale#	Brachina Gorge	808	394	128.8	105.6
Trezona Formation	Brachina Gorge	814	26	881.8	5.4
Elatina Formation	Brachina Gorge	812	227	61.9	85.9
Brachina Formation	17.5 km NNW of Oraparinna Mine	769	2981	120.1	36.8
Brachina Formation#	11 km NNW of Oraparinna Mine	771	362	53.2	185.0
Brachina Formation#	Brachina Gorge	815	293	73.7	105.4
Brachina Formation#	30 km SW of Oraparinna Mine	829A	409	57.0	57.5
Brachina Formation#	30 km SW of Oraparinna Mine	829B	371	57.5	73.6
Mean concentration of all 15 samples, excluding sample no. 769			303	153	94
# Mean concentrations of a total of 9 samples, for the formations common in both Tables 9.3 and 9.4			381	88	107

According to these data, the mean Ba content of the rocks representing the entire Adelaide Fold Belt (419 ppm, Table 9.3) is higher than that for the central Flinders Ranges (303 ppm, Table 9.4), whereas the mean Sr and Rb contents are similar in both cases. Furthermore, the common formations between Tables 9.3 and 9.4 show that the mean concentration of samples of those formations in the Adelaide Fold Belt (528 ppm) is higher than the mean of samples from the central Flinders Ranges (381 ppm). However, the significance of this apparent difference should be treated cautiously, as not all of the whole rock samples in this experiment were examined for

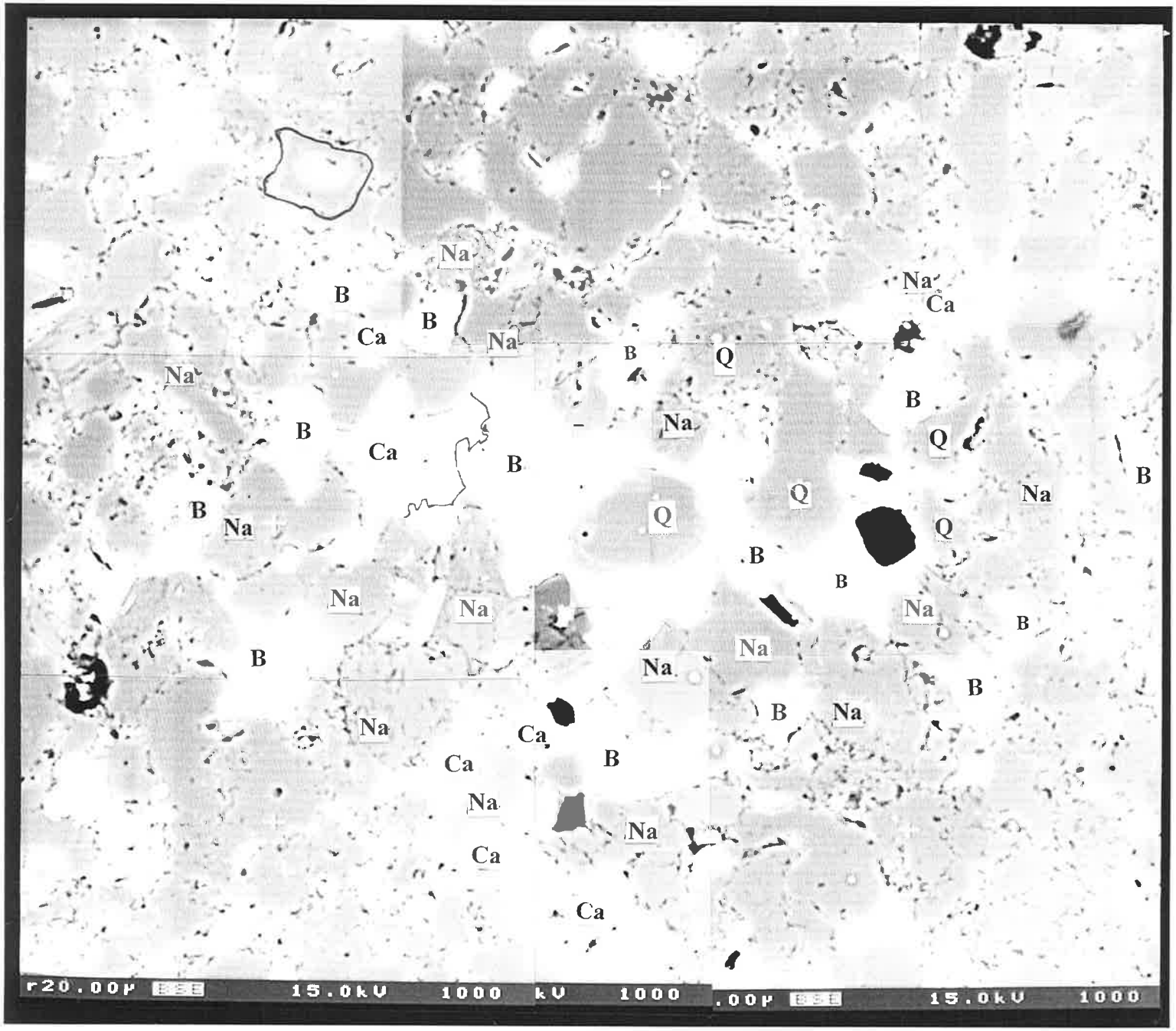

Fig. 9.6: Electron microprobe back scattered image showing Na-feldspar (Na), calcite (Ca), barite (B), quartz (Q) and CaSO4 (black) in the Brachina Formation, 17.5 km NNW of the Oraparinna Barite Mine (Sample 769).

0.02 mm

microscale barite mineralisation. The same observation applies to the samples analysed the Department of Mines of Energy and Energy (1996), and Turner *et al.* (1993) (Table 9.3).

9.6 Microprobe analyses for Ba in the Brachina Formation

The Brachina Formation was subjected to grain-scale investigations by electron microprobe, because the whole rock data on background Ba are ambiguous, due to the possible presence of barite mineralisation as grains and micro-veinlets (see above). The Brachina Formation is dominated by K- and Na-feldspars and quartz, and analyses using the electron microprobe showed that K-feldspars contain the highest concentrations of Ba. Cawley (1983) reported electron microprobe analyses up to 0.6 wt % Ba in the K-feldspars of Brachina Formation from the Oraparinna Mine. Therefore, K-feldspar grains of the Brachina Formation from the mine, as well as from non-mineralised areas (i.e. areas where barite deposits are not known to occur) in the Adelaide Fold Belt, were investigated in this study for Ba concentrations using the electron microprobe.

9.6.1 Ba content in K- and Na-feldspar grains

The Ba contents of K-feldspars in the Brachina Formation from non-mineralised areas in the Adelaide Fold Belt show a mean value of 0.4 wt %, ranging from 0 to 1.18 wt % for 24 spot analyses (Table 9.5a). The highest value of 1.18 wt % was obtained from sample 771, 11 km NNW of the Oraparinna Mine. The samples from Oraparinna Mine show a mean value of 0.2 wt % Ba, ranging from 0 to 0.79 wt % for 39 spot analyses (Table 9.5b). By comparison, the Ba content of Na-feldspars in the samples from the non-mineralised areas show a mean value of 0.04 wt %, ranging from 0 to 0.18 wt % for 15 analyses (Table 9.5a) and those from the mine show a mean of 0.02 wt %, ranging from 0 wt % to 0.06 wt % for 13 analyses (Table 9.5b). Therefore, the data suggest that the mean Ba contents of both of the K- and Na-feldspars in the samples of Brachina Formation in the Oraparinna Mine are of the order of 50 % of corresponding values of samples from non-mineralised areas. However, the Ba contents of the Na-feldspars are very low for all samples.

9.6.2 Ba mapping of K-feldspar grains

The Brachina Formation in the mine and from various other localities of the Flinders Ranges was subjected to detailed grain-scale analyses by the electron microprobe for K-feldspar grains. The grains were subjected to spot analyses for Ba, followed by slow scanning at a speed of 8-14 hrs per area scanned. The results are shown in Figures 9.7a – 9.10b, where a range of colours denotes the Ba concentrations.

Table 9.5: Summary of Ba analyses by electron microprobe of K-feldspar, Na-feldspar and muscovite/sericite grains in the Brachina Formation from **(A) non-mineralised areas**, well away from barite deposits, in the Adelaide Fold Belt and **(B) the Oraparinna Mine**.
See section 9.3 and Table 9.4 for additional information of regional sample locations.

(A) Non-mineralised areas

Sample no.	Location	Ba analyses					
		K-feldspar grains			Na-feldspar grains		
		No. of analyses	Range (wt %)	Mean (wt %)	No. of analyses	Range (wt %)	Mean (wt %)
769	17.5 km NNW of Oraparinna Mine	-	-	-	7	0.002-0.109	0.063
771	11 km NNW of Oraparinna Mine, within 2km	10	0.078-1.183	0.582	1	-	0
772		9	0-0.629	0.338	1	-	0
829	30km SW of mine	4	0.136-0.171	0.151	1	0.019	0.019
91/536	Pichi Richi	-	-	-	3	0-.012	0.004
A987/W1	Witinna	-	-	-	1	0.007	0.007
6/8/80-1	Hallet Cove	1	0.04	0.04	1	0.181	0.181
Total		**24**	**0-1.18**	**0.4**	**15**	**0-0.18**	**0.04**

(B) The Oraparinna Mine

Sample no.	Ba analyses					
	K-feldspar grains			Na-feldspar grains		
	No. of analyses	Range (wt %)	Mean (wt %)	No. of analyses	Range (wt %)	Mean (wt %)
OM104	3	0.071-0.691	0.35	4	0-0.057	0.036
OM125	-	-	-	2	0-0.058	0.029
OM137B	5	0.075-0.198	0.122	1	-	0
2/90/1	5	0-0.416	0.135	-	-	-
2/90/9	-	-	-	-	-	-
2/90/20	2	0.179-0.411	0.295	-	-	-
2/90/28a	-	-	-	-	-	-
2/90/38	20	0.006-0.785	0.199	5	0-0.019	0.010
A815CR7*	4	0-0.168	0.102	1	0.064	0.064
Total	**39**	**0-0.79**	**0.2**	**13**	**0-0.06**	**0.02**

*Sample collected by Cawley (1983)

A back-scattered electron image of sample 2/90/38 from the Brachina Formation in the Oraparinna Mine shows K-feldspar and quartz as the major minerals, with accessory amounts of siderite (Fig. 9.7a). Spot analyses of a K-feldspar grain show the Ba content ranges from 0.01 wt % to 0.30 wt % for 18 analyses, with a mean of 0.18 wt % (Table 9.6). The scan-map of the grain

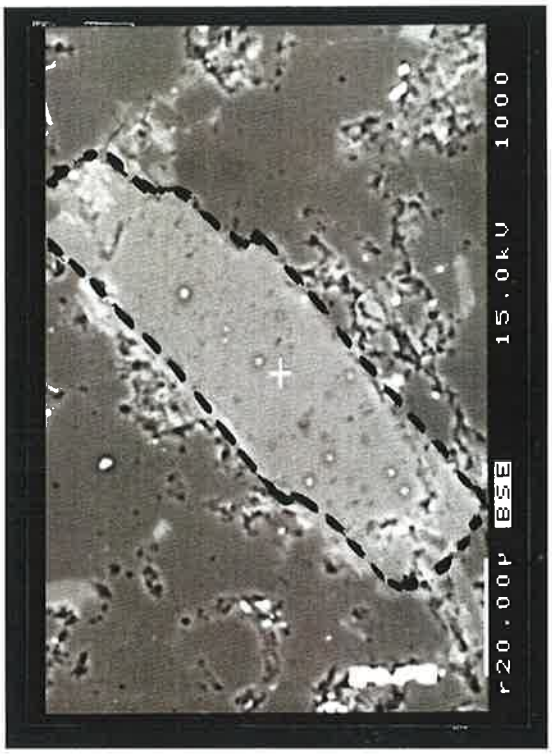

Fig. 9.7: Microprobe analyses of Brachina Formation in the Oraparinna Mine. Sample no. 2/90/38, 8m SE of 1D Lode along Drill Hole 2/90.
(a) Back scattered electron image showing a large K-feldspar grain (centre) surrounded by quartz grains. Minor siderite (white, bottom right) is also present. White circular spots are analytical points.
(b): Scan map of the central K-feldspar grain and adjacent quartz grains showing Ba distribution from highest (red) to lowest (white). The white grain at top right is siderite. White bar scales, both bottom right of (a) and bottom left of (b) are 0.02 mm.

(a)

(b)

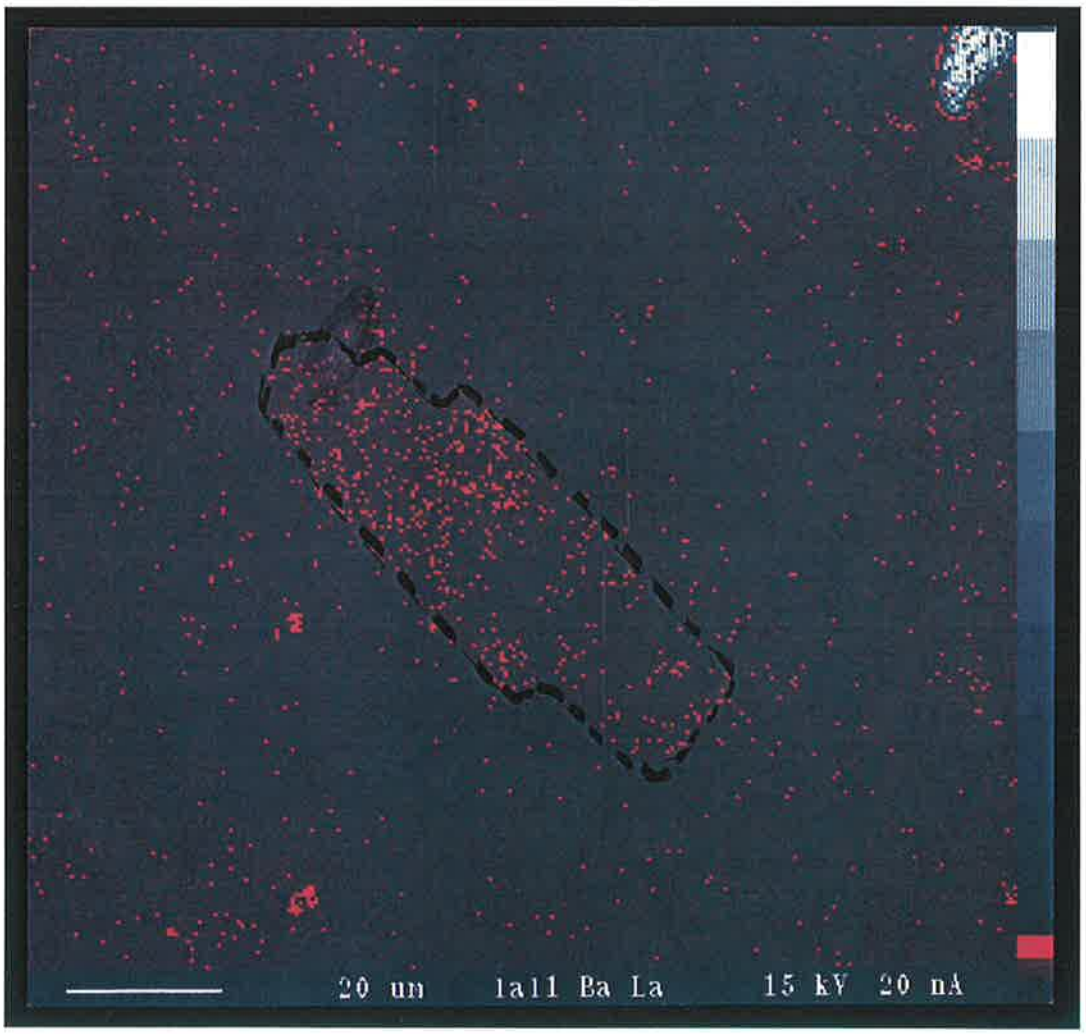

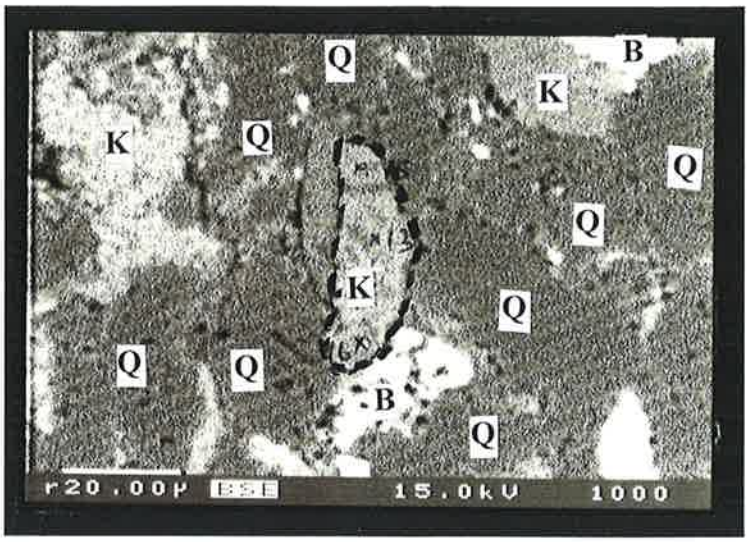

(a)

Fig. 9.8: Microprobe analyses of Brachina Formation, 11 km NNW of the Oraparinna Mine. Sample no. 772. (a) Back scattered electron image showing K-feldspar (K), quartz (Q), and barite (B) grains. (b): Scan map of the centre K-feldspar grain and adjacent grains showing Ba distribution from highest (red) to lowest (purple). Bottom left bar scales of both (a) white and (b) red, are 0.02 mm.

(b)

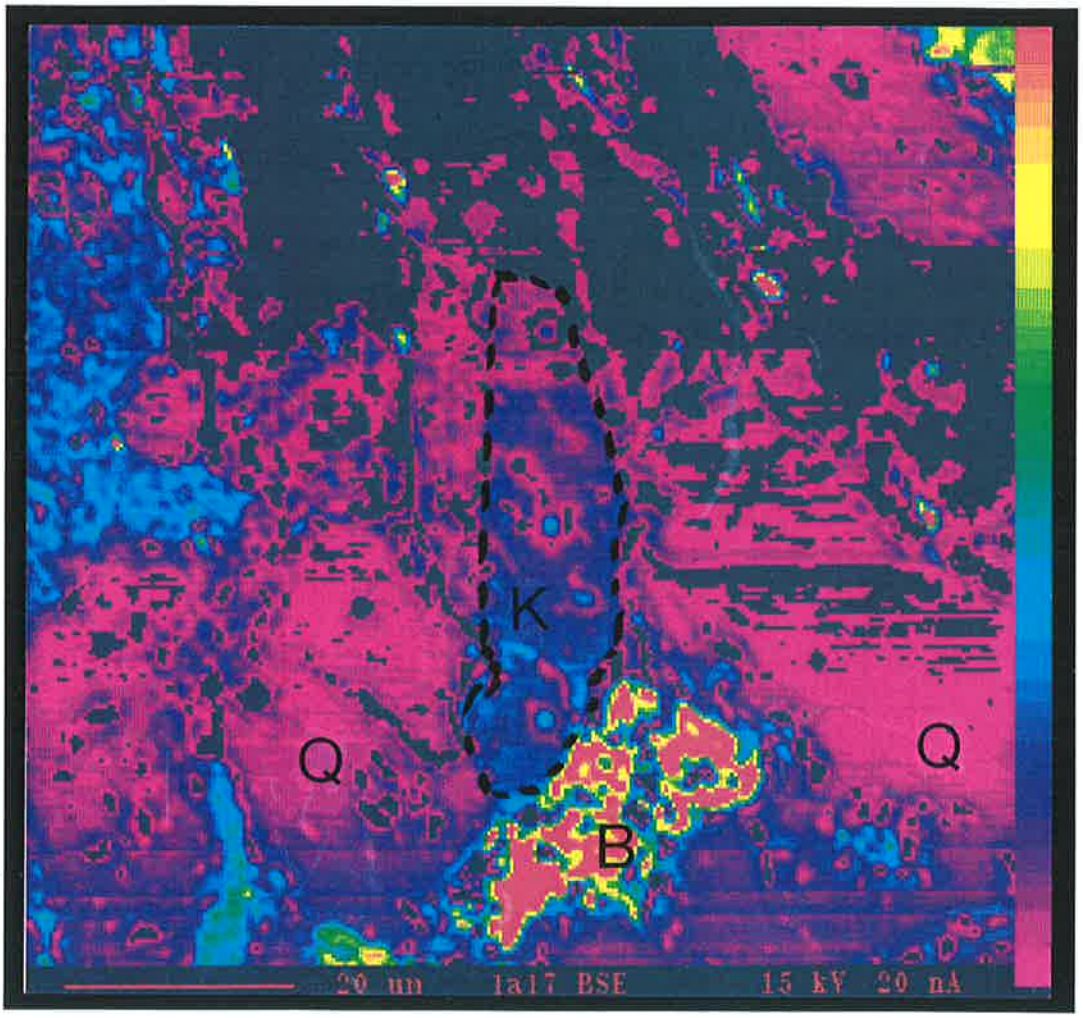

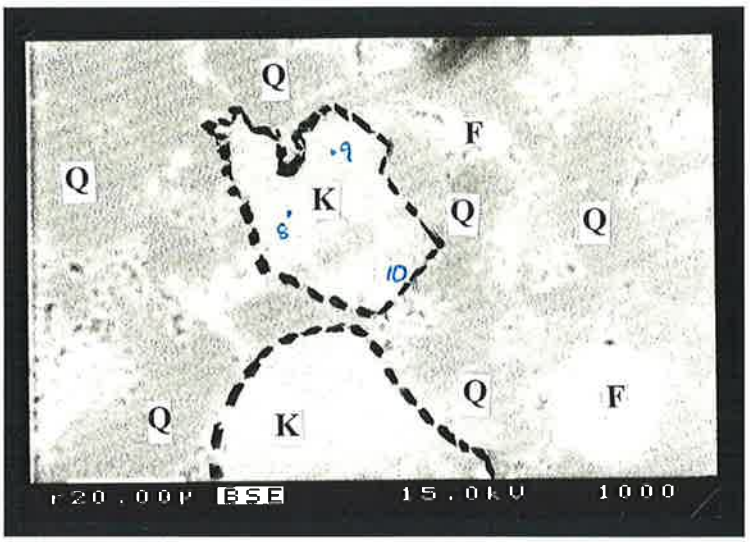

(a)

(b)

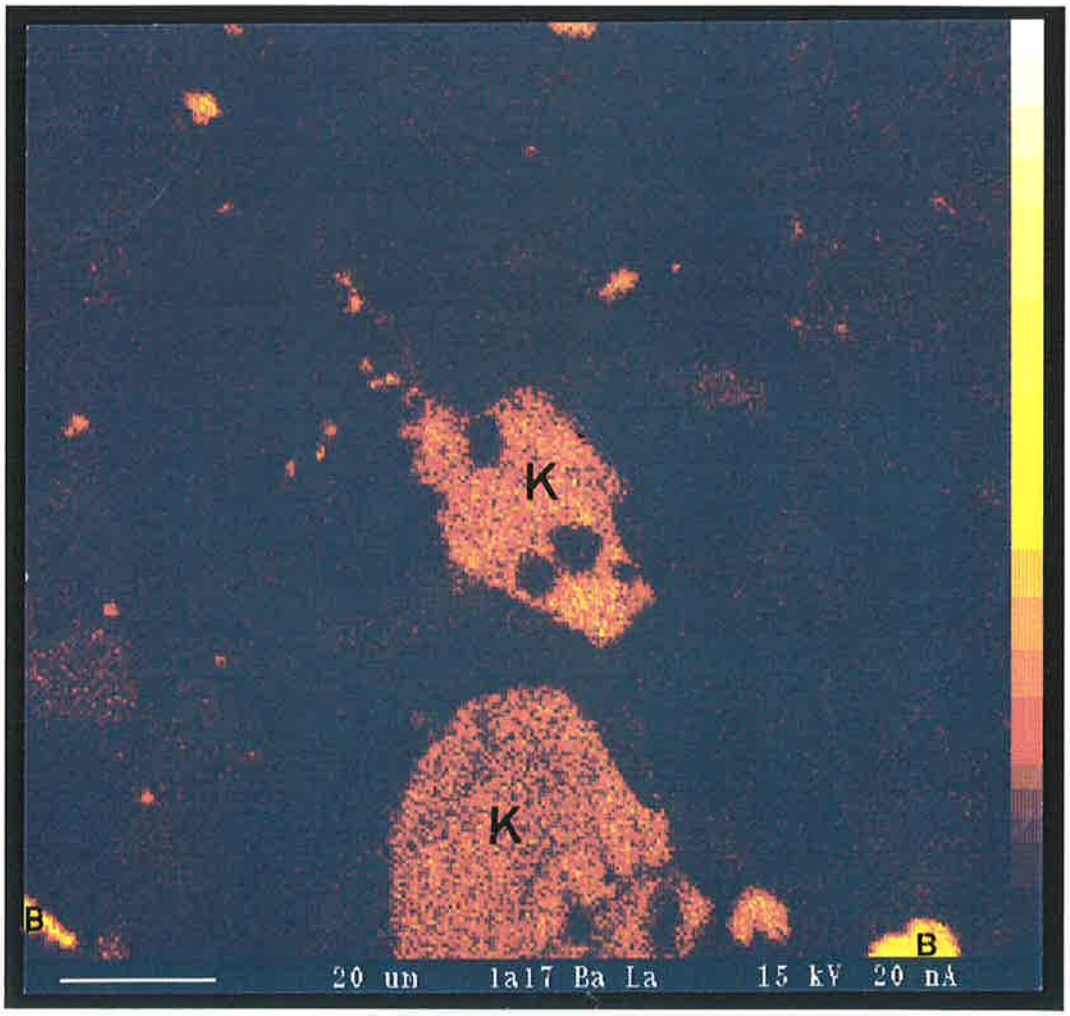

Fig. 9.9: Microprobe analyses of Brachina Formation, 11 km NNW of the Oraparinna Mine. Sample no. 771.
(a) Back scattered electron image showing K-feldspar (K), quartz (Q), barite (B) and $FeCO_3$ (F) grains.
(b): Scan map showing Ba distribution from highest (white) to lowest (black). Both central and lower K-feldspar grains show increasing Ba (indicated by yellow spots) towards the barite grain (yellow) in lowest right. Bottom left white bar scales of both (a) and (b) are 0.02 mm.

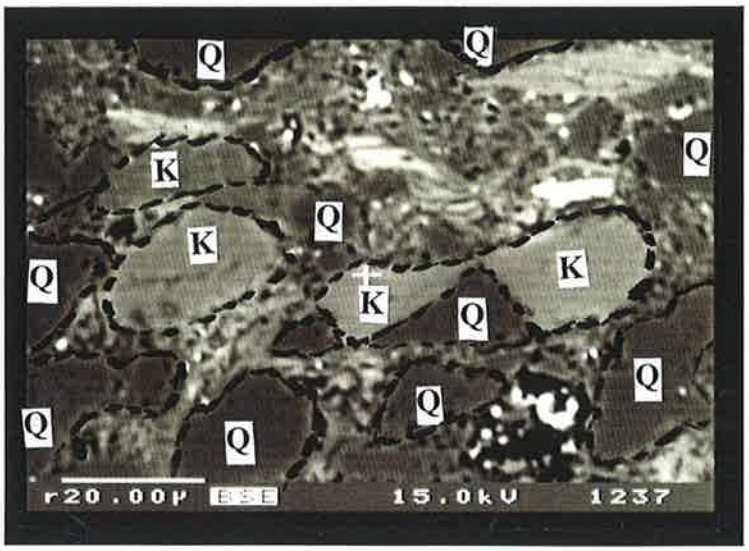

(a)

Fig. 9.10: Microprobe analyses of Brachina Formation, 30 km SW of the Oraparinna Mine. Sample no. 829.
(a) Back scattered electron image showing K-feldspar (K) and quartz (Q) grains.
(b): Scan map of the central K-feldspar grains and adjacent grains showing Ba distribution. The blue-green colour surrounding quartz grains (purple) indicates a higher concentration of Ba along grain boundaries.
Bottom left bar scales of both (a) white and (b) red, are 0.02 mm.

(b)

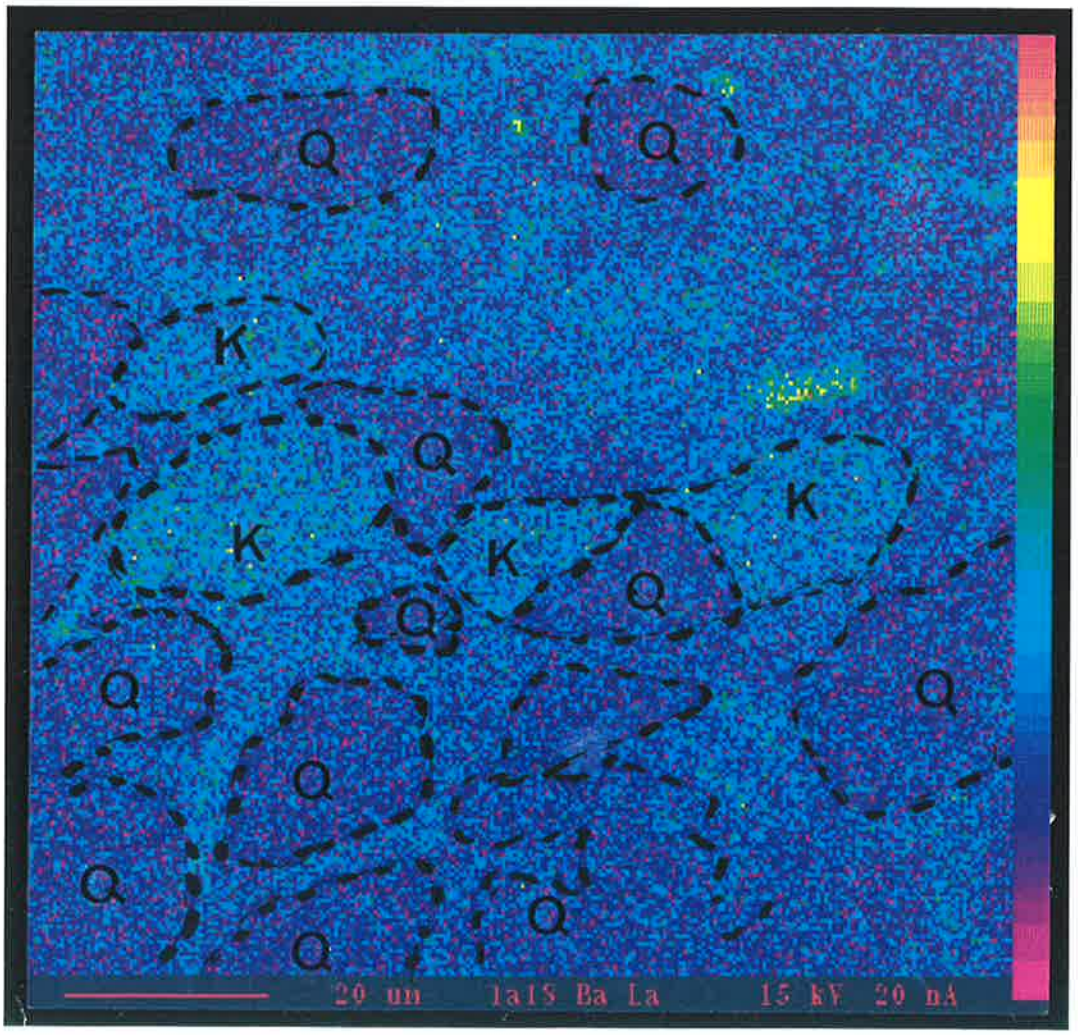

shows an inhomogeneous distribution of Ba, with higher concentrations in one half of the grain (Fig. 9.7b).

Table 9.6: Ba contents of a K-feldspar grain in the Brachina Formation in the Oraparinna Mine (Sample 2/90/38, Fig. 9.7a).

Analytical point no.	Ba (wt %)	Analytical point no.	Ba (w t %)	Analytical point no.	Ba (wt %)
503	0.09	509	0.17	515	0.21
504	0.24	510	0.01	516	0.18
505	0.23	511	0.25	517	0.17
506	0.26	512	0.23	518	0.19
507	0.10	513	0.21	519	0.03
508	0.22	514	0.30	520	0.06
Mean of 18 analyses					**0.18**

Sample 772 is from the Brachina Formation, collected 11 km NNW of the mine. The electron back-scattered image of the sample shows K-feldspar, quartz and barite (Fig. 9.8a). Spot analyses of a K-feldspar grain that is in contact with a barite grain indicate Ba contents ranging from 0.53 wt % to 0.67 wt % for 3 analyses, with a mean of 0.61 wt % (lower centre grain of Figs. 9.8a&b). Both the spot analyses and the scan map show the Ba concentration within the K-feldspar grain increases towards the adjoining barite grain.

The sample 771, collected 2 km west of 772, is also from the Brachina Formation and shows K-feldspar and quartz as major constituents, and siderite and barite as minor constituents (Fig. 9.9a). Spot analyses of the central K-feldspar grain close to, but not in contact with, two barite grains indicate Ba contents from 0.82 wt % to 1.18 wt % for 3 analyses, with a mean of 1.01 wt %. The scan map of the sample shows the Ba concentration within the both K-feldspar grains increases towards the closest barite grain (lower right, Fig. 9.9b).

The electron back-scattered image of sample no. 829 from the Brachina Formation, collected 30 km SW of the Oraparinna Mine, dominantly contains K-feldspar and quartz (Fig. 9.10a). Quartz grains usually surround K-feldspar grains and no barite grains were found in the thin section, although the gypsum grains contain minor concentrations of Ba. Spot analyses of K-feldspar grains show Ba contents ranging from 0.14 wt % to 0.17 wt %, for 3 analyses, with a mean of 0.15 wt %. The scan map shows Ba concentration gradually decreases away from K-feldspar grains, along grain boundaries of adjacent quartz grains (Fig. 9.10b).

The scan maps show that Ba concentration is inhomogeneous within K-feldspar grains of the Brachina Formation and increases towards the closest barite grain in the near vicinity. Further, Ba concentrations gradually decrease away from the grains, along the grain boundaries, as seen

between adjacent quartz grains. None of the K-feldspar grains subjected to analyses showed alteration to sericite (cf. Cawley, 1983) but indicate migration of Ba within and away from the grains.

9.7 Discussion

K-feldspar ($KAlSi_3O_8$) is an important Ba-carrier (Puchelt, 1972) and forms a continuous solid solution series with celsian ($BaAl_2Si_3O_8$) at high temperatures (Gay and Roy, 1968). The Ba contents of K-feldspar may vary up to 9.5 wt %, as found in the orthoclase-celsian series from the Magnet Cove Complex (Erickson and Blade, 1963). The highest Ba content in K-feldspars of the Adelaide Fold Belt reported previously was 0.6 wt %, from the Brachina Formation in the Oraparinna Mine (Cawley, 1983). However, present research found Ba up to 1.2 wt % from the same formation, 17.5 km NNW of the mine.

9.7.1 Source of Ba for barite vein formation

The Brachina Formation and siltstone lithology are the dominant features of the distribution of barite deposits in the Adelaide Fold Belt. For deposits with production + reserves of more than 2000 tonnes, the Brachina Formation is the most important stratigraphic unit, hosting 59 % of barite in the Adelaide Fold Belt. Siltstone hosts 57 % of the barite, and up to 72 % in association with other lithologies, mainly shale. Whole rock analyses have shown high Ba contents for both the siltstone (546 ppm) and Brachina Formation in the Adelaide Fold Belt (Tables 9.3a,b, 9.4, 9.7). In the present analyses, samples from a variety of formations in non-mineralised areas showed the highest value of 2981 ppm from the Brachina Formation, and samples of the Oraparinna Mine showed values up to 3.3 wt % (Tables 9.4, 9.7). However, the possible presence of barite in the form of veinlets and grains in samples prevents a clear interpretation of these data.

Whole rock analyses by the Mines Department and Turner *et al.* (1993) of rocks from the Adelaide Fold Belt show a mean Ba content of 419 ppm (Table 9.3a), compared to 303 ppm for analyses from the central Flinders Ranges (Table 9.4). The formations that are common to both sets of analyses show a mean Ba content of 528 ppm in the Adelaide Fold Belt and 381 ppm in the central Flinders Ranges. The lowest Ba content recorded in Brachina Formation, in the non-mineralised areas of the central Flinders Ranges was 293 ppm, and that at 600 m NW and south of the

Oraparinna Mine was 327 and 332 ppm, respectively; altogether showing a mean value of 315 ppm approximately, for those away from the mine (Table 9.7). The lowest Ba content recorded in the present analyses in Brachina Formation within the mine is 155 ppm (sections 9.4.1 and 9.4.2) and that of Cawley (1983) is 162 ppm (Table 9.7); showing an overall mean value of 159 ppm. Therefore, the evidence suggests that the Ba content of the Brachina Formation in the central Flinders Ranges is depleted with respect to the Adelaide Fold Belt as a whole, and further depleted in the Oraparinna Mine. This agrees with the depletion of Ba contents by 50 % in both the K- and Na- feldspars in the Oraparinna Mine compared to non-mineralised areas (Table 9.5). Therefore, it can be suggested that Ba released from the host formations, in particular from K-feldspars of the Brachina Formation, contributed to barite deposition.

Microprobe scanning maps show inhomogeneous Ba concentrations in K-feldspar grains of the Brachina Formation in the Flinders Ranges (Figs. 9.7b, 9.8b, 9.9b, 9.10b). The Ba^{2+} ions in K-feldspar grains have firstly migrated within the grains towards the edges closest to a forming barite grain, in the event of barite formation (Figs. 9.8b, 9.9b). When barite was not forming adjacent to the K-feldspar, the Ba^{2+} ions migrated away from the grain, to the depositional site, as indicated along grain boundaries of non-feldspathic grains (Fig. 9.10b). Therefore, Ba^{2+} migration dominantly from K-feldspar grains of the Brachina Formation was apparently responsible for contributing Ba for barite vein formation.

In summary, the evidence from the current research suggests that the reason for the relationship of barite deposits with the Brachina Formation was the release of Ba from K-feldspars to form barite. The research also suggests K-feldspars need not necessarily alter to sericite, to provide Ba for barite formation (cf. Cawley, 1983). The mechanism of migration of Ba is discussed in Chapter 13. Diapirs in the Fold Belt host only a minor amount of known barite deposits (1 wt %, Table 9.1) and it is unlikely that there is a genetic relation between diapiric fluids and barite vein formation.

Table 9.7: Summary of Ba contents of the Brachina Formation of the central Flinders Ranges from known locations with reference to mineralisation.

Location	Ba content (ppm)			no. of	Reference
	Lowest	Highest	Mean	analyses	
Non-mineralised areas of the central Flinders Ranges, tens of kilometres from the Oraparinna Mine	293	2981	883	5	Table 9.4
600 m NW of the Oraparinna Mine, in the Oraparinna National Park	327	1080	532	11	Cawley (1983)
600 m south of the Oraparinna Mine	332	5446	1470	9	Cawley (1983)
Oraparinna Mine	162	17400	2153	19	Cawley (1983)
Oraparinna Mine	155	32940	5234	22	Appendix 9.3

9.7.2 Guides for drill holes in barite exploration

All the three sections of the host rocks analysed in the research show decreasing trends of Ba away from the veins within a few hundreds of metres from the vein (Figs. 9.3, 9.4 and 9.5; Table 9.8). On the contrary, both the whole rock and grain-scale analyses of the Brachina Formation show Ba content increases away from the Oraparinna Mine to non-mineralised areas (see above). Therefore, decreasing trends of Ba content away from major veins apparently is due to the formation of barite in veinlets and grains adjacent to the veins, and suggest the potential to use Ba content of the host rock as a geochemical tool in drilling exploration for barite deposits.

Table 9.8: General direction of the increasing or decreasing trends of element content of the host rock with reference to distance from barite veins. The arrows show increasing (>), or decreasing (<) element concentration away from the vein, and varying trends of concentration as ><< (a general increase adjacent to the vein but decrease thereafter) or <>> (a general decrease adjacent to the vein but an increase thereafter). Inconsistent and flat trends are shown by /\/\ and ---, respectively.

Element /oxide	Level 5 (OBM), 0-24.8m from 1D Lode	Drill hole OU2/90, Level 7 (OBM), 0-45.8m from 1D Lode	Far Western Lode, 0-400m from lode excluding 110m-275m
SiO_2	>	not analysed	<
Al_2O_3	>	not analysed	<>>
Fe_2O_3	/\/\	not analysed	<>>
MnO	<	not analysed	---
MgO	>	not analysed	<>>
CaO	<	not analysed	<>>
Na_2O	>	not analysed	<>>
K_2O	>	not analysed	<>>
TiO_2	>	not analysed	>
P_2O_5	---	not analysed	<>>
Ba	<	<	><<
Sr	<	<>>	<>>
Rb	>	<>>	<>>
Cu	<	>	---
Zn		/\/\	<>>
Ni	>	/\/\	
Co	>	<>>	><<
Sc	/\/\	<>>	<>>
V	>	<>>	>
Ce	>	/\/\	<>>
Nd	>	/\/\	>
La	>	/\/\	>
Ga	>	<>>	>
Cr	>	/\/\	>
Y	<	<>>	>
Nb	>	<>>	<>>
Zr	/\/\	/\/\	>
Th	---	<>>	>
Pb	>	<>>	<>>
U	/\/\	<	/\/\

The Sr content of the samples of the Brachina Formation from the non-mineralised regional areas averages 76 ppm, varying from 53 to 120 ppm for 7 analyses (Table 9.4 and Turner *et al.,* 1993). Samples of the Brachina Formation in the mine average to 160 ppm, varying from 102 to 285 ppm for 14 analyses (Appendix 9.3). This significant increase of Sr in the Brachina Formation in the mine is again possibly due to the presence of barite ($(Ba,Sr)SO_4$) or strontianite ($SrCO_3$) in veinlets or grains. All three sections analysed, i.e. Level 5 and Drill Hole OU2/90 of the Oraparinna Mine, and the Far Western Lode indicate decreasing trends away from the vein up to 25m, and thereupon the latter two sections show increasing trends (Figs. 9.3*f*, 9.4c, 9.5n, Fig. Table 9.8). Therefore, caution is needed when using Sr as an exploration guide due to the variability of the data.

K_2O and Pb increase in the host rocks away from the veins (Table 9.8), possibly due to replacement of K^{2+} and Pb^{2+} adjacent to the veins by Ba^{2+}, due to similarities in ionic radii. The K_2O/Ba ratios increase away from veins (Fig. 9.11), and Ba/Pb ratios decrease (Fig. 9.12). Cu/Zn ratios show a general decrease away from barite veins (Fig. 9.13). $K_2O/(K_2O+Na_2O)$ and $Na_2O/(Na_2O+K_2O)$ ratios were also plotted against distance from the veins (Figs. 9.14 and 9.15). Excluding the interval between 110 - 275 m of the Far Western Lode section, the $K_2O/(K_2O+Na_2O)$ ratio decreases away from the veins, while the $Na_2O/(Na_2O+K_2O)$ increases.

Therefore, careful consideration of decrease of Ba contents of the host rocks away from barite veins and the respective gradients of K_2O/Ba, Ba/Pb, Cu/Zn, $K_2O/(K_2O+Na_2O)$ and $Na_2O/(Na_2O+K_2O)$ ratios also can be considered worthy of application as aids in the discovery of barite veins during exploratory drilling.

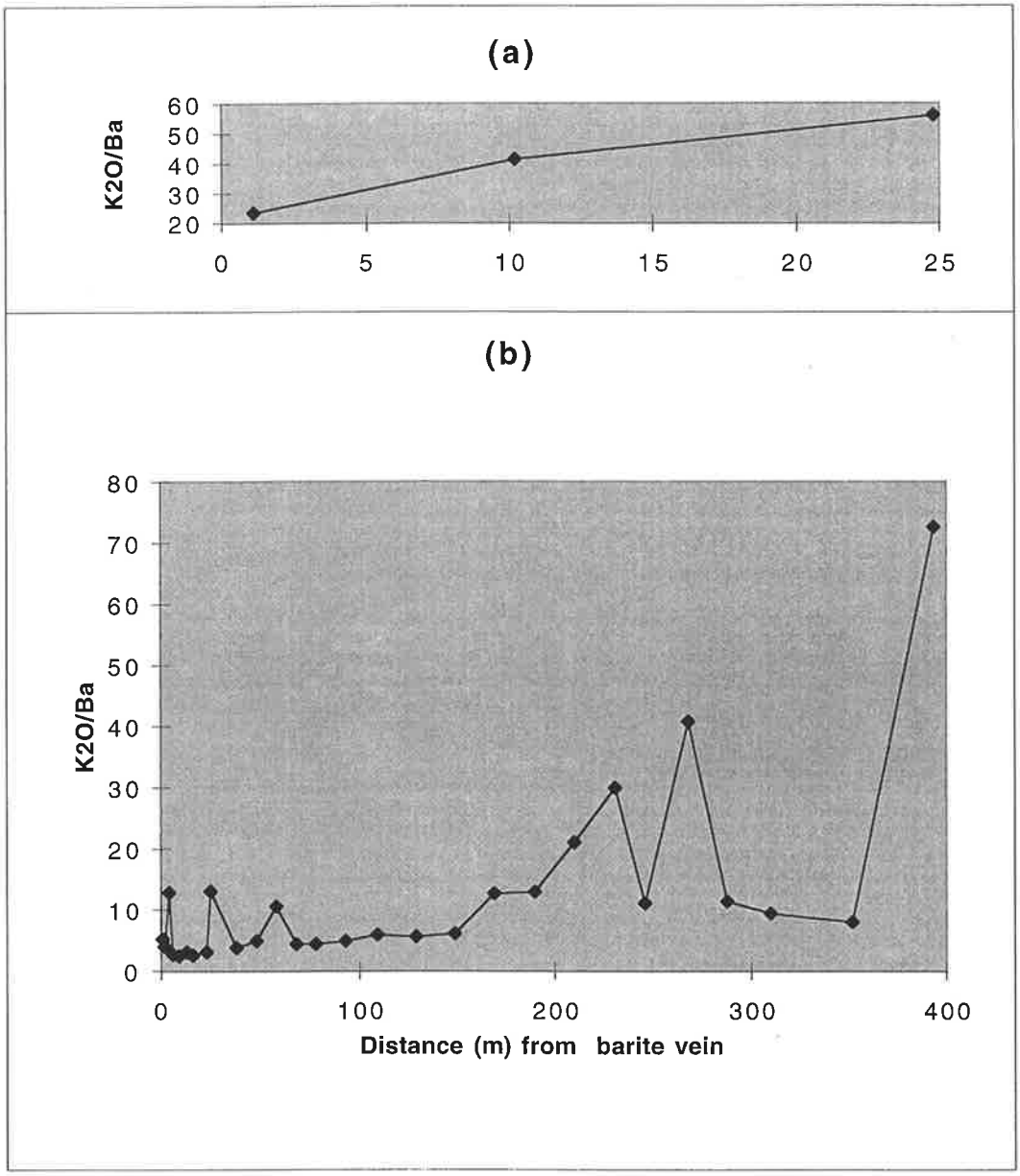

Fig. 9.11: Variation of K_2O/Ba ratio with distance from major barite veins. (a) 1D Lode level 5 of the Oraparinna Barite Mine and (b) Far Western Lode.

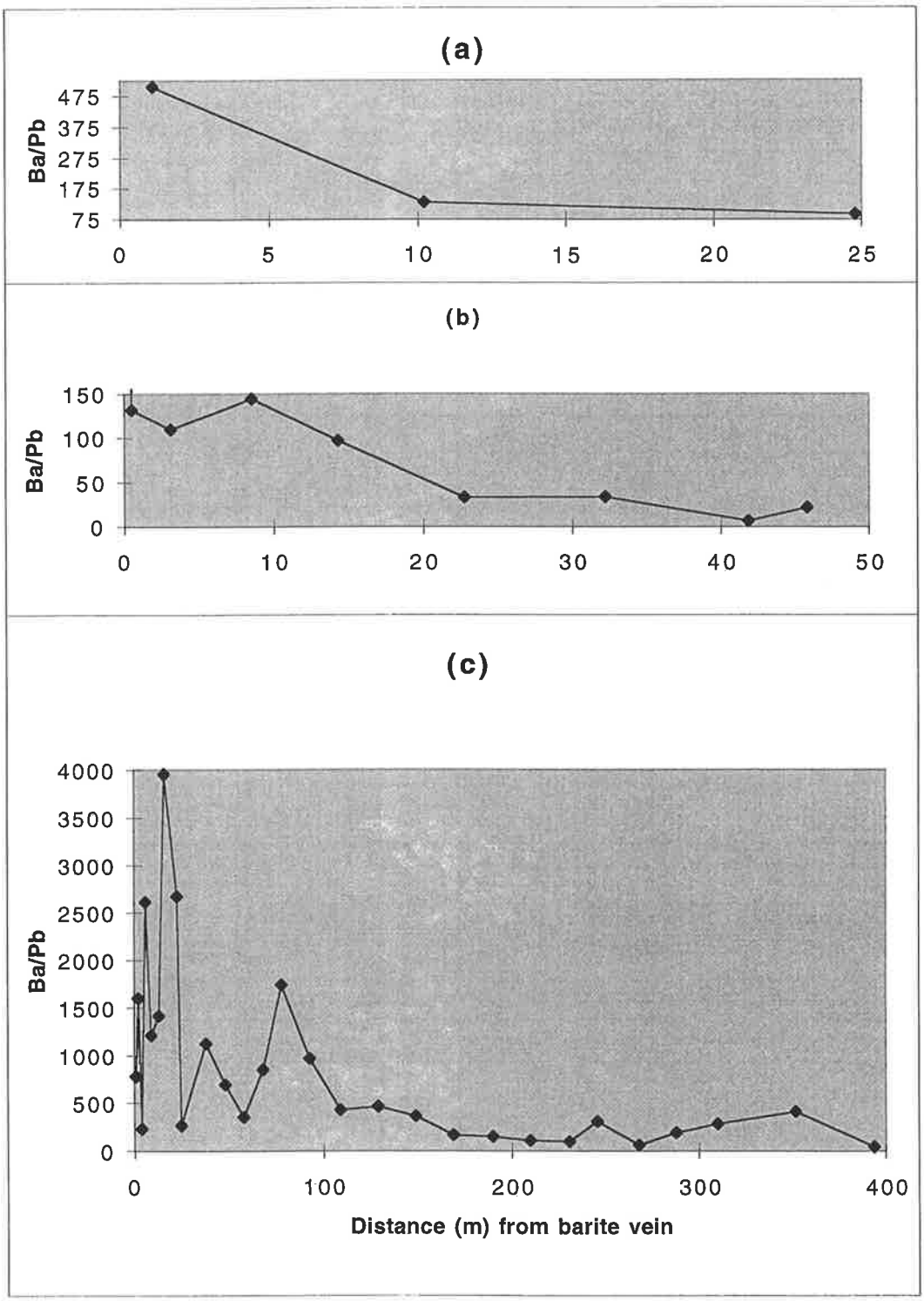

Fig. 9.12: Variation of Ba/Pb ratio with distance from major barite veins. (a) 1D Lode on level 5 and (b) Drill Hole OU2/90 in the Oraparinna Barite Mine, and (c) Far Western Lode.

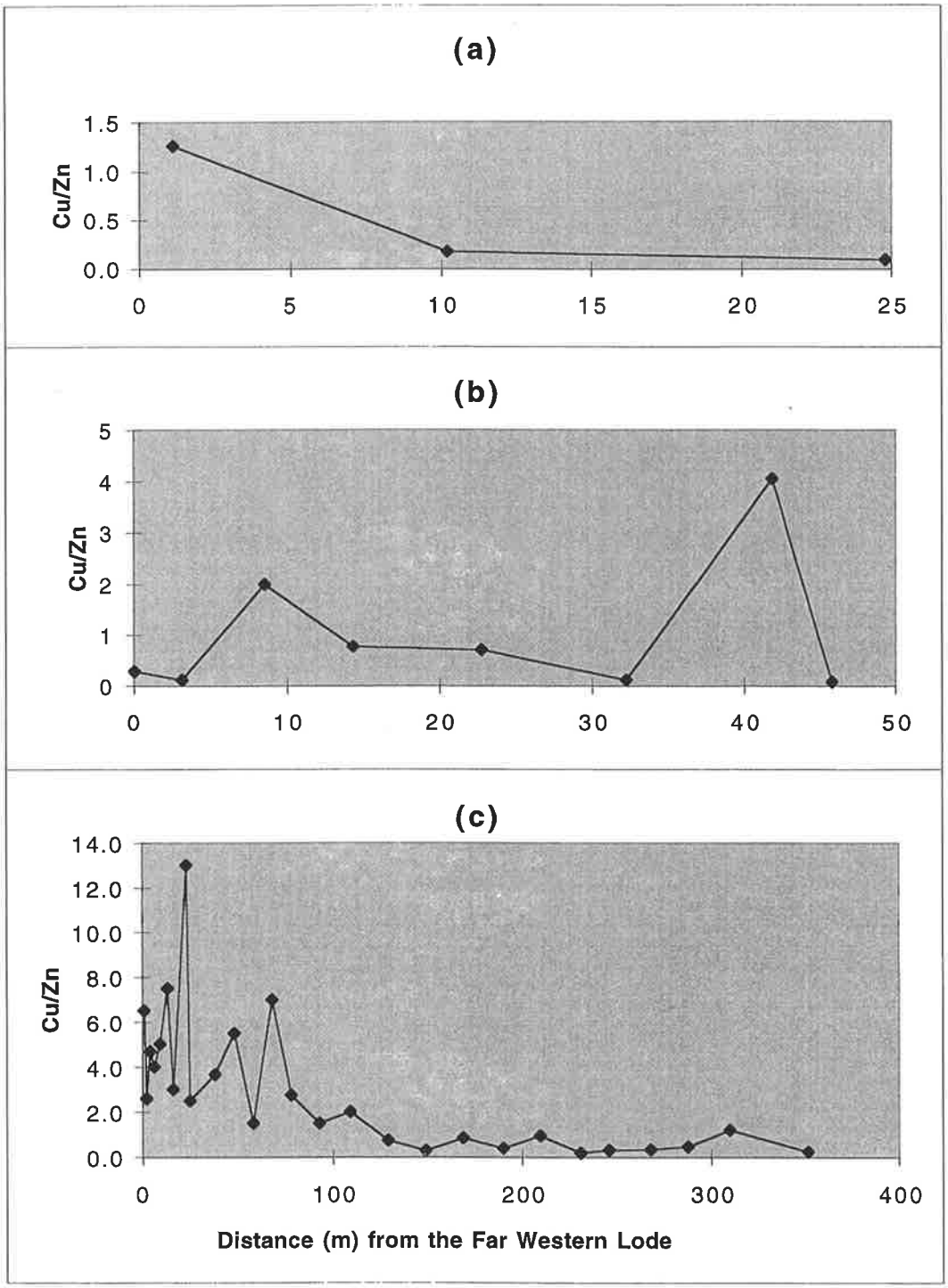

Fig. 9.13: Variation of Cu/Zn ratio with distance from major barite veins. (a) 1D Lode level 5 and (b) Drill Hole OU2/90 in the Oraparinna Barite Mine, and (c) Far Western Lode.

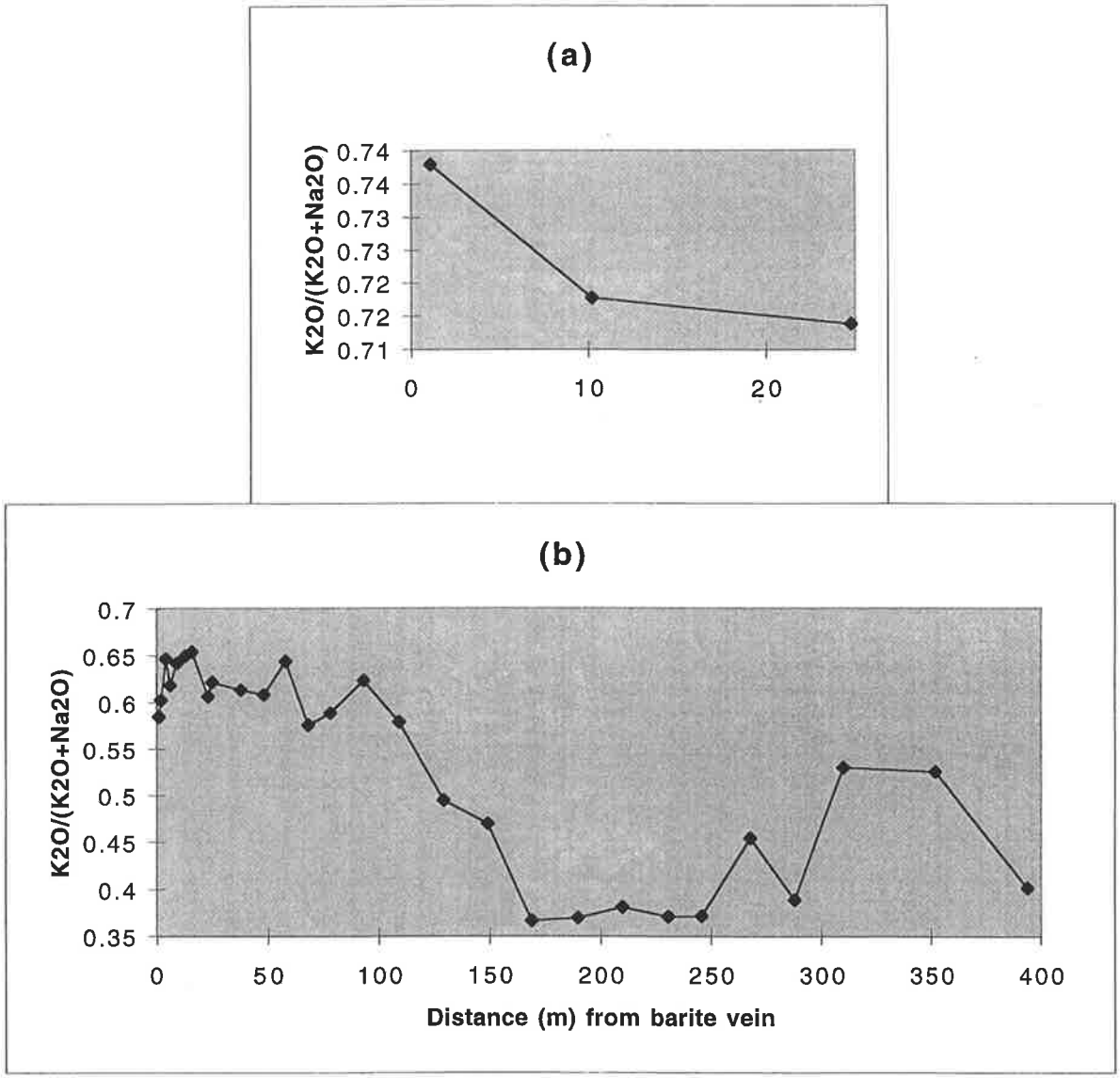

Fig. 9.14: Variation of $K_2O/(K2O+Na2O)$ ratio with distance from major barite veins. (a) 1D Lode on level 5 of the Oraparinna Barite Mine and (b) Far Western Lode.

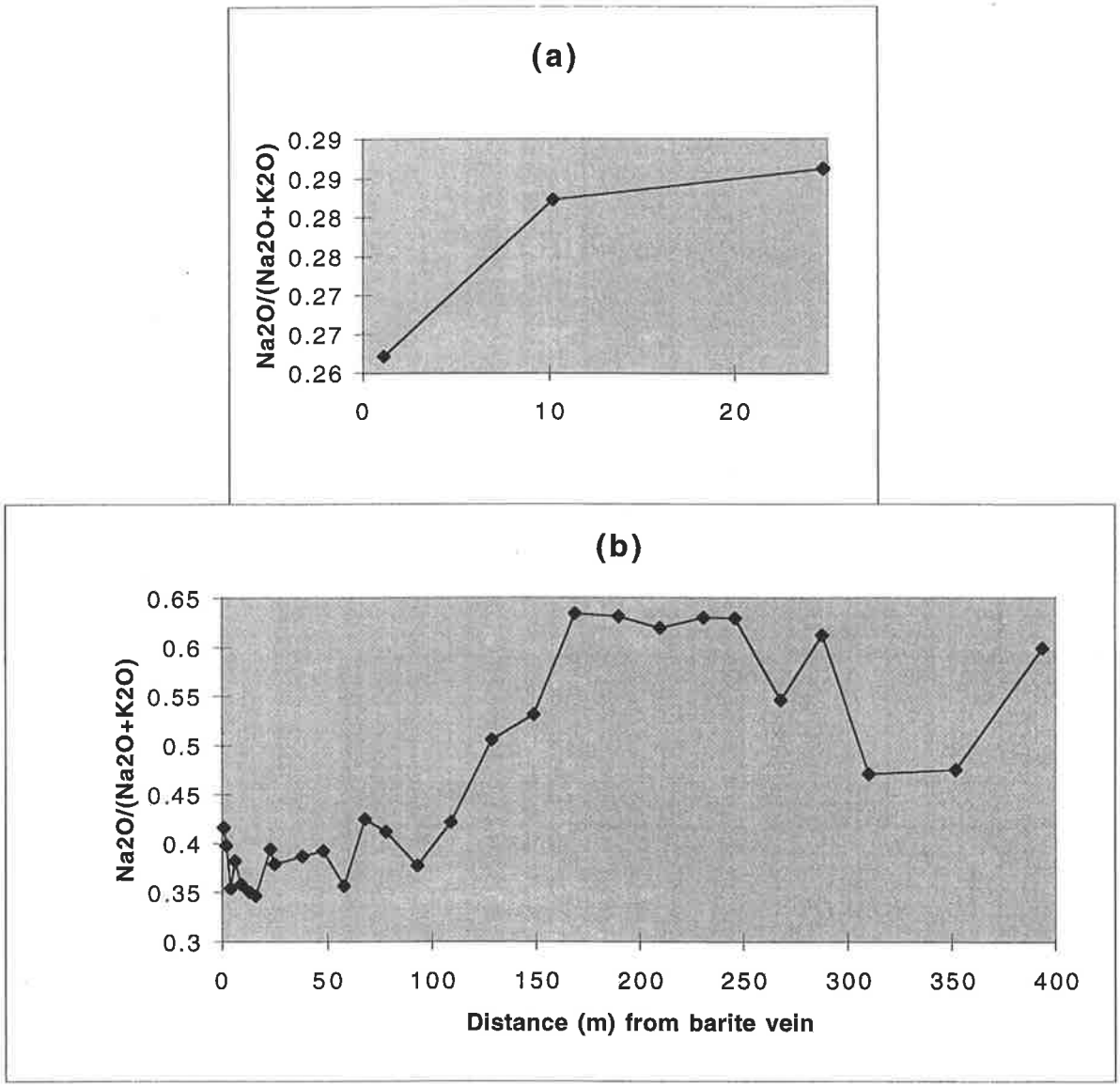

Fig. 9.15: Variation of Na2O/(Na2O+K2O) ratio with distance from major barite veins. (a) 1D Lode on level 5 of the Oraparinna Barite Mine and (b) Far Western Lode.

Chapter 10

STRONTIUM ISOTOPE GEOCHEMISTRY OF BARITE VEINS

10.1 Introduction

Rb and Sr are trace elements, concentrations in terrestrial materials ranging from a few parts per million to several hundred parts per million. Rubidium has an ionic radius of 1.48Å , very close to that of potassium (1.33Å), and therefore has coherence of geochemical behaviour with K, and is mainly enriched in minerals such as mica, K-feldspar, clay minerals, sylvite and carnallite. Similarly, strontium (ionic radius, 1.13Å) can also substitute for Ca (ionic radius = 0.99Å), and is therefore found also in plagioclase, apatite and carbonates. Sr is also a minor constituent of seawater, with an average concentration of 13.3 mg/kg of water (Sverdrup *et al.*, 1946) and a residence time of 10^7 years. Strontium in seawater derives mostly by the weathering of young volcanic rocks, old sialic rocks of the continental crust, and Phanerozoic marine limestones (Faure, 1986).

Rubidium has two naturally occurring isotopes, ^{85}Rb and ^{87}Rb, having relative abundances of 72.1654% and 27.8346%, respectively. Strontium has four natural isotopes: ^{84}Sr, ^{86}Sr, ^{87}Sr, and ^{88}Sr, having isotopic abundances of 0.56%, 9.87%, 7.04%, and 82.53%, respectively. The isotope ^{87}Rb is radioactive, and β-decays to stable ^{87}Sr. The isotopic abundance of Sr in natural minerals and rocks is modified depending on: the concentration of rubidium in the original materials, its age, processes of mixing, and metamorphism, diagenesis and hydrothermal processes.

If two reservoirs (e.g. magmas, sedimentary rocks, or waters) are isolated, and have different initial concentrations of Rb, the amount of radiogenic ^{87}Sr produced is obviously different, and the relative Sr isotopic ratios differ. If, by virtue of a given geological process, these reservoirs become open to one another, they can mix. The products of mixing have intermediate chemical and isotopic compositions, depending on the isotopic and chemical compositions of the starting materials (the "end members") at the time of mixing, and also on the proportion of each end member entering the mixture.

Several papers on barite deposits in Australia, Europe, Canada and North America have described the successful use of strontium isotopes ($^{87}Sr/^{86}Sr$) in studying the evolution of hydrothermal fluids (e.g. Cecile, 1983; Kelser *et al.*, 1988; Whitford *et al.*, 1992; Martin *et.al.*, 1995, Naehr *et.al.*, 2000 and Paytan *et al.*, 2002). The present study looks in detail at the Sr isotopic signatures of the vein barites

with respect to vein dilation and deformation, and attempts to clarify the provenance of the Sr and the time of the emplacement and evolution of veins.

10.2 Previous work

The bulk of the disrupted material now found in the diapirs of the central Flinders Ranges is considered to have been brought up from the Willouran Callanna Group (Coats, 1965; Dalgarno and Johnson, 1968; Mount, 1975; Haslett, 1976; Murrell, 1977; White, 1983; Preiss, 1985, 1987; Lemon, 1988). Turner *et al.* (1993) reported $^{87}Sr/^{86}Sr$ ratios of shales of the Willouran Callanna Group from the Blinman Diapir and from Arkaroola are 0.77728 and 0.84297 respectively. The authors calculated the initial $^{87}Sr/^{86}Sr$ ratios to be 0.71665 and 0.56947 respectively, assuming that the said formations have an age of 850 Ma (cf. Preiss, 1987). The latter isotopic ratio is well below the depleted mantle value, which, at the considered time of 850 Ma ago, would have been around 0.7 (Faure, 1986), and would represent the lowest possible Sr isotopic ratio for a terrestrial material of that age. Foden (1994) and Foden *et al.* (2001) explained this discrepancy as due to a massive mobilisation of Sr and Rb, probably during the late Neoproterozoic. According to Foden *et al* (2001), Sr-isotope data from Adelaide Geosyncline shales show evidence of significant post-depositional mobility, and combined data yield an apparent "isochron" age of approximately 586± 30 Ma.

Some barite samples collected during honours projects from the Oraparinna Mine (Cawley, 1983) and Artipena Lodes (Fig. 2.6; Robertson, 1981) in the central Flinders Ranges were analysed for $^{87}Sr/^{86}Sr$ by D. Whitford (CISIRO) for R. Both. The data for the veins at the Oraparinna Mine are: 0.711145 to 0.711600 for 1A Lode (4 analyses), 0.711387 to 0.711560 for 1C Lode (2 analyses) and 0.711193 for Link Lode (1 analysis; Fig. 7.4a). One analysis for Dunbar Lodes gave a value of 0.724447 and the Artipena Lodes range from 0.710170 to 0.711065 (4 analyses).

10.3 Sampling for $^{87}Sr/^{86}Sr$ ratio analyses

Barite and host rock samples analysed for $^{87}Sr/^{86}Sr$ signature were those described in Chapters 8 and 9 (Fig. 8.1). Seventeen barite samples from the Oraparinna Mine (OM) were analysed, representing all major veins and some minor veins (Fig. 8.1).

Non-recrystallised and recrystallised grains in barite samples also were analysed for $^{87}Sr/^{86}Sr$ signature (Chapter 8). The recrystallised grains commonly occur as colourless tiny mottles in the non-recrystallised white barite. The carefully selected mottles were drilled with a dental drill to collect powder samples. Similarly, the adjoining non-recrystallised grains were also drilled and powdered samples were collected. Samples NL50^{r} and NL50^{n} (Chapter 8) were used from the Noarlunga Lodes. The dominantly strontianite sample (OM156) collected between the two sub-veins of the 1D Lode contains minor quantities of barite (Figs. 8.1, 8.4a). This barite consists of recrystallised grains (OM156B^{r}), surrounded by non-recrystallised grains (OM156B^{n}), and was used for the isotope analyses. Similarly, part of sample BN144 from Bainbridge no.3 Lode was also used after separation into recrystallised grains (BN144^{r}) and non-recrystallised (BN144^{n}) grains (Fig. 7.12b). Sample HL301 from the Hall Lode was also separated into HL301^{r} and HL301^{n}.

Four samples from the Brachina Formation hosting 1D Lode on Level 5 of the Oraparinna Mine (OM121, OM 123, OM124 and OM125; Fig. 8.1) were analysed for Sr isotope composition. Two of these samples (OM123 and OM125) contain minor visible barite veins in fine cracks (Chapter 9, Appendix 9.3). Three samples were analysed from diapiric breccia in the Oraparinna Diapir; consisting of shale (OD823), shale within calcareous matrix (OD715), and dolomite (OD722; Table 9.4).

10.4 Analytical methods

Approximately 200 mg of powder from each barite sample were dissolved in 2.5N HCl in pre-cleaned polypropylene bottles. Each sample was dissolved in 5 ml of cation exchange resin (BIO-RAD AG50W-X8, <400 mesh). Dissolution took place over a period of 7 days. Though the dissolution of the samples was incomplete, it is known from previous experiments (J. Mawby, pers. communication) that Sr and Rb would be completely leached into the solution. Cations from the dissolved barite were then stripped from the resin by 6N HCl. Chemical extraction of Sr from the solutions was carried out by conventional ion exchange techniques (Pott, 1987) using the cation-exchange resin BIO-RAD AG50W-X8 (200-400 mesh). Sr was then loaded on single Ta filaments. The $^{87}Sr/^{86}Sr$ ratios were analysed using a Finnigan MAT 261 mass spectrometer, interfaced to a Hewlett-Packard 9845B for data processing, normalised to an $^{87}Sr/^{86}Sr$ value of 0.1194. Analyses of NBS 987 standard gave an average of 0.710153 ± 40 (2σ).

The element concentrations of Ba, Rb and Sr in samples from the barite veins and whole rock samples were determined by conventional XRF analysis.

10.5 Results

Including the Sr isotope data previously analysed for Oraparinna Mine, Dunbar and Artipena Lodes, by D. Whitford of CSIRO for R. Both, $^{87}Sr/^{86}Sr$ values for the barite veins from the Adelaide Fold Belt vary from 0.710695 to 0.733382 (48 values, Table 10.1). Data for the various lodes, in decreasing order of the mean $^{87}Sr/^{86}Sr$ values, are: Dunbar Lodes 0.721108 to 0.733382 with a mean value of 0.727521 for 6 analyses; Bowering Lode, 0.723435 for 1 analysis; Hall Lode 0.715397 to 0.718412 with a mean value of 0.716906 for 2 analyses; Noarlunga Lodes 0.711216 to 0.716613 with a mean value of 0.714671 for 6 analyses; Oraparinna Mine including Bainbridge Lodes and the fault zone deposits 0.710695 to 0.711955 with a mean value of 0.711347 for 29 analyses; and Artipena Lodes 0.710170 to 0.711065 with a mean value of 0.710763 for 4 analyses. Three samples from the Oraparinna Diapir show a range from 0.708514 to 0.822058 (Table 10.2). Samples of the Brachina Formation in Oraparinna Mine show $^{87}Sr/^{86}Sr$ ratios of 0.762477 (OM121) and 0.749393 (OM124) but those containing barite veinlets show low ratios of 0.717533 (OM123) and 0.716087 (OM125) with a mean value of 0.718611, Table 10.2).

10.6 Interpretation

10.6.1 Inter-vein relationship of $^{87}Sr/^{86}Sr$ ratios

The Dunbar Lodes occur next to a breccia offshoot emanating from the Oraparinna Diapir (Fig. 1.3). The diapir shows a mean $^{87}Sr/^{86}Sr$ ratio of 0.731775 (Table 10.2). The mean $^{87}Sr/^{86}Sr$ ratios of barite deposits around the Oraparinna Diapir decrease with increasing distance from the diapir or its off-shoot: 0.727521 (Dunbar Lodes, 0 m), 0.723435 (Bowering Lode, 30 m), 0.716906 (Hall Lode, 100 m) and 0.711347 (Oraparinna Mine, 2.4 km; Table 10.1). The decreasing $^{87}Sr/^{86}Sr$ ratios correlate approximately with logarithmically increasing distance from the diapir (Fig. 10.1).

For the Noarlunga Lodes, the barite samples NL51D, NL50 and NL51B were collected at 20m, 50m and 100m respectively, from the dolomitic Seacliff Sandstone Unit (Fig. 2.7). The samples show increasing $^{87}Sr/^{86}Sr$ ratios of 0.711216, (0.715007 and 0.715041), and 0.716613 (Table 10.1), respectively, with logarithmically increasing distance from the dolomite unit (Fig. 10.2).

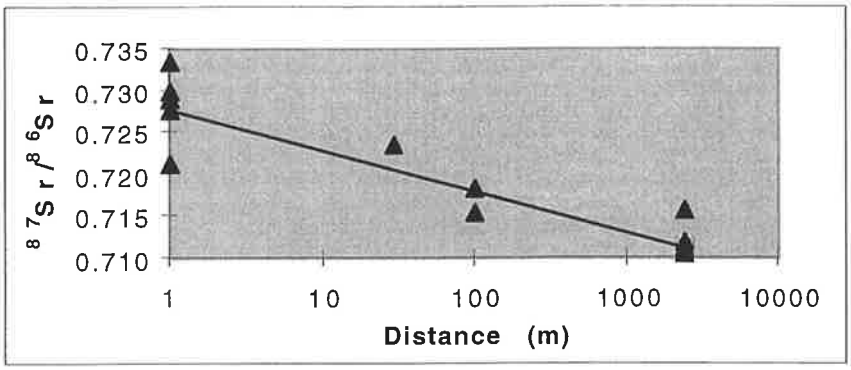

Fig. 10.1: Distance (m) from the Oraparinna Diapir or its breccia off-shoots vs $^{87}Sr/^{86}Sr$ ratios for barite veins. All the data at 1 m distance represent Dunbar Lodes (5 analyses), followed by Bowering Lode (30 m, 1 analysis), Hall Lode (100 m, 2 analyses), and Oraparinna mine area (2400 m, 29 analyses).

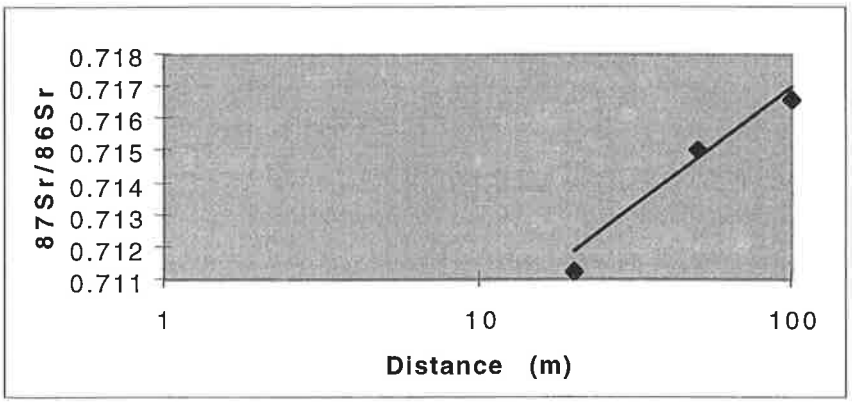

Fig. 10.2: Distance (m) from the dolomite unit, located between the Wilpena Group and the Umberatana Group sediments, vs $^{87}Sr/^{86}Sr$ ratios for barite lodes at Noarlunga. Lodes at distance: NL51D (20 m), NL50 (50 m) and NL51B (100 m).

Table 10.1: Sr isotope analyses of barite veins.

Sample*	Rb (ppm)	Sr (wt %)	$(^{87}Sr/^{86}Sr)m$	Remarks
Dunbar Lodes				
DL251[c]	Nd.	1.37	0.729799	
DL252	Nd.	1.50	0.728802	
DL253[b]	7.8	2.78	0.727590	
DL255[a]	Na.	1.60	0.721108	} from single vein
DL257[c]	Na.	1.47	0.733382	
72783***			0.724447	
Mean of 6 values			0.727521	
Bowering Lode				
BW200	0.9	1.31	0.723435	
Hall Lode				
HL301[n]	2.3**	0.24**	0.715397	
HL301[r]	**	**	0.718412	
Mean of 2 values			0.716905	
Oraparinna Mine				
OM111[c]	Na.	NA	0.711293	1A Lode, Level 6
OM113[c]	3.4	2.19	0.711469	1A Lode, Level 6
OM114[b]	1.1	3.28	0.710864	1A Lode, Level 6
OM141[c]	2.3	3.39	0.711094	1A Lode, Level 7
72776***			0.711160	1A Lode, Level 4
72777***			0.711145	1A Lode, Level 4
72778***			0.711600	1A Lode, Level 4
72779***			0.711279	1A Lode, Level 7
OM109	4.0	3.87	0.711158	1B Lode, Level 6
OM106[b]	1.9	3.74	0.711005	1C Lode, Level 6
72780***			0.711560	1C Lode, Level 4
72781***			0.711387	1C Lode, Level 4
OM108[a]	2.3	3.46	0.710695	1D Lode, Level 6
OM127[c]	Nd.	3.07	0.711167	1D Lode, Level 5
OM128[a]	4.3	3.46	0.710896	1D Lode, Level 5
OM140[a]	5.8	3.67	0.711722	1D Lode, Level 7
OM156B[n]	1121**	>50**	0.711466	} Minor barite from sample
OM156B[r]	**	**	0.711955	} OM156,dominantly strontianite
OM120[a]	4.9	3.64	0.711088	Link Lode
OM157[c]	0.5	2.80	0.711399	Link Lode
72782***			0.711193	Link Lode, Level 4
OM130	4.3	1.89	0.711706	minor vein
OM131	17.3	0.66	0.711724	minor vein
OM132	7.5	0.05	0.711935	minor vein
Oraparinna Bainbridge Lodes				
BN143	114	0.75	0.711464	
BN144[n]	0.6**	2.00**	0.711638	
BN144[r]	**	**	0.711857	
Oraparinna Fault zone				
OF158	2.8	3.19	0.711020	
OF159	0.6	2.64	0.711118	
Mean of 29 values for the Oraparinna area				0.711347

Contd.

Table 10.1: Sr isotope analyses of barite veins. (contd from previous page)

Sample*	Rb (ppm)	Sr (wt %)	$(^{87}Sr/^{86}Sr)m$	Remarks
Noarlunga				
NL50[n]	0.8**	0.90**	0.715007	
NL50[r]	**	**	0.715041	
NL51B	Nd.	1.11	0.716613	
NL51D	Nd.	0.72	0.711216	
NL52	2.9	0.66	0.714836	
NL53	4.6	0.62	0.715315	
Mean of 6 values			0.714671	
Artipena				
72784***			0.710894	Lode no.2
72785***			0.710170	Lode no.5
72786***			0.711065	Lode no.4
72787***			0.710922	Lode no.2
Mean of 4 values			0.710763	

*Abbreviations: [a]-Median Layer (ML), [b]- between ML and border, and [c]-border; [n]-non-recrystallised and [r]-recrystallised grains. $(^{87}Sr/^{86}Sr)m$ - ratio measured, Nd. - Not detectable, Na - not analysed. **: XRF analyses for Rb and Sr contents of these samples were performed on the mixed non-recrystallised and recrystallised barite. *** Analyses by D.Whitford of CSIRO for R. Both.

Table 10.2: Sr isotope analyses of rock samples.

(A) Diapiric breccia from the Oraparinna Diapir:

Sample	Rb (ppm)	Sr (ppm)	Ba (ppm)	$(^{87}Sr/^{86}Sr)m^*$ T=0	$^{87}Sr/^{86}Sr$ T=500Ma	Remarks
OD715	127	95	207	0.758248	0.730552	shale in calcareous matrix
OD722	6	256	42	0.708514	0.708031	dolomite
OD823	141	45	270	0.822058	0.756741	siltstone
Mean					0.731775	

(B) Brachina Formation of the Oraparinna Mine:

Sample	Rb (ppm)	Sr (ppm)	Ba (ppm)	$(^{87}Sr/^{86}Sr)m^*$ T=0	$^{87}Sr/^{86}Sr$ T=500Ma	Distance to 1D Lode (m) and remarks
OM121	201	105	553	0.762477	0.724125	24m
OM123	86	557	18072	0.717533	0.714347	17m, Minor visible barite veins in shale
OM124	184	136	778	0.749393	0.721388	10m
OM125	63	865	24705	0.716087	0.714584	4m, Minor visible barite veins in shale
Mean of 4 values					0.718611	

*(87Sr/86Sr)m = ratio measured

Artipena Lode no. 5 is located bordering dolomite of the Nuccaleena Formation (Fig. 2.6). The $^{87}Sr/^{86}Sr$ ratios of lodes increase from 0.710170 (Lode no. 5), to 0.710894 and 0.710922 (Lode no. 2), and to 0.711065 (Lode no. 4) with the increasing distance from the dolomite unit.

10.6.2 Intra-vein relationship of $^{87}Sr/^{86}Sr$ ratios

The $^{87}Sr/^{86}Sr$ ratios of samples collected *along the direction of vein fibres* (Section 8.2) were compared. The ratios increase from 0.710896 to 0.711167, for samples OM128[a] and OM127[c], respectively, collected 1 m apart from the median layer and border of the 1D Lode, on Level 5 of the Oraparinna Mine (Table 10.3, Fig. 10.3a). Similarly, the ratios increase from 0.721108 to 0.733382 for samples DL255[a] and DL257[c], respectively, collected 0.6 m apart from one of the Dunbar Lodes (Table 10.3, Fig. 10.3d). Therefore, it can be suggested that the $^{87}Sr/^{86}Sr$ ratios increase from median layer to border, *along the direction of vein fibres.*

The $^{87}Sr/^{86}Sr$ ratios of samples that were collected along lines *inclined to the direction of vein fibres* also were compared. 1A Lode shows an increase of $^{87}Sr/^{86}Sr$ ratios from 0.710864 (OM114[b]) between the median layer and border on Level 6 of the mine, to {0.711293 (OM111[c]) and 0.711469 (OM113[c])} at the border, on the same level (Table 10.3, Fig. 8.1). Likewise, the ratios increase from the OM114[b] to 0.711094 for OM141[c] on the adjoining Level 7 (Table 10.3, Fig. 10.3b). Link Lode in the mine also shows an increase in $^{87}Sr/^{86}Sr$ ratio from median layer on Level 6 (0.711088, OM120[a]) to border on the adjoining Level 7 (0.711399, OM157[c]; Table 10.3, Fig. 10.3c). However, the ratio decreases from median layer of the 1D Lode on Level 7, 0.711722 (OM140[a]), to 0.711167 (OM 127[c]) at the border on distant Level 5. Therefore, the increasing relationship of $^{87}Sr/^{86}Sr$ ratios from median layer to border along lines *inclined to the direction of vein fibres* is not valid always, especially between distant levels.

Samples collected from nearby parallel veins on the same level in Dunbar show an increase of Sr isotope ratios from median layer (0.721108, DL255[a]) to 0.72759 (DL253[b]) and 0.729799 (DL251[c]) of adjacent veins (Table 10.3).

Table 10.3: $^{87}Sr/^{86}Sr$ ratios of barite samples collected from defined positions of the veins (Extracted from Table 10.1).

Lode	$^{87}Sr/^{86}Sr$ ratio			Comments
	Median layer[a]	Between median layer and border[b]	Adjacent to the border[c]	
1D Lode	0.710896 (OM128[a])		0.711167 (OM127[c])	Level 5 of the mine
	0.710695 (OM108[a])			Level 6 of the mine
	0.711722 (OM140[a])			Level 7 of the mine
1A Lode		0.710864 (OM114[b])	0.711293 (OM111[c]) 0.711469 (OM113[c])	Level 6 of the mine
			0.711094 (OM141[c])	Level 7 of the mine
Link Lode	0.711088 (OM120[a])			Level 6 of the mine
			0.711399 (OM157[c])	Level 7 of the mine
Dunbar Lodes	0.721108 (DL255[a])		0.733382 (DL257[c])	Single vein
		0.727590 (DL253[b])	0.729799 (DL251[c])	Different veins

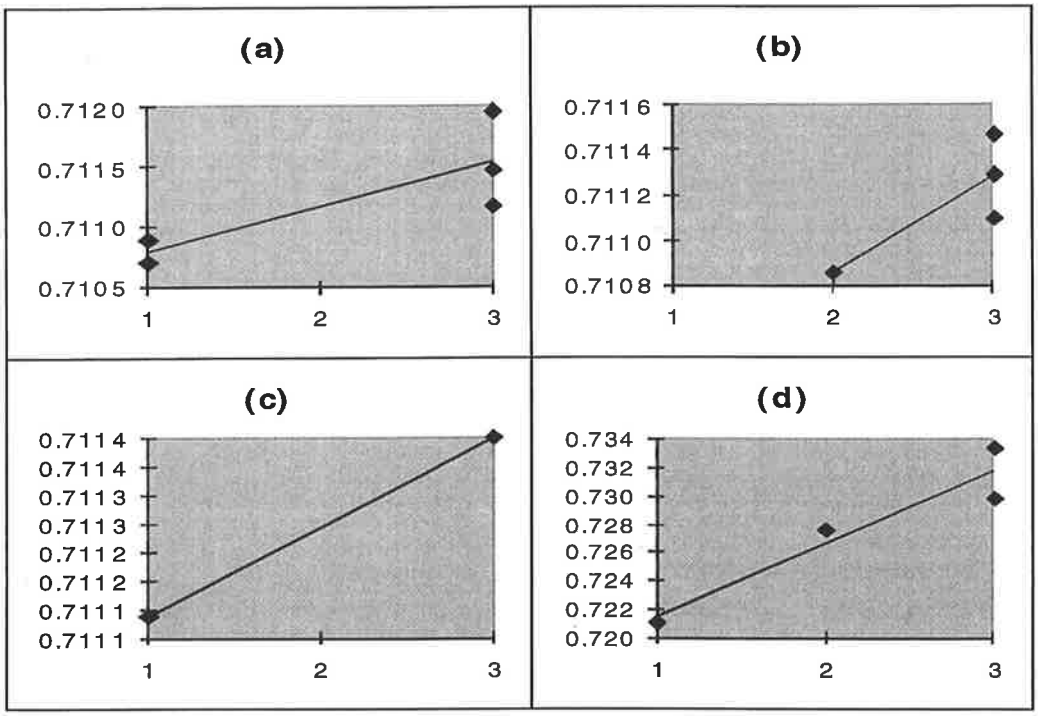

Fig. 10.3a-d: $^{87}Sr/^{86}Sr$ ratios with respect to the sample position of barite veins denoted by (1) median layer, (2) between median layer and border and (3) border of barite veins. (a): 1D Lode, (b): 1A Lode and (c): Link Lode of the Oraparinna Mine and (d): Dunbar Lodes.

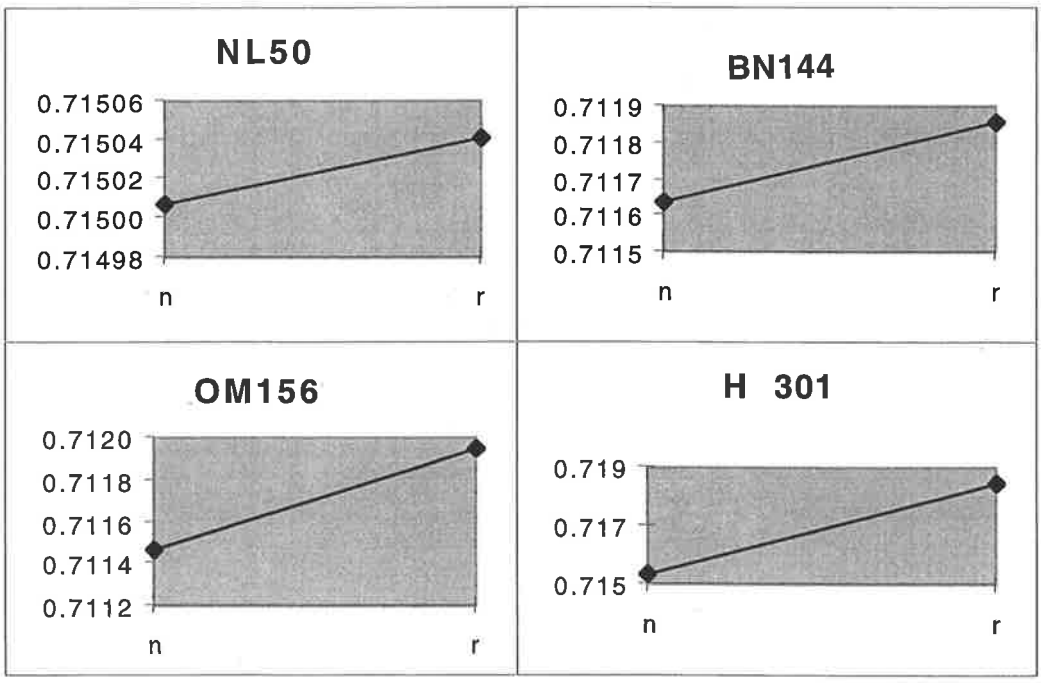

Fig. 10.4: Comparison of $^{87}Sr/^{86}Sr$ ratios (vertical axis) between non-recrystallised (n) and recrystallised (r) barite grains (horizontal axis) from Noarlunga Lodes (NL), Bainbridge Lodes (BN), Oraparinna Mine (OM) and Hall Lode (H).

10.6.3 $^{87}Sr/^{86}Sr$ ratio variation during recrystallisation

All the recrystallised barite grains show slightly higher $^{87}Sr/^{86}Sr$ ratios than adjoining non-recrystallised grains (Table 10.4, Fig. 10.4).

Table 10.4: $^{87}Sr/^{86}Sr$ ratios of recrystallised grains and adjoining non-recrystallised grains (Extracted from Table 10.1).

Location	$^{87}Sr/^{86}Sr$ ratio	
	Recrystallised grains	**Non- recrystallised grains**
Oraparinna Mine	0.711955 (OM156B^{r})	0.711466 (OM156B^{n})
Bainbridge Lode	0.711857 (BN144^{r})	0.711638 (BN144^{n})
Hall Lode	0.718412 (HL301^{r})	0.715397 (HL301^{n})
Noarlunga Lodes	0.715041 (NL50^{r})	0.715007 (NL50^{n})

10.7 Discussion

The discussion presumes barite veins in the Adelaide Fold Belt were formed approximately around 500 Ma, during the Delamerian Orogeny, as suggested by the vein geometry and relationship with host structure (Chapter 7).

10.7.1 Strontium sources

Potential sources for the Sr component in barite are plagioclase, apatite, carbonate including dolomite etc., and fluids contained in sedimentary sequences and diapirs, and Cambrian seawater.

The $^{87}Sr/^{86}Sr$ composition of Neoproterozoic seawater at 600 Ma was 0.7076 and that of Cambrian seawater at 500 Ma was 0.7092 (Asmerom *et al.*, 1991).

Breccia from the Oraparinna Diapir indicates a mean $^{87}Sr/^{86}Sr$ ratio of 0.7317765 at 500 Ma, varying from 0.708031 (dolomite) to 0.756741 (shale).

Previous data on $^{87}Sr/^{86}Sr$ ratios for the Tapley Hill Formation (approx. age 750 Ma) from the Flinders Ranges, calculated back to the 500 Ma are 0.713158 (carbonate), 0.713981 (carbonate) and 0.721825 (shale) (Jane, 1994), and 0.725619 (Turner *et al.* 1993). Therefore, the Tapley Hill Formation indicates a mean $^{87}Sr/^{86}Sr$ ratio of 0.718665 at 500 Ma, varying from 0.713158 to 0.725619.

Two samples out of four analysed for Sr isotope ratios of the Brachina Formation in the Oraparinna Mine show high Ba contents of 18072 and 24705 ppm, and high Sr contents of 557 and 865 ppm, respectively (Table 10.2b). These values are quite high to represent the Brachina Formation, probably due to contamination by micro-scale mineralisation (Fig. 9.6, Section 9.5); therefore, their $^{87}Sr/^{86}Sr$ ratios were not considered as representative of the formation. The other two samples show Ba contents of 553 and 778 ppm and were considered close enough to represent the formation (Table 9.7). $^{87}Sr/^{86}Sr$ ratios of these samples, calculated back to the age of 500 Ma, are 0.724125 and 0.721388 with a mean of 0.722757, which was considered as an approximate value for the Brachina Formation.

The mean $^{87}Sr/^{86}Sr$ ratio at 500 Ma for Dunbar Lodes of 0.727521 (ranging from 0.721108 to 0.733382, 6 analyses) suggests veins may have received Sr from both the adjacent Oraparinna Diapir (mean $^{87}Sr/^{86}Sr$ at 500 Ma, 0.734206) and the host Tapley Hill Formation (mean $^{87}Sr/^{86}Sr$ ratio at 500 Ma, 0.718665).

Bowering Lode shows a $^{87}Sr/^{86}Sr$ ratio of 0.723435. The lode is 30 m from the diapir and is likely to have received Sr from both the diapir (mean $^{87}Sr/^{86}Sr$ at 500 Ma, 0.734206) and the host Wilyerpa Formation, for which the $^{87}Sr/^{86}Sr$ ratio is unknown, but presumably less than that of the Callanna Beds in the diapir, due to the younger age of the formation.

The $^{87}Sr/^{86}Sr$ ratio for Hall Lode (0.715397 to 0.718412), 100 m from the diapir, is within the range of the host Tapley Hill Formation from 0.713158 to 0.725619 at 500 Ma, but possibly includes a minor contribution from the diapiric fluids as well.

Contributions from Cambrian seawater ($^{87}Sr/^{86}Sr$ = 0.7092, Asmerom *et al.*, 1991) and connate waters of overlying sequences to the Dunbar, Bowering and Hall Lodes were possible, but cannot be distinguished due to the effect of diapiric fluids.

The Oraparinna, Artipena and Noarlunga deposits have formed far away from diapirs. The Oraparinna and Artipena deposits are located respectively at 2.4 km and 25 km from the nearest diapirs. There are no known diapirs in the vicinity of the Noarlunga deposits. The $^{87}Sr/^{86}Sr$ ratios of the Oraparinna deposits vary from 0.710695 to 0.711955 with a mean value of 0.711347 (29 analyses), those of the Artipena Lodes vary from 0.710170 to 0.711065 with a mean value of 0.710763 (4 analyses), and those of Noarlunga Lodes vary from 0.711216 to 0.0.716613 with a mean value of 0.714671 (6 analyses). Therefore, the $^{87}Sr/^{86}Sr$ ratios of barite veins of the Oraparinna Mine and the Artipena Lodes are quite similar. The Brachina Formation (approx. age 600 Ma) is common to these three deposits and solely hosts the Oraparinna deposits, while a

sequence from the Etina Formation (approx. age 650 Ma) up to the Brachina Formation hosts the Artipena Lodes, and that from the Elatina Formation (approx. age 620 Ma) up to the Brachina Formation hosts the Noarlunga Lodes. The Sr isotope compositions of veins from these deposits are not explained by the approximate ratio for the Brachina Formation in the Oraparinna Mine, calculated back to 500 Ma (0.722757). Therefore, it is likely that Cambrian seawater ($^{87}Sr/^{86}Sr$ at 500 Ma of 0.7092; Asmerom *et al.*, 1991) or the connate waters of overlying formations contributed in achieving isotopic homogeneity of these deposits, since there are no known breccia intrusions in the vicinity of these deposits.

The $^{87}Sr/^{86}Sr$ ratios of both Noarlunga Lodes and Artipena Lodes show a relationship with increasing distance from dolomitic formations. The age of these dolomites is about 600 Ma and the $^{87}Sr/^{86}Sr$ ratios of dolomites remain approximately unchanged, due to their low Rb contents, whereas associated silicate hosts increase gradually due to decay of Rb. Therefore, veins formed closer to dolomite formations received less radiogenic isotopes than those formed further away.

10.7.2 Vein growth

Veins grew by adding tips to the fibre-ends while adding growth zones along the border of veins, during incremental opening of fractures (Fig. 7.15a). The Sr received by veins was mainly derived from the host rocks (see above), in which decay of Rb produced radiogenic Sr with time. The growth zones that formed in any incremental time period around single or adjacent multiple veins were likely to have similar $^{87}Sr/^{86}Sr$ ratios, provided that uniform isotopic conditions prevailed around veins, at the time of vein formation. During vein dilation $^{87}Sr/^{86}Sr$ ratios of the hosts increased with time, thereby increasing the ratios of both the newly added tip-ends and growth zones. Therefore, the $^{87}Sr/^{86}Sr$ ratios of veins essentially increased along *the direction of vein fibres* from median layer to border, as evidenced by the 1D Lode in the Oraparinna Mine and the Dunbar Lode (Fig. 7.15b). Furthermore, this relationship was also observed from median layer to border of adjacent veins in Dunbar, suggesting that the veins in question formed simultaneously. The relationship was also seen applicable *in directions inclined to vein fibres* on the same level or between adjacent levels but was not valid in directions steeply inclined to vein fibres, as seen between distant levels of the 1D Lode. This can be explained by increasing $^{87}Sr/^{86}Sr$ ratios along both vein-fibres from median line to border, but also from vein centre to border along the median line, following the tension-gash or lens shape growth zones (Fig. 7.15b). Therefore, a late-formed median line may show higher $^{87}Sr/^{86}Sr$ ratios than an early-formed border.

The slightly higher $^{87}Sr/^{86}Sr$ ratios in recrystallised barite grains than in adjoining non-recrystallised grains (Table 10.4, Fig. 10.4) is probably due to addition of radiogenic Sr to grains during recrystallisation. Recrystallised grains contain higher Sr contents than surrounding non-recrystallised grains and were formed during grain boundary migration in deformation (Table 8.5; Chapter 8). The source of added radiogenic Sr is not well understood but may be due to decay of minor Rb in barite or Rb from the incorporation of wall-rock inclusions in vein dilation.

10.7.3 Time duration of barite vein growth

The $^{87}Sr/^{86}Sr$ ratios of the median layer and borders of a barite vein represent the isotopic composition of Sr received, respectively, at the beginning and end of deposition of the vein formation. 1D Lode on Level 5 of the Oraparinna Mine shows $^{87}Sr/^{86}Sr$ ratios of 0.710896 (OM128[a]) in the median layer and 0.711167 (OM127[c]) in the border. The vein grew to a two-metre thickness from border to border, with one metre between median layer and border, during this change in isotope ratio.

The following calculation assumes that the Sr was supplied only by the host rock. The seawater input is neglected for calculation purposes.

$$^{87}Sr/^{86}Sr = (^{87}Sr/^{86}Sr)o + (^{87}Rb/^{86}Sr)\,(e^{\lambda t} - 1), \text{ where}$$

$^{87}Sr/^{86}Sr$ = isotope ratio for the Brachina Formation at the end of vein formation, obtained from vein border.

$(^{87}Sr/^{86}Sr)_o$ = initial isotope ratio for the Brachina Formation at the beginning of vein formation, obtained from median line.

$^{87}Rb/^{86}Sr$ = present isotope ratio for the Brachina Formation and assumed to be equal to the value at the time of vein border formation = Rb/Sr x 2.88216 (pers. commn. J. Foden, Dept of Geology and Geophysics, University of Adelaide)

λ = Rb decay constant, t = time duration for the vein formation.

The shale sample OM121, 24m SE of 1D Lode in the Brachina Formation at Level 5, Oraparinna Mine, has Sr = 105 ppm, Rb = 201 ppm. This sample was selected for the calculation because the

Sr and Rb concentrations do not show abnormal concentrations compared to the values of the same formation elsewhere in the central Flinders Ranges given in Turner *et al.* (1993).

Therefore,

$$0.711167 = 0.710896 + 5.54964694\ (e^{1.42x10\text{-}11t\ -1})$$

and

$$t = 3.438\ \text{Ma}$$

According to this calculation, the 1D Lode took 3.4 Ma to form. However, this assumes (a) the Sr and Rb concentrations of the host Brachina Formation remained unchanged after formation of barite veins, and (b) there was no seawater contribution. If seawater also had participated, the time of vein formation may have been more than 3.4 Ma.

10.7 Summary

The Sr isotope studies suggest a range of sources of Sr for barite vein formation. Neoproterozoic host formations were the main Sr source for all the deposits and there is evidence that Sr was also supplied by dolomites in the near vicinity of veins in Artipena and Noarlunga deposits. Dunbar, Bowering and possibly Hall Lodes have evidently received some Sr from the nearby Oraparinna Diapir. The deposits that are further away on the scale of kilometres from diapirs show no diapiric influence. All the deposits may have received Sr from additional sources such as Cambrian sea and/or connate waters from overlying sequences but this cannot be distinguished for lodes adjacent to the Oraparinna Diapir, due to the diapiric influence. However, the Oraparinna, Noarlunga and Artipena vein deposits show Sr was provided by sources in addition to the Neoproterozoic hosts.

The increase of $^{87}Sr/^{86}Sr$ ratios in the direction of barite vein fibres from median layer to border supports the theory of antitaxial mechanism of vein formation in the Adelaide Fold Belt.

Chapter 11

SULPHUR ISOTOPES

11.1 Introduction

The formation of barite deposits in the Adelaide Fold Belt required the supply of both Ba^{2+} and SO_4^{2-} during vein dilation. There are three isotopically distinct sulphur reservoirs, with differing values for $\delta^{34}S$ (Rollinson, 1995), viz. (1) mantle derived sulphur with $\delta^{34}S$ in the range of $0 \pm 3‰$ (Chaussidon and Lornard, 1990); (2) seawater sulphate which through geological time has varied from $\delta^{34}S‰$ of about 11 to 34‰ (Claypool *et al.*, 1980; Strauss, 1993; Shields *et al.*, 1999); (3) strongly reduced (sedimentary) sulphur with large negative $\delta^{34}S$ values.

The oceans constitute a major reservoir of sulphur, *ca* 1.3×10^{15} metric tons, in the form of sulphate ions in solution (Bowen, 1988). This represents about 10 wt % of the sulphur in the crust + ocean system (Ohmoto, 1986). The average sulphur content of crustal rocks is about 5000 ppm for sedimentary rocks and about 200 ppm for igneous and high-grade metamorphic rocks (Ohmoto, 1986). Sulphur in sedimentary rocks (i.e. recycled seawater sulphur) constitutes about 60 wt % of the total sulphur in the crust + ocean system, compared to about 30 wt % for igneous rocks (Holland, 1978). Hence, it is understood that seawater sulphur, either through direct or indirect pathways, plays an important part in the genesis of many ore deposits.

Physical and chemical controls of stable isotope fractionation are temperature, pressure (minimal for sulphur), kinetic effects, diffusion, distillation, major element chemistry, crystal structure etc. (Rollinson, 1995). A related process to diffusion that affects sulphur isotopes is microfiltration, in which sulphur isotopes are fractionated by adsorption onto clay minerals in sediments, leading to enrichment of the heavier isotope in formation waters (Ohmoto and Rye, 1979). Experiments by Nriagu (1974) with sulphate rich solutions showed that the isotopically lighter sulphate was preferentially adsorbed by clay minerals, leading the solution to be enriched with ^{34}S by 0.9 to 6.0‰.

Ohmoto (1972), Rye and Ohmoto (1974), and Ohmoto and Rye (1979) have shown quantitatively the effects of the chemical nature of ore-forming solutions on the sulphur isotope composition of minerals in hydrothermal systems. The magnitude of sulphur isotope exchange reactions between sulphate and sulphide species in solution is a function of fO_2, temperature, and pH value at the depositional environment. Large equilibrium fractionation factors exist between oxidised and reduced sulphur species, with a tendency towards preferential enrichment of heavier isotopes in

compounds with higher oxidation states (Ohmoto 1986). Under equilibrium conditions, $\delta^{34}S_{sulphates} > \delta^{34}S_{SO2} > \delta^{34}S_{sulphides}$. The magnitude of fractionation between the most oxidised and most reduced forms, i.e. $\Delta_{SO4-H2S}$, is 29‰ at 200 °C (Ohmoto and Lasaga, 1982).

Most hydrothermal fluids are neutral or slightly acidic. Their ΣS content typically falls in the range of 10^{-3} to 10^{-1} m with a tendency to decrease with decreasing temperature (Ohmoto, 1986). Such pH conditions and ΣS contents indicate that isotopic and chemical equilibrium between sulphides and sulphates is not likely to be attained in most geologic fluids at temperatures less than 150°C, except in some connate waters in which the residence time of sulphur species may exceed 10,000 years (Ohmoto, 1986). If isotopic equilibrium is achieved, the isotopic signature of an individual species may no longer be similar to that of the source area.

Barite occurrences in the Adelaide Fold Belt are characterised by a lack of associated sulphides, other than very minor occurrences such as disseminated chalcopyrite and pyrite. Significant amounts of iron in Bowering Lode (Fe_2O_3 = 0.27 - 2.06 wt %; Townsend and Barnes, 1981) and Dunbar Lodes (Fe_2O_3 = 0.3-8.0 wt %; Scott, 1979) occur as siderite or hematite and not as sulphides. This lack of sulphides means that the fluid was characterised by high fO_2, so that sulphate species were the dominant form of sulphur, with negligible reduced sulphur species. Robertson (1981) and Cawley (1983), on the basis of sulphur isotope analysis on the Artipena and Dunbar Lodes, respectively, proposed that sulphur was derived from the host Adelaidean sediments in the form of trapped seawater (i.e. connate water).

11.2 Materials and methods

Sulphur isotope analyses were undertaken on barite from the Oraparinna Mine (Fig. 8.1), Dunbar Lodes (Fig. 7.6a), Hall Lode and Bowering Lode (Figs. 1.3), as well as Noarlunga Lodes (Fig. 2.7). The analyses were performed in the Department of Geology and Geophysics, University of Adelaide using the method described by Coleman and Moore (1978). $^{34}S/^{32}S$ ratio measurements were made on a Micromass 602E mass spectrometer. The precision of the analyses was ± 0.5‰.

11.3 Results

All $\delta^{34}S$ values obtained, as well as previous data from Robertson (1981) and Cawley (1983), for the barite veins fall in the range of 16.8 to 31.0‰ (Table 11.1). In decreasing order, these values are,

Artipena Lodes (22.1 - 31.0‰, 2 analyses), Dunbar Lodes (21.0 - 30.8‰, 9 analyses), Oraparinna area (22.1 - 27.8‰, 29 analyses), Hall Lode (20.7 - 21.7‰, 2 analyses), Noarlunga Lodes (19.5 - 21.4‰, 7 analyses), and Bowering Lode (16.8 - 17.4‰, 2 analyses).

11.4 Interpretation

The barite veins were apparently deposited from fluids in which sulphates were the dominant sulphur species (see above), hence it can be assumed that $\delta^{34}S$ barite $\approx \delta^{34}S$ fluid. The range of $\delta^{34}S$ values of 16.8 to 31.0‰ suggests that sulphur for barite vein formation was largely derived from a marine source, i.e. coeval seawater, connate water or evaporites in the associated marine sedimentary formations in the Adelaide Fold Belt (cf. Robertson 1981; Cawley, 1983). In this case, the sulphur isotope characteristics of the barite deposits can be compared with the seawater sulphur isotope data and curves presented by Claypool *et al.* (1980), Strauss (1993) and Shields *et al.* (1999, Fig. 11.1). The present investigation attempts a detailed examination of the barite sulphur isotope data in relation to the seawater curve, in order to assess the possibility of mixing of fluids from various sedimentary rock units.

11.4.1 Dunbar

The $\delta^{34}S$ values of barite obtained in both the present study and Cawley (1983) for Dunbar Lodes range from 26.1 to 30.8‰ (8 analyses), and one analysis of 21.0‰ (Cawley, 1983; Table. 11.1). The values of present analyses fall in a narrow range of 29.6 to 30.8‰ (4 analyses). These values for Dunbar Lodes are higher than that expected for connate water of the host Tapley Hill Formation (seawater $\delta^{34}S$ for 750 Ma $\approx$ 14 - 25‰, Fig. 11.1).

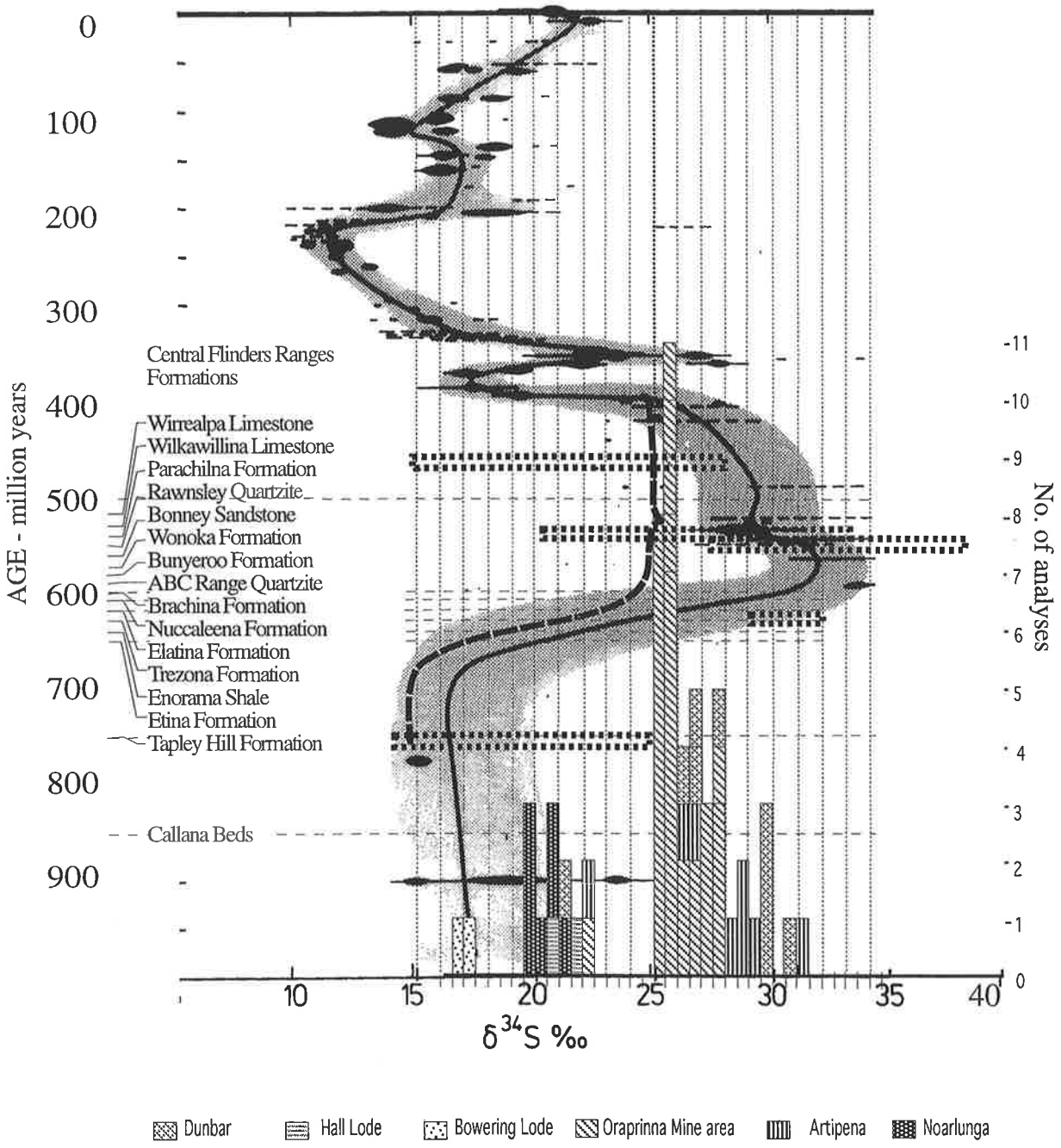

Fig. 11.1: Comparison of $\delta^{34}S‰$ values for vein barite from the Adelaide Fold Belt, with summary sulphur isotope age curve for sulphate, after Claypool *et al.*, 1980 (thick line with shaded area denoting the uncertainty of the curve), and additional information after Strauss (1993) ▬▬▬, and Shields *et al* (1999) ▪▪▪▪▪▪▪▪▪▪▪▪▪▪▪▪▪▪▪▪ .

Table 11.1: Sulphur isotope analyses of barite veins in the Adelaide Fold Belt.

Sample No.*	$\delta^{34}S$ (‰)	Host rock	Approximate age (Ma) of host	Remarks
Oraparinna Mine				
OM106b	25.8	Brachina Formation	600	1C Lode
OM108a-1	25.2	"	"	1D Lode
OM108a-2	25.6	"	"	1D Lode
OM109-1	26.5	"	"	1B Lode
OM109-2	25.6	"	"	1B Lode
OM111c	25.3	"	"	1A Lode
OM113c	26.8	"	"	1A Lode
OM113c	27.4	"	"	1A Lode
OM114b	26.2	"	"	1A Lode
OM120a	25.1	"	"	Link Lode
OM127c	25.4	"	"	1D Lode
OM128a	25.7	"	"	1D Lode
OM130	26.8	"	"	minor vein
OM131	22.1	"	"	minor vein
OM140a	25.4	"	"	1D Lode
OM141c-1	25.8	"	"	1A Lode
OM141c-2	26.3	"	"	1A Lode
OM157c-1	27.4	"	"	Link Lode
OM157c-2	27.1	"	"	Link Lode
OP-39*1	27.8	"	"	
OP-61*1	25.5	"	"	
OP-113*1	25.5	"	"	
Oraparinna Bainbridge Lode				
BN143	25.4	"	"	
BN144n	25.8	"	"	
BN144r-1	26.8	"	"	
BN144r-2	27.6	"	"	
Oraparinna fault zone				
OF158-1	25.2	"	"	
OF158-2	25.7	"	"	
OF159	25.2	"	"	
Dunbar				
DL251c	29.8	Tapley Hill Formation	750	
DL252	29.6	"	"	
DL253b-1	29.8	"	"	
DL253b-2	30.8	"	"	
DL1*2	21.0	"	"	
DL-2*2	26.6	"	"	
DL-3*2	27.7	"	"	
DL-4*2	26.1	"	"	
DL-5*2	26.6	"	"	
Bowering Lode				
BW-200-1	16.8	Wilyerpa Formation	>750	
BW-200-2	17.4	"	"	
Hall Lode				
HL301n	20.7	Tapley Hill Formation	750	
HL301r	21.7	"	"	

Contd.

Table 11.1: Contd.

Sample No.	$\delta^{34}S$ (‰)	Host rock	Approximate Age (Ma) of host rock	Remarks
Artipena				
AT52*3	28.6	Elatina /Trezona	620 /630	No. 1 Lode
AT58*3	29.4	"	"	No. 1 Lode
AT63*3	28.9	Brachina /Enorama	600 /640	No. 5 Lode
AT71*3	31.0	Enorama Shale	640	No. 3 Lode
AT29*3	22.1	"	"	No. 4 Lode
AT34*3	26.3	"	"	No. 4 Lode
AT34*3	26.8	"	"	No. 4 Lode
AT37*3	28.1	Etina Formation	650	No. 2 Lode
Noarlunga				
NL52	19.5	Brachina Formation	600	
NL53	19.8	Seacliff Sandstone	610	
NL50n	20.0	Elatina Formation	620	
NL50r	19.8	"	"	
NL51B-1	20.8	"	"	B Lode
NL51B-2	21.4	"	"	B Lode
NL51D	20.6	"	"	D Lode

*Sample order in Noarlunga and Artipena areas is arranged on the basis of the age of the host formation. (a), (b) and (c) denote sample position of the vein i.e. (a) - Median Layer (ML), (b) - between ML and border, and (c) - border. (n) and (r) denote non-recrystallised and recrystallised stages of the sample respectively. Suffixes to the sample numbers such as - 1 and - 2 denote repeated analyses.
*1 = R. Both (unpublished data), *2 =Cawley (1983), *3 = Robertson (1981).

Sulphides in the Tapley Hill Formation show a very wide range of $\delta^{34}S$. Lambert *et al.* (1987) reported $\delta^{34}S$ values from -1 to +46‰ from Mt. Gunson, Myall Creek and Kapunda, and analyses by R. Both (unpublished data) from the Blinman 2 diamond-drillhole, Frontier Exploration drill hole at Blinman, show values from 17.7 to 40.4‰. These are unusually high for what is clearly biogenic sulphide, and a sulphate source around 40‰ is indicated, i.e. much higher than coeval seawater, according to Claypool *et al.* (1980), Strauss (1993) and Shields *et al.* (1999) (Fig. 11.1). Lambert *et al.* (1987) suggested that during diagenesis (when the sulphides were deposited), the pore waters in the Tapley Hill Formation had sulphate with much higher $\delta^{34}S$ than "normal" seawater for that age. The Blinman 2 was drilled 2 km east of the Blinman Diapir, to a 2030 m depth (Preiss, 1999), on to the moderately and easterly dipping décollement surface on the eastern limb of the Blinman Anticline (See Figure 3.8a for the model). The Tapley Hill Formation extends from approximately 60 m to 1617 m (unpublished interpretation of Blinman 2 drill core by W.V. Preiss, 1991 and Preiss, 1999). Diapiric breccia intrusions or tongues occur commonly below 1040 m, where the rock is expected to have interacted with diapiric fluids.

The occurrence of the Oraparinna Diapir, adjacent to the Dunbar Lodes is a factor clearly to be considered in regard to sulphur source since strontium isotope data (Chapter 10) indicate that barite

in Dunbar Lodes received Sr from both the diapir and the Tapley Hill Formation. Field relations show that an offshoot of breccia from the Oraparinna Diapir cuts across the Dunbar Lodes (Fig. 7.6). The veins may have formed in the fractures dilated in the near vicinity of the forming Oraparinna Diapir. Therefore, a diapiric source of sulphates mixed with the connate waters of the Tapley Hill Formation should also be considered. The Oraparinna Diapir is known to be dominated by Callanna Group sediments (Dalgarno and Johnson, 1966; Preiss, 1987) with an approximate age of 850 Ma. The $\delta^{34}S$ value of seawater sulphate at 850 Ma is not well constrained but may have been approximately 15 - 21‰ (Fig. 11.1), which is lower than the values for the lodes.

Following deposition, the shales and brecciated formations in the diapirs, as well as the host Tapley Hill Formation, may have preferentially adsorbed ^{32}S from the connate water, increasing the $\delta^{34}S$ value of the fluids (cf. Nriagu, 1974). $\delta^{34}S$ in diapiric fluids may also have been increased by removal of ^{32}S as a result of the formation of diagenetic Fe and Cu sulphides (cf. Blinman Cu deposits, Coats, 1964a; Newton and Crettenden, 1984), during low-grade deformation in the diapirs (cf. Mount, 1975). However, these mechanisms may not be sufficient to account for the increase in $\delta^{34}S$ required by the difference in $\delta^{34}S$ value between 850 Ma seawater sulphate and Dunbar barite.

During the Delamerian deformation, the Adelaidean sequences were thrust over gently dipping décollements on the basement, causing eastern limbs to pass-over western limbs (Chapter 3). This process formed folds, especially detachment/fault-propagation folds, in which the major breccia deposits were emplaced as diapirs (Fig. 3.8a, Chapters 6, 13). The décollement surfaces were extended into the sedimentary rocks as steeply dipping listric-thrust surfaces, for which the host rock at the tip-end is unknown for the Oraparinna Anticline/Diapir. The rocks that were brecciated over these thrust surfaces formed the main breccia deposit. It consisted of clasts from the continuous sedimentary sequence of Callanna Group (approx. age 850 Ma) up to Nuccaleena Formation (approx. age 610 Ma) that occurs on the border with the Bunkers Graben (Chapter 4), so that a seawater-derived fluid with $\delta^{34}S$ values between approximately 14 - 34‰ may have been involved in the Oraparinna Diapir (Fig. 11.1). However, the diapir also contains clasts from the basement igneous rocks ($\delta^{34}S_{sulphide} \approx$?0‰).

The Dunbar Lodes (Fig. 7.6c) were formed in the vicinity of the Oraparinna Diapir during the D_1 deformation (Chapter 7). It is likely that the lodes ($\delta^{34}S$ = 21.0 to 31‰) incorporated sulphate derived mainly from the host Tapley Hill Formation and the Oraparinna Diapir. Percolation of coeval Cambrian seawater ($\delta^{34}S \approx$ 25 – 32‰) and connate water from overlying formations,

especially those aged between 530 – 550 Ma that have a seawater $\delta^{34}S$ range between 20 – 39‰ (Fig. 11.1; Claypool *et al.*, 1980; Shields *et al.*, 1999 and Strauss, 1993) is a further possibility, but is not distinguishable because of the overlapping ranges of isotope values.

11.4.2 Hall Lode

$\delta^{34}S$ values for Hall Lode vary from 20.7 to 21.7‰ (2 analyses), within the range expected for connate waters of the host Tapley Hill Formation (14 - 25‰, Fig. 11.1). As seen with Sr isotopes (Chapter 10), diapiric fluids from the Oraparinna Diapir (Section 11.4.1) could have participated because of the distance of 100 m from the diapir to the lode, but is not distinguishable because the $\delta^{34}S$ values for the lode are within the overlapping range of both sources. Alternatively, percolation of Cambrian seawater or connate waters from overlying formations could have also been possible but is not distinguishable as well. However, the host Tapley Hill Formation probably have been the major contributor of sulphur isotopes to the Hall Lode.

11.4.3 Bowering Lode

The two $\delta^{34}S$ values of 16.8 and 17.4‰ for the Bowering Lode are the lowest obtained for all barite veins analysed in the region. The vein is disrupted and displaced within brecciated Wilyerpa Formation on the eastern border of the Oraparinna Diapir (Fig. 1.3) and is intimately associated with a large mass of dolerite and breccia injected from the diapir (Townsend and Barnes, 1981). Sulphur in the Bowering Lode may have been derived from (a) connate water in the host ($\delta^{34}S$ of coeval seawater, >750 Ma $\approx$ 14 - 25‰, Fig.11.1); (b) sulphur associated with dolerite ($\delta^{34}S \approx 0$‰); and (c) diapiric fluids ($\delta^{34}S \approx$ 14 - 34‰, section 11.4.1). Sr isotope studies suggest contributions of diapiric fluids for the Bowering Lodes (Chapter 10). If diapiric fluids had been involved, they could have leached sulphides from dolerite ($\delta^{34}S \approx$?0‰), thereby producing average isotopic composition of 16.8 - 17.4‰, while mixing with sulphur from the host formation. The $\delta^{34}S$ values for the Bowering Lode lie close to the lower margin of the range for isotopes for both the sources of diapiric fluids and the Tapley Hill Formation and may suggest that sulphur from dolerites were also involved. Alternatively, percolation of Cambrian seawater or connate waters from overlying formations could have also been possible.

11.4.4 Oraparinna Mine

$\delta^{34}S$ values of barite from the Oraparinna Mine, including nearby Bainbridge Lodes and minor barite deposits in the fault zone adjacent to the mine, range from 22.1 to 27.8 (29 values, Table 11.1). Except for one value of 22.1‰ for a minor barite vein associated with carbonates, all other $\delta^{34}S$ values range between 25 - 28‰. There is no evidence of any breccia off-shoot intrusions in the area. Sr isotope data suggest that influence of diapiric fluids from the Oraparinna Diapir is unlikely, possibly because the horizontal distance of 2.4 km and vertical depth of 5.3 km to the diapiric breccia deposit (Section 10.7.1, Chapter 3). Percolation of Cambrian seawater or connate waters from overlying formations could have also been possible. However, the sulphur isotope values are well within the range expected for connate water from the host Brachina Formation ($\delta^{34}S \approx 23$ - 34‰ at 600 Ma, Fig. 11.1); therefore, connate water of the host formation is considered to be the most likely source of sulphur for the veins in the Oraparinna Mine.

11.4.5 Artipena Lodes

The Artipena Lodes (nos. 1-5) are hosted along fractures and faults, cross cutting the major syncline that consists of a continuous series of Neoproterozoic formations from the lowermost Etina Formation (approx. 650 Ma) to the uppermost Brachina Formation (600 Ma; Fig. 2.6). The $\delta^{34}S$ values of lodes hosted by the lower formations show slight deviation from the range expected for connate water from those formations (Table 11.2). However, all the barite lodes can be explained by connate water sourced from the uppermost Brachina Formation. Therefore, the evidence suggests that the deposition of veins possibly involved fluid mixing between formations. Furthermore, since the fractures hosting the lodes crosscut the Delamerian folds, it can be confidently suggested that the veins were formed simultaneously with or immediately after the Delamerian folding. Percolation of Cambrian seawater or connate waters from overlying formations could have also been possible but is not distinguishable.

Table 11.2: Summary of $\delta^{34}S$ values for the Artipena Lodes with reference to the same of the coeval seawater of the host formations (Fig. 11.1).

Lode no.	Host Formation		$\delta^{34}S$(‰)	
	Name	Age (Ma)	Coeval seawater	Barite (No. of analyses)
5	Brachina/Enorama Fm.	600/640	16-36	28.9 (1)
1	Trezona/Elatina Fm.	630/620	18-32	28.6 - 29.4 (2)
3,4	Enorama Shale Fm.	640	16-28	22.1 - 31.0 (4)
2	Etina Fm.	650	16-26.5	28.1 (1)

11.4.6 Noarlunga

The Noarlunga Lodes are hosted by a short continuous series of Neoproterozoic formations from Elatina Formation (620 Ma) to Brachina Formation (600 Ma, Fig. 2.7). The $\delta^{34}S$ value of the barite lodes in the Brachina Formation falls outside the predicted range for connate water for the Brachina Formation (Table 11.3). However, all the values for lodes can be explained by connate water sourced from the Elatina Formation or Seacliff Sandstone. This suggests vein deposition, as described for Artipena, involved fluid mixing between formations. The corresponding range for Cambrian seawater at 500 Ma ≈ 25 - 32‰ (Fig. 11.1), does not explain the range of $\delta^{34}S$ values between 19.8 – 21.4‰ for barite veins. However, mixing with connate waters from overlying formations, especially those aged between 530 – 550 Ma that have a coeval seawater $\delta^{34}S$ range between 15 – 39‰ (Fig. 11.1) could be possible but is not distinguishable due to overlapping ranges. There are no diapirs in the area, thus a contribution from diapiric sources is not to be expected.

Table 11.3: Summary of $\delta^{34}S$ values for the Noarlunga Lodes with reference to coeval seawater of the host formations (Figs. 2.6, 11.1)

Sample no.	Host Formation		$\delta^{34}S$(‰)	
	Name	Age (Ma)	Coeval seawater	Barite (No. of analyses)
N52	Brachina Fm.	600	23-36	19.5 (1)
N53	Seacliff Sandstone.	610	20-33.5	19.8 (1)
N51B, N51D	Elatina Fm.	620	18-32.5	19.8-21.4 (5)

11.5 Conclusion

The $\delta^{34}S$ values for the barite vein deposits in the Adelaide Fold Belt, including data of Robertson (1981) and Cawley (1983), range from 16.8 to 31.0‰, and thus mainly represent a marine origin.

The study shows that $\delta^{34}S$ values of barite vein deposits in the Fold Belt, have received sulphur of ultimate seawater origin from host formations as well as adjacent sources. The Dunbar Lodes have received part of the sulphur from the bordering breccia off-shoot of the Oraparinna Diapir. However, the $\delta^{34}S$ values of other barite vein deposits adjacent to the Oraparinna Diapir, i.e. the Bowering and Hall Lodes, as well as the Oraparinna Deposits at 2.4 km NE of the diapir, can be explained by respective connate water sources of host formations. Noarlunga and Artipena vein deposits clearly show evidence of mixing of connate waters in adjacent Neoproterozoic sequences. Veins in these two deposits are associated with major Delamerian folds, thus fluid mixing could

have been enhanced during deformation that formed folding. However, other sources such as dolerites adjacent to Bowering Lode, Cambrian seawater and connate waters of overlying formations could have also supplied sulphur to any of the deposits but cannot be distinguished due to overlapping ranges of $\delta^{34}S$ values for barite veins with that of host formations.

Chapter 12

FLUID INCLUSION STUDY

12.1 Introduction

A microthermometric study has been made of the fluid inclusions trapped in minerals in the barite veins, in an attempt to obtain information on the composition and temperature of the hydrothermal fluid of the ore-forming environment. It is well known that fluid inclusions in barite are prone to leakage and hence the data obtained in this study must be treated with caution. However, in view of the limited presence of other more suitable minerals, it was considered appropriate to study fluid inclusions in barite samples.

12.2 Sampling of barite veins

Doubly-polished thick sections of samples from Noarlunga, Oraparinna Mine, Bainbridge Lodes, Bowering Lode, Hall Lode and Dunbar Lodes were selected for fluid inclusion studies. Fluid inclusions studied on the heating/freezing stage ranged up to 10 μm; one of 20 μm was found at Bowering Lode but leaked during heating. Very few samples of barite proved to be satisfactory for microthermometric measurements, due to low clarity and excessive fracturing, the latter having resulted in partial or complete escape of fluids from the inclusions. Suitable fluid inclusions in barite were found only in samples from Noarlunga, Bowering Lode and Dunbar Lodes. Twenty sections of barite from various veins at the Oraparinna Mine and another two sections from the NE trending fault zone immediately east of the mine (Fig. 2.5) were examined and, although abundant small fluid inclusions (up to 2 μm in size) were found, they were too small for microthermometric measurements. A small number of fluid inclusions suitable for microthermometry were found in quartz from Hall Lode.

The microthermometric measurements were carried out using a Reynolds heating-freezing stage attached to a Leitz S Lux-POL binocular microscope in the Department of Geology and Geophysics of the University of Adelaide. Temperatures were recorded to within 0.1°C on a Fluid Inc. 410A Trendicator. Data were obtained for first melting (eutectic) temperature (T_{FM}), melting temperature of hydrohalite (T_{mh}), final melting temperature of ice (T_M), and homogenisation

temperature (T_H). T_{mh} was not observed in all fluid inclusions. Salinities were calculated from T_M according to Potter *et al.* (1978). No CO_2 phases were observed in the fluid inclusions.

12.3 Freezing measurements

The fluid inclusions were rapidly cooled down to –150°C, and observed during slow recovery of temperature.

The fluid inclusions in barite from Dunbar have T_{FM} values of approximately –52°C and correspond to the H_2O-NaCl-$CaCl_2$ ternary eutectic (Shepherd *et al.*, 1985). In fluid inclusions where T_{mh} could be observed, the values were in the narrow range of –22.8°C to –22.2°C (except for one value of –15.5°C), indicating NaCl:$CaCl_2$ ratios of approximately 2:1 (Fig. 12.1). T_M values range from –9.8°C to –8.6°C, corresponding to a salinity range of 13.8 to 12.4 wt % NaCl equivalent.

Fluid inclusions in barite from Noarlunga show similar results to those of Dunbar, with T_{FM} values approximately of –52°C, thus corresponding to the H_2O-NaCl-$CaCl_2$ ternary eutectic. The two T_{mh} values measured are –22.4°C and –22.2°C, indicating NaCl:$CaCl_2$ ratios of approximate 2:1 (Fig. 12.1). T_M values for the same fluid inclusions are –9.3°C and –9.2°C, corresponding to salinities of 13.2 and 13.1 wt % NaCl equivalent, respectively.

Bowering Lode barite shows T_{FM} values varying from –22.8°C to –21.5°C, close to the eutectic temperatures for the H_2O-NaCl or H_2O-NaCl-KCl systems (Shepherd *et al.*, 1985). T_M values range from –13.2°C to –0.3°C, indicating salinity ranging from 17.2 to 0.5 wt % NaCl equivalent.

The measured values of T_{FM} for fluid inclusions on quartz from Hall Lode range from –96.3°C to –43.7°C (Table 12.1). The low values (approximately –90°C) are well below the eutectic temperatures for geologically common H_2O-salt systems and it is likely that these measurements reflect either the difficulty in observing T_{FM} in small (<10 μm) fluid inclusions or the melting of a metastable phase. If metastable phases form during freezing of fluid inclusions, when the fluid inclusion is heated these phases may begin melting at a lower temperature than the first melting temperature of the stable assemblage (Goldstein and Reynolds, 1994). It is therefore likely that the T_{FM} value of –47°C is the only reliable measurement and would indicate a fluid in the system H_2O-NaCl-$CaCl_2$.

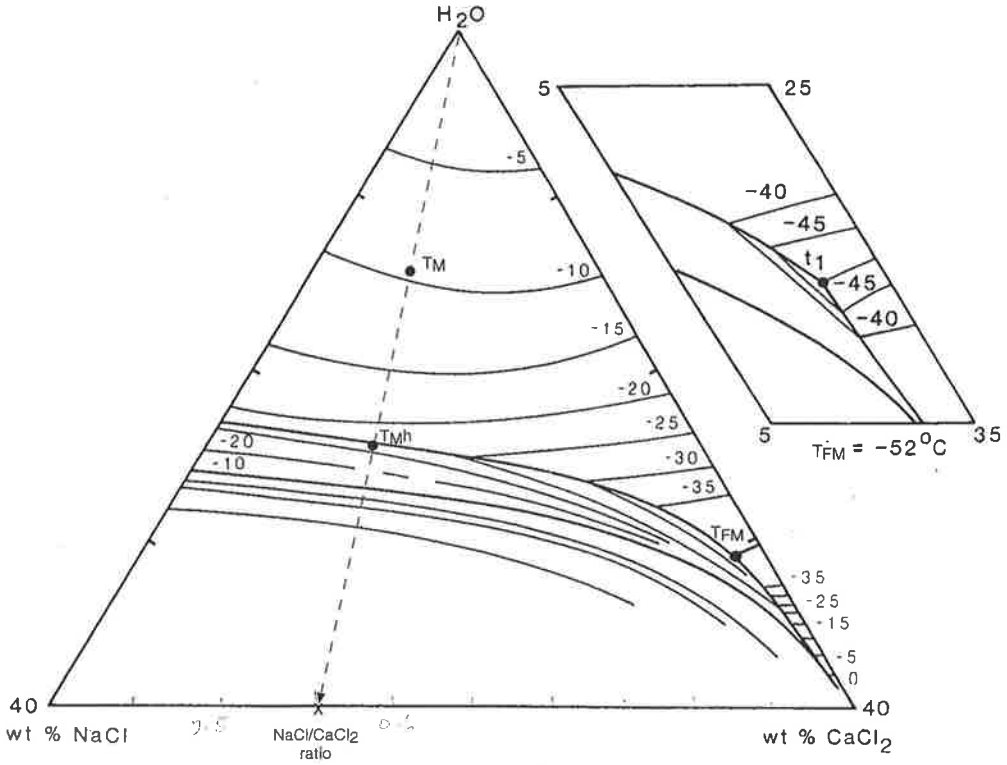

Fig. 12.1: Isotherms for the system H_2O-NaCl-$CaCl_2$ showing the melting path of fluid inclusions from Dunbar and Noarlunga Lodes. The insert shows an enlargement of the area around the ternary eutectic, T_{FM} at -52 °C (modified after Shepherd *et al.*, 1985).

T_M values for fluid inclusions in quartz from Hall Lode range from –6.5°C to –3.8°C, corresponding to a salinity range of 9.9 to 6.1 wt % NaCl equivalent.

Table 12.1: Microthermometric data for fluid inclusions in barite veins.

Sample No.	Lode	Host mineral	Volume ratios	T_{FM} (°C)	T_{Mh} (°C)	T_m (°C)	T_H (°C)	Salinity (wt % NaCl equivalent)
A987/50	Noarlunga	Barite	L95V5				242.1	
A987/50	Noarlunga	Barite	L95V5				223.2	
A987/50	Noarlunga	Barite	L90V10				263.9*	
A987/50	Noarlunga	Barite	L95V5				225.5	
A987/50	Noarlunga	Barite	L90V10	–51.1	–22.2	–9.2		13.1
A987/50	Noarlunga	Barite	L95V5	–52.8	–22.4	–9.3	230/238	13.2
A987/200	Bowering Lode	Barite	L95V5	–21.5		–0.3		0.5
A987/200	Bowering Lode	Barite	L90V10	–22.2		–0.5	132.4	0.9
A987/200	Bowering Lode	Barite	L90V10	–22.4		–9.8		13.8
A987/200	Bowering Lode	Barite	L100	–22.8		–13.2		17.2
A987/252	Dunbar Lode	Barite	L95V5	–52.3	–15.5	–9.2		13.1
A987/252	Dunbar Lode	Barite	L95V5	–55.8	–22.2	–9.4	149.8	13.3
A987/252	Dunbar Lode	Barite	L90V10	–53.1	–22.2	–9.1		13.0
A987/252	Dunbar Lode	Barite	L90V10	–52.6	–22.2	–8.6		12.4
A987/252	Dunbar Lode	Barite	L95V5	–51.9	–22.6	–9.2		13.1
A987/252	Dunbar Lode	Barite	L95V5	–52.6	–22.8	–9.3	153.0	13.2
A987/252	Dunbar Lode	Barite	L95V5	–54.1	–22.4	–9.8	169.0	13.8
A987/253	Dunbar Lode	Barite	L70V30				98.0	
A987/253	Dunbar Lode	Barite	L80V20				87.0	
A987/253	Dunbar Lode	Barite	L70V30				92.0	
A987/301	Hall Lode	Quartz	L40V60	–94.7		–4.5		7.2
A987/301	Hall Lode	Quartz	L92V8	–95.0		–3.8	127.4	6.1
A987/301	Hall Lode	Quartz	L80V20	–96.3		–6.5	122.5	9.9
A987/301	Hall Lode	Quartz	L92V8	–95.8		–4.2	130.8	6.7
A987/301	Hall Lode	Quartz	L88V12	–43.7		–4.8	142.8	7.6

T_{FM} = first melting (eutectic) temperature, T_{Mh} = melting temperature of hydrohalite, T_M = melting temperature of ice and T_H = temperature of homogenisation. * leaked

12.4 Heating measurements

Four measurements of fluid inclusions in barite from Noarlunga show T_H values from 223.2°C to 263.9°C. The fluid inclusion, which gave the highest T_H leaked at 263.9°C along cracks developed during heating. This indicates the true T_H for this inclusion may be higher than that recorded, unless there had also been leakage prior to the micro-thermometric study. Repeat measurements of another fluid inclusion in barite from Noarlunga showed a range of T_H from 230°C to 238°C. Fluid inclusions in two samples of barite from Dunbar showed ranges of 149.8°C to 169°C (3 measurements) and 87°C to 98°C (3 measurements). Fluid inclusions in quartz grains from Hall

Lode show T_H values ranging from 127.4°C to 142.8°C. The only measurable fluid inclusion in barite from Bowering Lode showed a T_H value of 132.4°C.

12.5 Summary

Fluid inclusion studies indicate that the fluids from which barite of the Noarlunga, Bowering, Dunbar and Hall Lodes were deposited had salinities in the range 0.5 - 17.2 wt % NaCl equivalent. These values are lower than salinities in fluid inclusions reported for other barite deposits of the Adelaide Fold Belt; Artipena (24.0 - 26.0 wt % NaCl, 12 data; Robertson, 1981), McRae deposit at the southern margin of the Oraparinna Diapir (23.5 - 25.5 wt % NaCl, 14 data, Robertson, 1981) and Oraparinna Mine (23.3 - 24.5 wt % NaCl, 9 data; Cawley, 1983).

Low eutectic temperatures were observed in fluid inclusions from all veins except from Bowering Lode. The Bowering Lode eutectic temperature data indicate the presence of NaCl±KCl in the ore forming fluids. The eutectic temperature data for other veins indicate the fluids contain cations such as Ca^{2+} in addition to Na^{+} and T_{mh} values for Dunbar and Noarlunga Lodes indicate NaCl:$CaCl_2$ ratios of approximately 2:1.

T_H values for fluid inclusions in barite show a large overall range (87°C to 242°C). In comparison, Cawley (1983) obtained T_H values between 85.5°C and 174.5°C for the Oraparinna Mine, and Robertson (1981) obtained those values between 340°C and 370°C for the Artipena and McRae vein deposits. However, as explained above, the data for barite must be treated with caution. The T_H values for fluid inclusions in quartz from Hall Lode (127.4°C to 142.8°C) are a more reliable indicator of the trapping temperature of the fluids. These temperatures have not been corrected for pressure effects.

Chapter 13

DISCUSSION AND CONCLUSION: ORIGIN OF THE GEOLOGICAL STRUCTURES, DIAPIRS, GRABENS AND BARITE VEINS IN THE FLINDERS RANGES

Sediments in the Adelaide Fold Belt were deposited between the expansion and closure of a sea from approximately 850 Ma to 480 Ma and were subjected to deformation during the Cambro-Ordovician Delamerian Orogeny that was responsible for the major geological structures (500 - 480Ma, Preiss, 1987).

13.1 The D_1 deformation

The D_1 structures are:

- SW verging Enorama F_1 Anticline (fault-propagation fold). Here, the sediments on the eastern (back) limb were thrust initially over a décollement surface on the basement and subsequently over the sediments on the western (eastern) limb, along a listric thrust fault (Fig. 3.8a). Therefore, the process brought up the lower sequences on the eastern limb against that on the western limb, adjacent to the hinge line. The tip-end of the thrust fault is unknown. During thrusting, the eastern limb dips increased from gentle to steep towards the hinge line, through a series of fault-bend folds, while the western limb showed a constant gentle dip. Section balancing calculation suggests a 5.3km depth to the breccia deposit over the décollement. Thickness of the breccia zone over the décollement is unknown but at least 2-3 km thickness may be expected.

- A series of parasitic structures formed on either limb of the Enorama – Oraparinna F_1 Anticlines. The western limb contains: (a) symmetric upright parallel folds (Fig. 4.2a-f) that show no vergence, (b) ramp thrust faults associated with fault breccia displaying gouge fabric (McClay, 1987; Fig. 4.4a-c). Both limbs show a NE-SW oriented L_1 bedding-slip lineation that disappears on the hinge line (Figs. 4.5a,b & 4.6a).

- A series of major anticlines was formed across the Ranges i.e. from west to east: the Moralana Anticline, Arkaba Anticline, Beltana - Worumba Anticlines and Copley – Mt. Roebuk Anticlines. Major synclines formed were Mernmerna Syncline, Wilpena – Kanyaka

Synclines, Puttapa – Wirrealpa Synclines, respectively. These show corrugated cardboard type folds (Fig. 3.2).

All the major and minor structures parallel the major axial traces, except the nearly perpendicular L_1 lineation. The vergence of major fault-bend folds, transportation of the eastern limbs over the western limbs, minor ramp thrust faults and kinematics of the L_1 lineation suggest the structures were formed during the NE-SW compressions of the D_1 deformation, verging SW. The geometric and sequential similarities between the Enorama Anticline and the other anticlines suggest imbricate fan type (Boyer and Elliot, 1982), SW verging fault-propagation fold geometry for the series of anticlines.

13.2 The D_2 deformation

The D_2 structures are:

- A series of corrugated cardboard type major F_2 folds oriented between NE and ENE (Fig. 3.3).
- Minor gentle folds that trend between NNE and NE, but may vary up to ESE (Figs. 5.1a-d, 5.3).
- Minor fault-propagation folds that are oriented between NE and east (Figs. 6.1, 6.3; Section 6.3).
- Conjugate kink folds oriented NE-SW (Fig. 4a-e).
- Conjugate reverse-thrust faults with intersection axis oriented NE-SW (Figs. 5.5a-d).
- A strong bedding-slip lineation (L_2) defined by ridge-in-groove striations that occur nearly perpendicularly to the F_2 fold axis (Fig. 4.6b).

All these minor structures are parallel to the major F_2 fold axes, to which the L_2 lineation is perpendicular. Therefore all these structures have formed during a NNW-SSE compression of the D_2 phase of shortening deformation. These structures generally plunge gently, but moderate plunges can also be found on the fold limbs adjacent to diapirs (Figs. 5.1b,c).

13.3 Interference and dextral rotation of structures

The Flinders Ranges show a series of overprinting structures including a dextral rotation:

(a) The major F_1 axial traces in the Flinders Ranges show a series of dextral kinks (Fig. 3.2). The axial trace from Beltana to Upalinna Anticlines shows kilometre scale dextral kinks between many anticlines along the trace. The same axial trace from Upalinna to Worumba Anticlines shows a tens of kilometre scale dextral kink that forms the Nackara Arc to which the earlier kinks are parasitic. Therefore, the Nackara Arc is considered to be a D_2 structure.

(b) Occurrence of dome and basin, egg-carton structures with a dextral sense of rotation, formed by superimposition of F_1 and F_2 folds. These can be observed at both major scale in the northern and southern Flinders Ranges (Chapter 3, Fig. 3.4), and at minor scale in the central Flinders Ranges (Figs. 4.2h, 5.6).

(c) Overprinting of L_2 ridge and groove lineation by L_1 (Fig. 4.4g);

The dextral rotation is further evidenced by the following:

(d) The satellite barite vein deposits that were produced during the D_1 deformation adjacent to the Oraparinna Mine have intersection axes dextrally rotated from N21°E to N55°E, towards an ENE trending major fault zone (Fig. 7.5b). Furthermore, their host F_2 fold axes also rotated from N21°E to N64°E, towards the fault zone (Figs. 5.3b).

(e) The minor F_2 fault-propagation folds on the eastern limb of the Enorama – Oraparinna F_1 Anticlines shows SE vergence and those on the western limb show NW vergence (Chapter 6).

(f) Rotation of the otherwise nearly vertical barite vein intersection axis of the Dunbar Lodes (product of D_1 deformation) to plunge 54°->113° (Fig. 7.6c), thereby indicating northwesterly movement of sequences.

Therefore, the sedimentary package in the Flinders Ranges clearly shows minor to major scale evidence for the two D_1 and D_2 deformations, by NE-SW and NNW-SSE compressions, respectively. The F_1 folds show prominence over the F_2 folds, thus the D_1 phase was stronger than

the D_2. The evidence suggests D_2 post-dated D_1, an interpretation that agrees with Richart (1976) and Li and Powell (1993, Chapter 2). The evidence also suggests the sedimentary package in the Flinders Ranges was accompanied by a dextral rotation of the structures during the D_2 deformation. The rotation can be explained by applying the D_2 NNW – SSE compression along the Northwest Fault, and in the south through the Nackara arc. The Northwest Fault has resulted in thrusting lower Torrensian sediments over the Upper Marinoan sediments.

Origin of the NW and NE trending folds in the Flinders Ranges in a single or two folding events has been suggested uncertain because of lack of cleavage (Richert, 1976; Preiss, 1987). Even though cleavage was not found, current studies suggest two distinct groups of folds of F_1 and F_2 belonging to D_1 and D_2 deformations respectively, that have been superimposed at both major and minor scale.

The NW and NE trending synclines in the Flinders Ranges have also been interpreted to have formed due to salt withdrawal during sedimentation (Dyson, 1997, 1998, 1999, 2002a,b), assuming that salt could have disappeared over a period of time. However, it is well known that large-scale salt deposits occur in association with the regions of salt-diapirs (Cramez and Jackson, 2000) and there has been no evidence of large scale salt deposits in the Fold Belt, other than a few isolated salt casts (Preiss, 1987; McCallum, 1988). The specific geometries of fault-propagation folds are extremely unlikely to have formed by salt withdrawal. Instead, there are thrust structures as documented in this thesis. Therefore, in the face of the geometry of F_1 and F_2 fault-propagation folds, parasitic and interference structures, these folds are strongly suggested to have formed during thrusting, related to the D_1 and D_2 deformations that occurred in the Delamerian Orogeny.

The style of kilometre to tens of kilometer-scale dextral kinks along the Beltana to Worumba F_1 anticlines suggest that these are parasitic to the hundreds of kilometer-scale dextral kinks between Worumba and Kangaroo Island (Fig. 1.1). Furthermore, these dextral movements are likely to have caused dextral rotations along faults to the east of the Adelaide Fold Belt, towards Broken Hill. All these dextral rotations can be explained by the NNW-SSE compressions of the D_2 deformation that occurred during the Cambro-Ordovician. In contrast, the 'S' shape of the major kink between the Nackara Arc and Kangaroo Island was not considered likely to be an 'oroclinal' bending where the axial traces bend around a large obstructing object of the basement (Marshak and Flottmann, 1996). However, occurrence of parasitic 'S' shape dextral kinks between Beltana and Worumba Anticlines, as well as other F_1 axial traces, including dextral rotations in minor structures within the sedimentary package in the Flinders Ranges (see above), indicates that the 'S' shape bending of the

axial traces associated with Kangaroo Island was formed during dextral rotation of the D_2 deformation.

13.4 Diapirs

Mud diapirism is one of the processes for producing large volumes of mélanges in modern accretionary wedges (Brown and Westbrook, 1988; Brown, 1990; Cita and Camerlenghi, 1990; Henry *et al.,* 1990; Limonov *et al.,* 1994; Cronin *et al.,* 1995; and Monaco and Tortorici, 1996). In ancient accretionary terranes, mud diapirism was caused by the highly overpressured and underconsolidated sediments along basal detachment of the wedge (Larue and Speed, 1984; Torrini *et al.,* 1985). Therefore, mud diapirism in thrust belts has been interpreted as the occurrence of the accretionary process with the underplating of sediment at the base of the wedge (Monaco and Tortorici, 1996). Here, fluids and mud that were extruded from the basal detachment reach upper levels of the sedimentary pile via major thrust faults and fractures, giving rise to mud volcanos, mud ridges and mud diapirs, and rip up different rock-units of the wedge during their emplacement (Brown and Westbrook, 1988).

Doming in relation to diapirism has been studied by many authors (Snowden and Bickle, 1976; Soula, 1982; Hippert, 1994; Choukroune *et al.,* 1995; Shackleton, 1995; Dirks *et al.,* 1997; Aerden and Malavielle, 1999; Calvert *et al.,* 1999; and Soula *et al.*, 2001). In the granitoid-rich upper basement of the Montagne Noire, the frontal orogenic wedge of the Southern French Hercynian Belt, Soula *et al.* (2001) interpreted anatectic rise of diapirs within antiforms that formed during contractional deformation. The authors further suggested the deformation was simultaneous with regional metamorphism and diapirs were formed by propagation of fold-and-thrust structures and related syn-contractional decompression with local partial melting. Antiformal stacking was suggested to be responsible for a local increase in pressure and crustal thickening of a previously thinned lithosphere, which enhanced local partial melting and further development of the ridge by diapiric rise in the middle to upper crust. These structures increased the amplitude of folds and thus the relative altitude of the basement high behind a developing foreland basin, giving rise to unusually wide spreading of overturning strata. The authors concluded that the apparent differences between the Montagne Noire ridge and 'ordinary' frontal ridges of orogenic wedges are the consequence of diapirism and related syn-contractional decompression metamorphism.

Ridge formation resulting from mud diapirism within anticlines has also been studied by Morley (1994) for the Osen-Rea thrust sheet, Norway, where thrust-related fold evolutionary models were produced (Fig. 6.5).

In the Flinders Ranges, ridge formation is evident by both F_1 and F_2 folds, formed in contractional deformations. There, the origin of diapirs (mud diapirs including dolerite, basalt and granitoid clasts from the basement) has been debated over much of the last century, arguing between syntectonic (Howchin, 1922; Mount, 1975) and synsedimentary (Webb, 1960; Lemon, 1988; Dyson, 1996, 2002a,b) origins. However, ridge formation and diapirism in the Flinders Ranges is evident by similarities between corrugated and ridge-forming major anticlines (Figs. 3.2, 3.8a) and minor anticlines (Figs. 6.1, 6.2, 6.3, 6.4), where breccia deposits formed along décollement surfaces have mainly localised in the core.

The present study suggests breccia deposits in the Flinders Ranges were different manifestations of mud diapirism. There are three associations:

(a) Anticlines; detachment/fault-propagation folds

The main breccia deposit has formed, migrated and deposited along a detachment surface and core of the fold and the profile has generally taken the 'upside down, plunging curvy-cucumber' shape (Figs. 3.8a, 6.1f-i, 6.2, 6.3, 6.4c). Perched breccia deposits have commonly formed on different levels of the back limb, as seen at the minor scale (Figs. 6.1f-i), extended to the hinge on the respective level (Figs. 6.1g-i), and between the Etina Formation and Enorama Shale at 5.3km NE of the Enorama Diapir (Fig. 4.5b).

(b) Associated with detachment thrust surfaces adjacent to apices of grabens; e.g. Yudnapunda Diapir (Fig. 3.6) and

(c) Faults; e.g. Mooloolloo Diapir at the Northwest Fault, (Fig. 3.7a).

These associations indicate that the mud diapirs were driven by thrust tectonics during the Delamerian Orogeny. This agrees with previous authors who suggested a syntectonic origin caused by: (a) vertical and lateral faulting (Howchin, 1922), (b) much disturbed and faulted (Mawson, 1942), (c) thrust complexes (Sprigg, 1949), and (d) diapiric emplacement after Adelaidean sedimentation, during the Delamerian Orogeny (Mount, 1975). However, the tectonic theory of diapir formation does not agree with theories based on disappearance of the original salt (Dyson,

1997, 1998, 1999, 2002a,b) and mud breccia movement triggered by differential loading (Lemon, 1988; Fig. 1.5).

13.4.1 Lemon's (1988) synsedimentary model for diapirs

In his experiments, Lemon (1988) produced the presumed shapes of diapirs from pillow to overturned water-drop, by using tension of a string attached to the centre of a rubber membrane (Figs. 1.4). Even though no complete profiles other than plan views of map scale diapirs have been documented, those experimental shapes were presumed to be similar to those of diapirs, with no evidence (Figs. 1.5, 2.3). However, the pillow to overturned water-drop shapes can be compared with diapirs formed in detachment folds (Fig. 6.4a,b) but these have commonly developed into fault-propagation folds during progressive deformation in the Flinders Ranges (Figs. 6.4c, 6.1-6.3).

Lemon's (1988) diapir modelling by laboratory sandbox experiments in relation to the Adelaide Fold Belt shows the following weaknesses (Figs. 1.4, 1.5, 2.2, 2.3, Chapter 6):

(a) The diapirs, and their breccia deposits, rose under compression but were modeled under tension.

(b) Breccia is expected to interact with the host during rising, by means of lateral intrusions, but observation was not possible due to the rubber membrane.

(c) Breccia rose under outward deviatoric pressures through the sedimentary column but was modelled under inward deviatoric pressures of a partial vacuum.

(d) Peripheral sinks around the model diapirs have formed as a result of the inward collapse of the flanks due to a lack of continuous supply of breccia. Formation of peripheral sinks otherwise, under continuous supply condition, is not understood.

(e) The shapes that the model developed from pillow to overturned waterdrop have not yet been demonstrated from the diapirs in the Adelaide Fold Belt, and are therefore not confirmed.

Therefore, the material and methodology applied in Lemon's sandbox experiments contradicted that of the diapirs in the Adelaide Fold Belt. The model excludes the geometry of hosts under condition of continuous supply of breccia, and tongues of breccia intrusions emanated laterally

from the diapir. While diapiric fluids were represented by inappropriate parameters, the shapes produced by the rubber membrane have never been demonstrated by example in the Adelaide Fold Belt.

13.4.2 Comparison of evidence: syntectonic or synsedimentary origin for diapirs in the Flinders Ranges?

The evidence used by Lemon (1988) to suggest a synsedimentary origin for diapirs is not unique for such a cause, and can be explained by a syntectonic origin as well. The supporting evidence used is:

(a) Occurrence of tongues of gravel beds emanating from the Enorama-Oraparinna Diapirs (Dalgarno and Johnson, 1968). The authors observed that the grain sizes in the tongues grade from fine to coarse, while the largest boulder lies at the border of the diapir. The tongues generally extend to 200m, with a maximum of 500m, and are limited to the western limb of the respective anticlines.

- Explanation by synsedimentary model: The wedges were not modeled in the sandbox experiments, but were thought to be synsedimentary turbidite facies formed by cannibalisation of diapiric debris from the top of diapirs, onto the surrounding sediments (Figs. 2.2, 2.3; Lemon, 1988; Reilly *et al.*, 2002). The tongues were considered to be bedding-parallel or incised valleys deposited with reworked grains from the diapir, formed during pulses created by differential overloading. The pulses do not form in any regular order of increasing or decreasing strength throughout sedimentation, therefore strong pulses that released larger sizes of clasts or boulders could have followed weaker pulses that released fine material. This process could have been repeated until overlying sedimentation took place. Furthermore, there have been no strong currents as the gravel beds do not extend for more than 500m from the diapir. Large boulders pushed/spilled out of the diapir may well travel onto the bottom of the peripheral sink, well away from the diapir (Fig. 2.2). Therefore, the mechanism of increasing sizes of clasts towards the diapir and occurrence of the largest boulder on the edge of the diapir (Dalgarno and Johnson, 1968) may not be well explained by a synsedimentary origin. However, the dominant occurrence of these tongues on the western border of the diapir has been considered to be due to a westward current direction.

- Explanation by syntectonic model: In fault-propagation fold models, these tongues form on the forelimb (Fig. 6.1i,i^) and both above and under the décollement (Figs. 6.1f,f^, g,g^, h,h^ and i,i^). The tongues commonly emanate from the main breccia deposit associated with the core (Fig. 6.1i^), but not necessarily all the time (Fig. 6.1g^). These tongues dilate in incremental openings within non-continuous progressive deformation, synchronously filling with clasts flowing from the diapir or in situ mineralisation, comprising barite or dolomite. During thrusting, breccia was under outward deviatoric pressure; therefore both clasts and fluids were flowing into the fractures that were in contact with the main breccia body. Sizes of gravel were controlled by that of the fracture opening at the diapir end. As the fracture dilated, larger gravel was able to enter the tongue, thus forming the grading. Early-entered finer material moved into the tapering edge of the wedge, allowing coarser material to enter. Boulders that were larger than the available opening of the wedge could not enter and stayed inside the diapir. The tongues may vary from bedding-parallel and bedding incising, and have especially formed during advancement of the breccia deposit in the core onto forelimb (Figs. 6.1i,i^). Therefore, grading of breccia in tongues on the western limb of the Enorama – Oraparinna Diapirs agrees with incremental opening of wedges and may suggest the breccia deposit has advanced further onto the same limb.

(b) Occurrence of peripheral sinks showing, 'downward dipping limbs towards the troughs', around diapirs (Fig. 1.4; Lemon, 1988).

- Explanation by synsedimentary model: Even though Lemon (1988) demonstrated the Oratunga Diapir as the best example for 'inward dipping peripheral sinks', the 'sink' does not continue around the periphery (Fig. 13.1). Instead, it is limited only to the western border. Such sinks are non-existent completely around diapirs in the Adelaide Fold Belt. In support of the 'inward dipping peripheral sink' theory, Lemon (1988) speculated the occurrence of sinks around the Enorama Diapir, shown in one of his E-W cross sections, "ENORAMA DIAPIR - A summary of the influence on surrounding sediments" (Fig. 2.3). However, no such sinks are shown in his section constructed across the same diapir, "Sketch section across Enorama – Oraparinna Diapirs" (Fig. 3.1). The evidence is contradictory and

STRATIGRAPHY OF SURROUNDING SEDIMENTS

CAINOZOIC

River beds and slope talus

Gravel terrace

LATE PRECAMBRIAN

Brachina Formation
- Moorillah Member
- Mooloolloo Member

Red / Green

Nuccaleena Formation

Elatina Formation

Trezona Formation

Enorama Shale

Etina Formation

DIAPIRIC ROCK TYPES

Dolomite / dolomitic sediments

Siltstone, mudstone

Silty sandstone

Basic volcanics, dolerite

Diapiric breccia (undifferentiated)

Diapiric breccia (mainly sandy siltstone)

Fault

Syncline axial trace

20° 76° Bedding, dip / overturned dip

A A' Line of section

Unconformity

Fig. 13.1: Geological Map – Oratunga Diapir (after Lemon, 1988). Note: The host sequences of the diapir dip gently between N and NNE. The 'inward dipping peripheral sink' is limited on to the western flank of the diapir.

careful mapping conducted across the diapir during the current research confirmed no existence of such a sink (Fig. 3.8a).

- Explanation by syntectonic model: Occurrences of forelimb synclines are characteristic in fault-propagation folds (Marrett and Bentham, 1997). If the fold is formed on initially horizontal sequences, the fore limb of the syncline would dip horizontally or gently, while its back limb dip moderately or steeply (Figs. 3.8a,b, 6.2a). Furthermore, if the fold is formed on dipping sequences, verging downward, the fore limb of the syncline would dip gently along bedding, while its back limb would dip moderately or steeply (Fig. 6.3). In both of these situations, fore limb synclines would not show 'downwardly dipping limbs towards the trough'. The only situation is formation of the fault-propagation fold on dipping sequences, verging upward (Figs. 6.1c,g^). Besides, parasitic folds that form around core breccia deposits in fault-propagation folds may also form on both limbs, forming peripheral sinks (Fig. 6.1g^,h^). Therefore, peripheral sinks can form around diapirs as parasitic folds, while fore limb synclines do not continue around the periphery of diapirs that are controlled by fault-propagation folds.

  Oratunga Diapir is formed on the eastern limb of the Beltana – Worumba Anticlines, adjacent to the F_1 axial trace (Fig. 3.4). The eastern limb generally dips NE but being adjacent to the nose of the doubly plunging F_1 anticlinal axial trace, the host sequences of the Oratunga Diapir dip NNE. Thus, according to the syntectonic model, the Oratunga Diapir is formed on a dipping sequence, verging upward (SW). As a result, the forelimb syncline shows 'downward dipping limbs towards the trough' (e.g. Fig. 6.1c,g^). The 'peripheral sink' that is limited to the west of the Oratunga Diapir can be better explained by a syntectonic model than the synsedimentary model (Fig.1.4).

(c) Occurrence of entrained debris derived from breccias in the surrounding hosts (Webb, 1960; Coats, 1964a,b, 1965, 1973; Dalgarno and Johnson, 1968).

- Explanation by synsedimentary model: Brought up by diapirs and distributed through erosion (Fig. 2.2).

- Explanation by syntectonic model: Piping of diapiric breccia clasts and fluids through fissures into the host (Fig. 6.4b), followed by bedding-slip displacement.

(d) Change of facies adjacent to diapirs (Lemon, 1988):

- Explanation by synsedimentary model: Erosion of diapirs during rise (Fig. 2.2).

- Explanation by syntectonic model: Escape of carbonate fluids accompanied by sands and gravel have formed a calcareous matrix in the adjacent host, thereby causing facies changes around diapirs (Fig. 6.4b).

A comparison of the ability to explain criteria associated with diapirs formed in anticlines by using fault-propagation fold models representing the syntectonic theory, and sandbox models representing the synsedimentary theory of Lemon (1988), is given in Table 13.1.

Table 13.1: Comparison between syntectonic and synsedimentary origins for diapirs in the Adelaide Fold Belt.

Phenomenon associated with diapirs	**(A) Explanation by syntectonic origin**	**(B) Explanation by synsedimentary origin (Lemon, 1988)**
a) Enorama Anticline contains a gently dipping forelimb, steeply to gently dipping back limb with increasing dips defined by fault-bend folds towards axial trace, steeply to moderately dipping remnants of the host rocks on the margins of the Enorama Diapir that occurs along the axial trace, 26% shortening (Figs. 3.8a-c).	The balanced section suggests Enorama Anticline follows the geometry of an asymmetric, SW verging fault-propagation fold that contains a décollement/listric thrust fault, which transported the eastern limb over both the basement and western limb, forming a thick layer of breccia and bringing lower sequences with increasing dips adjacent to the axial trace.	The sections constructed across the Enorama Diapir do not explain the geometric constraints of the host (Figs. 2.3, 3.1). Balanced sections were not constructed.
b) The Moralana Anticline confines its diapir, dominantly into the core and eastern limb. It shows a moderately dipping western limb, overturned and steeply to moderately dipping eastern limb (Fig. 2.4).	Dipping criteria of the Moralana Anticline are similar to that of the Enorama Anticline; therefore, the geometry is suggested to be an asymmetric, west verging fault-propagation fold.	Major thrust structures of detachment/fault-propagation folds have not been interpreted in the Flinders Ranges until current research.
c) Occurrence of NW trending, SW verging, series of corrugated cardboard type ridges of anticlines that hold a series of diapirs along axial traces (Fig. 3.2).	The anticlines were initiated as a series of SW verging imbricate thrusts, leading to fault-propagation fold geometry, during the D_1 deformation.	No interpretation
d) Occurrence of minor detachment/fault-propagation folds in the Flinders Ranges showing characters similar to a & b (see above) and shortening between 17-29% (Figs. 6.1, 6.2, 6.3, 6.4).	The folds are thrust structures possibly formed during D_2 shortening deformation.	Minor thrust structures of detachment/fault-propagation folds have not been discovered in the Flinders Ranges until current research.
e) Occurrence of ENE trending, series of corrugated cardboard type ridges of anticlines that hold diapirs along axial traces, e.g. Angepena Hill Diapir (Fig. 3.3).	Parasitic, minor F_2 detachment/fault-propagation folds (Figs. 6.1, 6.2, 6.3) suggest the major folds are to be of the same geometry.	No interpretation
f) Refolding of F_1 folds into dextral kinks forming the Nackara Arc and a series of parasitic arcs that remobilised diapirs mainly into domes (Fig. 3.4).	F_2 folds were superimposed onto F_1 folds during a dextral rotation of structures that occurred during the D_2 deformation.	No interpretation

Contd. From last page

Phenomenon associated with diapirs	**(A) Explanation by syntectonic origin**	**(B) Explanation by synsedimentary origin (Lemon, 1988)**
g) Major diapirs contain breccia dominantly clasts from the basement and the Callanna Group but may contain clasts up to Cambrian (e.g. the Beltana Diapir).	Breccia was initially formed on décollement surfaces by gouging the Callanna Group over the basement (Figs. 3.8a,b). The décollements were lately developed into listric thrust faults, transporting breccia over the forelimb while forming breccia from sequences up to the maximum of Cambro-Ordovician during Delamerian shortening.	Presumed synsedimentary diapirs were active until Cambrian.
h) Lack of diapirs in synclines, e.g. Mernmerna and Wilpena – Kanyaka Synclines (Fig. 3.2).	Breccia that was localised in detachment/fault-propagation folds which were anticlines and not synclines.	Observed the Wirrealpa Diapir has formed in the Wirrealpa Syncline (See below).
i) The Wirrealpa Diapir occurs on an F_1 Syncline (Fig. 3.2).	The diapir is controlled by F_1 and F_2 anticlines and wrench faults, but lies across the F_1 syncline (Figs. 3.3, 3.7).	Assumed the Wirrealpa Diapir is controlled by the Wirrealpa Syncline.
j) The Angepena Hill Diapir occurs on an F_1 syncline (Fig. 3.2).	The Angepena Hill diapir appears to have formed by the F_2 anticline that was superimposed on to an F_1 syncline (Figs. 3.3,3.4).	Unnoticed
k) The Enorama Diapir occurs across the F_2 syncline (Fig. 3.3).	The diapir was formed by the F_1 anticline and was F_1 elongated but was superimposed by F_2 syncline, thus decreased the width during remobilisation. The F_1 phase was more prominent than the F_2 phase.	Unnoticed
l) Occurrence of diapirs/breccia deposits in association with cores of anticlines (Enorama Diapir), limbs (Frontier 2 Drill Hole on the eastern limb of the Blinman Anticline, Chapter 3), and troughs of synclines (Wirrealpa Diapir).	Diapirs were largely formed during detachment/fault-propagation F_1 folding but remobilized during subsequent F_2 folding and wrench faulting (Figs. 3.4,3.8a,6.1-6.4). The Wirrealpa Diapir was not controlled by its syncline (See above).	Observed diapirs occur on Delamerian anticlines, limbs and synclines, thus misinterpreted that diapirs were not controlled by the Delamerian folds.
m) Occurrence of diapirs in domes that were formed by superimposition of anticlines (Fig. 3.4).	Both F_1 and F_2 anticlines contain breccia deposits, thus breccia was remobilized into domes.	Presumed growth of diapirs from pillow to overturned water-drop shape, similar to salt doming (Figs. 1.4, 1.5). However, the experimental shapes were not evidenced from the Adelaide Fold Belt.
n) Growth of diapirs as overturned, plunging cucumber shape from micro to major scale (Figs. 3.8a, 6.1f-i, 6.2, 6.3, 6.4).	Formation of breccia along décollement/listric thrust surfaces of fault-propagation folds and concentration in the cores.	
o) Occurrence of forelimb synclines adjacent to diapirs.	Fault-propagation folds commonly form forelimb synclines (Figs. 3.8a,b). However, 'synclines with downward dipping limbs' can be formed only if the forelimbs continue upwards (e.g. Oratunga Diapir; Figs. 6.1c,g^, 13.1).	Speculated peripheral sinks all around diapirs according to the experimental model, but do not exist (Figs. 1.4, 13.1). In the models, those sinks were formed due to collapse of limbs as a result of lack of continuous supply of breccia. On the contrary, the forelimb syncline of the Oratunga Diapir was formed due to upward continuation of the forelimb (Figs. 6.1a,g^). The Enorama Diapir was extrapolated to have peripheral sinks that do not exist (Figs. 2.3, 3.1, 3.8a).

Contd. From last page

Phenomenon associated with diapirs	(A) Explanation by syntectonic origin	(B) Explanation by synsedimentary origin (Lemon, 1988)
p) Occurrence of parasitic anticlines in association with fault-propagation folds that confine diapirs (Figs. 6.1g,g^).	The axial traces of parasitic folds are essentially parallel to that of the major fault-propagation fold.	Presumed as Teepee structures of sedimentary origin.
q) Occurrence of tongues of gravel beds that increase grain size towards diapir (Dalgarno and Johnson, 1968).	Synchronous filling of gravel into dilating fractures emanating from the diapir, where the sizes of gravel were controlled at the entrance(Figs. 6.1i,i^).	Erosion and spilling of clasts from the diapir, during pulses of differential loading (Fig. 1.5).
r) Thickening or thinning of limb sequences adjacent to the hinge.	Common with fault-propagation folding (Table 6.1, Marrett and Bentham, 1996).	Primary thickening.
s) Well-defined bedding-slip lineation on the limbs, nearly perpendicular to the fold axes.	Tectonic movement during shortening deformation (Figs. 4.5a, 4.6a).	Not modeled.
t) Occurrence of a positive Bouger gravity anomaly to the NE of Blinman, Oraparinna diapirs (Reid and Preiss, 1999).	Possible translational movement of hinge line towards the forelimb (Figs. 6.1i,i^), as a result of thrusting the back limb over forelimb in fault-propagation folds, leaving major breccia deposit under the back limb.	Not modeled.
u) Occurrence of a perched breccia deposit, 5.3km NE of the Enorama Anticline.	These may occur on different levels of limbs and hinges due to gouging ands thrusting (Figs. 6.1f-i).	Not modeled.
v) Temporal changes in composition and texture, increase of dolomite content of host sequences adjacent to the diapir.	Piping of breccia and fluids into the limbs (Fig. 6.4b) and precipitation of dolomite in the host in near vicinity of diapir (Figs. 6.1g,g^).	Presumed change of facies adjacent to diapirs due to mixing of spilled breccia onto hosts during synsedimentation (Fig. 2.2).
w) Occurrence of large rafts, as long as 1.5 km in breccia deposits.	Unplugged rafts that detached from hosts up to 1/3 width of the breccia deposits occur within core breccia deposits in folds (Fig. 6.4c).	Not modeled but presumed floating of kilometre scale rafts due to salt movement.
x) Occurrence of some limited salt casts in breccia deposits.	These may form during partial evaporation of the breccia deposit evident by expansion of the core, during development of the fold.	Presumed salt movement was responsible in breccia movement, forming diapirs.
y) dolomite caps on the top of the diapir		Presumed change of sea level and rise of diapirs.
z) Formation of barite vein deposits around the diapir, e.g. Dunbar, Bowering, Hall, Howard, McRae and Southern Lodes (Fig. 1.3).	Provision of dilational fractures around the fold and under the detachment surface due to shearing and compression, and synchronous mineralisation with fracture dilation (Figs. 6.1f-i).	Not modeled

Therefore, the evidence used to suggest a synsedimentary origin for the diapirs in the Adelaide Fold Belt is better explained by a syntectonic origin. In fact, the peripheral sinks derived from sandbox experiments (Lemon, 1988) do not exist in the Fold Belt, and can not be applied to diapirs in the Fold Belt. Instead, forelimb synclines occur, due to diapir formation in association with thrust-related folding. Furthermore, the whole sandbox experiment of Lemon (1988) is not applicable in modeling the diapirs in the Adelaide Fold Belt, as a result of unrepresentative materials and methods. The current research strongly suggests diapirs in the Fold Belt have formed syntectonically, during the Delamerian Orogeny.

13.5 Grabens

The Bunkers Graben was assumed to have formed synsedimentarily and simultaneously with the rising Oraparinna Diapir, causing thickening of some of the graben sequences (Lemon, 1988). However, the present research suggests a series of grabens including the Bunkers Graben was formed syntectonically, during the D_1 deformation and tectonic thrusting-related thickening.

The grabens formed in pairs, opposite to each other along Riedel and conjugate Riedel shears (Harding, 1974; Hancock, 1985) across major F_1 anticlines, where apices formed close to the fold axial traces and open-ends away from them (Fig. 3.6). The sedimentary package within the Bunkers Graben moved SW along a 15°NE dipping décollement surface towards the apex during thrusting, as evidenced by the fault-bend folds in the Oraparinna Mine (Fig. 4.3c,f). The SW verging movement of the package is further evidenced by F_1 asymmetric folds and L_1 bedding-slip lineation in the Bunkers Graben (Figs. 4.1a, 4.3g). The fault-bend fold geometry explains the increase of dips from the open-end to the apex, respectively from gently to vertically (Fig. 3.5a,b). Therefore, sequences in the graben moved southwestwardly in reverse direction as: (a) a package along the décollement and (b) individually along bedding. Fault-bend folding and asymmetric folding obviously increased thickness of formations. The reverse movement of sequences along gentle dips at the open end resulted in an appearance of sinistral faulting against the hosts across the northern fault boundary of the graben. However, this sinistral appearance changed towards the apex due to movement of the whole package along the décollement and appeared as dextral faulting across the same fault boundary. Furthermore, the graben sequences underwent a complicated series of movements as the sequences moved into the conjugate boundary faults and thus were subjected to extensive faulting. The sequences were again subjected to the D_2 deformation as well.

The thrust model for the Bunkers Graben is analogous with that of the eastern limb of the Enorama Anticline (Figs. 3.5, 3.8a). Both the graben and anticline show similar increase of dips towards their respective anticlinal hinge, governed by the mechanism of fault-bend folding. Movements of sequences have occurred along décollement surfaces, which subsequently developed into listric thrust fault surfaces adjacent to hinge lines of respective anticlines. The décollement is likely to be the same one on which the eastern limb of the Oraparinna Anticline was transported, because of the occurrence of one single breccia deposit from the apex of the graben to the western border of the diapir. The décollement of the Oraparinna Anticline is supposed to be the basement

as evidenced by the occurrence of clasts gouged from the basement, within the diapir. Furthermore, the décollement is expected to have extended north to the Enorama Anticline, because both anticlines are on the continuation of the same axial trace and diapirs are connected to each other. A thick breccia zone of at least a few kilometers is expected on the basement, and the 5.3km distance to the basement, as calculated from the balanced section of the Enorama Anticline (Fig. 3.8a), was treated as depth to the upper surface of the breccia deposit.

Therefore, the SW verging thrust model for the Bunkers Graben explains the unusual, sinistral and dextral movements of its sequences along the northern fault boundary, while suggesting tectonic thickening of sequences.

13.6 Barite veins

The present research has demonstrated that barite veins in the Adelaide Fold Belt formed following the antitaxial mechanism of vein formation during the Delamerian Deformation. The veins consist of barite fibres that grew nearly perpendicularly to and from median line, to border. Vein dilation was synchronous during incremental fracture opening, adding barite on to the tip ends of fibres, leaving vein-boundary parallel host rock inclusions within veins. Barite veins were formed within essentially unconnected fractures and show three major orientations, named after the Lode identification in the Oraparinna Barite Mine. All the vein types initially formed nearly vertically, during the NE-SW compressions of the D_1 deformation. The dominant 1D Type formed in NE-SW tensional fractures that opened during pure shear of the NE-SW compression, while the subordinate types of Link (NNE-SSW) and 1A (ENE-WSW) formed in fractures opened in conjugate shear zones. These vein types suggest convergent vein configurations of Beach (1975) Type B (Fig. 7.1e) or weakly convergent to divergent configurations of Smith (1996, Fig. 7.1f).

The three vein types that formed during the early part of the NE-SW compression were subjected to rotation during the syntectonic formation of the Bunkers Graben and its southwestward thrusting. Veins in the Oraparinna Mine have rotated 45° anticlockwise around an axis oriented at 315°. This can be explained as a consequence of southwestward reverse movement of graben sequences, causing bedding-slip movement within the Oraparinna Mine. The bedding-slip resulted in rotation of the nearly vertical vein-network into a plunging intersection axis of 45°->041° in the mine (Fig. 7.4d). Similarly, the other vein systems around the mine also plunge moderately to the NE (Fig. 7.5). The southwesterly plunging intersection axis of the Dunbar Lodes, 54°->113°, on the western limb of the Oraparinna Anticline can be explained by the northwesterly verging

movement of the western limb of the Oraparinna Anticline that occurred during the D_2 deformation.

The Artipena Lodes have three types of veins which crosscut the Delamerian F_1 folds oriented ENE (Fig. 2.6). The Noarlunga Lodes also crosscut the host Delamerian F_1 folds and occur parallel to the axial trace (Fig. 2.7). Therefore, both Artipena and Noarlunga Lodes were also formed during the latter part of the D_1 deformation. Minor barite veins have formed in association with F_2 fault-propagation folds in the central Flinders Ranges (Figs. 7.7a-d).

The research suggests barite veins in the Adelaide Fold Belt were formed mainly during the D_1 deformation and to a lesser degree during the D_2 deformation. Veins that formed during the D_1 deformation in the Oraparinna Mine were nearly upright but rotated into moderate dips during deformation.

13.7 Ingredients for barite vein formation

In fibrous veins, the availability of ingredients in the host rocks plays a major role in deciding the geometry of veins (Ramsay and Huber, 1987). If the ingredients for vein formation occur in the hosts in major quantities, veins follow the syntaxial mechanism, because boundary walls of the dilating fractures have enough nuclei to generate fibres from the wall into the vein, e.g. calcite veins in carbonates. Alternatively, if the vein material occurs in trace levels in the host, there are not enough nuclei on the vein wall to grow inward; thus the veins grow to either side from nuclei on the median layer, following the antitaxial mechanism of vein formation.

The Brachina Formation hosts the highest amount of barite (59 % of known production+reserves) and its dominant lithology, siltstone, hosts 57 % of known barite production+reserves in the Adelaide Fold Belt (Chapter 9). Siltstone mixed with other sedimentary lithologies host 72 % of known barite production+reserves in the Fold Belt.

Ba occurs in very minor quantities in the rocks of the Adelaide Fold Belt, in which the Brachina Formation contains relatively high amounts of Ba. Whole rock analyses of the Brachina Formation show Ba contents up to more than 3 wt %, but the highest values reflect the presence of barite mineralisation as grains and veinlets (Appendix 9.3). Therefore, the high Ba values of the Brachina Formation do not represent the true background Ba values. On the basis of existing data and samples analysed in this study, the mean whole rock Ba content of rocks from the Adelaide Fold

Belt is 419 ppm, compared to 303 ppm in the central Flinders Ranges (Tables 9.3a, 9.4). The formations that are common to both the Adelaide Fold Belt and central Flinders Ranges data sets have mean values for Ba of 528 ppm and 381 ppm, respectively. The mean of the minimum Ba contents of the whole rock Brachina Formation samples 600 m away from the Oraparinna Mine in Cawley's (1983) analyses and tens of kilometres away from the mine in the present analyses is 315 ppm, compared to that of 159 ppm in the mine. Electron microprobe analyses of samples of the Brachina Formation show that K-feldspar is the most important Ba-bearing mineral, with a maximum of 1.2 wt % (mean 0.4 wt %) in non-mineralised areas, compared to 0.6 wt % (mean 0.2 wt %) in the Oraparinna Mine. Similarly, analyses of Na-feldspars from non-mineralised areas have a mean of 0.04 wt % Ba compared to a mean of 0.02 wt % in the mine. Therefore, these analyses suggest regional depletion of Ba in the formations in the central Flinders Rages that host a large number of vein barite deposits and a further depletion in the host rocks adjacent to the Oraparinna Mine vein system. This depletion of Ba in the sedimentary rocks is the most likely source of Ba in the vein deposits.

There is also evidence that the main source of Sr was the host formations. Barite veins that formed during the Cambro-Ordovician Delamerian deformation (approx. age 500 - 480Ma) show decreasing $^{87}Sr/^{86}Sr$ ratios towards dolomite units (approx. age 600 Ma), and suggests a contribution of low radiogenic Sr from dolomites. Therefore, Sr could have been obtained from sources such as carbonates, evaporites and plagioclase in silicates, substituting for Ca because of similar ionic radius. Sr has been contributed from other sources as well. Isotope data suggest that the diapiric sources have provided Sr to nearby lodes, especially to the Dunbar and Bowering Lodes, but any such contribution to the Hall Lode, at 100m from the diapir, is not distinguishable. There has been no diapir influence on the Oraparinna Deposits, at 2.4 km distance from the diapir, or on the Artipena and Noarlunga Deposits that are further away from known diapirs. Sr isotope studies suggest that there may have been some involvement of Cambrian seawater in the formation of these deposits, through percolation, assisted by fractures. Formation of the lodes around the Oraparinna Diapir might also have involved some Cambrian seawater, but this is not distinguishable on the basis of the Sr isotope data.

The sulphur isotope data suggest that sulphate for barite vein formation was mainly derived from the connate water of the host formations, but in the case of Noarlunga and Artipena lodes there was mixing with connate water of the adjacent formations during Cambrian folding. Participation of diapiric fluids was evident in the Dunbar Lodes but not distinguishable in the other two lodes adjacent to the diapir, i.e. the Bowering and Hall Lodes. Any contribution of Cambrian seawater to any of the deposits studied is not distinguishable due to overlapping ranges of $\delta^{34}S$ values.

In conclusion, the host formations and their connate waters have dominantly supplied the ingredients, Ba, Sr and sulphate for barite vein formation in the Adelaide Fold Belt (Table 13.2). However, other sources available at sites, at the time of vein formation, such as diapirs, connate waters of overlying formations and, possibly Cambrian seawater have also made minor contributions to the ingredients for some deposits. Ba is a relatively abundant trace element in the Brachina Formation, which is thus the main host for vein barite deposits. A contribution of ingredients from diapiric was been limited to a distance of 100m from the diapir, as shown by the studies of the Oraparinna Diapir.

Table 13.2: Summary of Sr and S isotopes, and salinity and temperature of the mineralising fluids of barite vein formation in the Adelaide Fold Belt.

Deposit/ Distance to closest diapir	Sr isotope analyses		S isotope analyses		Mineralising fluids		Overall possible sources
	$^{87}Sr/^{86}Sr$ (No. of samples)	Sr sources *	$\delta^{34}S$ (‰) (No. of samples)	SO_4^{2-} sources*	Salinity (wt. %) NaCl equivalent (measurements)	Temperature °C (measurements)	
Dunbar Lodes/ (0m)	0.721108-0.733382 (6)	NH (M) DS (M) CS (ND)	21.0-30.8 (9)	CW (M) DS (M) CS (ND)	12.4-13.8 (7)	87-169 (6)	NH/CW (M) DS (M) CS (ND)
Bowering Lode/ (30m)	0.723435 (1)	NH (M) DS (M) CS (ND)	16.8-17.4 (2)	CW (M) DS (ND) CS (ND)	0.5-17.2 (4)	132 (1)	NH/CW (M) DS (M) CS (ND)
Hall Lode/ (100m)	0.715397-0.718412 (2)	NH (M) DS (m) CS (ND)	20.7-21.7 (2)	CW (M) DS (ND) CS (ND)	6.1-9.9 (5)	123-143 (4)	NH/CW (M) DS (m) CS (ND)
Oraparinna/(2.4km)							
Mine	0.710695-0.711955 (24)	NH (M) DS (U) CS (M)	22.1-27.8 (22)	CW (M) DS (U) CS (ND)	23.3-24.5*2 (9)	85-175*2 (9)	NH/CW (M) DS (U) CS (M)
Bainbridge Lode	0.711464-0.711857 (3)		25.4-27.6 (4)				
Fault zone	0.711020-0.711118 (2)		25.2-25.7 (3)				
Artipena Lodes*1/ (25km)	0.710170-0.711065 (4)	NH (M) DS (U) CS (M)	22.1-31.0 (8)	CW (M) DS (U) CS (ND)	24.0-26.0 (12)	340-370	NH/CW (M) DS (U) CS (M)
Noarlunga Lodes/ (>25km)	0.711216-0.716613 (6)	NH (M) DS (U) CS (M)	19.5-21.4 (7)	CW (M) DS (U) CS (ND)	13.1-13.2 (2)	223-242 (4)	NH/CW (M) DS (U) CS (M)

*Abbreviations: NH - Neoproterozoic Host, DS - Diapiric Sources, CS – Cambrian Seawater, CW - Connate Water of the host formations; Level of participation of each source: (M) - major participation, (m) - minor participation, (ND) – not distinguishable and (U) - any participation unlikely; *1Robertson (1981) and *2Cawley (1983). Hall Lode data were obtained on fluid inclusions in quartz; all other data refer to fluid inclusions in barite.

13.8 Mechanism of Ba and Sr transportation

Ba is commonly present in a number of silicate structures, mainly feldspars and micas. The most important substitution is for K^+, due to the nearly identical ionic radii, and the somewhat more covalent character of the Ba-O bond (Puchelt, 1972). Ba may also substitute for large ions such as Pb^{2+} (Barbieri, 1989).

K-feldspar grains in the Brachina Formation show non-uniform Ba contents that are usually concentrated into edges of grains closest to forming barite grains. This can be explained by Ba^{2+} ion migration within K-feldspar grains during deformation, and by ion absorption and expulsion (Putnis, 1992; Figs. 13.2, 13.3). Reverse migration of ions from barite to the feldspar grains is unlikely due to the strong covalent bonds between Ba^{2+} and SO_4^{2-}. The Ba^{2+} ions then migrated in fluids or through similar grains that were subjected to strain. The mechanism is likely to be ion absorption in, and expulsion from, grains as lattice structures undergo a range of structural changes causing atom and ion transfer through the grain structures during deformation (Putnis, 1992). Both the whole rock K and Pb concentrations in the host rocks show depletion towards barite veins on a scale of hundreds of metres (Figs. 9.3h, 9.5g). The K^+ and Pb^{2+} ions possibly have been replaced by migrating Ba^{2+} ions due to similar ionic charge and/or radius.

Therefore, the research suggests that connate waters containing SO_4^{2-} from the host rocks occupied the fractures during initiation, thus requiring Sr^{2+} and Ba^{2+} to form barite as antitaxial veins. The fractures continued to dilate during non-continuous progressive deformation, leaving border parallel host rock inclusions. The process demanded more SO_4^{2-}, Sr^{2+} and Ba^{2+} from adjacent sources to add to the tip-ends of barite fibres. The Sr^{2+} and Ba^{2+} migration was likely to have followed ion absorption and expulsion during deformation.

13.9 Conclusions

The Neoproterozoic to Cambrian sediments in the Flinders Ranges underwent two phases of shortening deformations, D_1 and D_2, during the Delamerian Orogeny in the Cambro-Ordovician. Two series of major folding patterns were oriented between NW and NNW (F_1), and NE and ENE (F_2), respectively. These folds were commonly formed as fault-propagation folds and took the pattern of imbricate thrust folds in the Flinders Ranges.

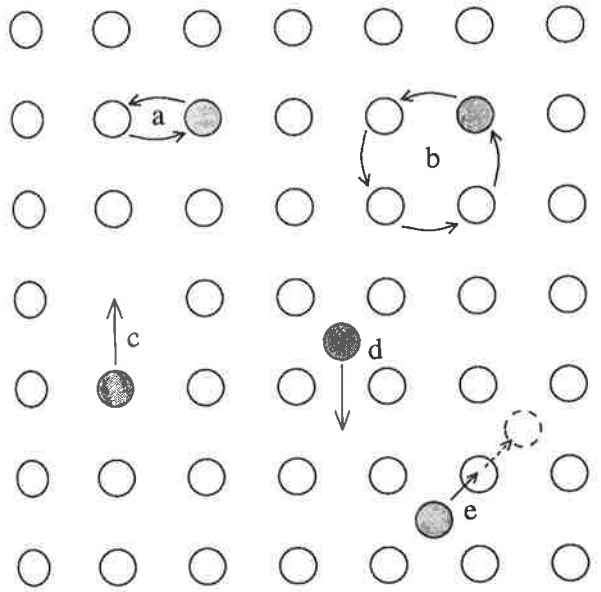

Fig. 13.2: Various atomic mechanisms for diffusion during deformation. (a) and (b) are exchange mechanisms without involving vacancies, (c) is a vacancy migration mechanism, (d) and (e) are interstitial migration mechanisms (After Putnis, 1992).

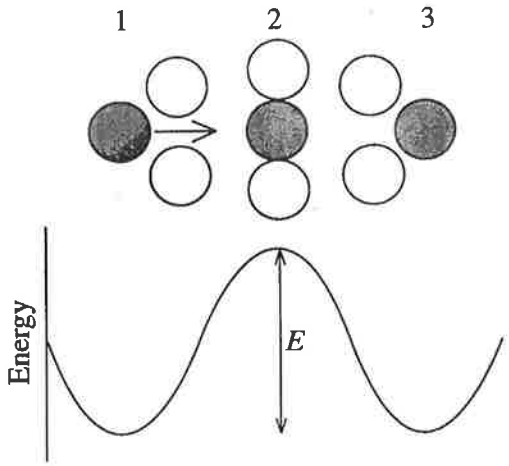

Fig. 13.3: Three stages in the migration of the shaded atom from one site to another during deformation. The starting position (1) and the final position (3) are equilibrium positions with free energy minima. The intermediate position involves lattice distortion and a maximum in energy, giving rise to an energy barrier (After Putnis, 1992).

The eastern limbs of F_1 folds were transported on décollements over the granitic basement and subsequently on listric thrust faults through the sediments over the fore limbs; thereby forming detachment/fault-propagation folds. The transportation caused underplating of material at the base of the sediments along a basal detachment, forming mud breccia that was enriched with ripped up different rock-units along the thrust surfaces extending into the upper sequences. In the Beltana, Worumba and Arkaba Diapirs, breccia clasts from the Cambrian sequences have been reported; suggesting the extension of the listric thrust faults into the Cambrian sequences. The mud diapirs show three different manifestations, mainly along anticlinal cores but on apices of grabens and faults. The western (fore) limbs of these folds generally dipped gently or moderately, while the eastern (back) limb dips increased from gentle to steep or overturned adjacent to hinge lines, and followed the fault-bend fold geometry. Sequences on eastern limbs were transported to upper levels against those on respective western limbs. The diapirs developed mainly during the D_1 deformation and were remobilized during the D_2 deformation, by localizing into superimposed folds, e.g. Blinman, Enorama and Oraparinna Diapirs. The D_1 phase was stronger than D_2, thus F_1 folds, including diapirs along fold hinges, commonly retained their elongations, even though they were refolded.

The D_1 phase also formed NE-SW trending grabens along Riedel and conjugate Riedel fractures oriented between NNE and ENE. NE-SW compression and associated thrusting of sequences bounded by major fractures between NNE-SSW and ENE-WSW formed grabens, commonly across anticlines. Graben sequences were transported towards respective apices over the basement, initially along the same décollements as the anticlines, but subsequently along listric thrust surfaces. The graben sequences followed fault-bend fold geometry, in addition to parallel folding, similar to the eastern limbs of anticlines; thus dips increase adjacent to apices.

The barite veins were also formed in the D_1 deformation in extension fractures dominantly oriented NE and subordinately oriented NNE and ENE within Riedel and conjugate Riedel shears.

The D_2 deformation formed a range of structures including conjugate kink folds, reverse thrust faults and bedding-slip lineation. Folds of both deformations were superimposed, forming a complex egg-carton structure containing domes and basins. The northern and southern components of the D_2 compression appear to have acted along the Northwest Fault in the northern Flinders Ranges and through the Worumba Anticline in the southern Flinders Ranges, respectively, thereby forming a series of dextral kinks along the F_1 axial traces including the most prominent Nackara Arc. These arcs are likely to be parasitic to the southern arc of the Adelaide Fold Belt through Kangaroo Island.

Barite veins were mainly formed antitaxially and nearly vertically in dilational tensional fractures during the D_1 deformation. The dominant 1D Type veins oriented NE-SW were formed along extensional fractures, while the subordinate Link and 1A Types were oriented NNE-SSW and ENE-WSW, respectively, and were formed in conjugate shear zones. Veins were subjected to deformation and rotation as evident from the Oraparinna Mine.

Geochemical evidence supports the antitaxial origin for barite veins. During incremental vein dilation, connate waters containing marine sulphates instantly occupied the dilated space, thus requiring Ba^{2+} and Sr^{2+} to form barite. The main source for these ions was the host formations but there also is evidence of these ions having been obtained from adjacent sources such as diapirs. Sr^{2+} ions may also have been contributed by Cambrian seawater to some deposits, especially those formed in association with the Brachina Formation. Other deposits studied were hosted by lower sequences, such as Tapley Hill Formation and Wilyerpa Formation and located within 100 m from the Oraparinna Diapir that has contributed some ingredients to the veins. The influence of Cambrian seawater to these deposits around the diapir was not distinguishable.

Siltstones are the preferred host lithology for barite in the Adelaide Fold Belt, and the siltstone-dominated Brachina Formation is the preferred host formation for barite. K-feldspars in the Brachina Formation contain up to 1.2 wt % Ba. Analyses of K- and Na-feldspars, as well as whole rock analyses of the Brachina Formation, indicate lower Ba contents within the Oraparinna Mine, compared to areas away from the mine. The mechanism of Ba^{2+} migration is suggested to be ion migration in strained grains during the Delamerian Deformation, following the theory of Putnis (1992), and is supposed to have occurred on a kilometre scale.

Fluid inclusion studies of quartz from Hall Lode suggest that temperatures of the fluid during formation of the veins were less than 150°C.

In summary, the research suggests the Flinders Ranges have been subjected to two deformations, producing its major geological structure and barite veins. The D_1 and D_2 deformations occurred in the Cambro-Ordovician Delamerian Orogeny, by NE-SW and NNW-SSE compressions and formed a series of superimposed folds oriented NW-SE and ENE-WSW, respectively. During the D_1 deformation the Adelaidean was transported over the basement, forming a polymict variety of clasts including rocks from basement and the lowest Adelaidean sequences, subsequently forming the breccias of major diapirs in the cores of detachment/fault-propagation folds. These diapirs carried clasts up to the sequences in which décollement faults ended as listric thrust faults and were re-deformed by the D_2 deformation. Thrusting during the D_1 deformation resulted in riedel and

anti-riedel fractures, forming major grabens over décollements that produced breccia, which were emplaced as piercement structures on the apices of grabens. Compression in the D_1 deformation formed barite veins following the antitaxial mechanism of vein formation in extensional and conjugate fractures. The veins were most likely formed at temperatures less than 150°C and received ingredients mainly from the Neoproterozoic hosts but also from connate waters, Cambrian seawater and adjacent diapiric sources.

REFERENCES

Aerden, D. G. A. M. & Malavielle, J. 1999. Origin of a large-scale fold nappe in the Montagne Noire, Variscan belt, France. *J. Struct. Geol.* **21**, 1321-1333.

Agar, S. M. 1990. Fracture evolution in the upper ocean crust: evidence from DSDP hole 504B. In: *Deformation mechanisms, rheology and tectonics* (edited by Knipe, R. J. & Rutter, E. H.). The Geol. Soc., London, 41-50.

Al Saffar, M. 1993. Geometry of fault-propagation folds: method and application. *Tectonophysics* **223**, 363-380.

Anderson, D. E. 1971. Kink Bands and Major Folds, Broken Hill, Australia. *Geol. Soc. Am. Bull.* **82**, 1841-1862.

Anderson, T. B. 1974. The relationship between kink-bands and shear fractures in the experimental deformation of slate. *J. Geol. Soc. Lond.* **130**, 367-382.

Ashby, M. F. & Verrall, R. A. 1973. Diffusion-accommodation flow and superplasticity. *Acta metall.* **21**, 149-163.

Asmerom, Y., Jacobsen, S. B., Knoll, A. H., Butterfield, N. J. & Swett, K. 1991. Strontium isotopic variations of Neoproterozoic seawater: Implications for crustal evolution. *Geochim. Cosmochim. Acta* **55**, 2883-2894.

Barbieri, M. 1989. Geochemistry of Barium. In: *Nonmetalliferous sratabound ore fields* (edited by de Brodtkorb, M.). Van Nostrand Reinhold, New York.

Barker, A. J. 1990. *Introduction to metamorphic textures and microstructures*. Blackie and Son Ltd, London.

Barnes, L. C. 1972. Geological investigations of the Burr Crush Zone. *Min. Res. Rev., Dept. of Mines and Energy, South Australia* **132**.

Barnes, L. C. & Robertson, R. S. 1983. Artipena Barite Deposits, geological investigations, 1980-81 Out of hundreds. Co. Derby, Flinders Ranges. Dept. of Mines and Energy, South Australia, Report 83/93.

Barnes, L. C. & Robertson, R. S. 1985. Artipena Barite Deposits. *Min. Res. Rev., Dept. of Mines and Energy, South Australia* **155**, 66-67.

Bates, R. L. & Jackson, J. A. 1987. *Glossary of Geology (Third Edition)*. Am. Geol. Inst., Alexandria, VA.

Beach, A. 1975. The geometry of en-echelon vein arrays. *Tectonophysics* **28**, 245-263.

Becker, A. & Gross, M. R. 1999. Sigmoidal wall-rock fragments: application to the origin, geometry and kinematics of en echelon vein arrays. *J. Struct. Geol.* **21**(7), 703-710.

Billings, M. P. 1972. *Structural Geology*. Prentice-Hall, Englewood cliffs.

Bowen, R. 1988. *Isotopes in the Earth Sciences*. Elsevier Applied Science Publishers Ltd.

Boyer, S. E. & Elliott, D. 1982. Thrust systems. *AAPG Bull.* **66**(9), 1196-1230.

Boyle, R. W. 1972. The geology, geochemistry and origin of the barite, manganese, and lead-zinc-copper-silver deposits of the Walton-Cheverie area, Nova Scotia. *Canadian Geol. Surv. Bull.* **166**, 181.

Broadhurst, E. 1946. Blinman Barytes Mine, Oraparinna Station (near the Bunker). *Min. Res. Rev., Dept. of Mines and Energy, South Australia*(82), 82-83.

Broadhurst, E. 1968. Future development of the Oraparinna Mine. South Australian Barytes Ltd. Unpublished report In South Australian Dept. Mines and Energy, Open File Envelope 3757.

Brown, K. M. 1990. The nature and hydrogeologic significance of mud diapirs and diatremes for accretionary systems. *J. Geophys. Res.* **95**, 8969-8982.

Brown, K. M. & Westbrook, G. K. 1988. Mud diapirism and subcretion in the Barbados ridge accretionary complex: the role of fluids in accretionary processes. *Tectonics* **7**, 603-640.

Callen, R. A. & Reid, P. W. 1994. Geology of the Flinders Ranges National Park. 1:75,000, Geol. Surv. of South Australia.

Calvert, A. T., Gans, P. B. & Amato, J. M. 1999. Diapiric ascent and cooling of a sillimanite gneiss dome revealed by (Super 40)Ar/(super 39)Ar thermochronology: the Kigluaik Mountains, Seward Peninsula, Alaska. *Geol. Soc. Sp. Publ.* **154**, 205-232.

Cawley, J. 1983. A geochemical investigation of the Oraparinna Barite Mine, Eastern Flinders Ranges, South Australia. Unpublished B.Sc. thesis, Dept. of Geol. and Geophy., Univ. of Adelaide.

Cecile, M. P., Shakur, M. A. & Kruouse, H. R. 1983. The isotopic composition of western Canadian barites and the possible derivation of oceanic sulfate ^{34}S and ^{18}O age curves. *Canadian J. Earth Sci.* **20**, 1528-1535.

Chaussidon, M. & Lorand, J. P. 1990. Sulfur isotope composition of orogenic spinel Iherzolite massifs from Ariege (N.E. Pyrenees, France): An ion microprobe study. *Geochim. Cosmochim. Acta* **54**, 2835-2846.

Chester, J. S. & Chester, F. M. 1990. Fault-propagation folds above thrusts with constant dip. *J. Struct. Geol.* **12**, 903-910.

Choukroune, P., Bouhallier, H. & Arndt, N. T. 1995. Soft lithosphere during periods of Archean crustal growth or reworking. In: *Early Precambrian Processes* (edited by Coward, M. P. & Ries, A. C.). Geol. Surv. Sp. Publ. 95, 67-86.

Cita, M. & Camerlenghi, A. 1990. The Mediterranean Ridge as an accretionary prism in collisional context. *Mem. Soc. Geol. Ital.* **45**(463-480).

Clarke, G. L. & Powell, R. 1989. Basement/ cover interaction in the Adelaide Fold Belt, South Australia: the development of an arcuate foldbelt. *Tectonophysics* **158**, 209-226.

Clarke, J. D. A. 1986. Stratigraphy and sedimentology of the upper part of the Wilkawillina Limestone, Wilkawillina Gorge, Flinders Ranges. *Quarterly Geol. Notes, Geological Surv. of South Australia* **100**.

Claypool, G. E., Holser, W. T., Kaplan, I. R., Sakai, H. & Zak, I. 1980. The age curves of sulfur and oxygen isotopes in marine sulfate and their mutual interpretation. *Chem. Geol.* **28**, 199-260.

Coats, R. P. 1964a. The geology and mineralisation of the Blinman Dome Diapir **26**. Geol. Surv. of South Australia Report of Investigations, and map.

Coats, R. P. 1964b. Umberatana Group (new Name). *Quarterly Geol. Notes, Geol. Surv. of South Australia* **9**, 7-12.

Coats, R. P. 1965. Diapirism in the Adelaide Geosyncline. *Aust. Petrol. Explor. Ass.* **5**, 98-102.

Coats, R. P. 1973. Copley map sheet SH 54-9,1:250 000 Series and Explanatory Notes. Geol. Surv. of South Australia.

Coleman, M. L. & Moore, M. P. 1978. Direct reduction of sulfates to sulfur dioxide for isotope analysis. *Analytical Chemistry* **50**(11), 1594-1595.

Coney, P. J., Edwards, J., Hine, R., Morrison, F. & Windrim, D. 1990. The regional tectonics of the Tasman orogenic system, eastern Australia. *J. Struct. Geol.* **12**, 519-544.

Coward, M. P. 1976. Large scale Palaeozoic shear zone in Australia and present extension to the Antarctic Ridge. *Nature* **259**, 648-649.

Cox, S. F. 1987. Antitaxial crack-seal vein microstructures and their relationship to replacement paths. *J. Struct. Geol.*, 779-787.

Cox, S. F. & Etheridge, M. A. 1983. Crack-seal fibre growth mechanisms and their significance in the development of oriented layer silicate microstructures. *Tectonophysics* **92**, 147-170.

Cramez, C. & Jackson, M. P. A. 2000. Superposed deformation straddling the continental-oceanic transition in deep-water Angola. *Marine and Petroleum Geol.* **17**(10), 1095-1109.

Crawford, A. R. & Campbell, K. S. W. 1973. Large-scale horizontal displacement within Australo-Antartica in the Ordovician. *Nature Phys. Sci.* **241**, 61-64.

Cronin, B. T., Lucchi, R. G., Cramp, A. & Kidd, R. B. 1995. Mid diapirs and mud volcanoes in the eastern Mediterranean Sea: the alternative source for thick conglomeratic deposits in deep-water setting. In: *Abstracts, Annual meeting of the Tectonic Studies Group*, Cardiff, U.K.

Currie, J. B. 1956. Role of concurrent deposition and deformation of sediments in development of salt-dome graben structures. *AAPG Bull.* **40**, 1-16.

Dahlstrom, C. D. A. 1990. Geometric constraints derived from the law of conservation of volume and applied to evolutionary models for detachment folding. *AAPG Bull.* **74**(3), 336-344.

Daily, B., Jago, J. B. & Milnes, A. R. 1973. Large-scale horizontal displacenent within Australo-Antarctica in the Ordovician. *Nature Phys. Sci.* **244**, 61-64.

Dalgarno, C. R. & Johnson, J. E. 1964. Wilpena Group (new name). *Quarterly Geol. Notes, The Geol. Surv. of South Australia* **9**, 12-16.

Dalgarno, C. R. & Johnson, J. E. 1965. Oraparinna map sheet, 1:63360, map no 670, zone 6. Geol. Surv. of South Australia.

Dalgarno, C. R. & Johnson, J. E. 1966. Parachilna Geological Map, Sheet H 54-13 zones 5 & 6, 1:250,000. Dept of Mines and Energy, The Geol. Surv. of South Australia.

Dalgarno, C. R. & Johnson, J. E. 1968. Diapiric structures and late Precambrian-Early Cambrian sediments in Flinders Ranges, South Australia. *Diapirism and diapirs, AAPG, Oklahoma, USA* **8**, 301-314.

Dirks, P. H. G., Zhang, J. S. & Passchier, C. W. 1997. Exhumation of high-pressure granulites and the role of lower crustal advection in the North China Craton near Datong. *J. Struct. Geol.* **19**(8), 1343-1358.

Durney, D. W. 1979. Dilation in shear zones and its influence on the development of en echelon fractures. In: *Int. Conf. on Shear Zones in Rocks*, University of Barcelona, 30.

Durney, D. W. 1985. Attitude variation of en-echelon fractures in generalized Riedel experiments (abstracts). *J. Struct. Geol.* **7**, 491-492.

Durney, D. W. & Ramsay, J. G. 1973. Incremental strains measured by syntectonic crystal growths. In: *Gravity and Tectonics* (edited by Jong, K. A. D. & Scholten, R.). Wiley, New York, 67-96.

Dyson, I. A. 1992. Geology of the Upalinna Diapir, central Flinders Ranges, South Australia. *Geol. Surv. Quarterly Geol. Notes (South Australia)* **124**, 2-19.

Dyson, I. A. 1996. A new model for diapirism in the Adelaide Geosyncline. *MESA Journal (Quarterly Earth Res. J. of Primary Industries and Resources South Australia)* **3**, 41-48.

Dyson, I. A. 1997. The evolution of salt tectonics in the Adelaide Geosyncline. In: *Abstracts, Australian Sedimentologists Group Conference, Geol. Soc. Australia* **47**, 9.

Dyson, I. A. 1998. The breakup unconformity, salt tectonics and development of mini-basins in the Neoproterozoic succession of the Adelaide Geosyncline. In: *The assembly and breakup of Rodinia, Workshop proceedings* (edited by Bird, R. T.). Geol. Soc. Australia, 7-8 September, Perth, 29-33.

Dyson, I. A. 1999. The Beltana Diapir. *MESA Journal (Quarterly Earth Res. J. of Primary Industries and Resources South Australia)* **15**, 40-46.

Dyson, I. A. 2002a. Evolution of the Oladdie Diapir near Carrieton, southern Flinders Ranges. In: *Geoscience 2002: Expanding Horizons. Abstracts of the 16th Australian Geological Convention* (edited by Preiss, V. P.) **No. 67**, Adelaide convention Centre, Adelaide, South Australia, 379.

Dyson, I. A. 2002b. Adelaidean sedimentation and the timing of salt tectonics in the east Willouran Ranges. In: *Geoscience 2002: Expanding Horizons. Abstracts of the 16th Australian Geological Convention* (edited by Preiss, V. P.) **No. 67**, Adelaide Convention Centre, Adelaide, South Australia, 380.

Elliot, D. 1983. The construction of balanced cross-sections. *J. Struct. Geol.* **5**, 101.

Erickson, R. L. & Blade, L. V. 1963. Geochemistry and petrology of the alkali igneous complex at Mannet Cove, Arkansas. *U.S. Geol. Surv., Profess. Papers* **425**.

Etheridge, M. A. & Wilkie, J. C. 1979. Grain size reduction, grain boundary sliding and the flow strength of mylonites. *Tectonophysics* **58**, 159-178.

Faure, G. 1986. *Principles of isotope geology*. John Wiley and Sons, New York.

Fleuty, M. J. 1975. Slickensides and slickenlines. *Geological Magazine* **112**, 319-322.

Flottmann, T. & James, P. J. 1997. Balanced cross sections and strain distribution across two superposed and reactivated basins: structure of the southern Adelaide Fold-Thrust Belt. *J. Struct. Geol.* **19**(8), 1093-1110.

Flottmann, T., James, P. R., Rogers, J. & Johnson, T. 1994. Early Palaeozoic foreland thrusting and basin reactivation at the southeastern Paleo-Pacific margin of the Australian Precambrian Craton: a reappraisal of the structural evolution of the southern Adelaide Fold-Thrust Belt. *Tectonophysics* **234**, 95-116.

Foden, J. 1994. Nd- Sr isotope studies and the provenance of sediments in the Neoproterozoic and early Palaeozoic, eastern Australia. In: *Newsletter, Geological Society of South Australia.*

Foden, J., Barovich, K., Jane, M. & O'Halloran, G. 2001. Sr isotopic evidence for Late Neoproterozoic rifting in the Adelaide Geosyncline at 586 Ma: implications for a Cu ore forming fluid flux. *Precambrian Research* **106**(3-4), 291-308.

Forbes, B. G. 1972. Parachilna, South Australia. In: *Explanatory Notes, 1:250,000 Geological Series, Sheet SH/54-13*. Dept. of Mines, Geol. Surv. of South Australia.

Forbes, B. G. 1983. Noarlunga Preliminary Geological Map. Sheet 6627-IV and PT 6527-I. 1:250,000, Geol. Surv. of South Australia.

Forsyth, R. K. 1978. Geology of the Bunkers Graben, central Flinders Ranges. *S. Aust. Dept. Mines and Energy. Open file Envelope* **3424**.

Gay, P. & Roy, N. N. 1968. The mineralogy of the potassium - barium feldspar series. III. Sub-solidus relationships. *Mineral Mag.* **36**, 914.

Gayer, R. A., Powell, D. B. & Rhodes, S. 1978. Deformation against metadolerite dykes in the Caledonides of Finnmark, Norway. *Tectonophysics* **46**, 99-115.

Ghosh, S. K. & Ramberg, H. 1968. Buckling experiments on intersecting fold patterns. *Tectonophysics* **5**, 89-105.

Gibson, A. A. 1957. Oraparinna Barite Mine. *Min. Res. Rev., Dept. of Mines and Energy, South Australia* **102**, 84-100.

Goldstein, R. H. & Reynolds, T. J. 1994. Systematics of fluid inclusions in diagenetic minerals. SEPM Short Course 31, Society for Sedimentary Geology.

Groshong, R. H. & Epard, J. L. 1994. The role of strain in area-constant detachment folding. *J. Struct. Geol.* **16**, 613-618.

Hancock, P. L. 1985. Brittle microtectonics: principles and practice. *J. Struct. Geol.* **7**(3/4), 437-457.

Harding, T. P. 1974. Petroleum traps associated with wrench faults. *AAPG Bull.* **60**, 35-378.

Harris, R. J. 1979. Far Western Barite Occurrences, Oraparinna, Out of Hundreds, Co. Taunton, Flinders Ranges. *South Australian Dept. of Mines and Energy. Report 79/16.*

Haslett, P. G. 1976. Lower Cambrian carbonate stratigraphy and sedimentology, Old Wirrealpa Springs, Flinders Ranges, South Australia. Unpublished Ph.D. thesis, Dept. of Geol. and Geophy., Univ. of Adelaide.

Henry, P., Le Pichon, X., Lallemant, S., Foucher, J. P., Westbrook, G. & Hobart, M. 1990. Mud volcano field seaward of the Barbados Accretionary Complex: a deep-towed side sean sonar survey. *J. Geophys. Res.* **95**, 8917-8929.

Hiern, M. N. & Olliver, J. G. 1973. Statement of Ore Reserves. Oraparinna Barytes Mine. Co Taunton. *South Australian Dept. Mines Unpublished Report* **73/110**.

Hippertt, J. 1994. Structures indicative of hilicoidal flow in a migmatitic diapir (Bacao complex, southern Brazil). *Tectonophysics* **234**, 169-196.

Hobbs, B. E., Means, W. D. & Williams, P. F. 1976. *An outline of Structural Geology*. John Wiley, New York.

Holland, H. D. 1978. *The chemistry of the atmosphere and oceans*. J. Wiley and Sons, New York.

Homza, T. X. & Wallace, W. K. 1995. Geometric and kinematic models for detachment folds with fixed and variable detachment depths. *J. Struct. Geol.* **17**, 575-588.

Homza, T. X. & Wallace, W. K. 1997. Detachment folds with fixed hinges and variable detachment depth, northeastern Brooks Range, Alaska. *J. Struct. Geol.* **19**(3-4), 337-354.

Horwitz, R. C. 1962. Some aspects of metal distribution in sediments of upper Proterozoic-Lower Cambrian of South Australia. *Eclogae Geologicae Helveticae* **55**, 275-279.

Howchin, W. 1922. A geological traverse of the Flinders Ranges from the Parachilna Gorge to the lake Frome Plains. *Trans. Roy. Soc. South Australia* **46**, 46-82.

Hudleston, P. J. 1973a. Fold morphology and some geometrical implications of theories of fold development. *Tectonophysics* **16**, 1-46.

Hudleston, P. J. 1973b. An analysis of 'single layer' folds developed experimentally in viscous media. *Tectonophysics* **16**, 189-214.

Hudleston, P. J. 1989. The association of folds and veins in shear zones. *J. Struct. Geol.* **11**(8), 949-957.

Jackson, M. P. A., Cornelins, R. R., Craig, C. H., Gansser, A., Stocklin, J. & Talbot, C. J. 1990. Salt diapirs of the Great Kavir, Central Iran. *Geol. Soc. Am. Memoir* **177**.

Jamison, W. R. 1987. Geometric analysis of fold development in overthrust terrains. *J. Struct. Geol.* **9**, 207-219.

Jane, M. 1994. A geochemical analysis of carbonates and shales comprising the Adelaidean depositional system, with particular emphasis on the strontium isotopic values. Unpublished B.Sc. thesis, Dept. of Geol. and Geophy., Univ. of Adelaide.

Jenkins, R. J. F. 1990. The Adelaide Fold Belt: Tectonic reappraisal. In: *The evolution of a Late Precambrian-Early Palaeozoic Rift Complex: The Adelaide Geosyncline* (edited by Jago, J. b. & Moore, P. S.) **16**. Geol. Soc. Australia Special Publication.

Kelser, S. E., Jones, L. M. & Ruiz, J. 1988. Strontium isotopic geochemistry of Mississippi Valley-type deposits, east Tennessee: Implications for age and source of mineralizing brines. *Geol. Soc. Am. Bull.* **100**, 1300-1307.

Lambert, I. B., Knutson, J., Donnelly, T. H. & Etminan, H. 1987. Stuart shelf-Adelaide Geosyncline copper province, South Australia. *Econ. Geol.* **82**, 108-123.

Lapidus, D. F. 1990. *Collins Dictionary of Geology*. Harper Collins, London and Glasgow.

Laubscher, H. P. 1977. Fold development in the Jura. *Tectonophysics* **37**, 337-362.

Laurue, D. K. & Speed, R. C. 1984. Structure of the accretionary complex of Barbados II, Bissex Hill. *Bull. Geol. Soc. Am* **95**, 1360-1472.

Leach, D. L. 1980. Nature of mineralizing fluids in the barite deposits of central and southeast Missouri. *Econ. Geol.* **75**, 1168-1180.

Leeson, B. 1970. Geology of the Beltana 1:63 360 map area/ Report of Investigations. Geol. Surv., South Australia.

Lemon, N. M. 1988. Diapir recognition and modeling with examples from the Late Proterozoic Adelaide Geosyncline, Central Flinders Ranges, South Australia. Unpublished Ph.D. thesis, Dept. of Geol. and Geophy., Univ. of Adelaide.

Li, Z. X. & Powell, C. M. 1993. Magnetic fabric in mid-Cambrian rocks of the Central Flinders Zone and implications for the regional tectonic history. *Tectonophysics* **223**, 165-176.

Limonov, A. F., Woodside, J. M. & Ivanov, M. K. 1994. Mud volcanism in the Mediterranean and Black Seas and shallow structure of the Eratosthenes Seamount **64**. Unesco reports in marine sciences.

Lin, S. & Williams, P. F. 1992. The origin of ridge-in-groove slickenside striae and associated steps in an S-C mylonite. *J. Struct. Geol.* **14**(3), 315-321.

Mancktelow, N. S. 1981. Variation in fold axis geometry and slaty cleavage microfaric associated with a major fold arc, Fleurieu Peninsula, South Australia. *J. geol. Soc. Australia* **28**, 1-12.

Mancktelow, N. S. 1990. The structure of the southern Adelaide Fold Belt, South Australia. *Sp. Publ. Geol. Soc. Australia* **16**, 369-395.

Mansfield. 1956. Noarlunga Barite Deposits - Hundred of Willunga. *Min. Rev., Geol. Surv., South Australia* **100**, 90-92.

Marrett, R. & Bentham, P. A. 1997. Geometric analysis of hybrid fault-propagation/detachment folds. *J. Struct. Geol.* **19**(3-4), 243-248.

Marshak, S. & Flottmann, T. 1996. Structure and origin of the Fleurieu and Nackara Arcs in the Adelaide fold-thrust belt, South Australia: salient and recess development in the Delamerian Orogeny. *J. Struct. Geol.* **18**(7), 891-908.

Marshak, S. & Mitra, G. 1988. *Basic methods in structural geology*. Prentice Hall, Englewood Cliffs, N.J.

Martin, E. E., Macdougall, J. D., Herbert, T. D., Paytan, A. & Kastner, M. 1995. Strontium and neodynium isotopic analyses of marine barite separates. *Geochim. Cosmochim. Acta* **59**(7), 1353-1361.

Mawson, D. 1942. The structural character of the Flinders Ranges. *Trans. Roy. Soc. South Australia* **66**, 262-272.

McCallum, W. S. 1982. Oraparinna Barite deposits. Geological investigations at the Oraparinna (Bunkers Hill) Mine, Co. Taunton, Flinders Ranges. Dept. of Mines and Energy, South Australia, Report book 82/52.

McCallum, W. S. 1988. Barite, diapirs and evaporites. In: *Sp. publ. no8, Dept. of Mines and Energy, South Australia*, 27-31.

McCallum, W. S. 1990. Oraparinna Barite Deposits. In: *Geology of the Mineral Deposits of Australia and Papua New Guinea* (edited by Hughes, F. E.). The Australian Institute of Mining and Metallurgy: Melbourne, 1159-1191.

McCallum, W. S. 1992. Data File - Vein Barite deposits in the Adelaide Fold Belt. Dept. of Mines and Energy, South Australia.

McCallum, W. S. & Johnson, P. D. 1981. Oraparinna Barite deposits, Turley Lode, Southern Lode, Nicholls Deposit, Flinders Rages. Dept of Mines and Energy, South Australia, Report book 81/41.

McClay, K. R. 1987. *The mapping of geological structures*. John Wiley & Sons.

McClay, K. R. 1992a. Glossary of thrust tectonics terms. In: *Thrust Tectonics* (edited by McClay, K. R., 1992). Chapman & Hall, London, 419-433.

McClay, K. R. 1992b. *Thrust Tectonics*. Chapman & Hall, London.

Means, W. D. 1987. A newly recognized type of slickenside striation. *J. Struct. Geol.* **9**, 585-590.

Mercier, E., Outtani, F. & De Lamotte, D. F. 1997. Late-stage evolution of fault-propagation folds: principles and examples. *J. Struct. Geol.* **19**(2), 185-193.

Mincham, H. 1964. The story of the Flinders Ranges. *Rigby, Adelaide*, 306.

Mitra, S. 1990. Fault-propagation folds: Geometry, kinematic evolution and hydrocarbon traps. *AAPG Bull.* **74**, 921-945.

Mitra, S. 1992. Balanced structural interpretations in fold and thrust belts. In: *Structural Geology of Fold and Thrust Belts* (edited by Mitra, S. & Fisher, G. W.). The Johns Hopkins University Press, Baltimore, 53-77.

Mitra, S. & Namson, J. 1989. Equal area balancing. *American J. Sci.* **289**, 563-599.

Monaco, C. & Tortorici, L. 1996. Clay diapirs in Neogene-Quaternary sediments of central Sicily: evidence for accretionary processes. *J. Struct. Geol.* **18**(10), 1265-1269.

Morley, C. R. 1994. Fold-generated imbricates: examples from the Caledonides of Southern Norway. *J. Struct. Geol.* **16**(5), 619-631.

Mortimer, G. E., Cooper, J. A., Paterson, H. L., Cross, K., Hudson, G. R. T. & Uppill, R. K. 1988. Zircon U-Pb dating in the vicinity of the Olympic Dam Cu-U-Au deposit, Roxby Downs, South Australia. *Econ. Geol.* **83**, 694-709.

Mount, T. J. 1975. Diapirs and diapirism in the Adelaide 'Geosyncline', South Australia. Unpublished Ph.D. thesis, Dept. of Geol. and Geophys., Univ. of Adelaide.

Mumme, I. A. 1961. Geophysical investigation of the Blinman Dome. *Trans. Roy. Soc. South Australia* **85**, 7-11.

Murrell, B. 1977. Stratigraphy and tectonics across the Torrens Hinge Zone between Andamooka and Maree, SA. Unpublished Ph.D. thesis, Dept. of Geol. and Geophys., Univ. of Adelaide.

Naehr, T. H., Stakes, D. S. & Moore, W.S. 2000. Mass wasting, ephemeral fluid flow, and barite deposition on the California continental margin. *Geology* **28**(4), 315-318.

Neuman, E. W. 1933. Solubility relations of barium sulfate in aqueous solutions of strong electrolytes. *J. Am. Chem. Soc.* **55**, 879-884.

Newton, A. W. & Crettenden, P. P. 1984. Blinman Copper Mine - re-evaluation of mine dumps and review of geology. *Min. Res. Rev., Geol. Surv., South Australia* **154**, 72-73.

Nriagu, J. O. 1974. Fractionation of sulfur isotopes by sediment adsorption of sulfate. *Earth and Planetary Sci. Letters* **22**, 366 - 370.

O'Driscoll, E. S. 1964. Interference patterns from inclined shear fold systems. *Bull. Can. Petrol. Geol.* **12**, 279-310.

Ohmoto, H. 1972. Systematics of sulfur and carbon isotopes in hydrothermal ore deposits. *Econ. Geol.* **67**, 551-579.

Ohmoto, H. & Lasaga, A. C. 1982. Kinetics of reactions between aqueous sulphates and sulphides in hydrothermal systems. *Geochim. Cosmochim. Acta* **46**, 1727-1745.

Ohmoto, H. & Rye, O. 1979. *Isotopes of sulfur and carbon. In H. L. Barnes (Ed.), Geochemistry of hydrothermal ore deposits*. John Wiley & Sons.

Ohomoto, H. 1986. Stable isotope geochemistry of ore deposits. In: *Reviews in Mineralogy* (edited by J. W. Vallet, H. P. Taylor & O'Neil, J. R.). Mineral. Soc. America, 460-570.

Olliver, J. G. & Scott, D. C. 1978. Barite deposits near Mount John. *Min. Res. Rev., Geol. Surv., South Australia* **145**, 22-32.

Olliver, J. G., Spencer, W. G. & Cooper, R. 1979. Unusual mottled barite from Matthews deposit, Flinders Ranges. *Quarterly Geol. Notes, Geol. Surv., South Australia* **59**, 13-16.

Parkin, L. W., Reyner, M. L., Pitman, R. K. & K, J. R. 1953. Serle map sheet, Geological Atlas of South Australia, 1:63,360. Geol. Surv., South Australia.

Passchier, C. W. & Trouw, R. A. J. 1996. *Microtectonics*. Springer-Velag, Berlin.

Paul, E., Flottman, T. & Sandiford, M. 1999. Structural geometry of the Northern Flinders Ranges in the Adelaide Fold Belt, South Australia. *Australian J. Earth Sci.* **46**(3), 343-354.

Payton, A., Mearon, S., Cobb, K. & Kastner, M. 2002. Origin of marine barite deposits: Sr and S isotope characterizations. *Geology* **30**(8), 747-750.

Petit, J. P. 1987. Criteria for the sense of movement on fault surfaces in brittle rocks. *J. Struct. Geol.* **9**(5/6), 597-608.

Philippot, P. 1990. Opposite vergence of napes and crustal extension in the French Italian Alps. *Tectonics* **9**, 1143-1164.

Pluijm Van Der, B. A. 1984. An unusual 'crack-seal' vein geometry. *J. Struct. Geol.* **6**(5), 593-597.

Pollard, D. D. & Segall, P. 1987. Theoretical displacements and stresses near fractures in rock with applications to faults, joints, veins, dikes, and solution surfaces. In: *Fracture mechanics of rock* (edited by Atkinson, B. K.). Academic Press, London, 27-65.

Pott, P. J. 1987. *A hand-book of silicate rock analysis*. Blackie, Glasgow and London.

Potter, R. W., Clynne, M. A. & Brown, D. L. 1978. Freezing point depression of aqueous sodium chloride solutions. *Geochem. Cosmochim. Acta* **73**, 284-285.

Preiss, W. V. 1983. Adelaide Geosyncline and Stuart Shelf Geological Map: Precambrian and Palaeozoic geology (with special reference to the Adelaidean). Dept of Mines and Energy, South Australia.

Preiss, W. V. 1985. *Stratigraphy and tectonics of the Worumba Anticline and associated intrusive breccias.* Dept. of Mines and Energy, Geol. Surv., South Australia.

Preiss, W. V. 1987. *The Adelaide Geosyncline - late Proterozoic stratigraphy, sedimentation, palaentology and tectonics.* Dept. of Mines and energy, Geol. Surv., South Australia.

Preiss, W. V. 1995. Delamerian Orogeny. In: *The Geology of South Australia. Vol. 2 The Phanerozoic.* (edited by Dextral, J. F. & Preiss, W. V.) **54**. Geol. Surv. Bull., South Australia, 45-57.

Preiss, W. V. 1999. *Parachilna, South Australia, 1:250,000 Geological Series, Sheet SH54-13, Explanatory Notes.* Primary Industries and Resources, South Australia.

Puchelt, H. 1972. Barium. In: *Handbook of Geochemistry* (edited by Wedepohl, K. H.). Springer-Verlag, p56 A-1 to I-22.

Putnis, A. 1992. *Introduction to mineral sciences*. Cambridge Univ. Press, Cambridge.

Ramsay, J. G. 1980. The crack-seal mechanism of rock deformation. *Nature* **284**, 135-139.

Ramsay, J. G. & Huber, M. I. 1987. *The techniques of modern structural geology*. Academic Press, London.

Reid, P. & Preiss, W. V. 1999. Parachilna map sheet, 1:250,000. Geol. Surv., S. Australia.

Reid, R. B. 1969. A survey of Australian Barite. Unpublished B.Sc. thesis, Dept. of Econ. Geol., Univ. of Adelaide.

Reid, R. B. 1970. Final Report on SML 325, Oraparinna, Flinders Ranges, S.A. South Australian Barytes Ltd. *South Australian Dept. Mines and Energy. Open file Envelope 1381.*

Reilly, M. R. W., Lang, S. C. & Lemon, M. N. 2002. A basin floor fan outcrop analogue: reservoir heterogeneity and sequence stratigraphy. In: *Geoscience 2002: Expanding Horizons. Abstracts of the 16th Australian Geological Convention* (edited by Preiss, V. P.) **No. 67**, Adelaide Convention Centre, Adelaide, South Australia, 387.

Rich, J. L. 1934. Mechanics of low-angle overthrust faulting as illustrated by Cumberland thrust block, Virginia, Kentucky and Tennessee. *AAPG Bull.* **18**, 1584-1596.

Richert, J. P. 1976. Thrust Faulting in the northern Flinders Ranges, South Australia. *J. Geol. Soc. Australia* **23**, 361-366.

Robertson, A. 1981. An investigation of the barite deposits in the Artipena Area, Eastern Flinders Ranges, South Australia. Unpublished B.Sc. thesis, Dept. of Econ. Geol., Univ. of Adelaide.

Rollinson, H. R. 1995. *Using geochemical data: Evaluation, Presentation, Interpretation.* Longman Group Ltd.

Rothery, E. 1988. En echelon vein array development in extension and shear. *J. Struct. Geol.* **10**, 63-71.

Rowland, S. M. & Duebendorfer, E. M. 1994. *Structural analysis and synthesis, Second Edition.* Blackwell Scientific, Boston.

Rutland, R. W. R., Parker, A. J., Pitt, G. M., Preiss, W. V. & Murrell, B. 1981. The Precambrian of South Australia. In: *Precambrian of the southern Hemisphere* (edited by Hunter, D. R.). Elsevier, Amsterdam, 309-360.

Rye, R. O. & Ohmoto, H. 1974. Sulfur and carbon isotopes and ore genesis: A review. *Econ. Geol.* **69**, 826-842.

Sandiford, M., Paul, E. & Flottmann, T. 1998. Sedimentary thickness variations and deformation intensity during basin inversion in the Flinders Ranges, South Australia. *J. Struct. Geol.* **20**(12), 1721-1731.

Scott, D. C. 1979. Steetley's Barite Deposit - Linke's Lode, Flinders Ranges. ML 3414, Out of Hundreds, Co. Taunton, South Australia. Dept of Mines and Energy, S. Australia, Report book 79/98.

Seni, S. J. & Jackson, M. P. A. 1983a. Evolution of salt structures, East Texas diapir province, Part 1: Sedimentary record of halokinesis. *AAPG Bull.* **67**, 1219-1244.

Seni, S. J. & Jackson, M. P. A. 1983b. Evolution of salt structures, East Texas diapir province, Part II: Patterns and rates of halokinesis. *AAPG Bull.* **67**, 1245-1273.

Shackleton, R. M. 1995. Tectonic evolution in greenstone belts. In: *Early Precambrian Processes* (edited by Coward, M. P. & Ries, A. C.). Geol. Soc. London, Special Publication 95, 53-65.

Shainin, V. E. 1950. Conjugate sets of en echelon tension fractures in the Athens Limestone at Riverton, Virginia. *Bull. Geol. Soc. Am* **61**, 509-517.

Shepherd, T. J., Rankin, A. H. & Aldeton, D. H. M. 1985. *A practical guide to fluid inclusions.* Blackie.

Shields, G. A., Strauss, H., Howe, S. S. & Siegmund, H. 1999. Sulphur isotope composition of sedimentary phosphorites from the basal Cambrian of China: implications for Neoproterozoic-Cambrian biochemical cycling. *J. Geol. Soc. London* **156**, 943-955.

Sibson, R. H. 1986. Brecciation processes in fault zones: Inferences from earthquake rupturing. *Pure and applied geophysics* **124**, 159-175.

Skjernaa, L. 1975. Experiments on superimposed buckle folding. *Tectonophysics* **27**, 255-270.

Smith, J. V. 1996. Geometry and kinematics of convergent conjugate vein array systems. *J. Struct. Geol.* **18**(11), 1291-1300.

Snowden, P. A. & Bickle, M. J. 1976. The Chindomora Batholith: diapiric intrusion or interference fold? *J. Geol. Soc., London* **132**, 131.

Soula, J. C. 1982. Characteristics and mode of emplacement of gneiss domes and plutonic domes in central-eastern Pyrenees. *J. Struct. Geol.* **4**, 313-342.

Soula, J. C., Debat, P., Brusset, S., Bessiere, G., Christophoul, F. & Deramond, J. 2001. Thrust-related, diapiric, and extensional doming in a frontal orogenic wedge: example of the Montagne Noire, Southern French Hercynian Belt. *J. Struct. Geol.* **23**(11), 1677-1699.

Sprigg, R. C. 1949. Thrust tectonics in the Witchelina area, South Australia. *Trans. Roy. Soc. South Australia* **73**, 40-47.

Sprigg, R. C. 1952. Sedimentation in the Adelaide Geosyncline and the formation of the continental terrace. In: *Sir Douglas Mawson Anniversary Volume* (edited by Glaessner, M. F. & Rudd, E. A.). Univ. of Adelaide, p153-159.

Srivastava, D. C. 2000. Geometrical classification of conjugate vein arrays. *J. Struct. Geol.* **22**, 713-722.

Starke. 1962. Die strontiumgehalte de baryte. *Freiberg Forschungshefte* **c150**, 169.

Strauss, H. 1993. The sulfur isotope record of Precambrian sulfates: new data and a critical evaluation of the existing record. *Precambrian Research* **63**, 225-246.

Suppe, J. 1983. Geometry and kinematics of fault-bend folding. *American J. Sci.* **283**(7), 684-721.

Suppe, J. 1985. *Principles of Structural Geology*. Prentice Hall, N. Jersey.

Suppe, J. & Medwedeff, D. A. 1990. Geometry and kinematics of fault-propagation folding. *Eclogae Geologicae Helveticae* **83**, 409-454.

Sverdrup, H. U., Johnson, M. W. & Fleming, R. H. 1946. *The Oceans*. Prentice-Hall Inc, New York.

Tanner, P. W. G. 1989. The flexural-slip mechanism. *J. Struct. Geol.* **11**(6), 635-655.

Thorbjornsen, K. L. & Dunne, W. M. 1997. Origin of a thrust related fold: geometric vs kinematic tests. *J. Struct. Geol.* **19**, 303-319.

Torrini, R., Speed, R. C. & Mattioli, C. S. 1985. Tectonic relationships between forearc-basin strata and the accretionary complex at Bath, Barbados. *Bull. Geol. Soc. America* **96**(861-874).

Townsend, I. J. 1983. Patawarta Barite Deposit. *Min. Res. Rev., Dept. of Mines and Energy, Adelaide* **155**, 64-65.

Townsend, I. J. & Barnes, L. C. 1981. Oraparinna Barite Deposits, Bowering Lodes, Flinders Ranges, ML 4321, Out of hundreds, County Taunton, RB 81/79. Dept. of Mines and Energy, South Australia.

Turner, S., Foden, J., Sandiford, M. & Bruce, D. 1993. Sm-Nd isotopic evidence for the provenance of sediments from the Adelaide Fold Belt and southeastern Australia with implications for episodic crustal addition. *Geochim. Cosmochim. Acta* **57**, 1837 - 1856.

Twiss, R. J. & Moores, E. M. 1991. *Structural Geology*. W. H. Freeman and Company, New York.

Urai, J. L., Williams, P. F. & Van Roermund, H. L. M. 1991. Kinematics of crystal growth in syntectonic fibrous veins. *J. Struct. Geol.* **13**, 823-836.

Von der Borch, C. C. 1980. Evolution of late Proterozoic to Early Palaeozoic Adelaide foldbelt, Australia: comparison with post-Permian margins. *Tectonophysics* **70**, 115-134.

Wallace, W. K. & Homza, T. X. 1998. Detachment folds with fixed hinges and variable detachment depth, northeastern Brooks Range, Alaska: Reply. *J. Struct. Geol.* **20**(11), 1591-1595.

Wawryk, C. 1989. Strontium and rare earth element geochemistry of barite - fluorite mineralization at Olympic Dam, South Australia. Unpublished B.Sc. thesis, Dept. of Geol. and Geophys., Univ. of Adelaide.

Webb, B. P. 1960. Diapiric structures in the Flinders Ranges, South Australia. *Aust. J. Sci* **22**, 9.

Webb, B. P. 1961. The geological structure of the Blinman Dome. *Trans. Roy. Soc. S. Australia* **85**, 1-6.

Wedepohl, K. H. 1969. Composition and abundance of common igneous rocks. In: *Handbook of geochemistry* (edited by Wedepohl, K. H.). Springer-Verlag.

White, A. H. 1983. Speculations on the Adelaide rift and the origin of diapirs. In: *Adelaide Geosyncline sedimentary environments and tectonic setting symposium: Abstracts of the Geol. Soc. Aust.* **No. 10**, Adelaide, 3-6.

Whitford, D. J., Korsch, M. J. & Solomon, M. 1992. Strontium isotope studies of barites: Implications for the origin of base metal mineralisation in Tasmania. *Econ. Geol.* **87**, 953-959.

Will, T. M. & Wilson, C. J. L. 1989. Experimentally produced slickenside lineations in pyrophyllitic clay. *J. Struct. Geol.* **11**(6), 657-667.

Wiltschko, D. V. & Chapple, W. M. 1977. Flow of weak rocks in the Appalachian Plateau folds. *AAPG Bull.* **61**, 653-670.

Yassaghi, A. 1998. Geometry, kinematics, microstructures, strain analysis and *P-T* conditions of the shear zones and associated ductile trusts in the southern Mt. Lofty ranges/Adelaide Hills area, South Australia. Unpublished Ph.D. thesis, Dept. of Geol. and Geophy., Univ. of Adelaide.

Yassaghi, A., James, P. R. & Flottmann, T. 2000. Geometric and kinematic evolution of asymmetric ductile shear zones in thrust sheets, southern Adelaide Fold-Thrust Belt, South Australia. *J. Struct.Geol.* **22**, 889-912.

Appendix 8.1

XRF ANALYSES

PRELIMINARY SAMPLE PREPARATION

The samples were crushed in a jaw crusher to produce gravel-sized pieces and milled for a short time in a tungsten carbide mill vessel, to produce a fine powder suitable for analysis.

MAJOR ELEMENTS

SAMPLE PREPARATION, INSTRUMENTATION and RESULTS

The samples were dried in an oven at 110°C for over two hours to remove the absorbed moisture. They were then weighed into alumina crucibles and ignited overnight in a furnace at 960°C, to yield the Loss on Ignition (LOI) values. This comprises organic material, CO_2 from carbonate minerals, $H20^+$ (water in combination with the crystal structure), and possibly S, Cl and other volatiles, depending on the mineralogy of the samples. Nominally 1g of the ignited material was then accurately weighed with nominally 4g of flux (commercially available as type 12:22, comprising 35.3% lithium tetraborate and 64.7% lithium metaborate). The sample-flux mixture was fused in Pt-Au crucibles, using a propane-oxygen flame, at a temperature of approx. 1150°C, and cast into a preheated mould to produce a glass disc suitable for analysis.

The samples were analysed with a Philips PW 1480 X-ray Fluorescence Spectrometer, using an analysis program calibrated against several international and local Standard Reference Materials. A dual-anode (Sc-Mo) X-ray tube was used, operating at 40kV, 75mA.

Results

The results are presented on a "dry basis" in tabular form as oxides, which is the traditional form for silicate analyses. The analyses are on the "whole" sample, including any organic material that may be present. The iron is analysed as total Fe (combining the ferrous and ferric forms) expressed as Fe_2O_3. The method is suited particularly for silicate samples, and some difficulties are experienced in trying to analyse samples of extreme composition, such as barite.

TRACE ELEMENTS

SAMPLE PREPARATION, INSTRUMENTATION and RESULTS

About 5-8g of sample powder (depending on whether or not Boric Acid is used as a backing) was mixed with nominally 1ml of binder solution (Poly Vinyl Alcohol) and pressed to form a pellet. This was allowed to dry in air and was heated for a further 1 to 2 hours in a 70° C oven to ensure that the pellet was completely dry before analysis.

The samples were analysed with a Philips PW 1480 XRF Spectrometer, using several analysis programs covering suites of from 1 to 7 trace elements, with conditions optimised for the elements being analysed. The programs were calibrated against many (30 or more in some cases) local and international Standard Reference Materials. The both α dual-anode Sc-Mo tube (operated at sufficient voltage to excite the Mo) and a Au tube were used for

the analyses, to provide optimal excitation for different elements. Matrix corrections were made using either the Compton Scatter peak, or mass absorption coefficients calculated from the major element data.

Results

The results are presented as elements in tabular form, expressed as ppm. The calibrations assume trace levels of the elements, usually up to one to several thousand ppm. Samples containing one or more of these levels of "trace" elements cannot be successfully analysed using the general trace element programs.

Appendix 8.2 XRF Chemical analyses of barite samples. Concentrations for Ba and Sr are given as wt (%) and other elements as ppm.

*Sample	Deposit	Details	Ba	Sr	Rb	Cu	Zn	Ni	Co	Sc	V	Ce	Nd	La	Ga	Cr	Y	Nb	Zr	Th	Pb	U
NL50	Noarlunga		41.69	0.9	0.8	553	14	3	10.1	2.6	nd.	293	355	2	nd.	nd.	nd.	1.6	0.3	4.7	nd.	nd.
NL51B	Noarlunga	B Lode	40.81	1.11	nd.	594	10	nd.	8.6	3	nd.	280	339	2	nd.	nd.	nd.	1.5	nd.	5.8	nd.	nd.
NL51D	Noarlunga	D Lode	41.08	0.72	nd.	570	13	5	9.2	4.4	nd.	285	341	3	nd.	nd.	nd.	1.3	8.3	1.4	nd.	nd.
NL52	Noarlunga		40.68	0.66	2.9	553	24	10	9.9	0.8	nd.	281	338	nd.	nd.	nd.	nd.	2.1	nd.	5.5	nd.	0.2
NL53	Noarlunga	Riddles Lode	39.50	0.62	4.6	534	11	15	8.9	2.5	nd.	276	328	nd.	nd.	nd.	nd.	3.1	17	nd.	nd.	nd.
OM106[b]	Oraparinna Mine	1C Lode, Level 6	39.45	3.74	1.9	772	9	6	11.6	2.7	nd.	274	339	nd.	nd.	nd.	nd.	4.8	nd.	1	nd.	nd.
OM108[a]	Oraparinna Mine	1D Lode, Level 6	39.33	3.46	2.3	780	16	1	9.5	3.6	nd.	272	346	nd.	nd.	nd.	nd.	3.8	nd.	nd.	nd.	nd.
OM109	Oraparinna Mine	1B Lode, Level 6	37.74	3.87	4	753	8	8	7.4	2.1	nd.	268	310	nd.	nd.	nd.	nd.	2.5	nd.	nd.	nd.	nd.
OM113[c]	Oraparinna Mine	1A Lode, Level 6	39.68	2.19	3.4	680	13	2	8	3.1	nd.	274	324	5	nd.	nd.	nd.	4.1	nd.	0.5	nd.	nd.
OM114[b]	Oraparinna Mine	1A Lode, Level 6	39.50	3.28	1.1	721	15	0	8.4	3	nd.	276	352	2	nd.	nd.	nd.	4.7	nd.	4.2	nd.	nd.
OM120[a]	Oraparinna Mine	Link Lode, Level 6	38.95	3.64	4.9	751	15	5	7.9	2.4	nd.	273	334	nd.	nd.	nd.	nd.	4.1	nd.	nd.	nd.	nd.
OM127[c]	Oraparinna Mine	1D Lode, Level 5	39.67	3.07	nd.	724	12	1	8.6	3.3	nd.	280	336	1	nd.	nd.	nd.	3.3	nd.	3.5	nd.	nd.
OM128[a]	Oraparinna Mine	1D Lode, Level 5	39.29	3.46	4.3	728	13	0	8.6	2.2	nd.	274	334	nd.	nd.	nd.	nd.	5	nd.	nd.	nd.	nd.
OM130	Oraparinna Mine	breccia mixed	35.15	1.89	4.3	633	20	11	11.7	4.7	nd.	252	325	nd.	nd.	nd.	nd.	3.1	nd.	nd.	nd.	nd.
OM131	Oraparinna Mine	carbonate mixed	1.40	0.66	17.3	107	38	28	20.6	12.1	40.4	45	7	2	nd.	0	23	1.6	nd.	nd.	nd.	nd.
OM132	Oraparinna Mine	carbonate mixed	0.44	0.05	7.5	1	11	7	6.9	nd.	9.6	101	85	24	nd.	nd.	141	0.8	8.3	nd.	nd.	1.2
OM133	Oraparinna Mine	carbonate mixed	4.68	0.21	8.2	150	17	10	33.3	0	3.6	59	47	8	nd.	nd.	76	1.9	11	nd.	nd.	nd.
OM140[a]	Oraparinna Mine	1D Lode, Level 7	39.20	3.67	5.8	745	12	4	9.9	2.9	nd.	271	335	nd.	nd.	nd.	nd.	4.5	nd.	3.9	nd.	nd.
OM141[c]	Oraparinna Mine	1A Lode, Level 7	38.96	3.39	2.3	907	13	4	9.1	2	nd.	274	351	1	nd.	nd.	nd.	2.4	nd.	nd.	nd.	nd.
BN143[c]	Bainbridge	shale mixed	25.53	0.75	114.4	485	22	23	12.8	12.8	36.1	215	209	20	nd.	nd.	12	10.9	122	nd.	nd.	nd.
BN144	Bainbridge	No. 3 Lode	40.48	2	0.6	648	11	6	8.7	3	nd.	278	362	nd.	nd.	nd.	nd.	3.4	nd.	nd.	nd.	nd.
OM157[c]	Oraparinna Mine	Link Lode, Level 7	38.37	2.8	0.5	711	14	10	8.7	3.3	nd.	267	332	1	nd.	nd.	nd.	1.9	nd.	nd.	nd.	nd.
158	Oraparinna	fault zone	39.40	3.19	2.8	685	16	5	7.8	3.1	nd.	270	348	nd.	nd.	nd.	nd.	4.4	nd.	nd.	nd.	nd.
159	Oraparinna	fault zone	40.29	2.64	0.6	677	17	1	8.5	4.6	nd.	281	368	nd.	nd.	nd.	nd.	4.4	nd.	nd.	nd.	nd.
BW200	Bowering		40.19	1.31	0.9	577	11	2	8.4	4.9	nd.	280	350	1	nd.	nd.	nd.	2.9	nd.	nd.	nd.	nd.
D251[c]	Dunbar		39.46	1.37	nd.	591	14	nd.	9.2	3.2	nd.	275	362	1	nd.	nd.	nd.	2	nd.	4.7	nd.	nd.
D252	Dunbar		40.20	1.5	nd.	1132	13	6	9.7	2.7	nd.	283	363	1	nd.	nd.	nd.	2.1	nd.	4.4	nd.	nd.
D253[b]	Dunbar		39.94	2.78	7.8	656	17	3	12.6	3.5	nd.	272	330	0	nd.	nd.	nd.	2.9	nd.	8.5	nd.	nd.
D255[a]	Dunbar	1.5m thick lode	52.52	1.6	na.	na	na	na	na	0.7	na	na	na	na	na	na	na	na	na	na	na	na
D257[c]	Dunbar	0.6m from the centre	52.79	1.46	na	na	na	na	na	nd.	na	na	na	na	na	na	na	na	na	na	na	na
H301	Halls	quartz mixed	21.36	0.24	2.3	240	6	nd.	55.6	2.6	nd.	158	175	nd.	nd.	nd.	nd.	0.9	2.6	nd.	nd.	nd.

*Note: [a], [b] and [c] denote sampling positions in the lode as the centre median line ([a]), between centre and border ([b]) and border ([c]). All the samples were analysed using pressed pellets and Ba in high quantities may result in errors. Hence, relative concentrations of Ba may be believed rather than absolute values.
Sr was reanalysed later in comparison with laboratory made standards. D255[a] and D257[b] samples were also analysed later. Abbreviations: nd - not detectable, na - not analysed
All sample Nos. have the prefix "A987/", the authors index No. at the Dept. of Geology and Geophysics, Uni. of Adelaide.

Appendix 9.1: Barite deposits of the Adelaide Fold Belt, with estimated tonnages and host rock lithologies for deposits with combined production + reserves > 2000 tonnes. Data for some associated smaller deposits also included. Source of data: Mines and Energy Dept, S.A. 1992

Deposit	Map Sheet 1:250,000 scale	Barite prodution + reserves (Tonnes)	Proterozoic															Palaeozoic	Host Lithology*
			Pre-Adelaidean	Adelaidean														Cambrian	
				Torrensian				Sturtian			Marinoan							Cambrian	
				Burrra Group				Umberatana Group						Wilpena Group				Hawker Gp.	
				B1	B2	B3	B4	B7	U2	U6	U8	U9	U10	U13	W1	W2	W4	W5	W6	H1	H2	
Beltana No1	Copley	21																x				Lst,Sltst
Beltana No 2	Copley	3778																x				Sh,Sltst
Ediacara North	Copley	18000																x				Sh,Sdst,Q
Mount James No1, North	Copley	391?																x				Sltst,Lst
Mount James No1, South	Copley	11300																x				Sltst,Lst
Mount James No 2	Copley	4200																x				Sh-Sdst
Mount James No 3	Copley	7380																x				Lst,Sh-Sdst
Mount James No 4	Copley	1800																x				Sh
Nilpena, No 1(A->E)lodes	Copley	4477													x							Sltst
Nilpena, No 2(A->D)lodes	Copley	5094													x							Sltst
N Moolooloo, Copper King Bar	Copley	5500																x				Sla,Sltst,Do
Nankaburyana Deposit	Copley	2525																x				Sltst,Do,Lst
Mt. Serle No.1 Lode	Copley	3344													x							Sltst
Mt. Serle No.2 Lode	Copley	2169													x							Sltst,Sdst
Mt. Serle No.3 Lode	Copley	200?																		x		Do,Do-Sltst
Mt. Serle No.4 Lode	Copley	510?																		x		Do-Sltst

*Abbreviations; Lst: Limestone, Do: Dolomite, Slst: Siltstone, Do-Slst: Dolomitic Siltstone, Sh: Shale, Sdst: Sandstone, Sh-Sdst: Shaly Sandstone, Sla: Slate, Co: Conglamerate, Sch: Schist, Phy: Phyllite, Q: Quartzite, Orapr: Oraparinna

B1: Rhynie SdSt, B2: River Wakefield Subgroup, B3: Aldgate SdSt, B4: Woolshed Flat Shale, B7: Saddleworth Formation, U2: Holowilena Ironstone, U6: Wilyerpa Formation, U8: Tapley Hill Formation, U9: Enorama Shale, U10: Etina Formation, U13: Elatina Formation, W1: Nuccaleena Formation, W2: Brachina Formation, W4: ABC Range Quartzite, W5: Bunyeroo Formation, W6: Wonoka Formation, H1: Wilkawillina LSt, H2: Parara LSt.

Appendix 9.1 Contd.....

Deposit	Map sheet	Tonnes	Pre-Adelaidean	B1	B2	B3	B4	B7	U2	U6	U8	U9	U10	U13	W1	W2	W4	W5	W6	H1	H2	
Mt. Chambers Barite	Copley	4325														x						Sltst
Artipena (No.1 Lode)	Parachilna	724												x								SdSt
Artipena (No.2 Lode)	Parachilna	12472											x									Sh,Do-SltSt
Artipena (No.3 Lode)	Parachilna	600										x										Sh,Do-SltSt,SdSt
Artipena (No.4 Lode)	Parachilna	160										x										Sh,Do
Cement Square (No.1)Lode	Parachilna	7500														x	x	x				SltSt,Sh,SdSt
Cement Square (No.2)Lode	Parachilna	4300														x	x	x				SltSt,Sh,SdSt
Carey Hill No.2A Lodes	Parachilna	39598														x						SltSt
Carey Hill No.2B Lodes	Parachilna	1500														x						SltSt
Coadville, Coadsville	Parachilna	3414														x						Sh,SltSt
Moralana No.1	Parachilna	26427										x										Sh
Mt Folkland No.1	Parachilna	8490															x					SdSt
Mt Folkland No. 2	Parachilna	8307															x					SdSt
Mt Folkland No. 3	Parachilna	11622															x					SdSt
Mt. Frome	Parachilna	13863														x						SltSt,Sh
Mt. John Lode 1->10	Parachilna	9485																				Diapir
Mt. Neville	Parachilna	5200														x						SltSt
Orapr. Diapir-Bairstow Lode	Parachilna	15565									x											Sh,SltSt,Di
Orapr. Diapir-Bowering Lode	Parachilna	14834								x												Q,Do.SltSt,Di
Orapr. Diapir-Hall Lode	Parachilna	7700									x											SltSt,Sh
Orapr. Diapir-Howard Lode	Parachilna	100?							x?	x												SltSt,Sh,SdSt,Q
Orapr. Diapir-Linke's Lode	Parachilna	28542									x											Sh,SltSt
Orapr. Diapir-Mc Rue No.1	Parachilna	38406								x												Q,SltSt
Orapr. Diapir-Mc Rue No.2	Parachilna	7000								x												Q,SltSt
Orapr. Diapir-Nicolls Lode	Parachilna	20									x?											Diapir
Orapr. Diapir-Souhern Lode	Parachilna	1 - 500?												x								Sh,SltSt
Orapr. Diapir-Tom Hill Lode	Parachilna	16									x											Sh,SltSt
Orapr.-No.1 Lode System	Parachilna	333000														x						SltSt

Appendix 9.1 Contd....

Deposit	Map sheet	Tonnes	Pre-Adelaidean	B1	B2	B3	B4	B7	U2	U6	U8	U9	U10	U13	W1	W2	W4	W5	W6	H1	H2	
Orapr.-No.2 Lode System	Parachilna	5000														x						SltSt
Orapr.-No.3 Lode System	Parachilna	4000														x						SltSt
Orapr.-No.4 Lode System	Parachilna	6000?														x						SltSt
Orapr.-No.5 Lode System	Parachilna	20 - 25,000?														x						SltSt
Orapr.-Selsen Lode	Parachilna	15000															x	x				Sh,SltSt
Orapr.-Western Lode	Parachilna	2000														x						SltSt
Orapr.-Mathews Deposit	Parachilna	14315																x				SltSt
Orapr.-Far Western Lodes	Parachilna	1000?												x	x	x						SdSt,Q
Orapr.-Turley Lode	Parachilna	10-15,000														x						SltSt
Orapr.-Vincent Lode	Parachilna	1086							x													Sh,Do,SdSt,Q,Co
Potato Patch	Parachilna	3893																			x	SltSt,SdSt,LSt
Horseshoe Prospect	Orroroo	10000						x														Sh,Do
Oladdie	Orroroo	3000		x	x																	SltSt,Q,
Corunna Barite	Pt. Augusta	300?	Corunna Congl.																			SdSt
Mt. Whyalla	Pt. Augusta	2188	Pandura Form.																			SdSt,Co
Saltia	Pt. Augusta	809												x		x						SltSt,SdSt,Sla
Mt. Larva	Pt. Augusta	45	Moonabie Form.																			SdSt,Co
Julia Creek A	Adelaide	6043										x										Sla,Phy,Do
Julia Creek B	Adelaide	64																				Sla,Phy,Do
Torrens Barites Mine	Adelaide	9108					x															LSt,Sh,Sch
Woodside	Adelaide	3091																				SltSt
Aldgate	Barker	7327				x																SdSt,Sla
Crystal Barite Mine	Barker	16576				x																SdSt,Sla
Noarlunga Section 92	Barker	239												x								SltSt
Noarlunga Snowflake Sect. 82	Barker	72												x								SltSt,Sh
Noarlunga Snowflake Sec.102	Barker	42												x								Sla
Total production + reserves		824200																				

Appendix 9.2

Field geological log supplemented with some updated microscope information of Diamond Drill Core No. OU 2/90 drilled through the Brachina Formation in the Oraparinna Barite Mine. The hole was drilled from the main decline in the mine, through 1D Lode. The host in the NW (1 to 50.64m) of the Lode shows a strong post - vein slip-lineation developed more intensely close to the ore body. The slip lineation southeast of the lode from 61.22m to 70.91m is much weaker than NW of the lode.

Start : 1.1m Finish: 70.91m

Abbreviations:

Colour: grn. - green, blk. - black, rd. - red, ppl. - purple, br. - brown, wh. - white, brsh. - brownish, grnsh. - greenish, yelsh. - yellowish etc., dk. - dark, l. - light.

Texture: v.f.g. - very fine grained

lithology: qtz. - quartz, sltst. - , bar. - barite, cal. - calcite

Sample No.	Depth (m)	Description
	1.1-1.25	Dk. brsh. grn.; Thinly interbeded with l.br., v.f.g. sltst. Calcite occurs in tiny fractures.
	1.25-1.55	Dk. pplsh. grn; very thin calcite veins (<1mm) shows displacements along bedding planes.
2/90/1	1.35	
	1.55-8.80	Similar to 1.1-1.25m, with occurrence of minor chalcopyrite in association with l.br. thinly bedded sltst. beds. The sltst. is thinly interbedded from 4.02m onwards with l. ppl. sltst., except from 5.25-5.80m.
2/90/2	1.8	
2/90/3	3.0	High concentration of thin and folded calcite veins. (Contains deformed barite of wavy extinction, qtz, calcite of younger generation.)
2/90/4	3.75	Minor occurrence of chalcopyrite limited to l.br. sltst. patches. Strong chlorite lineation occurs.
2/90/5	4.80	Sltst.: Ppl. bands and calcite patches. Calcite occurs concordant as well as discordant to bedding.
2/90/6	5.45	
2/90/7	5.85	Bar. at the centre of carbonate, also in contact with ppl. Sltst.

2/90/8	6.35	Thin brsh. rd. barite in association with wh. calcite, l.br. sltst. and ppl. colour thin beds. Haematite needles are present.
2/90/9	7.90	Calcite in association with barite (l. yelsh. wh.). Chalcopyrite concentrated in thin bands parallel to the major calcite band.
2/90/10	8.65	Cores tend to break easily along ppl. colour bedding. Lineation is well developed. No association of calcite.
	8.80-9.55	Siltstone: Blk. spotted br., micaceous, thinly bedded. No lineation. Calcite bands are displaced along bedding.
2/90/11	8.80	Sample from the boundary between l.ppl. sltst. and dk brsh. grn sltst.
	9.55-10.95	Dk. brsh. grn and dk brsh. ppl. thinly interbeded sltst.. Slip lineation on bedding.
	10.95-11.78	Dk. brsh. grn. sltst. with random lenses of br. sltst., to which most chalcopyrite mineralisation is limited.
2/90/12	11.55	Calcite/ bar. mineralisation sheared along bedding.
	11.78-16.10	Siltstone: Dk. brsh. ppl interbeded with dk brsh. grn sltst.
2/90/13	12.75	Shearing between calcite and barite bands.
	16.10-17.30	Siltstone: Dk. brsh. grn. sltst. interbeded with br. sltst. Pyrite limited to br. sltst.
2/90/14	17.05	Well crystallised pyrite in fine grained bar., qtz., calcite occurrences.
	17.30-20.34	Siltstone: Dk. brsh. ppl inter layered with brsh. grn. sltst.
2/90/15	18.40	Brecciated calcite veins.
2/90/16	20.20	Calcite and barite associations
	20.34-23.40	Siltstone: Dk. brsh. grn. with calcite laminations.
2/90/17	22.60	Calcite in en-echelon tension gashes indicating a semi-brittle to semi-ductile shear zone
	23.40-23.80	Grn and ppl. sltst. inter layered with br. sltst.
	27.80-41.00	Siltstone: Grn. variety with calcite laminations.
2/90/18	27.90	Pyrite and barite localisations in calcite.

2/90/19	32.52	Shearing of calcite along bedding
2/90/20	23.11	Br., silty, folded laminations.
2/90/21	34.50	Calcite/bar. of wh./creamy wh. bands.
2/90/22	36.35	Calcite/barite veining
2/90/23	36.90	Shearing of calcite/bar. along bedding
2/90/24	39.40	Calcite/barite veining
	41.00-42.30	Siltstone: Ppl. sltst. interbeded with some shale at 42.00m.
2/90/25	42.10	Sltst. br.
	42.30-49.40	Siltstone with grn. sh. and calcite.
2/90/26	47.50	Calcite/barite association.
	49.40-50.64	Brsh. ppl. and grn. siltstone inter layered.
	49.40-50.64	Siltstone: Brsh ppl. and grn. sltst. inter layered.
2/90/27	49.80	Cal./bar. association.
2/90/28a	50.60	Siltstone/calcite/barite association adjoining the major barite lode
2/90/28b	50.64	Sheared and deformed, elongated small barite grains.
	50.64-61.22	Barite: 10.58m thick along the drill hole, reddish colour on boundary decreases towards interior.
2/90/29	51.80	Barite.
2/90/30	54.45	Barite and qtz mixed in lamellae
2/90/31	57.44	Barite: Creamy white, calcite relicts in barite. Folded lamellae in barite.
2/90/32	58.45	Barite mixed with calcite patches.
	61.22-62.20	Siltstone: Grn. and br. patches.
2/90/33	61.22m	End of Lode. Shear textures.
2/90/34	61.42	20cm away from the lode's boundary, barite in grnsh and br. sltst. Weak lineation in sltst.
	62.20-62.95	Siltstone: Ppl with minor bar. and calcite thin bands.

2/90/35	62.70	Ppl sltst. with bar. and calcite banding. Weak lineation in sltst..
	62.85-70.91	Grn and l. br. siltstone.
2/90/36	63.25	1cm thick barite vein in sltst.
2/90/37	67.00	Grn siltstone mixed with shale. Elongated barite grains in 60° angle.
2/90/38	69.20	Fibrous calcite in grn. sltst. Lineation in the host is not developed as on the other side of the lode.
2/90/39	70.30-70.91	Grn. sltst., slip lineation is developed, but not as on the other side of the lode.
	70.91	End of hole.

Appendix 9.3: XRF analyses of Brachina Formation in the Oraparinna Barite Mine.

Section 1: Brachina Formation samples from the Level 5, adjacent to the 1D Lode, Oraparinna Barite Mine.

Major element Analysis (%):

Sample*[1]	Distance (m) to lode border	SiO2	Al2O3	Fe2O3	MnO	MgO	CaO	Na2O	K2O	TiO2	P2O5	SO3	LOI	Total
OM121	24.8	62.9	16.66	7.27	0.03	2.1	0.4	1.72	4.29	1.22	0.14	0.1	3.23	100
OM123	16.9	63.33	9.43	6.61	0.26	1.59	2.8	2.32	1.75	0.94	0.09	1	5.08	95.2
OM124	10.2	62.39	16.47	7.38	0.06	2.11	1	1.62	4.12	1.21	0.14	0.2	3.5	100
OM125	4.2	70.4	6.71	3.24	0.13	0.64	3.3	1.75	1.45	0.79	0.07	1.6	3.81	93.8
OM126	1.1	58.38	14.38	7.10	0.18	1.61	4.8	1.3	3.66	1.17	0.17	0.3	6.37	99.4

Minor element Analysis (ppm):

Sample	Distance (m) to lode border	Ba	Sr	Rb	Cu	Zn	Ni	Co	Sc	V	Ce	Nd	La	Ga	Cr	Y	Nb	Zr	Th	Pb	U
OM121	24.8	765	107	198.2	7	75	47	56.1	26.1	246	103	51	51	23.4	139	39	18	230	18	8.4	3.8
OM123	16.9	24504	552	83.9	38	38	20	41.6	12.8	111	93	54	34	5.6	49	37	13	386	12	nd.	2.8
OM124	10.2	996	136	184.2	14	81	44	29.9	27.2	246	80	45	40	23	133	41	18	253	19	7.7	4.1
OM125	4.2	32940	865	62.8	52	28	15	63.2	9.7	67.5	64	47	16	0.3	22	26	8.8	182	2.2	nd.	0.6
OM126	1.1	1566	1785	165.5	72	57	43	25.9	24.2	204	78	42	36	20.3	109	42	17	242	19	3.1	2.7

Section 2: Brachina Formation samples from the Drill hole OU2/90 of the Oraparinna Barite Mine drilled through 1D Lode.

2/90/5	45.84 (NW)	378	131.8	189	5	68	45	18.7	19	182	79	38	37	23.3	137	42	19	280	18	8.4	5
2/90/11	41.84	155	170.3	27.1	73	18	11	48.3	4.8	56	29	13	11	6.9	24	27	12	281	8.4	10	1.6
2/90/15	32.24	491	130.2	144	8	74	47	19.1	15	146	70	34	31	18.9	126	39	16	280	15	4.6	2.8
2/90/18	22.74	287	101.9	135	54	77	43	9.8	16	168	76	35	37	19.9	131	31	14	186	11	4.7	2.2
2/90/22	14.29	476	284.6	80.7	26	34	56	60.5	12	65.9	41	21	19	10	41	38	10	297	11	38	3.7
2/90/25	8.54	2538	129.8	9.5	20	10	15	0.7	3.9	61	62	34	19	5.1	251	25	8.7	169	5.7	1.2	2.1
2/90/26	3.14	901	126.7	144	7	66	40	12.5	14	156	66	28	29	17.8	178	36	17	300	15	7.8	4
2/90/28a	0.04 (NW)	1027	210.6	158	6	22	25	13.8	14	118	61	31	28	16.6	63	43	15	211	9.8	8.2	2.5
2/90/33	0 (SE)	7064	477.7	148	40	16	46	23.2	11	105	63	30	33	14.6	110	17	12	215	11	18	5.2
2/90/34	0.2	5232	369	198	117	20	26	6	14	146	85	40	49	21.3	125	25	16	256	13	4.9	2.7
2/90/35	1.48	361	129.8	221	18	22	24	7.8	16	151	109	45	60	23.2	112	31	17	269	14	8.8	3.1
2/90/36	2.03	349	146.6	208	25	26	26	18.6	18	167	85	34	44	21.8	92	32	19	301	19	15	2.4
2/90/37	5.78	875	110.7	70.6	26	18	40	38.4	6.9	43.8	30	16	11	7.5	29	29	11	300	11	26	2.9
2/90/39	9.08 (SE)	480	106.9	162	23	55	36	23.7	16	147	67	31	32	19.8	82	38	17	313	18	17	4.2

Brachina Formation samples from Level 6, adjacent to the 1C Lode, Oraparinna Barite Mine.

OM101	1121	12780	238	83	50	43	7.4	17	171	42	21	19	27	124	35	20	288	20	9.5	nd.
OM104	32029	4660	208	223	22	28	9.4	12	131	64	32	17	9.8	97	26	19	262	8.3	nd.	nd.
OM105	713	211.2	186	71	18	24	8.6	16	156	114	47	62	19.1	121	26	16	262	17	8.5	4.3

Appendix 9.4: Major and trace element XRF analyses of Elatina Formation at the 'Far Western Lode' in the Third Plain area.

Sample	Distance (m) from vein	SiO2 %	Al2O3 %	Fe2O3T %	MnO %	MgO %	CaO %	Na2O %	K2O %	TiO2 %	P2O5 %	SO3 %	LOI %	Total %
987-730	1	90.30	4.39	0.68	0.00	0.09	0.21	1.16	1.63	0.07	0.06	0.16	0.53	99.28
987-731	2	91.01	3.90	0.48	0.00	0.07	0.21	0.99	1.50	0.05	0.07	0.21	0.62	99.10
987-732	4	92.38	3.70	0.71	0.02	0.07	0.13	0.81	1.48	0.04	0.07	-0.01	0.38	99.78
987-733	6	92.27	3.18	0.60	0.00	0.07	0.11	0.76	1.23	0.05	0.03	0.23	1.01	99.54
987-734	9	92.28	3.39	0.61	0.01	0.06	0.07	0.68	1.22	0.07	0.03	0.23	0.57	99.21
987-735	13	91.93	3.43	0.48	0.00	0.07	0.08	0.76	1.41	0.03	0.04	0.25	0.46	98.93
987-737	16	91.78	3.45	0.63	0.01	0.08	0.16	0.72	1.36	0.06	0.08	0.25	0.58	99.15
987-738	23	91.08	3.83	0.59	0.01	0.07	0.07	0.89	1.37	0.05	0.02	0.22	0.56	98.75
987-739	25	92.43	3.87	0.41	0.00	0.05	0.05	0.89	1.46	0.05	0.02	0.04	0.37	99.65
987-740	38	91.48	3.77	0.91	0.02	0.08	0.11	0.82	1.30	0.12	0.05	0.15	0.62	99.44
987-741	48	89.87	4.48	0.87	0.01	0.20	0.17	1.00	1.55	0.15	0.07	0.17	0.74	99.29
987-742	58	92.05	3.87	0.55	0.01	0.09	0.08	0.83	1.50	0.04	0.02	0.05	0.46	99.56
987-743	68	89.95	4.54	0.80	0.01	0.09	0.12	1.21	1.64	0.14	0.06	0.17	0.54	99.28
987-744	78	91.69	3.88	0.61	0.00	0.06	0.07	1.00	1.43	0.08	0.03	0.17	0.41	99.42
987-745	93	89.14	4.10	0.98	0.05	0.39	0.48	0.87	1.44	0.16	0.04	0.45	1.26	99.36
987-746	109	89.43	4.15	0.64	0.02	0.36	0.58	1.15	1.58	0.14	0.04	0.24	0.78	99.09
987-747	129	80.29	6.11	2.79	0.08	0.62	1.97	1.83	1.79	0.78	0.16	0.45	2.19	99.07
987-748	149	74.51	6.51	3.07	0.11	1.05	4.39	1.98	1.75	0.86	0.16	0.13	4.66	99.17
987-749	169	65.54	8.47	3.11	0.14	1.59	7.67	2.84	1.64	0.63	0.18	0.16	7.84	99.81
987-750	190	63.81	8.45	3.26	0.13	2.14	7.82	2.82	1.65	0.74	0.22	0.10	8.59	99.73
987-751	210	67.51	7.71	2.73	0.14	2.45	6.32	2.62	1.61	0.66	0.22	0.06	7.79	99.82
987-752	231	66.02	8.48	2.83	0.10	1.43	7.90	2.84	1.67	0.57	0.17	0.07	7.73	99.79
987-753	246	74.60	8.49	3.64	0.17	0.44	2.84	2.90	1.71	0.84	0.24	0.75	2.86	99.47
987-754	268	84.38	7.32	1.47	0.00	0.29	0.41	2.26	1.88	0.31	0.11	0.00	0.90	99.35
987-755	288	81.58	8.53	2.07	0.01	0.54	0.38	2.76	1.75	0.37	0.16	0.06	1.12	99.34
987-756	310	84.92	6.43	1.77	0.01	0.48	0.29	1.75	1.97	0.39	0.10	0.08	0.89	99.10
987-757	352	86.60	5.85	1.41	0.00	0.18	0.25	1.69	1.87	0.28	0.09	0.11	0.67	99.01
987-758	394	83.23	7.94	2.15	0.01	0.35	0.31	2.61	1.75	0.45	0.13	-0.01	0.71	99.62

Appendix 9.4: ....contd. Major and trace element XRF analyses of Elatina Formation at the 'Far Western Lode' in the Third Plain area.

Sample	Distance (m) from vein	Zr ppm	Nb ppm	Y ppm	Sr ppm	Rb ppm	U ppm	Th ppm	Pb ppm	Ga ppm	Cu ppm	Zn ppm	Ba ppm	Sc ppm	Co ppm	V ppm	Ce ppm	Nd ppm	La ppm	Cr ppm	Ni ppm
987-730	1	45.2	1.9	6.5	59.0	48.8	0.1	0.3	4.1	2.0	16	7	3184	1.3	129	14	11	1	4	5	0
987-731	2	40.5	1.4	5.3	66.2	45.9	0.6	0.0	2.4	1.3	13	2	3837	1.1	130	13	11	0	3	5	0
987-732	4	37.9	1.5	5.6	39.0	44.7	0.2	0.8	5.1	3.2	13	5	1152	2.0	61	16	9	7	4	5	0
987-733	6	40.3	1.4	5.7	54.8	36.7	0.6	0.0	1.8	0.6	14	3	4705	1.0	84	14	9	0	3	4	0
987-734	9	48.8	1.1	6.1	34.5	37.2	1.3	1.3	4.2	1.7	12	3	5071	1.4	169	16	13	1	4	9	0
987-735	13	33.4	1.3	4.9	67.8	41.8	0.6	0.5	3.3	0.9	5	1	4647	0.5	153	12	11	0	3	3	0
987-737	16	48.5	1.6	6.6	43.6	40.0	1.4	0.1	1.4	0.0	15	2	5533	0.7	91	17	10	0	4	5	0
987-738	23	39.6	1.6	6.5	40.9	41.1	0.9	0.3	1.7	1.7	9	3	4539	1.9	117	15	10	0	4	3	0
987-739	25	52.9	2.0	4.3	30.1	42.4	0.8	1.3	4.3	2.7	13	1	1126	0.7	173	10	8	2	3	5	0
987-740	38	95.9	2.1	8.3	33.1	40.2	0.0	1.7	3.1	1.9	10	4	3467	1.5	95	19	12	3	4	10	0
987-741	48	117.8	3.0	9.2	43.1	46.9	0.0	2.2	4.7	3.0	11	3	3241	1.6	152	21	16	4	5	14	0
987-742	58	35.7	1.5	5.1	34.7	45.3	0.0	0.6	4.1	2.4	11	2	1435	1.5	101	14	10	4	4	10	0
987-743	68	106.0	3.1	9.0	52.8	49.5	0.3	2.6	4.5	1.5	6	4	3794	1.6	110	19	17	4	5	11	0
987-744	78	65.6	1.4	6.0	44.6	41.1	0.1	1.8	1.9	2.1	14	2	3300	1.4	128	15	11	3	4	5	0
987-745	93	113.3	2.8	8.0	58.6	43.5	0.7	2.1	3.1	3.0	11	4	2991	2.0	87	19	18	3	6	14	1
987-746	109	116.1	2.6	7.8	60.0	45.1	0.3	1.3	6.4	1.2	6	4	2715	1.9	82	16	14	1	4	13	0
987-747	129	573.2	9.4	28.3	58.8	57.9	2.7	9.5	7.1	4.4	20	10	3254	5.1	60	59	39	14	20	59	4
987-748	149	668.8	11.1	28.2	56.4	58.4	2.8	13.2	8.0	4.0	11	15	2902	7.4	47	65	55	27	25	68	3
987-749	169	301.4	10.1	30.7	63.3	57.3	2.6	9.7	8.0	7.7	5	18	1305	8.6	71	73	48	20	20	99	16
987-750	190	359.9	10.8	34.9	71.0	59.4	3.0	11.3	8.8	8.7	15	18	1279	9.5	42	80	51	23	24	79	11
987-751	210	371.8	10.8	31.8	62.8	56.2	2.9	11.6	7.2	6.9	6	16	767	8.1	32	66	46	21	21	63	9
987-752	231	253.2	9.0	27.4	55.0	61.0	2.6	9.3	6.1	9.6	16	17	559	7.9	48	71	40	18	18	61	8
987-753	246	507.1	11.9	41.0	69.2	62.5	3.6	13.0	5.1	7.6	15	80	1555	9.0	99	80	57	27	28	85	64
987-754	268	158.2	5.4	16.7	50.9	73.7	1.6	3.8	8.1	6.6	7	23	462	4.3	94	31	20	11	10	25	0
987-755	288	142.3	6.4	18.9	60.8	64.4	1.5	4.8	8.2	7.3	15	45	1552	6.4	57	42	31	15	13	36	24
987-756	310	239.0	5.6	16.5	63.5	69.8	2.0	3.6	7.6	4.2	9	20	2114	4.9	61	37	29	12	11	27	4
987-757	352	198.4	4.4	15.8	79.4	66.8	0.9	3.7	5.8	4.6	13	11	2362	3.2	100	31	24	9	11	25	0
987-758	394	250.7	6.0	21.6	45.3	68.1	0.8	6.8	5.8	6.3	6	25	241	6.0	78	44	32	18	15	39	5

16th Australian Geological Convention
1-5 July 2002
Adelaide Convention Centre
Adelaide, South Australia

GEOSCIENCE 2002:
Expanding Horizons

Abstracts Volume No.67

Mendis, P.J. (Lal)., James, P.R., and Both, R.A., (2002) Geological structure of the Flinders Ranges, South Australia.
Abstracts – Geological Society of South Australia, v. 67, p. 183.

Mendis, P.J. (Lal)., Both, R.A., and James, P.R., (2002) Structural and geochemical control of barite veins in the Flinders Ranges, South Australia.
Abstracts – Geological Society of South Australia, v. 67, p. 337.

Mendis, P.J. (Lal)., James, P.R., and Both, R.A., (2002) Origin of diapirs in the Adelaide fold belt; synsedimentary or syntectonic?
Abstracts – Geological Society of South Australia, v. 67, p. 384.